2021

MECHANISMS OF INTERACTION BETWEEN HAEMOPHILUS PARAINFLUENZAE AND STREPTOCOCCUS MITIS

Dasith Perera
University of Rhode Island, dasithperera@uri.edu

MECHANISMS OF INTERACTION BETWEEN *HAEMOPHILUS PARAINFLUENZAE* AND *STREPTOCOCCUS MITIS*

BY

DASITH PERERA

A DISSERTATION SUBMITTED IN PARTIAL FULFILLMENT OF

THE

REQUIREMENTS FOR THE DEGREE OF

DOCTOR OF PHILOSOPHY

IN

CELL & MOLECULAR BIOLOGY

UNIVERSITY OF RHODE ISLAND

2021

DOCTOR OF PHILOSOPHY DISSERTATION

OF

DASITH PERERA

APPROVED:

Thesis Committee:

Matthew Ramsey, Major professor

David Nelson

David Rowley

Brenton DeBoef
DEAN OF THE GRADUATE SCHOOL

UNIVERSITY OF RHODE ISLAND
2021

ABSTRACT

The human oral cavity is a complex polymicrobial environment, home to an array of microbes that play roles in health and disease. Oral bacteria have been shown to cause an array of systemic diseases and are particularly concerning to type II diabetics (T2D) with numerous predispositions that exacerbate bacterial infection. In this dissertation, we investigated the serum of healthy subjects and T2D subjects to determine whether we see greater translocation of oral bacteria into the bloodstream of T2D individuals. We didn't observe any significant enrichment of oral taxa, however we detected the presence of an emerging pathogen, *Acinetobacter baumannii* that is also associated with impaired inflammation in T2D.

While some are associated with disease, many oral taxa are important in the prevention of disease. In this dissertation we investigated the interactions between two abundant health-associated commensal microbes, *Haemophilus parainfluenzae* and *Streptococcus mitis*. We demonstrated that *H. parainfluenzae* typically exists adjacent to Mitis group streptococci *in vivo* in healthy subjects. We revealed that this co-occurrence is density dependent and further influenced by H_2O_2 production. Additionally, Mitis group streptococci are likely the *in vivo* source of NAD for *H. parainfluenzae* further facilitating this co-occurrence. We also investigated *H. parainfluenzae*'s response to H_2O_2, which is composed of a redundant OxyR-controlled system. Furthermore, we showed that H_2O_2 likely elicits the SOS response in *H. parainfluenzae* which may be a mechanism of generating genetic diversity within this species. These findings reveal mechanisms behind why these two highly abundant taxa coexist in healthy individuals.

ACKNOWLEDGMENTS

I would like to thank Matthew Ramsey for the years of mentoring, advice, stimulating discussions, help and support. I would also like to thank my parents, brother and sister for the many decades of support and more things that could be written. I thank my wife, Phone who I know has made many sacrifices over the past few years and without whom I probably would not have finished this. I thank my in-laws for their help over the last few years and being there for Phone and me. I thank lab members Eric, Thais and Alex for being great lab members and the very interesting Friday talks. I thank Zach for the coffee runs to Dunkin and stimulating science discussions. I would also like to thank other grads students at URI that have helped maintain a great work environment, especially Eric, Thais, Alex, Zach, Kathleen, Tomali, Chris and Katie.

PREFACE

This dissertation has been written in manuscript format

TABLE OF CONTENTS

LIST OF TABLES

TABLE PAGE

LIST OF FIGURES

CHAPTER 1: Introduction

The human oral cavity is a complex environment, home to over 600 species of bacteria (1), most of whom are considered indigenous to this site (2). It is now well established that the oral microbiota plays a vital role in the development of many diseases. While intuitively, the oral microbiota plays a role in the development of oral diseases, oral microbes have also been associated with a range of systemic disorders beyond the oral cavity.

One of the best-established associations is that of cardiovascular disease. Oral bacteria belonging to the HACEK (*Haemophilus* species*, Aggregatibacter* species*, Cardiobacterium hominis*, *Eikenella corrodens* and *Kingella* species) are known causes of infective endocarditis (IE) (3). Oral microbes, including *Aggregatibacter actinomycetemcomitans* and *Porphyromonas gingivalis* have also been detected in atherosclerotic plaques (4). Additionally, the development of oral diseases including periodontitis has been shown to be an important risk factor for cardiovascular disease (5). The most common form of periodontal disease is gingivitis (6). Gingivitis is a reversible inflammatory disease caused by bacterial plaque that forms at the gingival margin (7). If left untreated, gingivitis may develop into periodontitis, which is a chronic, irreversible inflammatory disease that may result in destruction of connective tissue, vascular proliferation and bone destruction (8).

An important patient population that is affected by periodontal disease are type II diabetics (T2D). The association between T2D and periodontitis can be considered to occur both ways as periodontitis is regarded as a potential complication of poorly controlled diabetes and that periodontal pathogens can play a role in T2D (9). In fact diabetics have 3 times the risk of developing periodontitis compared to non-diabetics (10). Studies have shown differences in the composition of oral bacteria in T2D subjects compared to non-diabetics, including elevated numbers of some periodontal pathogens (11,12). The abundance of some periodontal pathogens has also been shown to worsen glycemic control. Notably, the lipopolysaccharide (LPS) of the periodontal pathogen *Porphyromonas gingivalis* can stimulate inflammatory cytokines that impair insulin activity (13).

Given the propensity of some oral bacteria to cause systemic disease, it is important to determine factors that can contribute to bacterial translocation into the bloodstream. This is particularly important among diabetics as they have multiple predispositions that can exacerbate bacterial infection. The presence of bacteria in the bloodstream outside of sepsis has been a contentious topic (14). While the advent of Next generation sequencing (NGS) has improved our ability to detect bacteria that are both unculturable and found in low abundance, the lack of appropriate controls in early studies investigating the “human blood microbiome” has hindered our understanding of this environment (14). It is now established that at least transient bacterial translocation occurs even after brushing teeth or mastication of food (15,16). Given that T2D subjects exhibit symptoms including poor circulation, decreased wound heal-

ing and diminished bacterial uptake by phagocytosis (17–19), it is important to determine whether there is a greater translocation of oral bacteria into the blood of T2D. Similarly, given that diabetics are disproportionately affected by periodontitis, it is important to determine the effects of these conditions on bloodstream colonization.

While the abundance of certain oral bacteria has been associated with both oral and systemic disease, the abundance and selection of commensal bacteria has been associated with health and prevention of disease (20).The oral cavity is not a unitary environment in fact, the oral cavity contains several different subsites which are composed of distinct microbial communities (7). These include dental plaque, tongue dorsum, buccal mucosa and keratinized gingiva, which are home to very distinct communities. In fact, most bacterial species in the oral cavity are found in only a single site (21). An exception to this specificity is *Haemophilus parainfluenzae*, which is found in high abundance in all these sites as well as the nasopharynx (1). While *H. parainfluenzae* is responsible for the majority of cases of HACEK endocarditis (3), it is more commonly associated with a healthy oral microbiome (22). In fact, the abundance of *H. parainfluenzae* has been associated with beneficial immunomodulatory and antiproliferative effects against cancerous cells (23,24). It is therefore important to understand the interactions of *H. parainfluenzae* within the oral cavity as this may improve our understanding of what maintains its healthy status and potentially prevents its translocation into distal sites where it may cause disease.

Another abundant commensal found in all sites of the oral cavity and nasopharynx are Mitis group Streptococci. The Mitis group is comprised of at least 13 *Streptococcus sp.* including *S. mitis*, *S. oralis*, *S. peroris* and *S. sanguinis* (25). Many of the

species within this group are amongst the first colonizers of the human oral cavity and facilitate both microbial-microbial and host-microbial interactions by being anchors for biofilm formation and provide surface proteins to enable attachment and integration of other bacteria (26,27). A key example of this is *S. mitis*, which is regarded as a pioneering colonizer of both the oral cavity and nasopharynx (28). *S. mitis* has been shown to induce expression of human-β-defensin 2, which is a host antimicrobial peptide that can kill oral pathogens and also dampen the effects of inflammation following coculture with oral pathogens (29,30).

S. mitis can also influence overall oral biofilm ecology. It can release extracellular DNA, which is crucial for the development and stabilization of biofilms and it can also produce hydrogen peroxide (H_2O_2), which has been shown to be an effective antimicrobial that can shape microbial community composition (27). Given the abundant presence of Mitis group Streptococci in the same environments as *H. parainfluenzae* it is prudent to investigate interactions between these two commensal taxa, especially in the context of H_2O_2 response and tolerance. The goals of this dissertation are to improve our understanding of *H. parainfluenzae- Streptococcus sp.* interaction with a focus on understanding *H. parainfluenzae's* response to H_2O_2.

References

1. Dewhirst FE, Chen T, Izard J, Paster BJ, Tanner ACR, Yu W-H, et al. The human oral microbiome. J Bacteriol. 2010 Oct;192(19):5002–17.
2. Palmer RJ. Composition and development of oral bacterial communities. Periodontol 2000. 2014 Feb;64(1):20–39.
3. Chambers ST, Murdoch D, Morris A, Holland D, Pappas P, Almela M, et al. HACEK infective endocarditis: characteristics and outcomes from a large, multi-national cohort. PLoS One. 2013;8(5):e63181.
4. Figuero E, Sánchez-Beltrán M, Cuesta-Frechoso S, Tejerina JM, del Castro JA, Gutiérrez JM, et al. Detection of periodontal bacteria in atheromatous plaque by nested polymerase chain reaction. J Periodontol. 2011 Oct;82(10):1469–77.
5. Dhadse P, Gattani D, Mishra R. The link between periodontal disease and cardiovascular disease: How far we have come in last two decades ? J Indian Soc Periodontol. 2010 Jul;14(3):148–54.
6. Kumar S. Evidence-Based Update on Diagnosis and Management of Gingivitis and Periodontitis. Dent Clin North Am. 2019 Jan;63(1):69–81.
7. Zhang Y, Wang X, Li H, Ni C, Du Z, Yan F. Human oral microbiota and its modulation for oral health. Biomed Pharmacother. 2018 Mar;99:883–93.
8. Pihlstrom BL, Michalowicz BS, Johnson NW. Periodontal diseases. Lancet. 2005 Nov 19;366(9499):1809–20.
9. Preshaw PM, Alba AL, Herrera D, Jepsen S, Konstantinidis A, Makrilakis K, et al. Periodontitis and diabetes: a two-way relationship. Diabetologia. 2012 Jan;55(1):21–31.
10. Novaes AB, Gonzalez Gutierrez F, Grisi MF, Novaes AB. Periodontal disease progression in type II non-insulin-dependent diabetes mellitus patients (NIDDM). Part II--Microbiological analysis using the BANA test. Braz Dent J. 1997;8(1):27–33.
11. Hintao J, Teanpaisan R, Chongsuvivatwong V, Ratarasan C, Dahlen G. The microbiological profiles of saliva, supragingival and subgingival plaque and dental caries in adults with and without type 2 diabetes mellitus. Oral Microbiol Immunol. 2007 Jun;22(3):175–81.

12. Casarin RCV, Barbagallo A, Meulman T, Santos VR, Sallum EA, Nociti FH, et al. Subgingival biodiversity in subjects with uncontrolled type-2 diabetes and chronic periodontitis. J Periodontal Res. 2013 Feb;48(1):30–6.
13. Kuo L-C, Polson AM, Kang T. Associations between periodontal diseases and systemic diseases: a review of the inter-relationships and interactions with diabetes, respiratory diseases, cardiovascular diseases and osteoporosis. Public Health. 2008 Apr;122(4):417–33.
14. Castillo DJ, Rifkin RF, Cowan DA, Potgieter M. The Healthy Human Blood Microbiome: Fact or Fiction? Front Cell Infect Microbiol. 2019;9:148.
15. Forner L, Larsen T, Kilian M, Holmstrup P. Incidence of bacteremia after chewing, tooth brushing and scaling in individuals with periodontal inflammation. J Clin Periodontol. 2006 Jun;33(6):401–7.
16. Sconyers JR, Crawford JJ, Moriarty JD. Relationship of bacteremia to tooth-brushing in patients with periodontitis. J Am Dent Assoc. 1973 Sep;87(3):616–22.
17. Cade WT. Diabetes-related microvascular and macrovascular diseases in the physical therapy setting. Phys Ther. 2008 Nov;88(11):1322–35.
18. Falanga V. Wound healing and its impairment in the diabetic foot. Lancet. 2005 Nov 12;366(9498):1736–43.
19. Gyurko R, Siqueira CC, Caldon N, Gao L, Kantarci A, Van Dyke TE. Chronic hyperglycemia predisposes to exaggerated inflammatory response and leukocyte dysfunction in Akita mice. J Immunol. 2006 Nov 15;177(10):7250–6.
20. Marsh PD. Role of the Oral Microflora in Health. null. 2000 Jan 1;12(3):130–7.
21. Mark Welch JL, Dewhirst FE, Borisy GG. Biogeography of the Oral Microbiome: The Site-Specialist Hypothesis. Annu Rev Microbiol. 2019 08;73:335–58.
22. Caselli E, Fabbri C, D'Accolti M, Soffritti I, Bassi C, Mazzacane S, et al. Defining the oral microbiome by whole-genome sequencing and resistome analysis: the complexity of the healthy picture. BMC Microbiol. 2020 May 18;20(1):120.

23. Tseng Y-C, Yang H-Y, Lin W-T, Chang C-B, Chien H-C, Wang H-P, et al. Salivary dysbiosis in Sjögren's syndrome and a commensal-mediated immunomodulatory effect of salivary gland epithelial cells. NPJ Biofilms Microbiomes. 2021 Mar 11;7(1):21.

24. Baraniya D, Jain V, Lucarelli R, Tam V, Vanderveer L, Puri S, et al. Screening of Health-Associated Oral Bacteria for Anticancer Properties in vitro. Front Cell Infect Microbiol. 2020;10:575656.

25. Zheng W, Tan TK, Paterson IC, Mutha NVR, Siow CC, Tan SY, et al. StreptoBase: An Oral Streptococcus mitis Group Genomic Resource and Analysis Platform. PLoS One. 2016;11(5):e0151908.

26. Kolenbrander PE, London J. Adhere today, here tomorrow: oral bacterial adherence. J Bacteriol. 1993 Jun;175(11):3247–52.

27. Zhu L, Kreth J. The role of hydrogen peroxide in environmental adaptation of oral microbial communities. Oxid Med Cell Longev. 2012;2012:717843.

28. Mitchell J. Streptococcus mitis: walking the line between commensalism and pathogenesis. Mol Oral Microbiol. 2011 Apr;26(2):89–98.

29. Ouhara K, Komatsuzawa H, Yamada S, Shiba H, Fujiwara T, Ohara M, et al. Susceptibilities of periodontopathogenic and cariogenic bacteria to antibacterial peptides, {beta}-defensins and LL37, produced by human epithelial cells. J Antimicrob Chemother. 2005 Jun;55(6):888–96.

30. Zhang G, Chen R, Rudney JD. Streptococcus cristatus attenuates Fusobacterium nucleatum-induced interleukin-8 expression in oral epithelial cells. J Periodontal Res. 2008 Aug;43(4):408–16.

Manuscript

CHAPTER 2: Impaired host response and the presence of *Acinetobacter baumannii* in the serum microbiome of type-II diabetic patients.

Published in iScience December 2020

Dasith Perera[1], Sarah Kleinstein[2], Benjamin Hanson[1], Hatice Hasturk[3], Ryan Eveloff[2], Marcelo Freire[2], Matthew Ramsey[1]

1. The University of Rhode Island, Department of Cell and Molecular Biology, Kingston, RI 02881, USA.
2. J. Craig Venter Institute, La Jolla, CA 92037, USA.
3. The Forsyth Institute, Cambridge, MA 02142, USA.

Impaired host response and the presence of *Acinetobacter baumannii* in the serum microbiome of type-II diabetics

Authors (alphabetical): [1]Perera, D., [2]Kleinstein, S.E., [1]Hanson, B., [3]Hasturk, H., [2]Eveloff, Ryan, [2,4]*Freire, M., [1†]*Ramsey M.

Affiliations: [1]The University of Rhode Island, Kingston, RI 02881; [2]J. Craig Venter Institute, La Jolla, CA 92037. [3]The Forsyth Institute, Cambridge, MA 02142. [4]University of California San Diego, School of Medicine, La Jolla, CA 92093. * co-corresponding authors, † denotes lead contact.

Keywords: *Acinetobacter baumanii*, type-2 diabetes, serum microbiome, periodontitis, chronic inflammation

Funding Sources: This work was supported by U.S. Public Health Service Grants R00 DE0234804 (Freire), DE018917 (Hasturk) and R01 DE027958 (Ramsey) from the National Institutes of Health/National Institute of Dental and Craniofacial Research.), NIGMS/RI-INBRE early career development award (P20GM103430 - Ramsey), and the Rhode Island Foundation Medical Research Fund (20164348 - Ramsey).

Summary

Type-II diabetes (T2D) affects over 10% of the United States population and is a growing disease worldwide that manifests with numerous comorbidities and defects in inflammation. This dysbiotic host response allows for infection of the host by numerous microorganisms. In the course of T2D disease, individuals can develop chronic infections including foot ulcers and periodontitis, which lead to further complications and opportunistic infections in multiple body sites. In this study, we investigated the serum of healthy subjects and T2D patients with (T2DP) or without periodontitis for both microbiome signatures in addition to cytokine profiles. Surprisingly, we detected the presence of *Acinetobacter baumanii* in the serum of 23% of T2D/T2DP individuals tested. In T2DP, IL-1β, TNF-α, MCP-1, IL-6, IL-8, and IFN-γ were significantly elevated in ABC positive subjects. As an emerging pathogen, *A. baumanii* infection represents a risk for impaired inflammation and the development of comorbidities in T2D subjects.

Introduction

Type-II diabetes (T2D) is a chronic inflammatory disease affecting 10.5% of the United States population, with rising prevalence both in the United States and worldwide ("National Diabetes Statistics Report | Data & Statistics | Diabetes | CDC," 2020; Whiting et al., 2011). Individuals with T2D typically have numerous comorbidities, and are at greater risk of both opportunistic and nosocomial infections, which can result in significant morbidity, including amputations, and lost quality of life (QOL) measures (Erben et al., 2013; Ferlita et al., 2019; Kim et al., 2019; McDonald et al., 2014; Vardakas et

al., 2007). Thus, care must be taken to prevent and monitor the infection status of these individuals, as the development of diabetic mucosal and skin lesions across the body can impact the host immune and diabetic responses. Key infection prevention includes minimizing portals of entry and colonization by numerous pathogens. One example of such a portal of entry is the emergence of diabetic foot ulcers, which can develop diabetic foot infections (DFIs). Roughly 15% of adult T2D subjects develop foot ulcers and ~14% of these subjects undergo amputation, with the remainder needing extensive debridement, negative pressure treatments and other therapies including antibiotics that result in prolonged hospitalization time, lengthy healing duration and increased treatment costs (Driver et al., 2010; Reiber et al., 1998).

In addition to DFIs, T2D subjects are ~3 times more likely to develop periodontitis (Emrich et al., 1991; Wu et al., 2020). Periodontitis is an inflammatory oral disease accompanied by a polymicrobial biofilm infection that can lead to tissue damage, chronic lesions and tooth/bone loss in the oral cavity (Genco et al., 2020; Irfan et al., 2001; Mann et al., 2020). During periodontal infection, the healthy oral microbiome, especially in the subgingival space (along teeth below the gumline, including periodontal ligament, epithelium, alveolar bone, and connective tissues), transitions to one enriched with several opportunistic pathogens that exacerbate inflammation and host tissue damage both locally and systemically (Curtis et al., 2020; Griffen et al., 2012; Hajishengallis and Lamont, 2012; Nowicki et al., 2018; Roberts and Darveau, 2015; Socransky et al., 1998). While protective, acute inflammation is a helpful immune response, it is characterized by rapid activation of inflammation and subsequent return to

homeostasis (resolution). Unresolved inflammation that fails to control the trigger leads to chronic lesions and is a hallmark of both periodontitis and T2D.

More acute bacteremia can manifest in diseases such as endocarditis or other distal infections by oral microbes (Carrizales-Sepúlveda et al., 2018; Lockhart and Durack, 1999; Parahitiyawa et al., 2009). Various systemic diseases are in fact influenced by microbial metabolism and host interactions. “How” and “why” immune system imbalance fails to control microbial pathogenic transition remains an active area of investigation. Increasing evidence implicates periodontal diseases, especially periodontitis in adults, as a potential risk factor for increased morbidity and mortality from systemic conditions including diabetes, cardiovascular diseases, adverse pregnancy outcomes, and others (Genco et al., 2020; S.E. Kleinstein et al., 2020). This is due to two plausible mechanisms: a direct pathway leading to migration of the bacteria to distal organs and an indirect pathway leading to production of microbial metabolites and/or activating inflammatory mediators that activate the immune system locally and systemically. This is likely made possible as periodontitis presents as a chronic inflammatory condition of the tooth-supporting structures occurring with oral microbiome dysbiosis and continuous inflammatory burden. Notably, oral microbes have also been detected (Dowd et al., 2008; Gardner et al., 2013) and isolated from DFIs (Bowler and Davies, 1999; Citron et al., 2007). Thus, we hypothesized that T2D patients might be at a greater risk of extraoral infection and may exhibit changes in microbiota that transiently occupy their bloodstream. We further hypothesized that these changes would be even more apparent in T2D patients with periodontitis (T2DP) and that these patients may carry potential

DFI-colonizing oral species in their bloodstream. Our initial investigations toward these hypotheses utilized samples derived from previous work on resolution of inflammation in T2D (Freire et al., 2017) and are reported here, with unexpected results.

To investigate the possibility of oral species presence in the bloodstream, we compared the serum V1-V3 16S microbiomes of T2D and T2DP subjects versus a healthy cohort. While our initial microbiome observations did reveal the presence of multiple oral taxa in human serum, it did not demonstrate that these were especially enriched in T2D or even T2DP subjects compared to non-diabetic subjects. Unexpectedly, we detected *Acinetobacter baumanii* in 23% of the T2DP subjects in our study with none detected in the healthy cohort. *A. baumanii* is an emerging infectious pathogen (Villar et al., 2014) notorious for its evolving antibiotic resistances (Gootz and Marra, 2008; Vázquez-López et al., 2020), nosocomial (Ayoub Moubareck and Hammoudi Halat, 2020; Dijkshoorn et al., 2007) and bloodstream infections (Peleg et al., 2008). *A. baumanii* is part of a cluster of *Acinetobacter* species with similar clinical manifestations known as the AB or ABC complex (Gerner-Smidt and Tjernberg, 1993) which are highly similar via ribotyping.

A. baumanii or ABC complex organisms present several particular risks to T2D subjects, specifically higher mortality rates for those with bacteremia (Leão et al., 2016) and for those with higher blood glucose concentrations (Leung and Liu, 2019). *A. baumanii* has recently emerged as medically important because of the increasing number of local and systemic infections produced by this organism. An inoculum of this pathogen

in a mouse pneumonia model led to increased proinflammatory cytokines, reduced neutrophil infiltration into the lung, and increased extrapulmonary dissemination (Qiu et al., 2009). In T2D, neutrophils present failure in early chemotaxis, but a hyper-inflammatory feedback loop emerges to compensate initial myeloid cell failure (Sarah E Kleinstein et al., 2020). Patients infected with *A. baumanii* after burns were 9.8 times more likely to develop glucose intolerance and ~3x more T2D burn patients developed *A. baumanii* infections (27%) than patients without T2D (8.5%) (Furniss et al., 2005). Additionally, *A. baumanii* has also been observed in DFIs, particularly alongside other multidrug resistant pathogens, presenting a grave concern for T2D individuals (Castellanos et al., 2019; Henig et al., 2020). In addition to DFIs, ABC complex organisms can also spread through the body and form infections in numerous organs (Al-Anazi and Al-Jasser, 2014; Peleg et al., 2008).

In this work, we first investigated whether or not we could detect signatures of oral bacteria in a *post hoc* microbiome analysis of serum samples collected in a previous study (Freire et al., 2017). Our findings indicated minor, yet significant, microbiome compositional changes between healthy cohort, type-II diabetics (T2D) and T2D subjects with periodontitis (T2DP). We discovered that nearly 1/4 of T2DP subjects in our study contained sequence reads identical to that of *A. baumanii,* which was not detected in any healthy, no-template, or mock control samples. The specific presence of *A. baumanii* was confirmed by further clone library and 16S rDNA Sanger sequencing. In addition, we assayed the host response by cytokine profiles of sera. Our findings revealed distinct differences between the healthy, T2D and T2DP groups, demonstrating

that diabetes presents the major proinflammatory forces via cytokine analysis, and periodontal diseases synergistically increased that profile when compared to healthy controls. When stratifying *A. baumanii* positive T2D versus *A. baumanii* negative T2D samples we observed unique cytokine profiles, suggesting a specific microbial impact on systemic inflammation. While our methodology cannot indicate if *A. baumanii* was transiently present or a subclinical colonizer of our T2DP cohort, we propose that these data reveal a much greater risk of currently 'uninfected' T2D individuals for *A. baumanii* exposure and infection than previously understood and should justify more intensive and thorough investigation into AB complex colonization of type-II diabetics.

Results

Patient demographics

Serum samples were generated from the population described in Table 1. A total of 81 subjects were investigated in this study, 57 with type-II diabetes (T2D), of which 29 had periodontitis (T2DP) as defined by the American Association of Diabetes (ADA) (American Diabetes Association, 2015) and American Association of Periodontology (AAP) (Armitage, 1999) criteria respectively. All T2D donors were poorly-controlled diabetic subjects that had not taken antimicrobials, non-steroidal anti-inflammatory drugs or insulin sensitizers within 3 months. Diagnostic serum glucose measures were taken for all subjects and HbA1C was measured for diabetics to stage disease status. As expected, poorly-controlled diabetics (HbA1c% >6.5%) showed significantly elevated

glucose levels ($p < 0.0001$; Table 1). There were no significant differences in gender or ethnicity between healthy volunteers and diabetic patients. Diabetic patients showed elevated BMI and tended to be older than healthy controls ($p< 0.05$), consistent with known disease biology. Periodontal condition was further stratified among the subjects according to severity of irreversible tissue loss (mild, moderate, severe) and reversible lesions called gingivitis according to American Association of Periodontology (AAP) (Armitage, 1999) criteria. Periodontal condition was significantly worse in diabetic compared to healthy subjects ($p< 0.0001$). All healthy subjects had healthy periodontal condition compared to only 11% of diabetic patients, with 15% of diabetic subjects suffering from severe periodontitis. Current and former smokers were near uniformly part of the T2D and T2DP groups with only 1 current smoker in the healthy group. The entire study population had a median age range of 53 +/- 11 years and all subjects were outpatient and thus not part of an extended hospital stay cohort.

Table 1. Clinical demographics of study subjects.

	Healthy (N=24)	Type 2 Diabetic (N=57)	Total Cohort (N=81)	p-value
Age (mean in years ± SD)	46 ± 10.74	56 ± 10.38	52.78 ± 11.40	0.0003
Gender (no., Male %)	14 (58%)	28 (49%)	42 (51.85%)	

	Female	10 (42%)	29 (51%)	39 (48.15)	0.62
Ethnicity	Caucasian	15 (63%)	26 (46%)	40 (49.38%)	
	Hispanic	2 (8%)	7 (12%)	9 (11.11%)	
	African-American	6 (25%)	23 (40%)	29 (35.80%)	
	Asian	0	2 (4%)	2 (2.47%)	
	Other	1 (4%)	0	1 (1.23%)	0.23
Smoking Status (no., %)	Smokers	1 (4%)	5 (9%)	6 (7.41%)	
	Former Smokers	0	21 (38%)	21 (25.93%)	
	Never Smokers	23 (92%)	31 (53%)	54 (66.67%)	0.002
BMI (kg/m^2; mean ± SD)		29.58 ± 2.82	32.89 ± 6.07	31.87 ± 5.48	0.001
Blood Cholesterol (mg/dl; mean ± SD)		148.50 ± 35.91	213.04 ± 78.81	194.00 ± 74.84	<0.0001
Blood Glucose (mg/dl; mean ± SD)	Normal (<100mg/dl)	83.00 ± 11.14	97.00 ± 1.41	85.33 ± 11.46	

	Pre-diabetes (100-125mg/dl)	104.80 ± 3.33	115.60 ± 7.44	108.90 ± 7.42	
	Diabetes (>126mg/dl)	165.20 ± 39.70	202.00 ± 56.45	198.60 ± 55.86	<0.0001
HbA1c % (mean ± SD)	Normal (<5.7% HbA1c)	-	5.20 ± 0.26	-	
	Pre-diabetes (5.7-6.4% HbA1C)	-	6.13 ± 0.21	-	
	Diabetes (>6.4% HbA1c)	-	8.07 ± 1.51	-	-
Periodontal Condition (no., %)	Healthy	25 (100%)	6 (10.71%)	31 (38.27%)	
	Mild	0	15 (26.79%)	15 (18.52%)	
	Moderate	0	11 (19.64%)	11 (13.58%)	
	Severe	0	12 (21.43%)	12 (14.81%)	
	Gingivitis	0	10 (17.86%)	10 (12.35%)	

	Stable Perio-dontitis	0	2 (3.57%)	2 (2.47%)	<0.0001
ABC Positive (no., %)	Positive	0 (0%)	13 (23%)	13 (16.05%)	
	Negative	19 (76%)	29 (51%)	48 (59.26%)	
	Not Tested	5 (24%)	15 (26%)	20 (24.69%)	0.07
Neutrophil Count (mil. of cells, mean ± SD)		76.48 ± 57.77	165.46 ± 97.12	131.90 ± 94.51	<0.0001
Monocyte Count (mil. of cells, mean ± SD)		66.15 ± 50.13	117.10 ± 62.99	99.22 ± 63.28	0.002

Table 1. Study subject demographics. *p-values* calculated by unpaired t-tests or $\chi 2$ (two-sided p-values; italicized $p<0.05$ significant). SD, standard deviation; BMI, body-mass index; ABC, *A. baumanii;* %, percentage; mg/dl, milligrams per deciliter; kg/m^2, kilograms per square meter.

Microbiome analysis controls for low template sequencing

Data generated here was part of a *post hoc* study of serum samples collected for a previous study (Freire et al., 2017) and thus not available in the larger volumes ideal for 16S microbiome dataset generation. Low template concentrations can produce microbiome signatures not derived from that in the biological samples due to amplification of contaminating gDNA in sterile buffers and reagents (Kennedy et al., 2014; Kim et al., 2017; Salter et al., 2014), which often manifests as aquatic species signatures, many of which are not compatible with growth in the human host (i.e. many do not even grow at 37°C) (Kim et al., 2017). A description of no-template / reagent only control samples is provided in the methods. Data within this study is provided as either minimally filtered (mitochondrial, human and chloroplast aligned reads removed) or strict filtered (reads removed based on homology with reagent-only controls) and indicated as such throughout the study. All sequence data is made available at NIH SRA Bioproject PRJNA664044, and all scripts used for data generation, filtering, and analyses are provided in the Supplemental Information.

We were able to generate abundant data from these samples with careful consideration paid to controls for amplification bias and background bacterial gDNA contamination of commercial sterile reagents. First, we utilized amplification of a mock standard library of 8 bacterial and 2 fungal species (Fig. S1A-B) at 10 and 1 ng of total template, which indicated that our library preparation protocol was suitable for species-level analysis where possible by V1-V3 sequence. Second, we utilized 13 separate no-template /

reagent only controls, which were subjected to our sequence analysis pipeline, revealing frequently encountered contaminating taxa. These taxa were filtered from each human-derived sample in the strict-filtered datasets only.

V1-V3 16S microbiome diversity analyses reveal minor but significant differences between diabetic and nondiabetic groups

Serum and control samples were subject to bead beater lysis and genomic DNA purification. Purified gDNA was amplified using the V1-V3 targeted 27F-519R primer pair (Stackebrandt and Goodfellow, 1991; Turner et al., 1999). Quality trimmed reads were subjected to DADA2 analysis (Callahan et al., 2016) and aligned to the SILVA database (Quast et al., 2013) to determine species-level identity where possible. Rarefaction curve analysis was performed to ensure adequate sequencing depth (Fig. S2) and resequencing of each Illumina index was performed to generate greater sequencing depth without further template amplification. Run to run variability between next-generation sequencing was found to be insignificant (Fig. S3). Data analysis and comparisons were performed via QIIME2 (Bolyen et al., 2019) as detailed in the methods.

We first quantified alpha and beta diversity between the healthy, T2D and T2DP subject groups for our strict filtered (Fig. 1) and minimally filtered data (Fig. S4). For both datasets, species richness for T2D and T2DP groups were significantly different than the healthy cohort which was also significantly different when compared to T2DP in each dataset for species evenness (T2D more rich, T2DP less rich and less even). Beta

diversity was significantly less for healthy subjects versus T2D and greater when compared to T2DP for either minimal or strict filtered datasets. Thus, we observed minor but significant shifts in microbiome composition between subject groups.

To begin investigating which taxa contributed to this composition difference we first looked at a phylum level display of our taxonomically assigned data (Fig. 2). Figure 2A and 2B respectively indicate phylum level data for strict versus minimal filtered datasets. Similar trends in phyla distribution were evident for either dataset and reveal minor phylum level changes between subject groups.

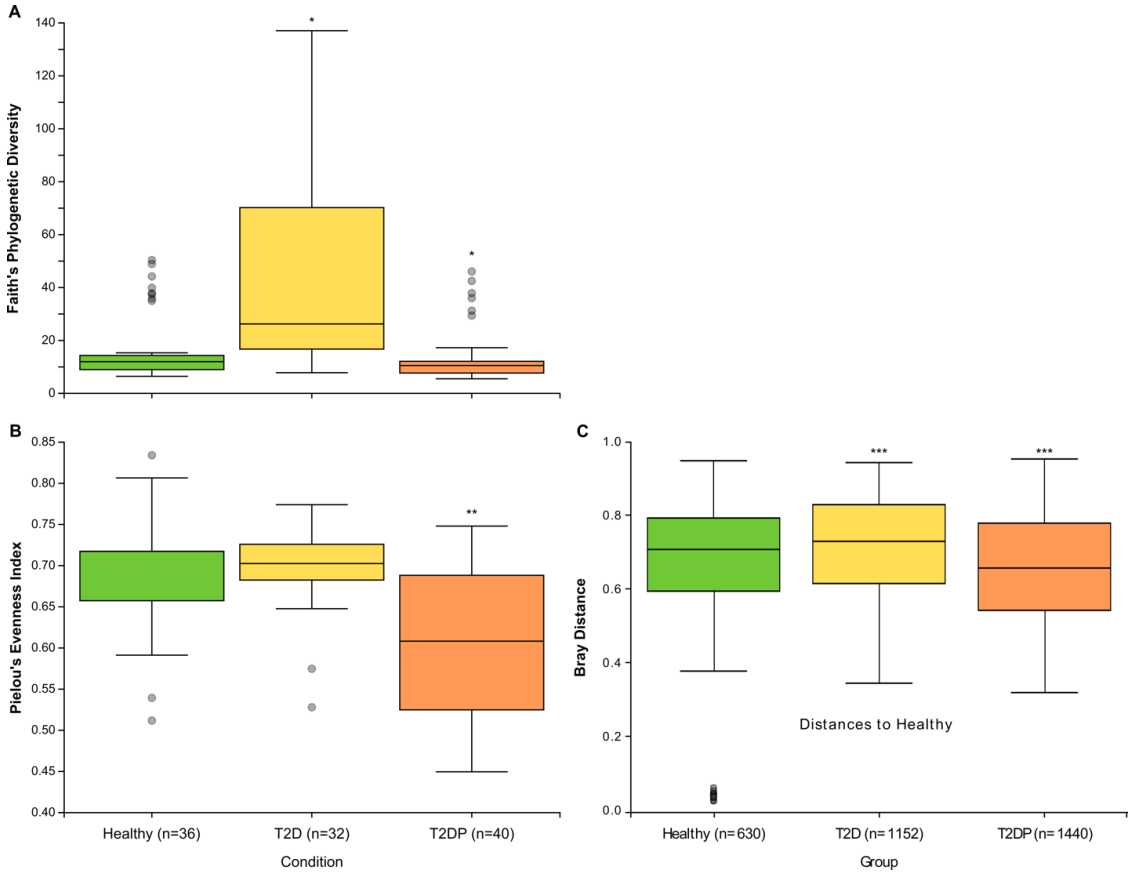

Figure 1.1. 16S Alpha and Beta diversity of serum microbiomes changes with subject status. Species richness is displayed based on Faith's phylogenetic diversity (Faith, 1992) (A) and species evenness based on Pielou's evenness index (Pielou, 1966) (B) for healthy, type-II diabetic (T2D) and type-II diabetics with periodontitis (T2DP) samples. Significance was determined by Kruskal-Wallis analysis of variance (Kruskal and Wallis, 1952) for each comparison indicated and Benjamini-Hochberg correction (Benjamini and Hochberg, 1995) was applied to generate adjusted q-values. All data used was strictly filtered based on no-template control indexes. * indicates q-value < 0.002 compared to Healthy, ** indicates q-value < 0.0004 compared to Healthy and to T2D, (C) Beta-diversity Bray Curtis distances. Pairwise PERMANOVA of each category vs each (group size of 3, n=112) was performed in 999 permutations. *** indicates q-value differs from 'healthy' < 0.001.

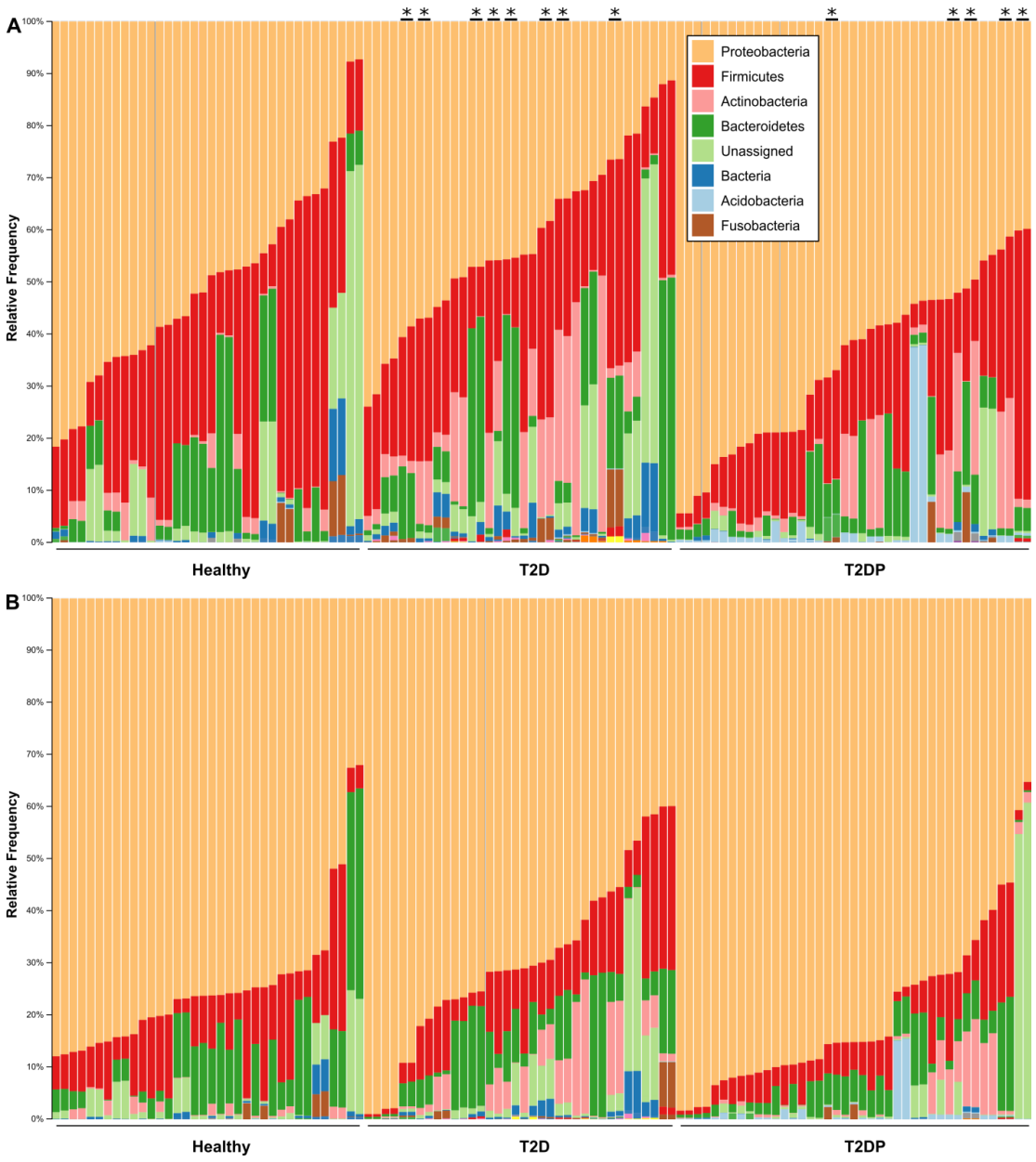

Figure 1.2. Phylum level diversity changes between subject status. DADA2 analyzed data was aligned to the SILVA database for taxonomical assignment via QIIME2 as described in methods. Data from both sequencing runs were collapsed to

phylum level taxa and displayed for (A) strict filtered and (B) minimally filtered conditions. Asterisks on the top indicate run-run sample pairs that were positive for *A. baumanii*.

MED and DADA2 analysis reveal the presence of Acinetobacter baumanii

Given our initial investigation into whether or not there were differences between T2D and T2DP microbiota and a preliminary hypothesis that oral taxa would be enriched in T2DP serum, we first used a minimal entropy decomposition (MED) analysis identical to one used previously to characterize oral microbiomes (Eren et al., 2014). Oligotyped "nodes" or representative sequences were aligned to both the Human Oral Microbiome (HOMD) (Escapa et al., 2018) and Ribosomal Database Project (RDP) (Cole et al., 2014) databases and species were assigned based on 98% or higher sequence identity when comparing nodes to reference databases. We next compared species assigned data between subject groups by linear discriminate analysis effect size measurements (LEfSe) (Segata et al., 2011). Using MED analyzed data for healthy vs all T2D subjects (Fig. 3) we detected significant enrichments of some oral species (*S. cristatus, N. flavescens*) but also some known reagent contaminants (*R. picketti, A. broomeae*). Surprisingly, we observed *Acinetobacter baumanii* significantly enriched in the T2D population as a whole. For MED analysis, reads assigned as *A. baumanii* were present from 0.01 to 7.3 % of total reads in 8 T2D and 5 T2DP subjects. No reads assigned to *A. baumanii* were detected in any healthy subjects. DADA2 amplicon sequence variants (ASV) are similar to MED nodes and we observed that one ASV node was a perfect

match to the singular MED node assigned to *A. baumanii* based on 100% RDP alignment across its full sequence.

In our DADA2 / QIIME2 based analysis we performed taxonomical assignment for each DADA2 amplicon sequence variant (ASV) node aligned to either the Greenegenes (DeSantis et al., 2006) (not shown) or SILVA database version 132 (Quast et al., 2013). Phylum level taxonomic assignments of DADA2 data aligned to SILVA were used in Figure 2. ASVs are similar to MED nodes and we observed that one ASV node was a perfect match to the singular MED node assigned to *A. baumanii* based on 100% RDP alignment across its full sequence. This ASV was assigned only to the *Acinetobacter* genus despite a 100% full length match to *A. baumanii* sequence at the RDP database and the NCBI non-redundant database (not shown). Based on this, we manually assigned this ASV to *A. baumanii* and found that reads now assigned to *A. baumanii* were present from 0.01 to 9.1 % of total reads in 8 T2D and 5 T2DP subjects with no reads assigned to *A. baumanii* detected in any healthy subjects. This demonstrated agreement between both MED and DADA2-based 16S data analysis. LEfSe analysis was again performed on healthy vs all T2D, as well as between all three subject groups and demonstrated again that *A. baumanii* was significantly elevated amongst all T2D samples (Fig. S5).

We next looked at differences in microbiome compositions across subjects by plotting Bray-Curtis distances via non-metric multidimensional scaling (NMDS) while distinguishing subject groups as well as presence or absence of *A. baumanii* complex (ABC)

bacteria (Fig. 4). Broadly, T2D and T2DP samples had less overlap in composition while healthy samples intersected either group. ABC status did not seem to form a distinct microbiome cluster, suggesting that there was no unique microbiota composition for ABC positive subjects apart from *A. baumanii* sequence detection.

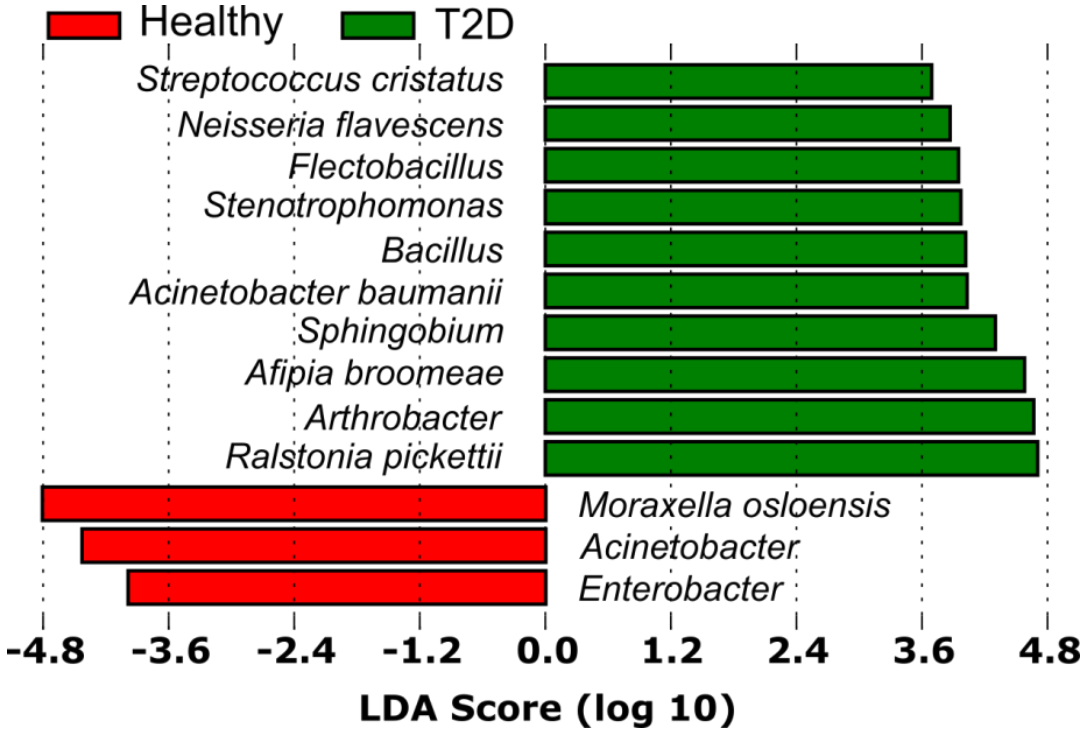

Figure 1.3. Healthy vs all T2D subjects reveal a potential enrichment of *A. baumanii*. Initial Minimal Entropy Decomposition (MED) analysis of 16S data with taxonomy assigned based on RDP database alignment to generate species level assignments was performed followed by linear discriminate analysis effect size quantification (LEfSe). This revealed enrichment of several species / genera in T2D subjects relative to healthy. DADA2 analysis of the same dataset was aligned to the SILVA database and shows similar patterns of enrichment (Fig. S5).

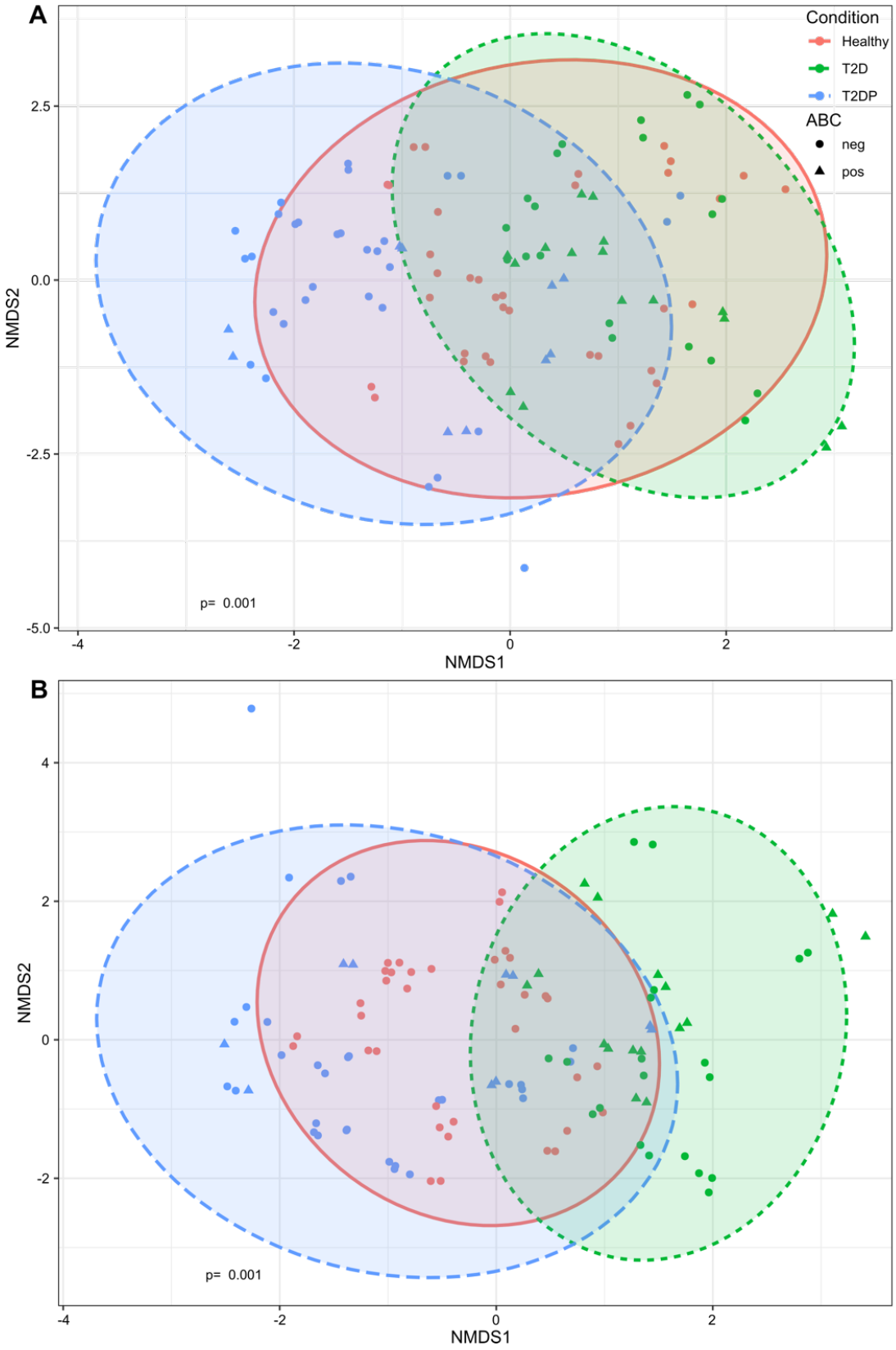
A
Condition
Healthy
T2D
T2DP
ABC
neg
pos
NMDS2
NMDS1
p= 0.001
B
NMDS2
NMDS1
p= 0.001

Figure 1.4. Beta diversity quantification between subject groups. SILVA assigned taxonomy of DADA2 analyzed 16S data was used to determine Bray-Curtis dissimilarity between samples for strictly filtered (A) and minimally filtered (B) data. Non-metric multidimensional scaling and statistical analysis for each subject group was performed in R using the *vegan* package as described in methods.

Validating the presence of A. baumanii in T2D subjects

The finding of ABC sequences was unexpected, as study participants were not hospitalized or under treatment for any infection(s), and we wished to confirm this result by other techniques. This was especially needed as the V1-V3 portion of the 16S rDNA sequence only differs between *A. baumanii* and *A. nosocomialis* by 1 nucleotide substitution. Using PCR primers for the 16S rDNA region that encompasses nearly all differentiating 16S nucleotides between *Acinetobacter* species we generated amplicons from a portion of our ABC positive samples alongside negative healthy and no-template control samples (Fig. 5). PCR products were ligated into a TA vector and individual colonies were propagated and subjected to Sanger sequencing of plasmid inserts. The 1242bp sequences were then aligned to the NCBI reference RNA sequence database (refseq_rna). Each sequence (12 clones across 5 samples) was identical and matched the *A. baumanii* 16S sequence across its length. This result validated our initial 16S detection of putative *A. baumanii*.

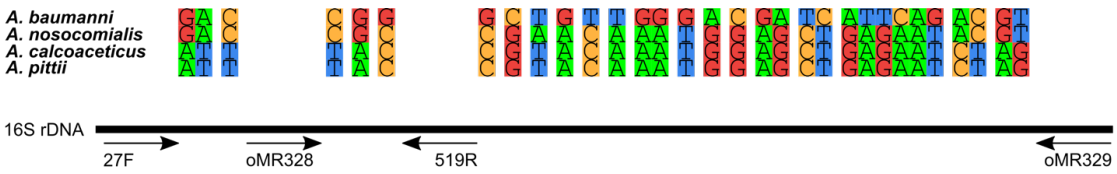

Group	% *A. baumanii* (V1-V3)	Clones Sequenced	Clones Positive	Clone Species
T2D	7.3	5	2	*A. baumanii*
T2D	1.2	2	2	*A. baumanii*
T2D	1.2	10	0	
T2DP	0.8	10	0	
T2DP	0.7	10	2	*A. baumanii*
T2D	0.4	4	2	*A. baumanii*
T2D	0.3	9	4	*A. baumanii*
T2D	0.3	10	0	
Healthy	0	10	0	
Healthy	0	10	0	
Control	0	10	0	
Control	0	10	0	

Figure 1.5. Clone library design to verify ABC complex member identity. Amplification with oMR328-329 primers produced an amplicon between 120-1306bp of the *A. baumanii* 16S rDNA sequence. This allowed for Sanger sequencing of information rich nucleotides indicated above allowing for species differentiation beyond initial V1-V3 sequencing with the 27F-519R primers. The table beneath indicated the total number of individual clones sequenced per sample and which species they aligned to with 100% identity in the NCBI non-redundant database.

Host cytokine responses to T2D and T2DP vs Health

In addition to serum microbiota, we also quantified twenty different human cytokines in serum samples across all 3 patient groups (Fig. 6). Based on relative abundance pro-

files, we observed that proinflammatory cytokines were significantly elevated in *A. baumannii* positive samples highlighted in the box (ABC+). MCP-1 and IL-1β, classic pro-inflammatory cytokines, were increased in diabetic patients. Intriguingly, T2D ABC-negative subjects did not show increase of these markers. ABC+ subjects showed significantly higher cytokine expression levels of IL-1β, IL-6, IL-8, MCP-1, and IFN- γ when compared to ABC-negative groups (I and V, $p<0.01$).

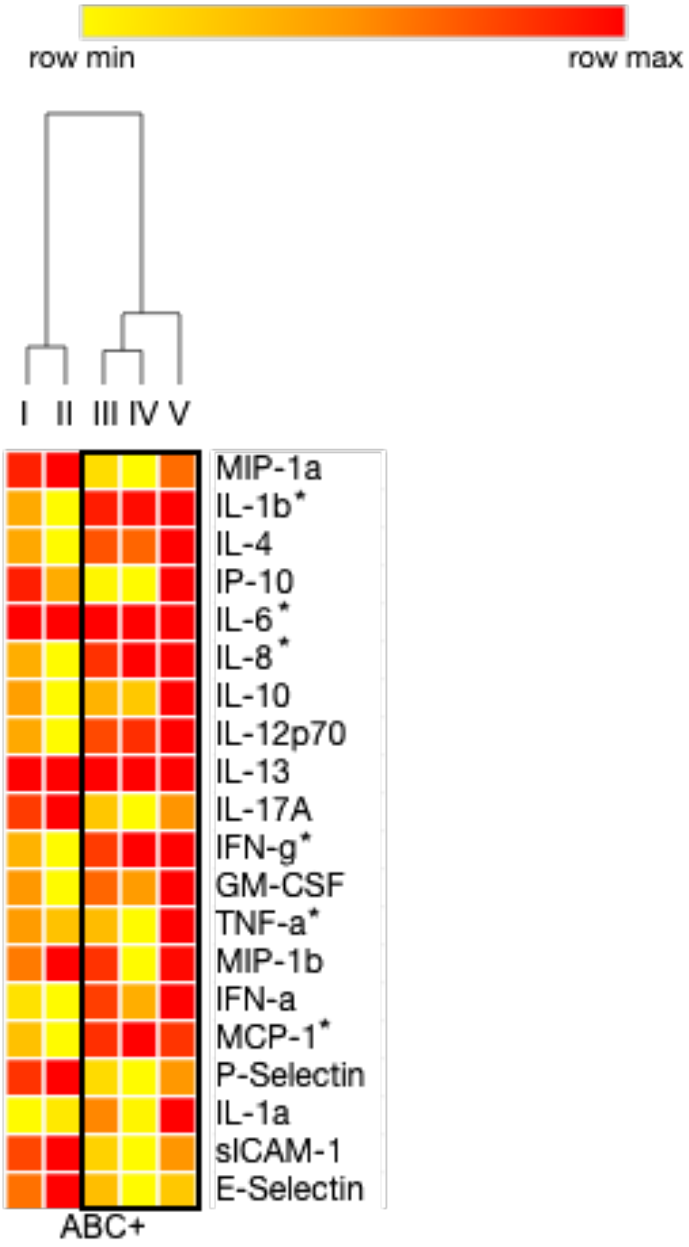

Figure 1.6. Cytokine profile quantification reveals distinct differences between subject groupings and *A. baumanii* presence. Heat map showing immune mediator concentrations derived from serum of diabetic and healthy samples (red, highest expression; yellow, lowest expression). Hierarchical clustering was employed by Morpheus from the Broad Institute (Morpheus, https://software.broadinstitute.org/mor-

pheus). Observations from hierarchical clustering are shown in a tree, with *A. baumannii* positive (ABC+) groups highlighted in the box. ABC+ groups (II, III and IV) showed significantly different ($p < 0.01$) levels of IL-1β, IL-6, IL-8, MCP-1, IFN- γ compared to ABC-negative (ABC-) groups (I and V). I) Diabetic/Healthy, II) ABC+/ABC, III) ABC+ Diabetic/ABC- Diabetic, IV) ABC+ Diabetic/Healthy, V) ABC- Diabetic/Healthy. Data are clustered according to comparison groups. * = p-value <0.01 between groups via unpaired Student's t-test.

Host cytokine responses to specific microbiota

Based on the cytokine abundance data and earlier microbiome sequencing, we were able to determine if any specific taxa were significantly correlated with cytokine presence or absence in T2D subjects (Fig. 7). *A. baumanii* was significantly correlated with elevated amounts of IFN-α, IFN-γ, IL-12p70, IL-8, and TNF-α. ABC+ subjects presented cytokine correlations consistent with a profile of chronic inflammation. IL-8 is a chemokine that impacts neutrophil phenotype and function, and excessive amounts of this cytokine lead to chronic activation of phagocytes (Moore and Kunkel, 2019). Excessive production of TNF-α increases failure of resolution of inflammation on innate immune cells by controlling a resolution receptor (Freire and Van Dyke, 2013). Here, TNF-α showed a significant increase in ABC+ subjects, suggesting co-existence with ABC in the serum of type-II diabetics. We also performed an identical analysis for healthy subjects and saw several genera or species with significant correlations (Fig. S6). In healthy subjects,

unique profiles were found, correlated with lower levels of proinflammatory cytokines and co-clustered with ABC-negative samples.

While low template concentration microbiome profiling presents many challenges, we were able to utilize numerous control steps to minimize the impact of contaminating taxa. We were also able to demonstrate that not only were there significant differences between subject groups that include taxa of likely biological origins; we also demonstrated that specific cytokines significantly correlated with the presence of distinct taxa. Most surprisingly, we were able to detect *A. baumanii* and confirm its presence in serum samples of type-II diabetics not known or currently diagnosed with any underlying infection. These data do not *per se* indicate active infection but could also indicate colonization or transient exposure to *A. baumanii* for these subjects compared to healthy subjects.

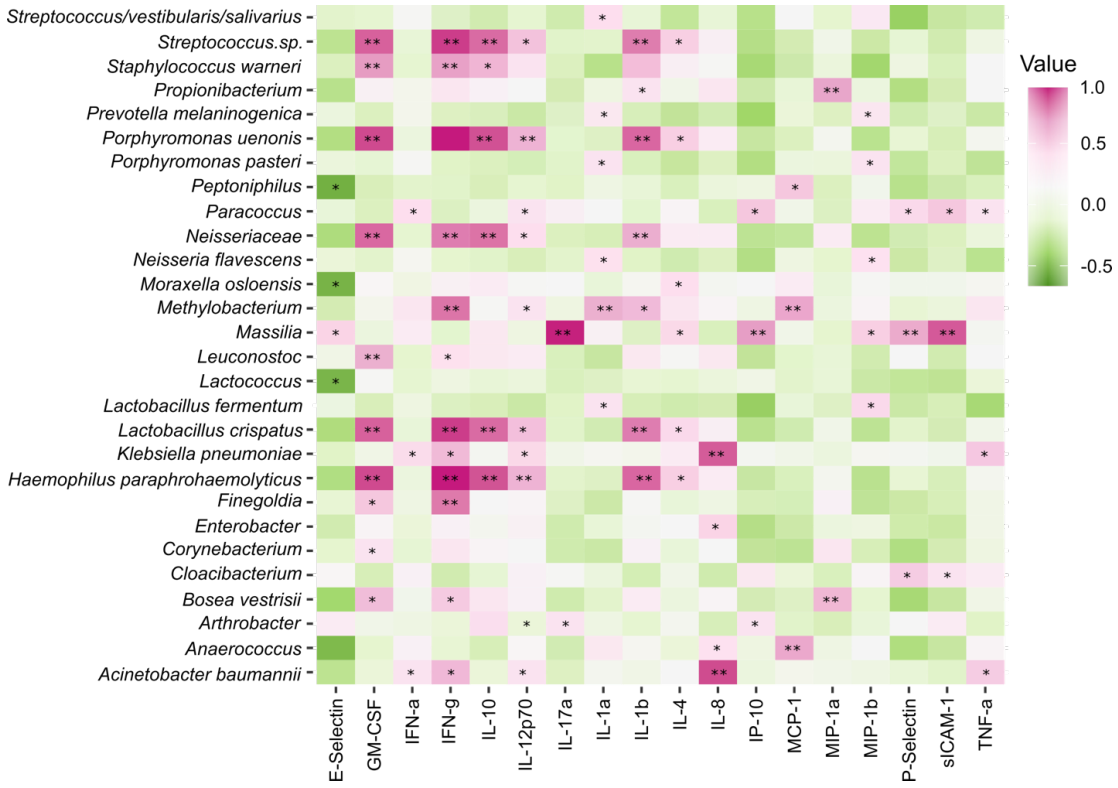

Figure 1.7. Host-microbial correlation resolved type-II diabetic associations with inflammatory cytokines. HOMD/RDP assigned taxonomy of MED analyzed 16S data for both T2D and T2DP samples and cytokine concentrations were analyzed via Pearson correlation coefficient in R using the *rcorr* function. Significance was determined using the asymptotic p-values generated by *rcorr* with * = p-value <0.05 ** = p-value <0.01. Data are strictly filtered with taxa present in no-template controls subtracted.

Discussion

Issues with amplification-based 16S studies from low template concentrations are well known (Kim et al., 2017; Pollock et al., 2018; Sinha et al., 2015). We began this study as a *post hoc* analysis of existing serum samples from a previous bank of anonymized specimens (Freire et al., 2017). As sample volumes of serum were mostly limited, we relied on amplification of 16S rDNA, using V1-V3 region primers to improve the likelihood of identifying oral taxa (Eren et al., 2014) that we hypothesized to exist in the diabetic with periodontitis part of our cohort. To minimize effects of amplification, we performed multiple high-throughput sequencing runs of amplified libraries to increase sequence depth as opposed to further amplification and using a higher capacity sequencing platform. Additionally, we also included numerous no-template controls throughout sample preparation and purification to identify as many outside contaminants as we could (Kennedy et al., 2014; Kim et al., 2017; Salter et al., 2014). As a further control, we carried out amplification of mock community libraries (Fig. S1) to determine if amplification bias or infidelity affected taxonomic assignment. We also used two separate methods for correction of Illumina-sequenced amplicon errors, DADA2 (Callahan et al., 2016) and minimal entropy decomposition / oligotyping (MED) (Eren et al., 2015), as well as comparing our data from multiple ribosomal databases for taxonomic assignment (Cole et al., 2014; DeSantis et al., 2006; Quast et al., 2013). In addition to Illumina sequencing, we performed a separate amplification of 16S rDNA followed by Sanger sequencing to independently confirm the identity of putative *A. baumanii* sequence presence in a subset of our diabetic samples (Fig. 5). Thus, we have made great efforts

to validate our findings as far as is feasible and have taken care not to over interpret data presented here.

We initially hypothesized that oral taxa would be enriched in the bloodstream of T2DP subjects, and potentially all T2D subjects, compared to healthy subjects. Our microbiome data revealed changes in composition between our three subject groups (Figs. 1-4, S4-5). However, while we observed oral taxa in our samples, there was only enrichment of few oral taxa in T2DP subjects, specifically *S. cristatus* and *N. flavescens* (Fig. 3), which are not associated with periodontitis. Given the limited template available for each sample, we cannot rule out that other oral taxa are not elevated in T2DP subjects, but more rigorous testing of that hypothesis would require larger serum volumes and using a longitudinal approach on individual subjects. By far the most surprising element of this dataset was the detection of *A. baumanii* (Fig. 3, 5, S5) assigned reads unique to 13 T2DP subjects and not present in any control or healthy subject samples.

A. baumanii represents a considerable risk to T2D subjects including higher mortality rates (Leão et al., 2016) and a higher risk of infection in burn wounds, as well as DFIs (Castellanos et al., 2019; Furniss et al., 2005; Henig et al., 2020). To confirm our V1-V3 amplicon data and to determine whether or not these were *A. baumanii* or another AB complex species, we used targeted near full-length 16S rDNA primers that allowed us to sequence the majority of differentiating nucleotides necessary for ribotyping. Sequencing individual clones of these amplicons revealed 100% matches to *A. baumanii* and no clones (n=50) were *A. baumanii* positive from indicated control samples (Fig.

5). This result was surprising, as none of the subjects in our T2D/P cohort were currently under in-patient treatment or had any indication of underlying infection (apart from periodontitis). Given the methodology here, we cannot speculate on the true infection status of these individuals, nor can we be certain if the *A. baumanii* present were circulating in the bloodstream or were on the skin and mixed with the sample during a blood draw. No matter the route of entry, we were able to determine significant cytokine profile changes in T2DP *A. baumanii* positive subjects, as well as broader inflammatory changes in cytokine profiles between T2DP, T2D and healthy subjects (Fig. 6).

Cytokine dysregulation can impact the host locally and systemically, making the subject more prone to severe infections and increased tissue damage (Tisoncik et al., 2012). Individuals that have T2D present an increased metabolic burden, while often comorbid periodontal disease promotes microbial dysbiosis, with both diseases resulting in a chronic state of inflammation. In the present study, *A. baumanii* was only found in the serum of diabetics, where an increase in proinflammatory cytokines was also observed (Figs. 6, 7). We utilized an unbiased panel of 20 human cytokines to survey specific immune responses to T2D and T2DP compared to those of healthy individuals. While there are complications presented by low template sizes in our samples, cytokine profiling from these same volumes were well within desired assay volumes. As mediators of inflammation, cytokine production feeds forward a cascade of signals that can impact tissue, organ and overall host immunometabolism. In T2D, IL-1β, TNF-α, MCP-1, IL-6, IL-8, and IFN-γ were significantly elevated in ABC+ subjects and not in ABC-negative subjects. Of these proinflammatory cytokines, IL-1β, TNF-α, and IL-8 suppression

has been investigated as therapeutic targets for clinical management of diabetes and associated chronic lesions (Feng et al., 2018; Peiró et al., 2017). We previously observed increased TNF-α levels in cell cultured neutrophils from T2D subjects relative to cells derived from healthy subjects (Sarah E Kleinstein et al., 2020). Co-occurrence of bacteria in the serum and cytokines also differed among controls. In the current study, co-occurrence among cytokines was more evident in diabetic subjects (100 significant co-occurrences) versus healthy individuals (30 significant co-occurrences) (Figs. 7, S6). *A baumannii* especially correlated with neutrophil inflammatory signaling cytokine IL-8, which was not observed in healthy subjects. We have previously shown differences in gene expression in neutrophils of T2D individuals, which are primed to mount an aberrant inflammatory response when compared to neutrophils of healthy individuals (Sarah E Kleinstein et al., 2020), consistent with production of inflammatory cytokines observed here. In contrast, IL-17α, P-selectin, and E-selectin levels were increased in diabetics that were ABC-negative compared to ABC+ diabetics. IL-4 and IL-10 did not co-occur with *A. baumanii* in any of the healthy versus diabetic groups. The cytokine results provide an initial glimpse into the host response to chronic inflammatory diseases, T2DP with and without the presence of *A. baumannii*, which may warrant further investigation in larger studies.

In conclusion, this study has revealed modest serum microbiome compositional changes and significant cytokine profile changes between T2D subjects with or without periodontitis versus non-T2D individuals, revealing an impaired host response when *A. bau-*

manii was present. We also present here the potential for lurking *A. baumanii* colonization in asymptomatic T2D subjects, possibly to a much larger extent than previously reported. In our opinion, these data present a strong justification for further monitoring of T2D individuals for *A. baumanii* colonization and support the need for a more robust study to characterize the potentially greater spread of *A. baumanii* amongst individuals with T2D.

Limitations of the Study

Limitations of this study primarily include small template volumes available for serum samples in this *post hoc* study. Blood and sera microbiome studies will always be more complex due to low bacterial template concentrations inherent to these types of sample. While we have done our utmost efforts to validate our main findings regarding *A. baumanii* presence, there are likely more interesting aspects to our study cohort microbiota that have been missed. These and other minor limitations have been indicated in the manuscript.

Resource Availability

Lead Contact – Further information and requests for resources, data, code, and reagents should be directed to and will be fulfilled by the Lead Contact, Dr. Matthew Ramsey (mramsey@uri.edu).

Materials Availability

This study did not generate new unique reagents or genetic constructs.

Data and Code Availability

All data is available at NIH – SRA Bioproject number PRJNA664044. All other code used for data analysis has been provided in the Transparent Methods section (see Scripts) in the Supplemental Information.

Acknowledgements

Thanks to the M. Ramsey and M. Freire lab members for their valuable input and assistance with both experimental work and writing. Thanks to Dr. Janet Atoyan at the Rhode Island Genomics and Sequencing Center for assistance with sequence library preparation and suggestions on sequence data analysis. Thanks to Dr. Thomas E. Van Dyke for helpful discussion and to the Forsyth Center for Clinical and Translational Research Center staff for recruiting patient samples and providing clinical data used in this study.

Author Contributions

DP, BH and SEK performed the work. DP, SEK, MF, and MR wrote and edited the manuscript. MF, HH, and MR provided reagents and samples. DP, RE, SEK, MF, and MR designed the experiments. MF and MR secured funding.

Declaration of Interests

The authors declare no competing interests.

References

Al-Anazi, K.A., Al-Jasser, A.M., 2014. Infections Caused by Acinetobacter baumannii in Recipients of Hematopoietic Stem Cell Transplantation. Front. Oncol. 4, 186. https://doi.org/10.3389/fonc.2014.00186

American Diabetes Association, 2015. (2) Classification and diagnosis of diabetes. Diabetes Care 38 Suppl, S8–S16. https://doi.org/10.2337/dc15-S005

Armitage, G.C., 1999. Development of a classification system for periodontal diseases and conditions. Ann. Periodontol. 4, 1–6. https://doi.org/10.1902/annals.1999.4.1.1

Ayoub Moubareck, C., Hammoudi Halat, D., 2020. Insights into Acinetobacter baumannii: A Review of Microbiological, Virulence, and Resistance Traits in a Threatening Nosocomial Pathogen. Antibiot. Basel Switz. 9. https://doi.org/10.3390/antibiotics9030119

Benjamini, Y., Hochberg, Y., 1995. Controlling the False Discovery Rate: A Practical and Powerful Approach to Multiple Testing. J. R. Stat. Soc. Ser. B Methodol. 57, 289–300. https://doi.org/10.1111/j.2517-6161.1995.tb02031.x

Bolger, A.M., Lohse, M., Usadel, B., 2014. Trimmomatic: a flexible trimmer for Illumina sequence data. Bioinforma. Oxf. Engl. 30, 2114–2120. https://doi.org/10.1093/bioinformatics/btu170

Bolyen, E., Rideout, J.R., Dillon, M.R., Bokulich, N.A., Abnet, C.C., Al-Ghalith, G.A., Alexander, H., Alm, E.J., Arumugam, M., Asnicar, F., Bai, Y., Bisanz, J.E., Bittinger, K., Brejnrod, A., Brislawn, C.J., Brown, C.T., Callahan, B.J., Caraballo-Rodríguez, A.M., Chase, J., Cope, E.K., Da Silva, R., Diener, C., Dorrestein, P.C., Douglas, G.M., Durall, D.M., Duvallet, C., Edwardson, C.F., Ernst, M., Estaki, M., Fouquier, J., Gauglitz, J.M.,

Gibbons, S.M., Gibson, D.L., Gonzalez, A., Gorlick, K., Guo, J., Hillmann, B., Holmes, S., Holste, H., Huttenhower, C., Huttley, G.A., Janssen, S., Jarmusch, A.K., Jiang, L., Kaehler, B.D., Kang, K.B., Keefe, C.R., Keim, P., Kelley, S.T., Knights, D., Koester, I., Kosciolek, T., Kreps, J., Langille, M.G.I., Lee, J., Ley, R., Liu, Y.-X., Loftfield, E., Lozupone, C., Maher, M., Marotz, C., Martin, B.D., McDonald, D., McIver, L.J., Melnik, A.V., Metcalf, J.L., Morgan, S.C., Morton, J.T., Naimey, A.T., Navas-Molina, J.A., Nothias, L.F., Orchanian, S.B., Pearson, T., Peoples, S.L., Petras, D., Preuss, M.L., Pruesse, E., Rasmussen, L.B., Rivers, A., Robeson, M.S., Rosenthal, P., Segata, N., Shaffer, M., Shiffer, A., Sinha, R., Song, S.J., Spear, J.R., Swafford, A.D., Thompson, L.R., Torres, P.J., Trinh, P., Tripathi, A., Turnbaugh, P.J., Ul-Hasan, S., van der Hooft, J.J.J., Vargas, F., Vázquez-Baeza, Y., Vogtmann, E., von Hippel, M., Walters, W., Wan, Y., Wang, M., Warren, J., Weber, K.C., Williamson, C.H.D., Willis, A.D., Xu, Z.Z., Zaneveld, J.R., Zhang, Y., Zhu, Q., Knight, R., Caporaso, J.G., 2019. Reproducible, interactive, scalable and extensible microbiome data science using QIIME 2. Nat. Biotechnol. 37, 852–857. https://doi.org/10.1038/s41587-019-0209-9

Bowler, P.G., Davies, B.J., 1999. The microbiology of infected and noninfected leg ulcers. Int. J. Dermatol. 38, 573–578. https://doi.org/10.1046/j.1365-4362.1999.00738.x

Callahan, B.J., McMurdie, P.J., Rosen, M.J., Han, A.W., Johnson, A.J.A., Holmes, S.P., 2016. DADA2: High-resolution sample inference from Illumina amplicon data. Nat. Methods 13, 581–583. https://doi.org/10.1038/nmeth.3869

Carrizales-Sepúlveda, E.F., Ordaz-Farías, A., Vera-Pineda, R., Flores-Ramírez, R., 2018. Periodontal Disease, Systemic Inflammation and the Risk of Cardiovascular Disease. Heart Lung Circ. 27, 1327–1334. https://doi.org/10.1016/j.hlc.2018.05.102

Castellanos, N., Nakanouchi, J., Yüzen, D.I., Fung, S., Fernandez, J.S., Barberis, C., Tuchscherr, L., Ramirez, M.S., 2019. A Study on Acinetobacter baumannii and Staphylococcus aureus Strains Recovered from the Same Infection Site of a Diabetic Patient. Curr. Microbiol. 76, 842–847. https://doi.org/10.1007/s00284-019-01696-7

Citron, D.M., Goldstein, E.J.C., Merriam, C.V., Lipsky, B.A., Abramson, M.A., 2007. Bacteriology of moderate-to-severe diabetic foot infections and in vitro activity of antimicrobial agents. J. Clin. Microbiol. 45, 2819–2828. https://doi.org/10.1128/JCM.00551-07

Cole, J.R., Wang, Q., Fish, J.A., Chai, B., McGarrell, D.M., Sun, Y., Brown, C.T., Porras-Alfaro, A., Kuske, C.R., Tiedje, J.M., 2014. Ribosomal Database Project: data and tools for high throughput rRNA analysis. Nucleic Acids Res. 42, D633-642. https://doi.org/10.1093/nar/gkt1244

Curtis, M.A., Diaz, P.I., Van Dyke, T.E., 2020. The role of the microbiota in periodontal disease. Periodontol. 2000 83, 14–25. https://doi.org/10.1111/prd.12296

DeSantis, T.Z., Hugenholtz, P., Larsen, N., Rojas, M., Brodie, E.L., Keller, K., Huber, T., Dalevi, D., Hu, P., Andersen, G.L., 2006. Greengenes, a Chimera-Checked 16S rRNA Gene Database and Workbench Compatible with ARB. Appl. Environ. Microbiol. 72, 5069–5072. https://doi.org/10.1128/AEM.03006-05

Dijkshoorn, L., Nemec, A., Seifert, H., 2007. An increasing threat in hospitals: multidrug-resistant Acinetobacter baumannii. Nat. Rev. Microbiol. 5, 939–951. https://doi.org/10.1038/nrmicro1789

Dodt, M., Roehr, J.T., Ahmed, R., Dieterich, C., 2012. FLEXBAR-Flexible Barcode and Adapter Processing for Next-Generation Sequencing Platforms. Biology 1, 895–905. https://doi.org/10.3390/biology1030895

Dowd, S.E., Wolcott, R.D., Sun, Y., McKeehan, T., Smith, E., Rhoads, D., 2008. Polymicrobial nature of chronic diabetic foot ulcer biofilm infections determined using bacterial tag encoded FLX amplicon pyrosequencing (bTEFAP). PloS One 3, e3326. https://doi.org/10.1371/journal.pone.0003326

Driver, V.R., Fabbi, M., Lavery, L.A., Gibbons, G., 2010. The costs of diabetic foot: the economic case for the limb salvage team. J. Am. Podiatr. Med. Assoc. 100, 335–341. https://doi.org/10.7547/1000335

Emrich, L.J., Shlossman, M., Genco, R.J., 1991. Periodontal disease in non-insulin-dependent diabetes mellitus. J. Periodontol. 62, 123–131. https://doi.org/10.1902/jop.1991.62.2.123

Erben, N., Ozgunes, I., Aksit, F., Doyuk Kartal, E., Colak, E., Usluer, G., 2013. Healthcare-associated infections and the distribution of causative pathogens in patients with diabetes mellitus. Eur. J. Clin. Microbiol. Infect. Dis. Off. Publ. Eur. Soc. Clin. Microbiol. 32, 821–825. https://doi.org/10.1007/s10096-013-1816-x

Eren, A.M., Borisy, G.G., Huse, S.M., Mark Welch, J.L., 2014. Oligotyping analysis of the human oral microbiome. Proc. Natl. Acad. Sci. U. S. A. 111, E2875-2884. https://doi.org/10.1073/pnas.1409644111

Eren, A.M., Morrison, H.G., Lescault, P.J., Reveillaud, J., Vineis, J.H., Sogin, M.L., 2015. Minimum entropy decomposition: unsupervised oligotyping for sensitive partitioning of high-throughput marker gene sequences. ISME J. 9, 968–979. https://doi.org/10.1038/ismej.2014.195

Escapa, I.F., Chen, T., Huang, Y., Gajare, P., Dewhirst, F.E., Lemon, K.P., 2018. New Insights into Human Nostril Microbiome from the Expanded Human Oral Microbiome Database

(eHOMD): a Resource for the Microbiome of the Human Aerodigestive Tract. mSystems 3, e00187-18, /msystems/3/6/msys.00187-18.atom. https://doi.org/10.1128/mSystems.00187-18

Faith, D.P., 1992. Conservation evaluation and phylogenetic diversity. Biol. Conserv. 61, 1–10. https://doi.org/10.1016/0006-3207(92)91201-3

Feng, S., Yu, H., Yu, Y., Geng, Y., Li, D., Yang, C., Lv, Q., Lu, L., Liu, T., Li, G., Yuan, L., 2018. Levels of Inflammatory Cytokines IL-1 β , IL-6, IL-8, IL-17A, and TNF- α in Aqueous Humour of Patients with Diabetic Retinopathy. J. Diabetes Res. 2018, 1–6. https://doi.org/10.1155/2018/8546423

Ferlita, S., Yegiazaryan, A., Noori, N., Lal, G., Nguyen, T., To, K., Venketaraman, V., 2019. Type 2 Diabetes Mellitus and Altered Immune System Leading to Susceptibility to Pathogens, Especially Mycobacterium tuberculosis. J. Clin. Med. 8. https://doi.org/10.3390/jcm8122219

Freire, M.O., Dalli, J., Serhan, C.N., Van Dyke, T.E., 2017. Neutrophil Resolvin E1 Receptor Expression and Function in Type 2 Diabetes. J. Immunol. Baltim. Md 1950 198, 718–728. https://doi.org/10.4049/jimmunol.1601543

Freire, M.O., Van Dyke, T.E., 2013. Natural resolution of inflammation. Periodontol. 2000 63, 149–164. https://doi.org/10.1111/prd.12034

Furniss, D., Gore, S., Azadian, B., Myers, S.R., 2005. Acinetobacter infection is associated with acquired glucose intolerance in burn patients. J. Burn Care Rehabil. 26, 405–408. https://doi.org/10.1097/01.bcr.0000176882.69354.7e

Gardner, S.E., Hillis, S.L., Heilmann, K., Segre, J.A., Grice, E.A., 2013. The neuropathic diabetic foot ulcer microbiome is associated with clinical factors. Diabetes 62, 923–930. https://doi.org/10.2337/db12-0771

Genco, R.J., Graziani, F., Hasturk, H., 2020. Effects of periodontal disease on glycemic control, complications, and incidence of diabetes mellitus. Periodontol. 2000 83, 59–65. https://doi.org/10.1111/prd.12271

Gerner-Smidt, P., Tjernberg, I., 1993. Acinetobacter in Denmark: II. Molecular studies of the Acinetobacter calcoaceticus-Acinetobacter baumannii complex. APMIS Acta Pathol. Microbiol. Immunol. Scand. 101, 826–832.

Gootz, T.D., Marra, A., 2008. Acinetobacter baumannii: an emerging multidrug-resistant threat. Expert Rev. Anti Infect. Ther. 6, 309–325. https://doi.org/10.1586/14787210.6.3.309

Griffen, A.L., Beall, C.J., Campbell, J.H., Firestone, N.D., Kumar, P.S., Yang, Z.K., Podar, M., Leys, E.J., 2012. Distinct and complex bacterial profiles in human periodontitis and health revealed by 16S pyrosequencing. ISME J. 6, 1176–1185. https://doi.org/10.1038/ismej.2011.191

Hajishengallis, G., Lamont, R.J., 2012. Beyond the red complex and into more complexity: the polymicrobial synergy and dysbiosis (PSD) model of periodontal disease etiology. Mol. Oral Microbiol. 27, 409–419. https://doi.org/10.1111/j.2041-1014.2012.00663.x

Henig, O., Pogue, J.M., Martin, E., Hayat, U., Ja'ara, M., Kilgore, P.E., Cha, R., Dhar, S., Kaye, K.S., 2020. The Impact of Multidrug-Resistant Organisms on Outcomes in Patients With Diabetic Foot Infections. Open Forum Infect. Dis. 7, ofaa161. https://doi.org/10.1093/ofid/ofaa161

Irfan, U.M., Dawson, D.V., Bissada, N.F., 2001. Epidemiology of periodontal disease: a review and clinical perspectives. J. Int. Acad. Periodontol. 3, 14–21.

Kennedy, K., Hall, M.W., Lynch, M.D.J., Moreno-Hagelsieb, G., Neufeld, J.D., 2014. Evaluating Bias of Illumina-Based Bacterial 16S rRNA Gene Profiles. Appl. Environ. Microbiol. 80, 5717–5722. https://doi.org/10.1128/AEM.01451-14

Kim, D., Hofstaedter, C.E., Zhao, C., Mattei, L., Tanes, C., Clarke, E., Lauder, A., Sherrill-Mix, S., Chehoud, C., Kelsen, J., Conrad, M., Collman, R.G., Baldassano, R., Bushman, F.D., Bittinger, K., 2017. Optimizing methods and dodging pitfalls in microbiome research. Microbiome 5, 52. https://doi.org/10.1186/s40168-017-0267-5

Kim, E.J., Ha, K.H., Kim, D.J., Choi, Y.H., 2019. Diabetes and the Risk of Infection: A National Cohort Study. Diabetes Metab. J. 43, 804–814. https://doi.org/10.4093/dmj.2019.0071

Kleinstein, Sarah E, McCorrison, J., Ahmed, A., Hasturk, H., Dyke, T.E.V., Freire, M., 2020. Transcriptomics of Type 2 Diabetic and Healthy Human Neutrophils (preprint). In Review. https://doi.org/10.21203/rs.2.21951/v1

Kleinstein, S.E., Nelson, K.E., Freire, M., 2020. Inflammatory Networks Linking Oral Microbiome with Systemic Health and Disease. J. Dent. Res. 99, 1131–1139. https://doi.org/10.1177/0022034520926126

Kruskal, W.H., Wallis, W.A., 1952. Use of Ranks in One-Criterion Variance Analysis. J. Am. Stat. Assoc. 47, 583–621. https://doi.org/10.1080/01621459.1952.10483441

Leão, A.C.Q., Menezes, P.R., Oliveira, M.S., Levin, A.S., 2016. Acinetobacter spp. are associated with a higher mortality in intensive care patients with bacteremia: a survival analysis. BMC Infect. Dis. 16, 386. https://doi.org/10.1186/s12879-016-1695-8

Leung, C.-H., Liu, C.-P., 2019. Diabetic status and the relationship of blood glucose to mortality in adults with carbapenem-resistant Acinetobacter baumannii complex bacteremia. J. Microbiol. Immunol. Infect. Wei Mian Yu Gan Ran Za Zhi 52, 654–662. https://doi.org/10.1016/j.jmii.2018.06.005

Lockhart, P.B., Durack, D.T., 1999. Oral microflora as a cause of endocarditis and other distant site infections. Infect. Dis. Clin. North Am. 13, 833–850, vi. https://doi.org/10.1016/s0891-5520(05)70111-2

Mann, J., Bernstein, Y., Findler, M., 2020. Periodontal disease and its prevention, by traditional and new avenues. Exp. Ther. Med. 19, 1504–1506. https://doi.org/10.3892/etm.2019.8381

McDonald, H.I., Nitsch, D., Millett, E.R.C., Sinclair, A., Thomas, S.L., 2014. New estimates of the burden of acute community-acquired infections among older people with diabetes mellitus: a retrospective cohort study using linked electronic health records. Diabet. Med. J. Br. Diabet. Assoc. 31, 606–614. https://doi.org/10.1111/dme.12384

Moore, B.B., Kunkel, S.L., 2019. Attracting Attention: Discovery of IL-8/CXCL8 and the Birth of the Chemokine Field. J. Immunol. 202, 3–4. https://doi.org/10.4049/jimmunol.1801485

National Diabetes Statistics Report | Data & Statistics | Diabetes | CDC [WWW Document], 2020. URL https://www.cdc.gov/diabetes/data/statistics/statistics-report.html (accessed 7.24.20).

NCBI Resource Coordinators, 2018. Database resources of the National Center for Biotechnology Information. Nucleic Acids Res. 46, D8–D13. https://doi.org/10.1093/nar/gkx1095

Nowicki, E.M., Shroff, R., Singleton, J.A., Renaud, D.E., Wallace, D., Drury, J., Zirnheld, J., Colleti, B., Ellington, A.D., Lamont, R.J., Scott, D.A., Whiteley, M., 2018. Microbiota and Metatranscriptome Changes Accompanying the Onset of Gingivitis. mBio 9. https://doi.org/10.1128/mBio.00575-18

Parahitiyawa, N.B., Jin, L.J., Leung, W.K., Yam, W.C., Samaranayake, L.P., 2009. Microbiology of odontogenic bacteremia: beyond endocarditis. Clin. Microbiol. Rev. 22, 46–64, Table of Contents. https://doi.org/10.1128/CMR.00028-08

Peiró, C., Lorenzo, Ó., Carraro, R., Sánchez-Ferrer, C.F., 2017. IL-1β Inhibition in Cardiovascular Complications Associated to Diabetes Mellitus. Front. Pharmacol. 8, 363. https://doi.org/10.3389/fphar.2017.00363

Peleg, A.Y., Seifert, H., Paterson, D.L., 2008. Acinetobacter baumannii: emergence of a successful pathogen. Clin. Microbiol. Rev. 21, 538–582. https://doi.org/10.1128/CMR.00058-07

Pessoa, L., Aleti, G., Choudhury, S., Nguyen, D., Yaskell, T., Zhang, Y., Li, W., Nelson, K.E., Neto, L.L.S., Sant'Ana, A.C.P., Freire, M., 2019. Host-Microbial Interactions in Systemic Lupus Erythematosus and Periodontitis. Front. Immunol. 10, 2602. https://doi.org/10.3389/fimmu.2019.02602

Pielou, E.C., 1966. The measurement of diversity in different types of biological collections. J. Theor. Biol. 13, 131–144. https://doi.org/10.1016/0022-5193(66)90013-0

Pollock, J., Glendinning, L., Wisedchanwet, T., Watson, M., 2018. The Madness of Microbiome: Attempting To Find Consensus "Best Practice" for 16S Microbiome Studies. Appl. Environ. Microbiol. 84, e02627-17, /aem/84/7/e02627-17.atom. https://doi.org/10.1128/AEM.02627-17

Qiu, H., KuoLee, R., Harris, G., Chen, W., 2009. High susceptibility to respiratory Acinetobacter baumannii infection in A/J mice is associated with a delay in early pulmonary recruitment of neutrophils. Microbes Infect. 11, 946–955. https://doi.org/10.1016/j.micinf.2009.06.003

Quast, C., Pruesse, E., Yilmaz, P., Gerken, J., Schweer, T., Yarza, P., Peplies, J., Glöckner, F.O., 2013. The SILVA ribosomal RNA gene database project: improved data processing and web-based tools. Nucleic Acids Res. 41, D590-596. https://doi.org/10.1093/nar/gks1219

Reiber, G.E., Lipsky, B.A., Gibbons, G.W., 1998. The burden of diabetic foot ulcers. Am. J. Surg. 176, 5S-10S. https://doi.org/10.1016/s0002-9610(98)00181-0

Roberts, F.A., Darveau, R.P., 2015. Microbial protection and virulence in periodontal tissue as a function of polymicrobial communities: symbiosis and dysbiosis. Periodontol. 2000 69, 18–27. https://doi.org/10.1111/prd.12087

Salter, S.J., Cox, M.J., Turek, E.M., Calus, S.T., Cookson, W.O., Moffatt, M.F., Turner, P., Parkhill, J., Loman, N.J., Walker, A.W., 2014. Reagent and laboratory contamination can critically impact sequence-based microbiome analyses. BMC Biol. 12, 87. https://doi.org/10.1186/s12915-014-0087-z

Segata, N., Izard, J., Waldron, L., Gevers, D., Miropolsky, L., Garrett, W.S., Huttenhower, C., 2011. Metagenomic biomarker discovery and explanation. Genome Biol. 12, R60. https://doi.org/10.1186/gb-2011-12-6-r60

Shannon, C.E., Weaver, W., 1975. The mathematical theory of communication. University of Illinois Press, Urbana.

Simpson, E.H., 1949. Measurement of Diversity. Nature 163, 688–688. https://doi.org/10.1038/163688a0

Sinha, R., Abnet, C.C., White, O., Knight, R., Huttenhower, C., 2015. The microbiome quality control project: baseline study design and future directions. Genome Biol. 16, 276. https://doi.org/10.1186/s13059-015-0841-8

Socransky, S.S., Haffajee, A.D., Cugini, M.A., Smith, C., Kent, R.L., 1998. Microbial complexes in subgingival plaque. J. Clin. Periodontol. 25, 134–144. https://doi.org/10.1111/j.1600-051x.1998.tb02419.x

Stackebrandt, E., Goodfellow, M. (Eds.), 1991. Nucleic acid techniques in bacterial systematics, Modern microbiological methods. Wiley, Chichester ; New York.

Tisoncik, J.R., Korth, M.J., Simmons, C.P., Farrar, J., Martin, T.R., Katze, M.G., 2012. Into the eye of the cytokine storm. Microbiol. Mol. Biol. Rev. MMBR 76, 16–32. https://doi.org/10.1128/MMBR.05015-11

Turner, S., Pryer, K.M., Miao, V.P., Palmer, J.D., 1999. Investigating deep phylogenetic relationships among cyanobacteria and plastids by small subunit rRNA sequence analysis. J. Eukaryot. Microbiol. 46, 327–338. https://doi.org/10.1111/j.1550-7408.1999.tb04612.x

Vardakas, K.Z., Siempos, I.I., Falagas, M.E., 2007. Diabetes mellitus as a risk factor for nosocomial pneumonia and associated mortality. Diabet. Med. J. Br. Diabet. Assoc. 24, 1168–1171. https://doi.org/10.1111/j.1464-5491.2007.02234.x

Vázquez-López, R., Solano-Gálvez, S.G., Juárez Vignon-Whaley, J.J., Abello Vaamonde, J.A., Padró Alonzo, L.A., Rivera Reséndiz, A., Muleiro Álvarez, M., Vega López, E.N.,

Franyuti-Kelly, G., Álvarez-Hernández, D.A., Moncaleano Guzmán, V., Juárez Bañuelos, J.E., Marcos Felix, J., González Barrios, J.A., Barrientos Fortes, T., 2020. Acinetobacter baumannii Resistance: A Real Challenge for Clinicians. Antibiot. Basel Switz. 9. https://doi.org/10.3390/antibiotics9040205

Villar, M., Cano, M.E., Gato, E., Garnacho-Montero, J., Miguel Cisneros, J., Ruíz de Alegría, C., Fernández-Cuenca, F., Martínez-Martínez, L., Vila, J., Pascual, A., Tomás, M., Bou, G., Rodríguez-Baño, J., GEIH/GEMARA/REIPI-Ab20101 Group, 2014. Epidemiologic and clinical impact of Acinetobacter baumannii colonization and infection: a reappraisal. Medicine (Baltimore) 93, 202–210. https://doi.org/10.1097/MD.0000000000000036

Whiting, D.R., Guariguata, L., Weil, C., Shaw, J., 2011. IDF diabetes atlas: global estimates of the prevalence of diabetes for 2011 and 2030. Diabetes Res. Clin. Pract. 94, 311–321. https://doi.org/10.1016/j.diabres.2011.10.029

Wu, C.-Z., Yuan, Y.-H., Liu, H.-H., Li, S.-S., Zhang, B.-W., Chen, W., An, Z.-J., Chen, S.-Y., Wu, Y.-Z., Han, B., Li, C.-J., Li, L.-J., 2020. Epidemiologic relationship between periodontitis and type 2 diabetes mellitus. BMC Oral Health 20, 204. https://doi.org/10.1186/s12903-020-01180-w

Appendix

Supplemental Information

Transparent Methods

Subject recruitment, sampling and storage

Subject recruitment has been described previously (Freire et al., 2017). Briefly, T2D and healthy subjects were recruited from the patient cohorts of the Center for Clinical and Translational Research at the Forsyth Institute under Forsyth Institute Institutional Review Board-approved protocols (Protocol #11-03 and #13-07). All subjects gave signed informed consent prior to study evaluations. Clinical periodontal data and peripheral venous blood were collected. The diagnosis of T2D was made by the subject's primary care physician following American Association of Diabetes guidelines (American Diabetes Association, 2015). Information was collected on subject demographics (age, gender, self-reported ethnicity, and self-reported smoking status), body-mass index (BMI; kg/m2), blood total cholesterol, blood glucose (point-of-care), percent hemoglobin A1C (HbA1c), and periodontal condition (Armitage, 1999). HbA1c was used to determine the level of glycemic control for diabetic subjects. One T2D individual lacked HbA1c measurements but fit based on all other diagnostic criteria (blood glucose >200 mg/dl) as well as cytokine profiles in accord with other T2D individuals. Neutrophil and monocyte cell counts were determined by lab assay (described below). Individuals were excluded if they were taking insulin sensitizers, nonsteroidal anti-inflammatory drugs, or antimicrobials within 3 months of study initiation. For this microbiome

study, a total of 81 subjects (N=24 healthy, N=57 T2D) were included for analysis, all of whom were unrelated and over 18 years of age (range: 28-79 years of age).

Sample preparation for 16S analysis

DNA Extraction

Frozen serum from N=81 samples (N=24 healthy, N=32 T2D and N=25 T2DP) were thawed on ice and aliquots were separated for DNA extraction. DNA was extracted using the Epicentre MasterPure Complete DNA and RNA Purification kit (Lucigen, WI, USA). Extraction was carried out using the manufacturer's instructions, with modifications that enabled bead beating. Briefly, 200µL of Tissue and Cell Lysis Solution (2x), 100µL of nuclease free water and 2µL of Proteinase K were added to Lysing matrix B (LMB) tubes (MP Biomedicals, Santa Ana, CA). Thereafter 100µL of serum was added to the tubes and placed in a Beadbeater (Biospec) for 30 seconds, then placed on ice for 3 minutes and then repeated. Each round of DNA extractions included a no template control, which consisted of 100µL nuclease free water instead of serum. The samples were then incubated and extracted as described in the manufacturer's instructions. Total DNA was precipitated using the manufacturer's instructions, however 300 µL of MPC Protein Precipitation Reagent was used to accommodate the increased volume. DNA was eluted in 50µL of nuclease free water.

16s rDNA primers 27F (TCGTCGGCAGCGTCAGATGTGTATAAGAGACAGA-GAGTTTGATYMTGGCTCAG) and 519R (GTCTCGTGGGCTCGGAGATGTG-TATAAGAGACAGGWATTACCGCGGCKGCTG) (Stackebrandt and Goodfellow, 1991; Turner et al., 1999) were used to amplify the V1-V3 regions of 16s rDNA in a 50 μL reaction using 2x Q5 HiFi mastermix (New England Biolabs, Ipswitch, MA) and 23 μL of extracted DNA (35 cycles).

Illumina MiSeq Library preparation

After the first round of PCR was carried out it was cleaned with Ampure XP beads (Beckman Coulter, Pasadena, CA) and then visualized by agarose gel electrophoresis. Full indices and adapters were added using the Illumina Nextera Index Kit (Illumina, San Diego, CA) by running the second round of PCR (50 ng of template DNA, 5 cycles) in 2x Phusion HF Master Mix (New England Biolabs, Ipswitch, MA). PCR were then cleaned with Ampure XP beads and analyzed by agarose gel electrophoresis and using the Agilent BioAnalyzer DNA1000 chip (Agilent Technologies, Santa Clara, CA). Samples were then quantified and normalized prior to pooling using a Qubit fluorimeter (Invitrogen, Carlsbad, CA). The final pooled library was quantified with the KAPA Biosystems Illumina Kit (KAPA Biosystems, Woburn, MA) via qPCR in a Roche LightCycler480. Samples were sequenced (2x250 bp paired-end) on an Illumina MiSeq (Illumina, San Diego, CA) at the Rhode Island Genomics and Sequencing Center (Kingston, RI).

Mock Community Standards Preparation

In order to quantify potential bias due to low template concentrations, PCR amplification, and contamination, we performed mock library assemblies with commercially available bacterial genomic DNA templates (Zymo Research #D6305). We amplified 2 libraries using 10 and 1 ng total starting templates in both sequencing runs for a total of 4 mock libraries synthesized.Total DNA species composition is provided in the manufacturer's instructions.

16S clone library resequencing

Primers were made to amplify regions of 16s rDNA that enable differentiation of the Acinetobacter species. Primers used were
oMR328 (TAGCGGCGGACGGGTGAGTAATGCTTA) and
oMR329 (TTCCGACTTCATGGAGTCGAGTTGCAGAC). 50 µL reactions in 2x Q5 mastermix (New England Biolabs, Ipswitch, MA) were run for 35 cycles using 23 µL of DNA extracted from serum as the template. The products were then purified using the Qiagen PCR purification kit according to the manufacturer's instructions. Gotaq 2x mastermix (Promega, Madison, WI) was used to generate 'A' overhangs via PCR for 5 cycles using 10 µL of purified DNA as the template. 4µL of the resulting PCR products were then used to generate clones using the TOPO TA Cloning Kit (Invitrogen, Carlsbad, CA) according to the manufacturer's instructions which was modified to use 0.5µL of TOPO vector. Clones were then transformed into NEB5α cells using the manufacturer's instructions and plated on LB plates supplemented with 0.1mM IPTG and 40µg/mL Kanamycin. Additionally, 40µl of 40mg/mL of X-gal was spread onto each

plate prior to plating to enable blue-white screening. The plates were incubated for 24 hours at 37°C. White colonies were inoculated into liquid cultures of LB supplemented with 40µg/mL kanamycin. Plasmids were extracted using QIAprep Spin Miniprep kit (Qiagen, Venlo, Netherlands). Inserts were sequenced using the M13 Forward (GTAAAACGACGGCCAGTG) and M13 Reverse (CACAGGAAACAGC-TATGACC) primers on an Applied Biosystems 3500xl using the "BigDye" Terminator v3.1 Cycle sequencing kit. Sequences were analyzed using NCBI BLAST (NCBI Re-source Coordinators, 2018). A maximum of 10 colonies were screened for each sample or until a sequence matched a species belonging to the *Acinetobacter baumanii- calco-aceticus* complex.

Cytokine Quantification

Frozen (-80°C) subject serum was brought up to room temperature and assayed using the Invitrogen human inflammation 20-plex ProcartaPlex cytokine panel (Thermo Fisher Scientific, Waltham, MA) on a Luminex 200 instrument (Luminex, Austin, TX) in universal assay buffer. Assayed cytokines included: MIP-1α, IL-1β, IL-4, IP-10, IL-6, IL-8, IL-10, IL-12p70, IL-13, IL-17A, IFN-γ, GM-CSF, TNF-α, MIP-1β, IFN-α, MCP-1, P-Selectin, IL-1α, sICAM-1, and E-Selectin. Following manufacturer proto-cols, all samples were run on a plate with 7 standards (diluted 1:4) and a control (uni-versal assay buffer only), with all samples, standards, and controls run in duplicate sim-ilar to our methods previously (Sarah E Kleinstein et al., 2020; Pessoa et al., 2019) .

Quality control (QC) steps were conducted according to manufacturer recommendations by xPONENT 4.2 software (Affymetrix eBioscience, San Diego, USA). Any standards with <70 or >130 % recovery of beads were invalidated. Samples were required to have a bead count of >30 beads recovered (all samples had >100 beads recovered and none were excluded at this step). Following QC, results were reported as average pg/mL for all measured cytokines. The lower limit of quantification (LLOQ) was determined based on the standard curve (after QC) as the average value of the lowest validated standards. Values at or below the LLOQ for each cytokine were reported at the LLOQ. As samples were run in two batches (with similar LLOQs for each batch), LLOQ for the cytokines (in pg/mL) were averaged across both runs: MIP-1α=1.79, IL-1β=5.58, IL-4=23.99, IP-10= 1.17, IL-6=18.89, IL-8=2.48, IL-10=2.01, IL-12p70=11.72, IL-13=5.63, IL-17A=4.63, IFN-γ=11.93, GM-CSF=14.57, TNF-α=9.66, MIP-1β=7.66, IFN-α=1.32, MCP-1=3.73, P-Selectin=1077.15, IL-1α=0.74, sICAM-1=442.80, and E-Selectin=441.00. To compare cytokine levels between study groups, unpaired t-tests were used with a significance threshold of $p<0.05$ and no assumption of consistent standard deviation.

Minimum Entropy Decomposition analysis of sequence libraries

Poor quality reads were discarded using flexbar (Dodt et al., 2012). Reads were then treated as single end reads and trimmed for quality and to a length of 160bp using Trimmomatic (Bolger et al., 2014). Minimum Entropy Decomposition (MED) was performed as described in the oligotyping pipeline (Eren et al., 2015), generating a list of

node representative sequences and their relative abundances. Taxonomic assignment of representative sequences were generated based on aligning 16s rRNA sequences at 98.5% identity against the eHOMD database (Escapa et al., 2018) and further evaluated using the Ribosomal Database Project (RDP) database (Cole et al., 2014). MED nodes were assigned species level taxonomy based on >98.5% identity matches to eHOMD and/or RDP with eHOMD designations used as 1st priority as our intial aim was to identify oral taxa. Node frequency tables now assigned taxonomy were then used in association with sample metadata for Linear Discriminate Effect Size analysis (LEfSe) (Segata et al., 2011).

QIIME2 analysis of sequence libraries

*All Scripts at end of this document. All work was performed on the University of Rhode Island High Performance Computing Bluewaves cluster:

https://web.uri.edu/hpc-research-computing/cluster-specifications/

Data Import

Fastq sequence data were imported using the **import-fastq.sh** script. Generated demux.qzv files were viewed using https://view.qiime2.org/ via the "quality viewer" function to determine location for sequence quality trimming used in the following step.

Fastq Trimming, DADA2 Analysis, Run-run Merging

A second sequencing run of the prepared Illumina libraries was performed to ensure maximum sequencing depth without further PCR amplification of starting template. At

the end of the "D2-merge.sh" script we then used the **Rarefaction-alpha.sh** script output (Fig. S2) to determine read depth (22,000) to use in downstream commands.

Initial Alpha and Beta Diversity Measurements and Run-run Comparison Testing

Merged libraries were used in the **Alpha-Beta-An.sh** script to determine initial phylogenetics on unfiltered data using the QIIME2 *core-metrics-phylogenetic* function, Alpha and Beta diversity calculations via QIIME2 *alpha-* or *beta-group-significance* functions as well as Beta diversity difference calculation (*beta-group-significance*) between sequencing Run 1 vs. Run 2 (Figs. S3, S4).

Mock Community Standards Quality Control Testing

This section uses the **mocklibQC1.sh** and **mocklibQC2.sh** scripts. Taxonomy files used are described below. The *-bar-plots.qzv file generated in the 1st script was viewed at https://view.qiime2.org/ and the level 6 data from this plot was exported as a .csv file which provides the reads per each taxa. This data was converted to proportion of total reads per each taxa and converted into the Zymo_actual.tsv file. The Zymo_expected.tsv file was generated by editing the Zymo_actual.tsv file with the proportion for each taxa present as provided in the manufacturers reference: https://files.zymoresearch.com/protocols/_d6305_d6306_zymobiomics_microbial_community_dna_standard.pdf

These .tsv inputs were then used in the **mocklibQC2.sh** script to output the visualizations seen in Figure S1.

Classifier Setup and Editing

Initial import of the SILVA 132 classifier was performed by running the following command:

wget https://data.qiime2.org/2019.7/common/silva-132-99-nb-classifier.qza

Classifier setup was then performed using the **classifier.sh** script. Upon searching the silva-taxonomy.qzv file generated, we noted that there were no reads that matched *A. baumanii* sequences at all. We used the rep-seqs.merge.qzv file output from the **D2merge.sh** script saved as a FASTA file from within the QIIME2 viewer function and performed a pairwise blast vs the full length *A. baumanii* 16S sequence from NCBI:

>A.baumanii 16s

AACGCTGGCGGCAGGCTTAACACATGCAAGTCGAGCGGGG-
GAAGGTAGCTTGCTACCGGAC-
CTAGCGGCGGACGGGTGAGTAATGCTTAGGAATCTGCCTATTAGTGGGGG
ACAACATCTCGAAAGGGATGCTAATACCGCATACGTCCTACGGGAGAAA-
GCAGGG-
GATCTTCGGACCTTGCGCTAATAGATGAGCCTAAGTCGGATTAGCTAGTTG
GTGGGGTAAAGGCCTACCAAGGCGACGATCTGTAGCGGGTCTGAGAG-
GATGATCCGCCACAC-
TGGGACTGAGACACGGCCCAGACTCCTACGGGAGGCAGCAGTGGGGAATA
TTGGACAATGGGGGGAACCCTGATCCAGCCATGCCGCGTGTGTGAA-
GAAGGCCTTATGGTT-
GTAAAGCACTTTAAGCGAGGAGGAGGCTACTTTAGTTAATACCTAGAGAT

AGTGGACGTTACTCGCAGAATAAGCACCGGCTAACTCTGTGCCAG-

CAGCCGCGG-

TAATACAGAGGGTGCGAGCGTTAATCGGATTTACTGGGCGTAAAGCGTGC

GTAGGCGGCTTATTAAGTCGGATGTGAAATCCCCGAGCTTAACTTGG-

GAATTGCATTCGA-

TACTGGTGAGCTAGAGTATGGGAGAGGATGGTAGAATTCCAGGTGTAGCG

GTGAAATGCGTAGAGATCTGGAGGAATAC-

CGATGGCGAAGGCAGCCATCTGGCCTAA-

TACTGACGCTGAGGTACGAAAGCATGGGGAGCAAACAGGATTAGATACCC

TGGTAGTCCATGCCGTAAACGATGTCTACTAGCCGTTGGGGCCTTT-

GAGGCTTTAGTGGCG-

CAGCTAACGCGATAAGTAGACCGCCTGGGGAGTACGGTCGCAAGACTAAA

ACTCAAATGAATTGACGGGGGCCCGCACAAGCGGTGGAG-

CATGTGGTTTAATTCGATGCAAC-

GCGAAGAACCTTACCTGGCCTTGACATACTAGAAACTTTCCAGAGATGGA

TTGGTGCCTTCGGGAATCTAGATACAGGTGCTG-

CATGGCTGTCGTCAGCTCGTGTCGTGA-

GATGTTGGGTTAAGTCCCGCAACGAGCGCAACCCTTTTCCTTACTTGCCAG

CATTTCGGATGGGAACTTTAAGGATACTGCCAGTGACAAACTGGAG-

GAAGGCGGGGACGAC-

GTCAAGTCATCATGGCCCTTACGGCCAGGGCTACACACGTGCTACAATGGT

CGGTACAAAGGGTTGCTACACAGCGATGTGATGCTAATCTCAAAAA-

GCCGATCGTAGTCCG-

GATTGGAGTCTGCAACTCGACTCCATGAAGTCGGAATCGCTAGTAATCGC

GGATCAGAATGCCGCGGTGAATACGTTCCCGGGCCTTGTACACAC-

CGCCCGTCACACCATGG-

GAGTTTGTTGCACCAGAAGTAGCTAGCCTAACTGCAAAGAGGGCGGTTAC

CACGGTGTGGCCGATGACTGGGGTGAAGT

One ASV from the rep-seqs.merge.qzv file (e875355f3179838110485d8f5013d4a6) returned a 100% match homology to the above *A. baumanii* sequence. This ASV was just annotated as *Acinetobacter* in the SILVA-132-99 taxonomy. We then edited the silva classifier taxonomy file by first exporting it using the following commands:

module load QIIME2/2019.7

*qiime tools export *

*--input-path silva-taxonomy.qza *

--output-path silva-taxonomy

This output the file in *.tsv format which was then opened in a text editor and searched for the ASV node identity and then modified as indicated here:

before

e875355f3179838110485d8f5013d4a6 D_0__Bacteria;D_1__Proteobacte-

ria;D_2__Gammaproteobacteria;D_3__Pseudomonadales;D_4__Moraxel-

laceae;D_5__Acinetobacter 0.9999662516375396

after

e875355f3179838110485d8f5013d4a6 D_0__Bacteria;D_1__Proteobacteria;D_2__Gammaproteobacteria;D_3__Pseudomonadales;D_4__Moraxellaceae;D_5__Acinetobacter;D_6__Acinetobacter baumanii 0.9999662516375396

The edited file was then saved as taxonomy-1.tsv and imported via the following command:

```
qiime tools import \
  --input-path /data/mramseylab/classifiers/silva-taxonomy/taxonomy-1.tsv \
  --type 'FeatureData[Taxonomy]' \
  --input-format TSVTaxonomyFormat \
  --output-path silva-mod-taxonomy.qza
qiime metadata tabulate \
  --m-input-file silva-mod-taxonomy.qza \
  --o-visualization silva-mod-taxonomy.qzv
```

The silva-mod-taxonomy.qza file was used for the rest of our analyses.

Data Filtering

Data presented throughout the manuscript is generally described as “Minimally Filtered” or “Strict Filtered”. We 1st began with all ASV assigned data from the above scripts and used metadata based filtering to separate out all data from control samples

which included no-template and PCR only control indexes. This was done using the **control-filter.sh** script. Data output from the script was exported so it could be viewed and then used to subtract taxa from human-derived datasets in downstream filtering steps. Next we applied the **meta-filter.sh** script to our data to extract only human derived samples for further analysis and filtering. After this we applied the **minimal-filter.sh** script. Outputs from this script were used in all "Minimally Filtered" described data in the manuscript. Minimal filtering included removal of instances of taxa that appeared in only 2 samples or less, features (ASV sequences) that appeared less than 10 times across all samples and any taxa with less than 20 reads per sample.

Next we took our output files from the above **control-filter.sh** script and used them as part of the input for the **auto-filter.sh** script to exclude these taxa from the remaining minimally filtered data. While this removed many spurious taxa from our samples we observed high abundance of known aquatic microbial contaminant sequences not typically human associated (ex: *Sphingomonas, Ralstonia*). These and other taxa were manually excluded using the **strict-filter.sh** script and further removal of highly abundant *Pseudomonas* sequences were also removed via the **nopa-filter.sh** script. Data filtered to this extent are referred to as "Strictly" filtered in the manuscript.

Re-analysis of Filtered Data

A reanalysis of filtered data was performed 1st for Alpha and Beta diversity measurements via the **alpha-beta2.sh** script (Fig. 1). Further description and statistical analysis of Beta diversity differences were performed in R using the *vegan* package via the

metaMDS and Adonis functions primarily as demonstrated in the **MMR20_ellipses_NMDS.R** script below.

LEfSe Analysis Comparison

Initial LEfSe analysis was performed using ASV output abundance data directly from the initial MED pipeline (Fig. 3). Further analysis on QIIME2 / DADA2 assigned strictly filtered data (Fig. S5) was performed first using the **lefse-noTax.sh** script to export and format data for analysis on the LEfSe Galaxy server (https://huttenhower.sph.harvard.edu/galaxy/). This script only outputs ASV node information without taxonomic assignment. Manual taxonomic assignment was performed comparing ASV node names to the rep-seqs-merge.qza file from the **D2merge.sh** script. LEfSe analysis was performed using default settings, *.svg output files were further edited in InkScape software for clarity.

Supplemental Figures and Legends

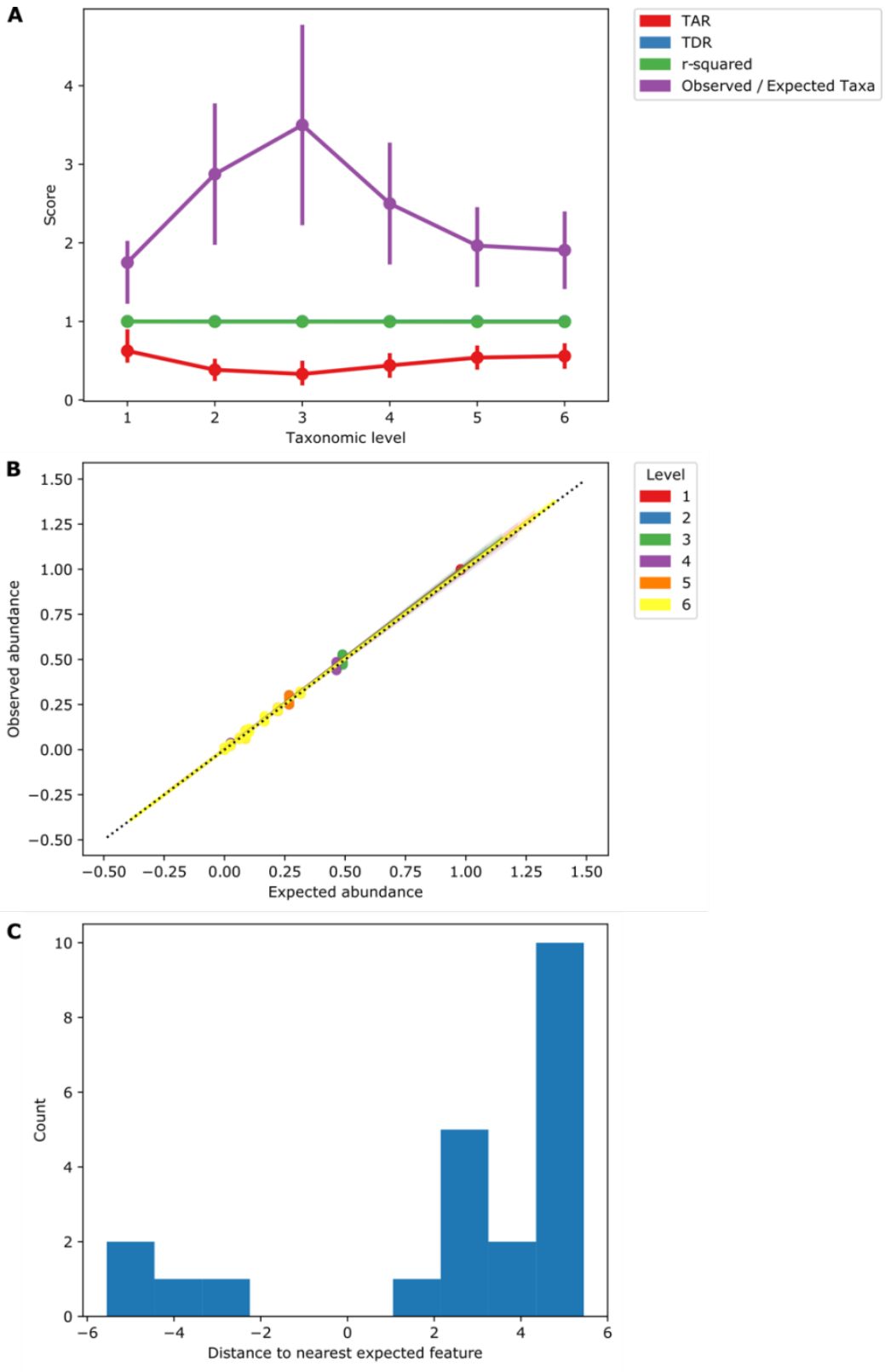
A
TAR
TDR
r-squared
Observed / Expected Taxa
Score
Taxonomic level
B
Level
1
2
3
4
5
6
Observed abundance
Expected abundance
C
Count
Distance to nearest expected feature

Figure S1.1. Mock library composition evaluation. A Zymogen mock community library was used for sequence library construction at 10 and 1 ng in duplicate between both sequencing runs. QIIME2 / DADA2 unfiltered data was given taxonomical assignment via SILVA and assessed via the "q2-quality-control" plugin. (A) Taxon accuracy rate (TAR), taxon detection rate (TDR) and linear regression scores (r-squared) are plotted at each taxonomic level. (B) Expected vs observed abundance of each species in the mock community is plotted at each taxonomic level. (C) Distance between false positive observations vs nearest expected feature. Misclassifications were unique to environmental contaminant taxa and no false negative features were observed (not shown).

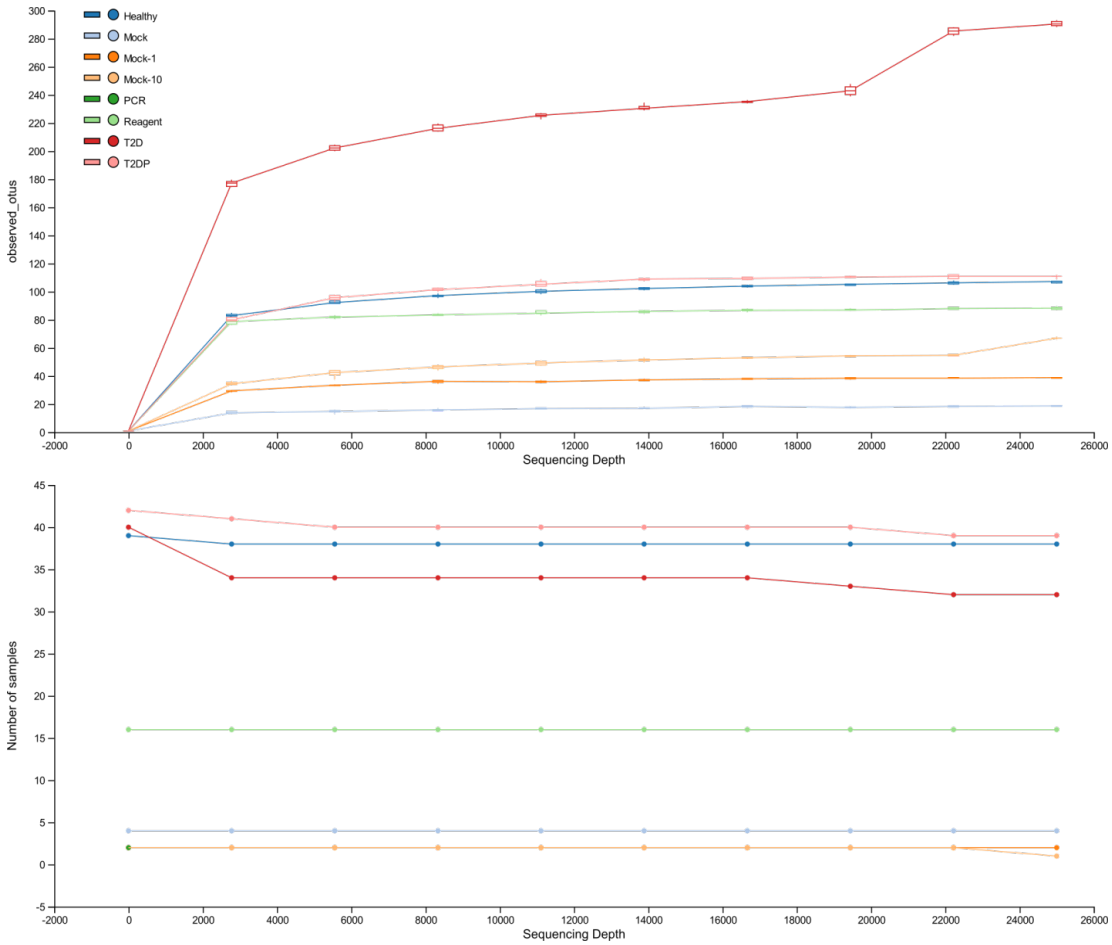

Figure S1.2. Alpha-diversity at different rarefaction levels. Total observed OTUs (here ASVs) are plotted (A) vs sequencing depth and each sample that can accommodate that sequencing depth is plotted in (B).

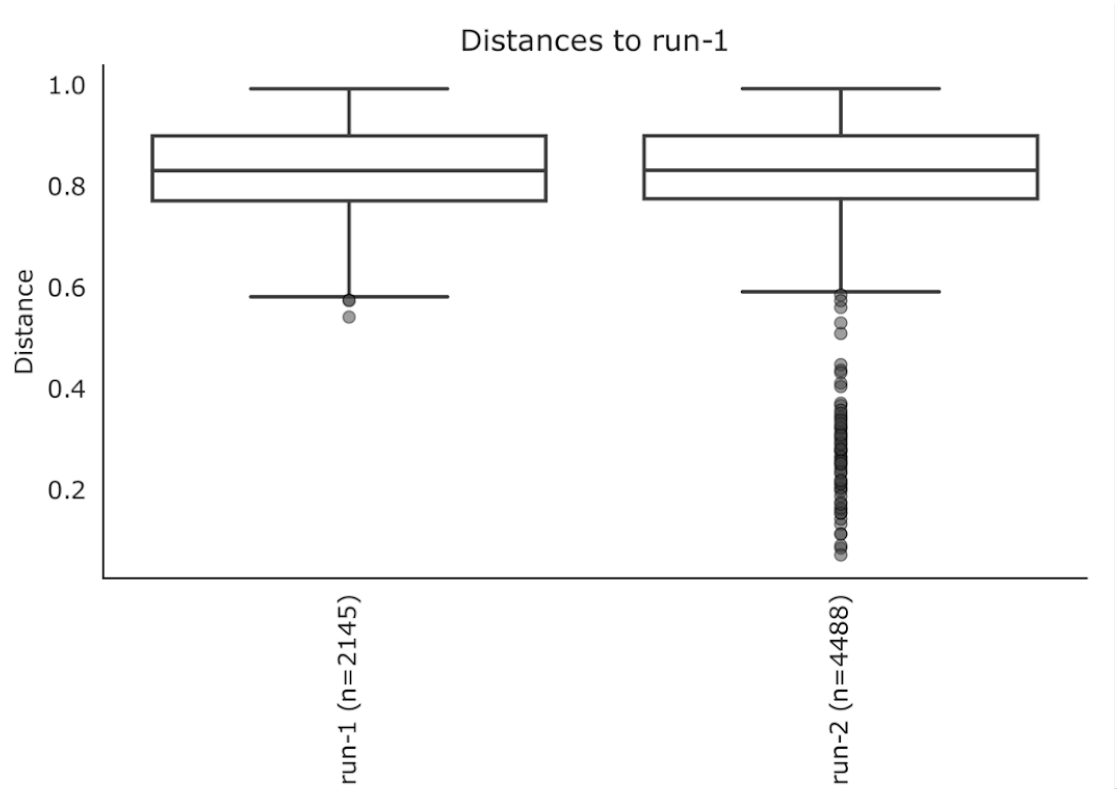
Distances to run-1
Distance
1.0
0.8
0.6
0.4
0.2
run-1 (n=2145)
run-2 (n=4488)

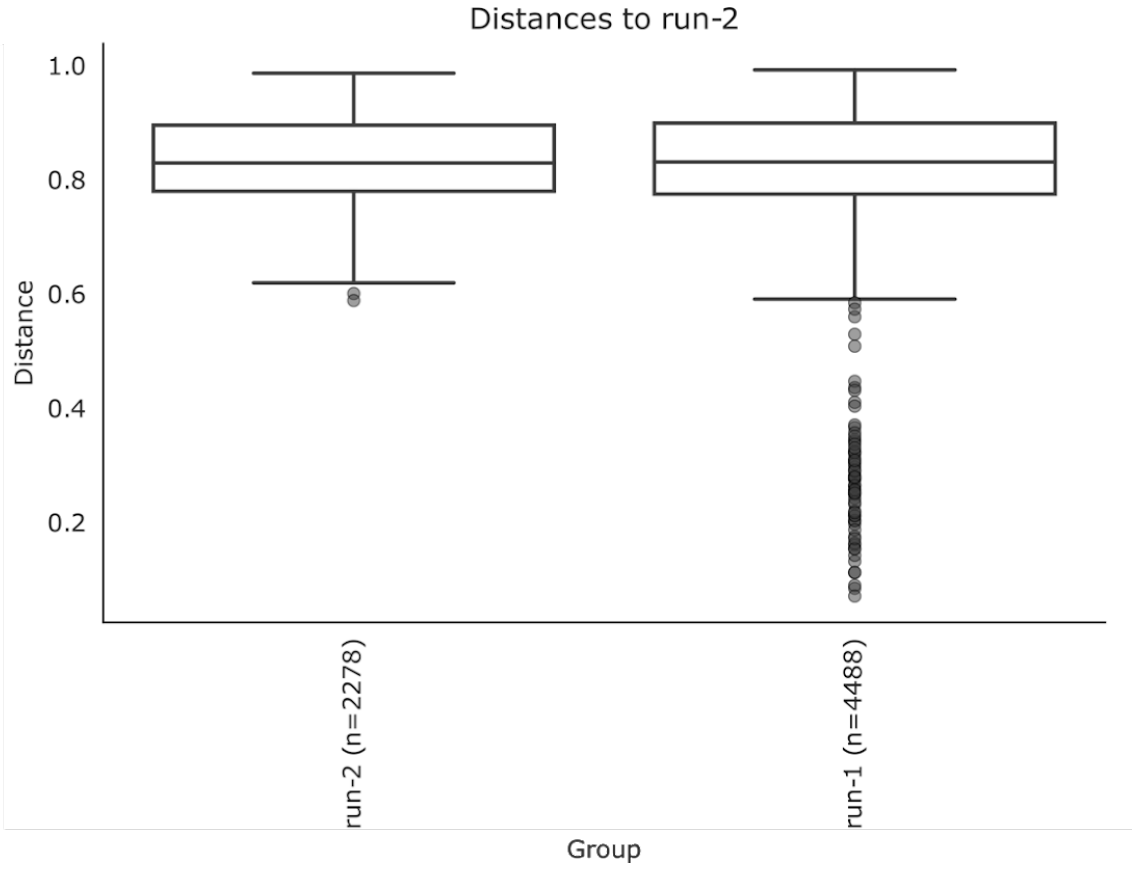
Distances to run-2
Distance
1.0
0.8
0.6
0.4
0.2
run-2 (n=2278)
run-1 (n=4488)
Group

Figure S1.3. Run to Run variability quantification. A Run vs Run Beta diversity comparison was performed for unfiltered data by comparing unweighted Unifrac distances as described in the methods. Pairwise PERMANOVA of Run-1 vs Run-2 (group size of 2, sample size of n=134 total indexes) was performed in 999 permutations resulting in a pseudo-F value of 0.567, p-value of 0.999 and corrected q-value of 0.999. No significant differences were observed between each run.

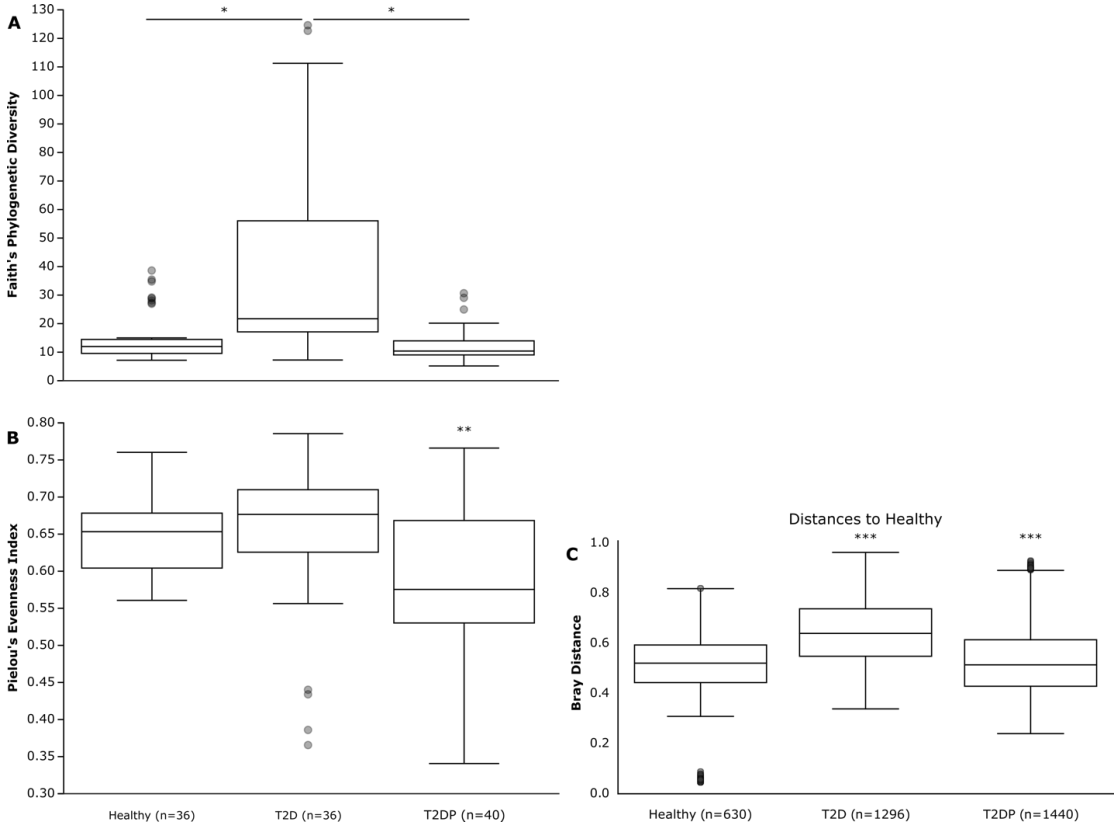

Figure S1.4. 16S Alpha and Beta diversity of serum microbiomes changes with subject status. Species richness is displayed based on Faith's phylogenetic diversity (Faith, 1992) (A) and species evenness based on Pielou's evenness index (Pielou, 1966) (B) for healthy, type-II diabetic (T2D) and type-II diabetics with periodontitis (T2DP) samples. Each graph used minimally filtered data for analysis. Significance was deter-

mined by Kruskal-Wallis analysis of variance (Kruskal and Wallis, 1952) for each comparison indicated and Benjamini-Hochberg correction (Benjamini and Hochberg, 1995) was applied to generate adjusted q-values. * indicates q-value < 2e-3 vs healthy, ** indicates q-value < 0.024 vs healthy, (C) Beta-diversity Bray Curtis distances. Pairwise PERMANOVA of each category vs each (group size of 3, n=112) was performed in 999 permutations. *** indicates q-value differs from healthy < 0.001.

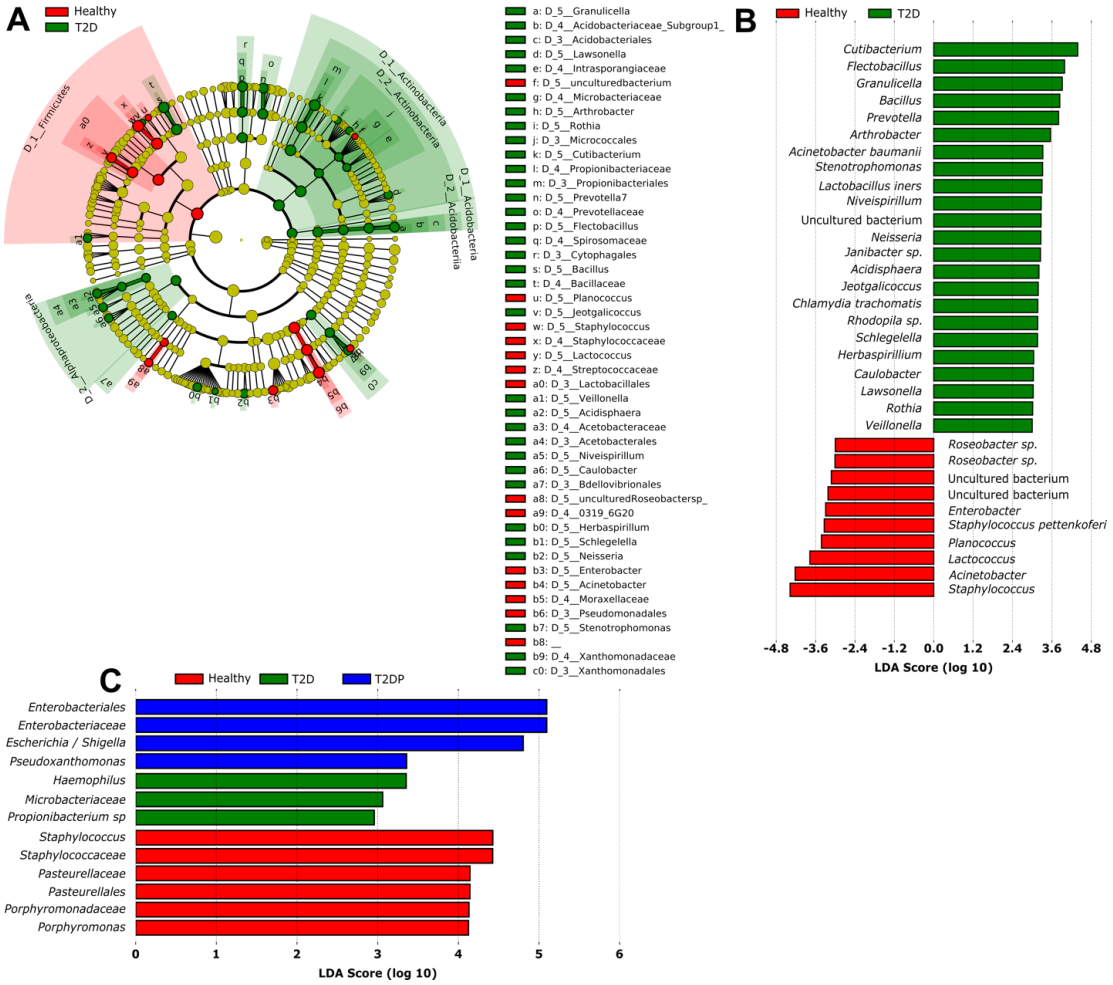

Figure S1.5. LEfSe Comparisons reveal taxonomical differences between subject groups. (A) LEfSe Cladogram plots (Segata et al., 2011) reveal general taxonomic shifts compared to (B) specifically enriched genera or species in all diabetics vs healthy

and (C) compared across all 3 subject groups. Data was generated from DADA2 / QIIME2 analyzed data aligned to the SILVA database that was then filtered for contaminating taxa abundant in no-template control indexes. *Pseudomonas* genus / species level results were also removed for clarity.

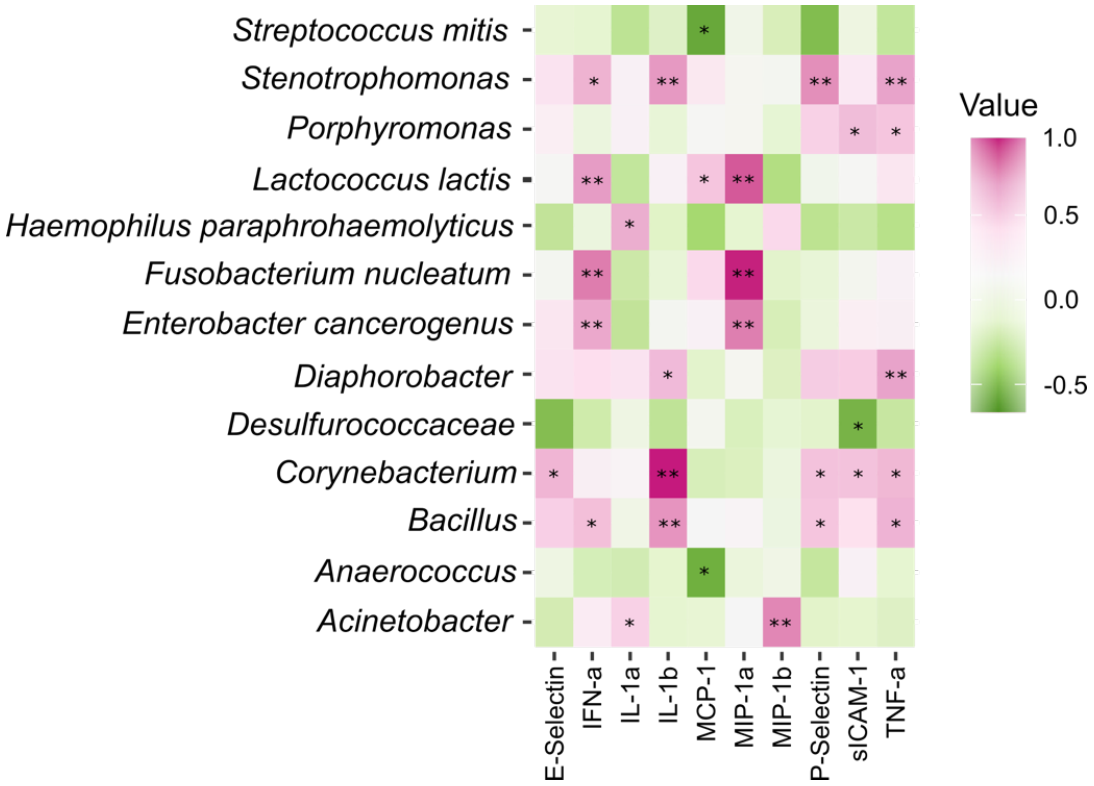

Figure S1.6. Cytokine correlation with specific taxa in healthy subjects. HOMD/RDP assigned taxonomy of MED analyzed 16S data for healthy samples and cytokine concentrations were analyzed via Pearson correlation coefficient in R using the *rcorr* function. Significance was determined using the asymptotic p-values generated by *rcorr* with * = p-value <0.05 ** = p-value <0.01. Data are strictly filtered with taxa present in no-template controls subtracted.

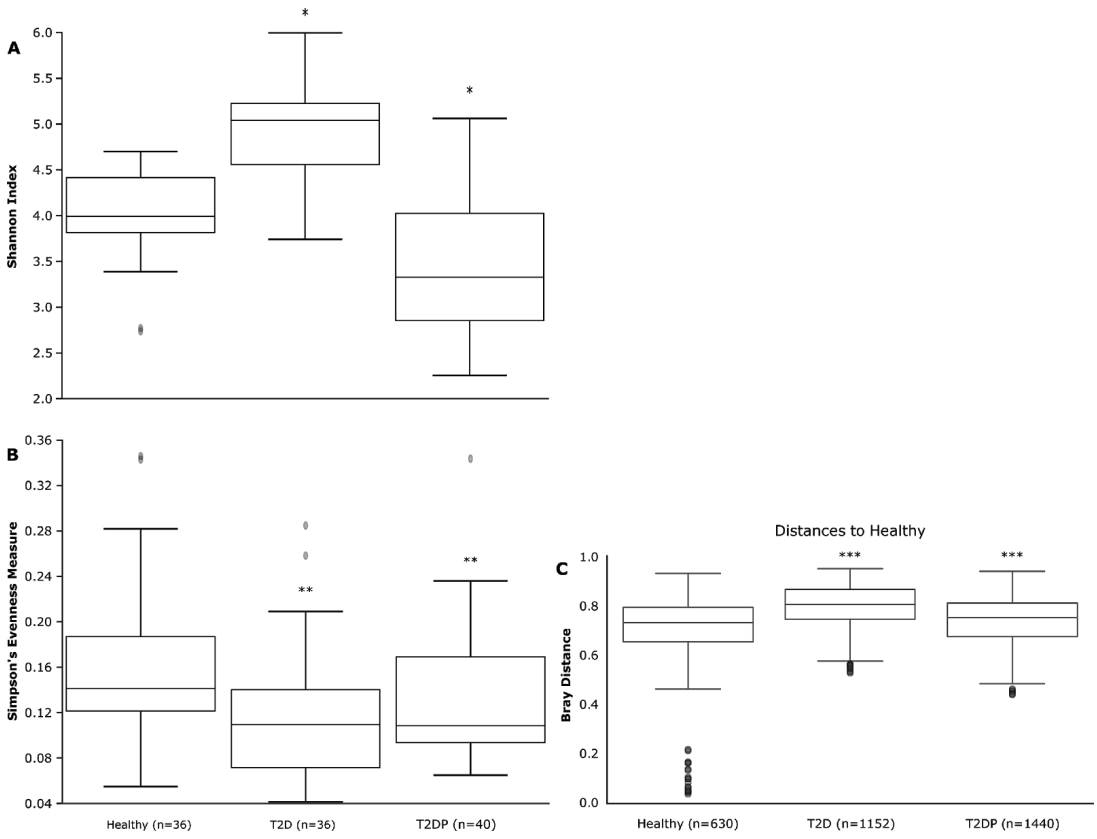

Figure S1.7. 16S Alpha and Beta diversity of serum microbiomes changes with subject status. Alpha diversity is displayed based on Shannon's index (Shannon and Weaver, 1975) (A) and species evenness based on Simpson's evenness measure (Simpson, 1949)) (B) for healthy, type-II diabetic (T2D) and type-II diabetics with periodontitis (T2DP) samples. Each graph used minimally filtered data for analysis. Significance was determined by Kruskal-Wallis analysis of variance (Kruskal and Wallis, 1952) for each comparison indicated and Benjamini-Hochberg correction (Benjamini and Hochberg, 1995) was applied to generate adjusted q-values. * indicates q-value < 1e-5, ** indicates q-value < 0.007, (C) Beta-diversity unweighted Unifrac distances. Pairwise PERMANOVA of each category vs each (group size of 3, n=112) was performed in 999 permutations. *** indicates q-value differs from 'healthy' < 0.02.

Supplemental References

Al-Anazi, K.A., Al-Jasser, A.M., 2014. Infections Caused by Acinetobacter baumannii in Recipients of Hematopoietic Stem Cell Transplantation. Front. Oncol. 4, 186. https://doi.org/10.3389/fonc.2014.00186

American Diabetes Association, 2015. (2) Classification and diagnosis of diabetes. Diabetes Care 38 Suppl, S8–S16. https://doi.org/10.2337/dc15-S005

Armitage, G.C., 1999. Development of a classification system for periodontal diseases and conditions. Ann. Periodontol. 4, 1–6. https://doi.org/10.1902/annals.1999.4.1.1

Ayoub Moubareck, C., Hammoudi Halat, D., 2020. Insights into Acinetobacter baumannii: A Review of Microbiological, Virulence, and Resistance Traits in a Threatening Nosocomial Pathogen. Antibiot. Basel Switz. 9. https://doi.org/10.3390/antibiotics9030119

Benjamini, Y., Hochberg, Y., 1995. Controlling the False Discovery Rate: A Practical and Powerful Approach to Multiple Testing. J. R. Stat. Soc. Ser. B Methodol. 57, 289–300. https://doi.org/10.1111/j.2517-6161.1995.tb02031.x

Bolger, A.M., Lohse, M., Usadel, B., 2014. Trimmomatic: a flexible trimmer for Illumina sequence data. Bioinforma. Oxf. Engl. 30, 2114–2120. https://doi.org/10.1093/bioinformatics/btu170

Bolyen, E., Rideout, J.R., Dillon, M.R., Bokulich, N.A., Abnet, C.C., Al-Ghalith, G.A., Alexander, H., Alm, E.J., Arumugam, M., Asnicar, F., Bai, Y., Bisanz, J.E., Bittinger, K., Brejnrod, A., Brislawn, C.J., Brown, C.T., Callahan, B.J., Caraballo-Rodríguez, A.M., Chase, J., Cope, E.K., Da Silva, R., Diener, C., Dorrestein, P.C., Douglas, G.M., Durall, D.M., Duvallet, C., Edwardson, C.F., Ernst, M., Estaki, M., Fouquier, J., Gauglitz, J.M., Gibbons, S.M., Gibson, D.L., Gonzalez, A., Gorlick, K., Guo, J., Hillmann, B., Holmes, S., Holste, H., Huttenhower, C., Huttley, G.A., Janssen, S., Jarmusch, A.K., Jiang, L., Kaehler, B.D., Kang, K.B., Keefe, C.R., Keim, P., Kelley, S.T., Knights, D., Koester, I., Kosciolek, T., Kreps, J., Langille, M.G.I., Lee, J., Ley, R., Liu, Y.-X., Loftfield, E., Lozupone, C., Maher, M., Marotz, C., Martin, B.D., McDonald, D., McIver, L.J., Melnik, A.V., Metcalf, J.L., Morgan, S.C., Morton, J.T., Naimey, A.T., Navas-Molina, J.A., Nothias, L.F., Orchanian, S.B., Pearson, T., Peoples, S.L., Petras, D., Preuss, M.L., Pruesse, E., Rasmussen, L.B., Rivers, A., Robeson, M.S., Rosenthal, P., Segata, N., Shaffer, M., Shiffer, A., Sinha, R., Song, S.J., Spear, J.R., Swafford, A.D., Thompson, L.R., Torres, P.J., Trinh, P., Tripathi, A., Turnbaugh, P.J., Ul-Hasan, S., van der Hooft, J.J.J., Vargas, F., Vázquez-Baeza, Y., Vogtmann, E., von Hippel, M., Walters, W., Wan, Y., Wang, M., Warren, J., Weber, K.C., Williamson, C.H.D., Willis, A.D., Xu, Z.Z., Zaneveld, J.R., Zhang, Y., Zhu, Q., Knight, R., Caporaso, J.G., 2019. Reproducible, interactive, scalable and extensible microbiome data science using QIIME 2. Nat. Biotechnol. 37, 852–857. https://doi.org/10.1038/s41587-019-0209-9

Bowler, P.G., Davies, B.J., 1999. The microbiology of infected and noninfected leg ulcers. Int. J. Dermatol. 38, 573–578. https://doi.org/10.1046/j.1365-4362.1999.00738.x

Callahan, B.J., McMurdie, P.J., Rosen, M.J., Han, A.W., Johnson, A.J.A., Holmes, S.P., 2016. DADA2: High-resolution sample inference from Illumina amplicon data. Nat. Methods 13, 581–583. https://doi.org/10.1038/nmeth.3869

Carrizales-Sepúlveda, E.F., Ordaz-Farías, A., Vera-Pineda, R., Flores-Ramírez, R., 2018. Periodontal Disease, Systemic Inflammation and the Risk of Cardiovascular Disease. Heart Lung Circ. 27, 1327–1334. https://doi.org/10.1016/j.hlc.2018.05.102

Castellanos, N., Nakanouchi, J., Yüzen, D.I., Fung, S., Fernandez, J.S., Barberis, C., Tuchscherr, L., Ramirez, M.S., 2019. A Study on Acinetobacter baumannii and Staphylococcus aureus Strains Recovered from the Same Infection Site of a Diabetic Patient. Curr. Microbiol. 76, 842–847. https://doi.org/10.1007/s00284-019-01696-7

Citron, D.M., Goldstein, E.J.C., Merriam, C.V., Lipsky, B.A., Abramson, M.A., 2007. Bacteriology of moderate-to-severe diabetic foot infections and in vitro activity of antimicrobial agents. J. Clin. Microbiol. 45, 2819–2828. https://doi.org/10.1128/JCM.00551-07

Cole, J.R., Wang, Q., Fish, J.A., Chai, B., McGarrell, D.M., Sun, Y., Brown, C.T., Porras-Alfaro, A., Kuske, C.R., Tiedje, J.M., 2014. Ribosomal Database Project: data and tools for high throughput rRNA analysis. Nucleic Acids Res. 42, D633-642. https://doi.org/10.1093/nar/gkt1244

Curtis, M.A., Diaz, P.I., Van Dyke, T.E., 2020. The role of the microbiota in periodontal disease. Periodontol. 2000 83, 14–25. https://doi.org/10.1111/prd.12296

DeSantis, T.Z., Hugenholtz, P., Larsen, N., Rojas, M., Brodie, E.L., Keller, K., Huber, T., Dalevi, D., Hu, P., Andersen, G.L., 2006. Greengenes, a Chimera-Checked 16S rRNA Gene Database and Workbench Compatible with ARB. Appl. Environ. Microbiol. 72, 5069–5072. https://doi.org/10.1128/AEM.03006-05

Dijkshoorn, L., Nemec, A., Seifert, H., 2007. An increasing threat in hospitals: multidrug-resistant Acinetobacter baumannii. Nat. Rev. Microbiol. 5, 939–951. https://doi.org/10.1038/nrmicro1789

Dodt, M., Roehr, J.T., Ahmed, R., Dieterich, C., 2012. FLEXBAR-Flexible Barcode and Adapter Processing for Next-Generation Sequencing Platforms. Biology 1, 895–905. https://doi.org/10.3390/biology1030895

Dowd, S.E., Wolcott, R.D., Sun, Y., McKeehan, T., Smith, E., Rhoads, D., 2008. Polymicrobial nature of chronic diabetic foot ulcer biofilm infections determined using bacterial tag encoded FLX amplicon pyrosequencing (bTEFAP). PloS One 3, e3326. https://doi.org/10.1371/journal.pone.0003326

Driver, V.R., Fabbi, M., Lavery, L.A., Gibbons, G., 2010. The costs of diabetic foot: the economic case for the limb salvage team. J. Am. Podiatr. Med. Assoc. 100, 335–341. https://doi.org/10.7547/1000335

Emrich, L.J., Shlossman, M., Genco, R.J., 1991. Periodontal disease in non-insulin-dependent diabetes mellitus. J. Periodontol. 62, 123–131. https://doi.org/10.1902/jop.1991.62.2.123

Erben, N., Ozgunes, I., Aksit, F., Doyuk Kartal, E., Colak, E., Usluer, G., 2013. Healthcare-associated infections and the distribution of causative pathogens in patients with diabetes mellitus. Eur. J. Clin. Microbiol. Infect. Dis. Off. Publ. Eur. Soc. Clin. Microbiol. 32, 821–825. https://doi.org/10.1007/s10096-013-1816-x

Eren, A.M., Borisy, G.G., Huse, S.M., Mark Welch, J.L., 2014. Oligotyping analysis of the human oral microbiome. Proc. Natl. Acad. Sci. U. S. A. 111, E2875-2884. https://doi.org/10.1073/pnas.1409644111

Eren, A.M., Morrison, H.G., Lescault, P.J., Reveillaud, J., Vineis, J.H., Sogin, M.L., 2015. Minimum entropy decomposition: unsupervised oligotyping for sensitive partitioning

of high-throughput marker gene sequences. ISME J. 9, 968–979. https://doi.org/10.1038/ismej.2014.195

Escapa, I.F., Chen, T., Huang, Y., Gajare, P., Dewhirst, F.E., Lemon, K.P., 2018. New Insights into Human Nostril Microbiome from the Expanded Human Oral Microbiome Database (eHOMD): a Resource for the Microbiome of the Human Aerodigestive Tract. mSystems 3, e00187-18, /msystems/3/6/msys.00187-18.atom. https://doi.org/10.1128/mSystems.00187-18

Faith, D.P., 1992. Conservation evaluation and phylogenetic diversity. Biol. Conserv. 61, 1–10. https://doi.org/10.1016/0006-3207(92)91201-3

Feng, S., Yu, H., Yu, Y., Geng, Y., Li, D., Yang, C., Lv, Q., Lu, L., Liu, T., Li, G., Yuan, L., 2018. Levels of Inflammatory Cytokines IL-1 β , IL-6, IL-8, IL-17A, and TNF- α in Aqueous Humour of Patients with Diabetic Retinopathy. J. Diabetes Res. 2018, 1–6. https://doi.org/10.1155/2018/8546423

Ferlita, S., Yegiazaryan, A., Noori, N., Lal, G., Nguyen, T., To, K., Venketaraman, V., 2019. Type 2 Diabetes Mellitus and Altered Immune System Leading to Susceptibility to Pathogens, Especially Mycobacterium tuberculosis. J. Clin. Med. 8. https://doi.org/10.3390/jcm8122219

Freire, M.O., Dalli, J., Serhan, C.N., Van Dyke, T.E., 2017. Neutrophil Resolvin E1 Receptor Expression and Function in Type 2 Diabetes. J. Immunol. Baltim. Md 1950 198, 718–728. https://doi.org/10.4049/jimmunol.1601543

Freire, M.O., Van Dyke, T.E., 2013. Natural resolution of inflammation. Periodontol. 2000 63, 149–164. https://doi.org/10.1111/prd.12034

Furniss, D., Gore, S., Azadian, B., Myers, S.R., 2005. Acinetobacter infection is associated with acquired glucose intolerance in burn patients. J. Burn Care Rehabil. 26, 405–408. https://doi.org/10.1097/01.bcr.0000176882.69354.7e

Gardner, S.E., Hillis, S.L., Heilmann, K., Segre, J.A., Grice, E.A., 2013. The neuropathic diabetic foot ulcer microbiome is associated with clinical factors. Diabetes 62, 923–930. https://doi.org/10.2337/db12-0771

Genco, R.J., Graziani, F., Hasturk, H., 2020. Effects of periodontal disease on glycemic control, complications, and incidence of diabetes mellitus. Periodontol. 2000 83, 59–65. https://doi.org/10.1111/prd.12271

Gerner-Smidt, P., Tjernberg, I., 1993. Acinetobacter in Denmark: II. Molecular studies of the Acinetobacter calcoaceticus-Acinetobacter baumannii complex. APMIS Acta Pathol. Microbiol. Immunol. Scand. 101, 826–832.

Gootz, T.D., Marra, A., 2008. Acinetobacter baumannii: an emerging multidrug-resistant threat. Expert Rev. Anti Infect. Ther. 6, 309–325. https://doi.org/10.1586/14787210.6.3.309

Griffen, A.L., Beall, C.J., Campbell, J.H., Firestone, N.D., Kumar, P.S., Yang, Z.K., Podar, M., Leys, E.J., 2012. Distinct and complex bacterial profiles in human periodontitis and health revealed by 16S pyrosequencing. ISME J. 6, 1176–1185. https://doi.org/10.1038/ismej.2011.191

Hajishengallis, G., Lamont, R.J., 2012. Beyond the red complex and into more complexity: the polymicrobial synergy and dysbiosis (PSD) model of periodontal disease etiology. Mol. Oral Microbiol. 27, 409–419. https://doi.org/10.1111/j.2041-1014.2012.00663.x

Henig, O., Pogue, J.M., Martin, E., Hayat, U., Ja'ara, M., Kilgore, P.E., Cha, R., Dhar, S., Kaye, K.S., 2020. The Impact of Multidrug-Resistant Organisms on Outcomes in Patients

With Diabetic Foot Infections. Open Forum Infect. Dis. 7, ofaa161. https://doi.org/10.1093/ofid/ofaa161
Irfan, U.M., Dawson, D.V., Bissada, N.F., 2001. Epidemiology of periodontal disease: a review and clinical perspectives. J. Int. Acad. Periodontol. 3, 14–21.
Kennedy, K., Hall, M.W., Lynch, M.D.J., Moreno-Hagelsieb, G., Neufeld, J.D., 2014. Evaluating Bias of Illumina-Based Bacterial 16S rRNA Gene Profiles. Appl. Environ. Microbiol. 80, 5717–5722. https://doi.org/10.1128/AEM.01451-14
Kim, D., Hofstaedter, C.E., Zhao, C., Mattei, L., Tanes, C., Clarke, E., Lauder, A., Sherrill-Mix, S., Chehoud, C., Kelsen, J., Conrad, M., Collman, R.G., Baldassano, R., Bushman, F.D., Bittinger, K., 2017. Optimizing methods and dodging pitfalls in microbiome research. Microbiome 5, 52. https://doi.org/10.1186/s40168-017-0267-5
Kim, E.J., Ha, K.H., Kim, D.J., Choi, Y.H., 2019. Diabetes and the Risk of Infection: A National Cohort Study. Diabetes Metab. J. 43, 804–814. https://doi.org/10.4093/dmj.2019.0071
Kleinstein, Sarah E, McCorrison, J., Ahmed, A., Hasturk, H., Dyke, T.E.V., Freire, M., 2020. Transcriptomics of Type 2 Diabetic and Healthy Human Neutrophils (preprint). In Review. https://doi.org/10.21203/rs.2.21951/v1
Kleinstein, S.E., Nelson, K.E., Freire, M., 2020. Inflammatory Networks Linking Oral Microbiome with Systemic Health and Disease. J. Dent. Res. 99, 1131–1139. https://doi.org/10.1177/0022034520926126
Kruskal, W.H., Wallis, W.A., 1952. Use of Ranks in One-Criterion Variance Analysis. J. Am. Stat. Assoc. 47, 583–621. https://doi.org/10.1080/01621459.1952.10483441
Leão, A.C.Q., Menezes, P.R., Oliveira, M.S., Levin, A.S., 2016. Acinetobacter spp. are associated with a higher mortality in intensive care patients with bacteremia: a survival analysis. BMC Infect. Dis. 16, 386. https://doi.org/10.1186/s12879-016-1695-8
Leung, C.-H., Liu, C.-P., 2019. Diabetic status and the relationship of blood glucose to mortality in adults with carbapenem-resistant Acinetobacter baumannii complex bacteremia. J. Microbiol. Immunol. Infect. Wei Mian Yu Gan Ran Za Zhi 52, 654–662. https://doi.org/10.1016/j.jmii.2018.06.005
Lockhart, P.B., Durack, D.T., 1999. Oral microflora as a cause of endocarditis and other distant site infections. Infect. Dis. Clin. North Am. 13, 833–850, vi. https://doi.org/10.1016/s0891-5520(05)70111-2
Mann, J., Bernstein, Y., Findler, M., 2020. Periodontal disease and its prevention, by traditional and new avenues. Exp. Ther. Med. 19, 1504–1506. https://doi.org/10.3892/etm.2019.8381
McDonald, H.I., Nitsch, D., Millett, E.R.C., Sinclair, A., Thomas, S.L., 2014. New estimates of the burden of acute community-acquired infections among older people with diabetes mellitus: a retrospective cohort study using linked electronic health records. Diabet. Med. J. Br. Diabet. Assoc. 31, 606–614. https://doi.org/10.1111/dme.12384
Moore, B.B., Kunkel, S.L., 2019. Attracting Attention: Discovery of IL-8/CXCL8 and the Birth of the Chemokine Field. J. Immunol. 202, 3–4. https://doi.org/10.4049/jimmunol.1801485
National Diabetes Statistics Report | Data & Statistics | Diabetes | CDC [WWW Document], 2020. URL https://www.cdc.gov/diabetes/data/statistics/statistics-report.html (accessed 7.24.20).

NCBI Resource Coordinators, 2018. Database resources of the National Center for Biotechnology Information. Nucleic Acids Res. 46, D8–D13. https://doi.org/10.1093/nar/gkx1095

Nowicki, E.M., Shroff, R., Singleton, J.A., Renaud, D.E., Wallace, D., Drury, J., Zirnheld, J., Colleti, B., Ellington, A.D., Lamont, R.J., Scott, D.A., Whiteley, M., 2018. Microbiota and Metatranscriptome Changes Accompanying the Onset of Gingivitis. mBio 9. https://doi.org/10.1128/mBio.00575-18

Parahitiyawa, N.B., Jin, L.J., Leung, W.K., Yam, W.C., Samaranayake, L.P., 2009. Microbiology of odontogenic bacteremia: beyond endocarditis. Clin. Microbiol. Rev. 22, 46–64, Table of Contents. https://doi.org/10.1128/CMR.00028-08

Peiró, C., Lorenzo, Ó., Carraro, R., Sánchez-Ferrer, C.F., 2017. IL-1β Inhibition in Cardiovascular Complications Associated to Diabetes Mellitus. Front. Pharmacol. 8, 363. https://doi.org/10.3389/fphar.2017.00363

Peleg, A.Y., Seifert, H., Paterson, D.L., 2008. Acinetobacter baumannii: emergence of a successful pathogen. Clin. Microbiol. Rev. 21, 538–582. https://doi.org/10.1128/CMR.00058-07

Pessoa, L., Aleti, G., Choudhury, S., Nguyen, D., Yaskell, T., Zhang, Y., Li, W., Nelson, K.E., Neto, L.L.S., Sant'Ana, A.C.P., Freire, M., 2019. Host-Microbial Interactions in Systemic Lupus Erythematosus and Periodontitis. Front. Immunol. 10, 2602. https://doi.org/10.3389/fimmu.2019.02602

Pielou, E.C., 1966. The measurement of diversity in different types of biological collections. J. Theor. Biol. 13, 131–144. https://doi.org/10.1016/0022-5193(66)90013-0

Pollock, J., Glendinning, L., Wisedchanwet, T., Watson, M., 2018. The Madness of Microbiome: Attempting To Find Consensus "Best Practice" for 16S Microbiome Studies. Appl. Environ. Microbiol. 84, e02627-17, /aem/84/7/e02627-17.atom. https://doi.org/10.1128/AEM.02627-17

Qiu, H., KuoLee, R., Harris, G., Chen, W., 2009. High susceptibility to respiratory Acinetobacter baumannii infection in A/J mice is associated with a delay in early pulmonary recruitment of neutrophils. Microbes Infect. 11, 946–955. https://doi.org/10.1016/j.micinf.2009.06.003

Quast, C., Pruesse, E., Yilmaz, P., Gerken, J., Schweer, T., Yarza, P., Peplies, J., Glöckner, F.O., 2013. The SILVA ribosomal RNA gene database project: improved data processing and web-based tools. Nucleic Acids Res. 41, D590-596. https://doi.org/10.1093/nar/gks1219

Reiber, G.E., Lipsky, B.A., Gibbons, G.W., 1998. The burden of diabetic foot ulcers. Am. J. Surg. 176, 5S-10S. https://doi.org/10.1016/s0002-9610(98)00181-0

Roberts, F.A., Darveau, R.P., 2015. Microbial protection and virulence in periodontal tissue as a function of polymicrobial communities: symbiosis and dysbiosis. Periodontol. 2000 69, 18–27. https://doi.org/10.1111/prd.12087

Salter, S.J., Cox, M.J., Turek, E.M., Calus, S.T., Cookson, W.O., Moffatt, M.F., Turner, P., Parkhill, J., Loman, N.J., Walker, A.W., 2014. Reagent and laboratory contamination can critically impact sequence-based microbiome analyses. BMC Biol. 12, 87. https://doi.org/10.1186/s12915-014-0087-z

Segata, N., Izard, J., Waldron, L., Gevers, D., Miropolsky, L., Garrett, W.S., Huttenhower, C., 2011. Metagenomic biomarker discovery and explanation. Genome Biol. 12, R60. https://doi.org/10.1186/gb-2011-12-6-r60

Shannon, C.E., Weaver, W., 1975. The mathematical theory of communication. University of Illinois Press, Urbana.

Simpson, E.H., 1949. Measurement of Diversity. Nature 163, 688–688. https://doi.org/10.1038/163688a0

Sinha, R., Abnet, C.C., White, O., Knight, R., Huttenhower, C., 2015. The microbiome quality control project: baseline study design and future directions. Genome Biol. 16, 276. https://doi.org/10.1186/s13059-015-0841-8

Socransky, S.S., Haffajee, A.D., Cugini, M.A., Smith, C., Kent, R.L., 1998. Microbial complexes in subgingival plaque. J. Clin. Periodontol. 25, 134–144. https://doi.org/10.1111/j.1600-051x.1998.tb02419.x

Stackebrandt, E., Goodfellow, M. (Eds.), 1991. Nucleic acid techniques in bacterial systematics, Modern microbiological methods. Wiley, Chichester ; New York.

Tisoncik, J.R., Korth, M.J., Simmons, C.P., Farrar, J., Martin, T.R., Katze, M.G., 2012. Into the eye of the cytokine storm. Microbiol. Mol. Biol. Rev. MMBR 76, 16–32. https://doi.org/10.1128/MMBR.05015-11

Turner, S., Pryer, K.M., Miao, V.P., Palmer, J.D., 1999. Investigating deep phylogenetic relationships among cyanobacteria and plastids by small subunit rRNA sequence analysis. J. Eukaryot. Microbiol. 46, 327–338. https://doi.org/10.1111/j.1550-7408.1999.tb04612.x

Vardakas, K.Z., Siempos, I.I., Falagas, M.E., 2007. Diabetes mellitus as a risk factor for nosocomial pneumonia and associated mortality. Diabet. Med. J. Br. Diabet. Assoc. 24, 1168–1171. https://doi.org/10.1111/j.1464-5491.2007.02234.x

Vázquez-López, R., Solano-Gálvez, S.G., Juárez Vignon-Whaley, J.J., Abello Vaamonde, J.A., Padró Alonzo, L.A., Rivera Reséndiz, A., Muleiro Álvarez, M., Vega López, E.N., Franyuti-Kelly, G., Álvarez-Hernández, D.A., Moncaleano Guzmán, V., Juárez Bañuelos, J.E., Marcos Felix, J., González Barrios, J.A., Barrientos Fortes, T., 2020. Acinetobacter baumannii Resistance: A Real Challenge for Clinicians. Antibiot. Basel Switz. 9. https://doi.org/10.3390/antibiotics9040205

Villar, M., Cano, M.E., Gato, E., Garnacho-Montero, J., Miguel Cisneros, J., Ruíz de Alegría, C., Fernández-Cuenca, F., Martínez-Martínez, L., Vila, J., Pascual, A., Tomás, M., Bou, G., Rodríguez-Baño, J., GEIH/GEMARA/REIPI-Ab20101 Group, 2014. Epidemiologic and clinical impact of Acinetobacter baumannii colonization and infection: a reappraisal. Medicine (Baltimore) 93, 202–210. https://doi.org/10.1097/MD.0000000000000036

Whiting, D.R., Guariguata, L., Weil, C., Shaw, J., 2011. IDF diabetes atlas: global estimates of the prevalence of diabetes for 2011 and 2030. Diabetes Res. Clin. Pract. 94, 311–321. https://doi.org/10.1016/j.diabres.2011.10.029

Wu, C.-Z., Yuan, Y.-H., Liu, H.-H., Li, S.-S., Zhang, B.-W., Chen, W., An, Z.-J., Chen, S.-Y., Wu, Y.-Z., Han, B., Li, C.-J., Li, L.-J., 2020. Epidemiologic relationship between periodontitis and type 2 diabetes mellitus. BMC Oral Health 20, 204. https://doi.org/10.1186/s12903-020-01180

CHAPTER 3: Mechanisms underlying proximity between oral commensal bacteria

Manuscript

Currently in review at The ISME Journal. *June 2021*

Dasith Perera[1], [2]Anthony McLean, [2]Viviana Morillo Lopez, [1]Kaileigh Cloutier-Le-blanc, [1]Eric Almeida, [1]Kiana Cabana, [2]Jessica Mark Welch, [1]Matthew Ramsey1

1. The University of Rhode Island, Department of Cell and Molecular Biology, Kingston, RI 02881, USA.
2. Marine Biological Laboratory, Woods Hole, MA 02543

Mechanisms underlying proximity between oral commensal bacteria

Authors: [1]Dasith Perera, [2]Anthony McLean, [2]Viviana Morillo Lopez, [1]Kaileigh Cloutier-Leblanc, [1]Eric Almeida, [1]Kiana Cabana, [2]Jessica Mark Welch, [1]Matthew Ramsey*

Institutional Affiliations: [1]The University of Rhode Island, Kingston, RI 02881; [2]Marine Biological Laboratory, Woods Hole, MA 02543

*Corresponding author: 120 Flagg Rd. Kingston, RI 02881, 401-874-9505, mramsey@uri.edu

Competing Interests: none

Abstract

Complex polymicrobial biofilm communities are abundant in nature particularly in the human oral cavity where their composition and fitness can affect health. While the study of these communities during disease is essential and prevalent, little is known about interactions within the healthy plaque community. Here we describe interactions between two of the most abundant species in this healthy microbiome, *Haemophilus parainfluenzae* and *Streptococcus mitis*. We discovered that *H. parainfluenzae* typically exists adjacent to Mitis group streptococci *in vivo* which it also positively correlated with based on microbiome data. By comparing *in vitro* coculture data to *ex vivo* microscopy, we revealed that this co-occurrence is density dependent and further influenced by H_2O_2 production. We discovered that *H. parainfluenzae* utilizes a more redundant, multifactorial response to H_2O_2 than related organisms and that this system's integrity enhances streptococcal fitness. Our results indicate that Mitis group streptococci are likely the *in vivo* source of NAD for *H. parainfluenzae* and also evoke patterns of carbon utilization *in vitro* for *H. parainfluenzae* similar to those observed *in vivo*. Our findings describe mechanistic interactions between two of the most abundant and prevalent members of healthy supragingival plaque that contribute to their *in vivo* survival.

Introduction

Taxon-taxon interactions are of great importance for understanding the structure and function of natural biofilms. Many bacteria occur in nature as part of complex polymicrobial biofilms (1). The behavior of individual species within these biofilms is elaborate and likely influenced by the spatial organization between physical and chemical substrates (1,2) produced by distinct species (3–5). Metagenomic and metatranscriptome techniques give us an unprecedented ability to observe group composition and behaviors, but cannot resolve which species might be influencing one another nor describe their spatial interactions. Metabolite-based interactions can influence community composition through cross feeding or trophic interactions (6,7), complementation of auxotrophies (8) as well as competition for nutrients and production of inhibitory substances (9–12). These types of polymicrobial associations have been shown to enhance the resiliency, fitness, and stability of these communities (4,13,14). Maintaining stable oral microbial communities can preserve oral health, thus there is a clear need to identify the interactions between prominent species in host-associated polymicrobial communities and how they might shape not only constituency but physical structure.

To delve into mechanisms underlying taxon-taxon interactions we chose to study the naturally occurring biofilm of human dental plaque. The human supragingival plaque (SUPP) biofilm has been long studied, dating to the very 1st microscopy observations of Antony von Leeuwenhoek in 1683 (ref. 15). Early work on both subgingival plaque and SUPP structure was aided by the study of physical aggregation between species from

these environments (16) generating hypotheses about direct interaction and assembly of plaque structures. Recently, much more detailed biogeography of SUPP structure was observed (17). One notable association was between *Streptococcus* and other genera at the margins of biofilm structures. Streptococci can influence community interactions due to their ability to rapidly consume carbohydrates, produce large amounts of acidic fermentation products, and excrete antimicrobial substances including reactive oxygen species. These properties can support the growth of some species while excluding others (9,18–20). Many oral *Streptococcus spp.* including Mitis group members are known to produce various anti-microbial substances, including hydrogen peroxide (H_2O_2) in aerobic conditions. Therefore, any bacterium adjacent to these *Streptococcus spp.* aerobically would need to have adapted the ability to withstand H_2O_2 (7,21). Alongside *Streptococcus* species within the Mitis group (*S. mitis, S. oralis, S. australis*, *S. infantis*, and others)*, Haemophilus parainfluenzae* is one of the most abundant and prevalent species in the SUPP of healthy individuals (22–26). Whilst frequently characterized as an opportunistic pathogen and implicated in diseases including endocarditis (27), in the oral cavity *H. parainfluenzae* is a commensal and is associated with beneficial immunomodulatory effects (28).

To identify mechanisms of interaction that take place within this healthy polymicrobial biofilm we investigated interactions between two of its most abundant members, *H. parainfluenzae* and *S. mitis*. Despite the frequent co-occurrence of these species in proximity *in vivo*, little is known about both the spatial relationship and metabolic mechanisms of interactions between these species. In this study, we observed that these taxa

exist in intimate proximity in SUPP and exhibit localized density dependences that also exist *in vitro* which are driven by streptococcal H_2O_2 production. We also discovered a highly redundant H_2O_2 resistance system in *H. parainfluenzae* that is different from other *Haemophilus* species. We then observed multiple mechanisms of *H. parainfluenzae* interaction including NAD auxotrophy complementation by Mitis group streptococci and the upregulation of alternative carbon and energy pathways during *in vitro* coculture that are also observed in *in vivo* gene expression data. These results provide a robust characterization of *H. parainfluenzae'*s role in the oral microbiota and reveal ways it has evolved to exist alongside streptococci in the oral cavity and likely beyond. This study details interactions between two prominent members of a complex natural biofilm community and allows us to demonstrate mechanisms of interaction that likely help drive micron-scale arrangements between these organisms.

Results

H. parainfluenzae co-occurs with S. mitis and related streptococci in human supragingival plaque

To determine which species *H. parainfluenzae* was most likely to interact with we used microbiome data from 117 subjects sampled by the Human Microbiome Project (HMP). Analysis of HMP species-assigned metagenomic data indicated that *H. parainfluenzae* is an abundant and prevalent member of SUPP detected in all 117 subjects averaging

7.6% relative abundance based on sequence reads (Fig. 1). We compared the upper quartile (n=29) of these subjects ranked by highest *H. parainfluenzae* abundance to the remainder of subjects (n=88) via LEfSe analysis (29) to determine which species were significantly likely to co-occur with *H. parainfluenzae* (Fig. 1). Interestingly, this indicated that individuals enriched in *H. parainfluenzae* have abundant *Streptococcus* sp. especially those in the Mitis group. These data were what led us to investigate *H. parainfluenzae* interactions with *S. mitis* as a Mitis group representative in order to examine the mechanisms of taxon-taxon interactions.

Species-specific FISH demonstrates frequent H. parainfluenzae - S. mitis co-proximity

To determine whether the large-scale co-occurrence of *H. parainfluenzae* and *S. mitis* was reflected in micrometer-scale spatial structure, we analyzed the organization of these two taxa using fluorescence *in situ* hybridization (FISH) and imaging. Within the supragingival plaque, *S. mitis* and related streptococci are frequent features of *H. parainfluenzae*'s micron-scale environment. Visualizing these species with FISH probes showed that 92% of *H. parainfluenzae* cells in supragingival plaque are located within 10 μm of cells labeled with a probe that hybridizes with a group of related streptococci including *S. mitis, S. oralis,* and *S. infantis* (Fig. 2A, Table S10, hereafter referred to as "*S. mitis*"). The median distance separating a *H. parainfluenzae* cell from the nearest *S. mitis* cell was 1.14 μm. Thus, most cells of *H. parainfluenzae* co-occur with *S. mitis* at micrometer scales.

In addition to proximity, images suggested a density-dependent relationship between these two taxa, with reduced densities of *H. parainfluenzae* in areas with the highest densities of *S. mitis* (Fig. 2C). We quantified this density effect by dividing each image into 1024 blocks of approximately 6 micrometers on a side (Fig. 2D) and measuring the density of *S. mitis*, *H. parainfluenzae*, and total bacteria within each block. The mean density of *H. parainfluenzae* increased as the percent of a block covered by *S. mitis* increased from 0 to around 20% (Fig. S1). This trend is likely due, at least in part, to variation in the overall quantity of plaque in each block because the density of each taxon has a positive linear relationship with the overall plaque density. As the density of *S. mitis* increased above 20%, the mean *H. parainfluenzae* density decreased, suggesting a density-dependent inhibitory effect of *S. mitis* on *H. parainfluenzae* growth. Given that both microbiome sequencing and microscopy imaging of *in vivo* supragingival plaque samples indicate significant co-occurrence and co-proximity between *H. parainfluenzae* and *S. mitis* (Fig. 1,2), it is important to determine the mechanisms that underlie these observations.

S. mitis eliminates H. parainfluenzae via production of H_2O_2

Culturing these two taxa together under controlled conditions in vitro revealed a dose-dependent interaction: *H. parainfluenzae* was killed by *S. mitis*, but only when abundance of *S. mitis* was high relative to that of *H. parainfluenzae*. We used a colony biofilm model (30,31) in which polycarbonate membranes were inoculated with *S. mitis*

and *H. parainfluenzae*, either separately or together, and permitted to grow for 24 hours; cell abundance was then assessed by resuspending the cells and plating for colony counts (see Methods). Cocultures inoculated at equal densities revealed that *S. mitis* reduced *H. parainfluenzae* numbers (Fig. 3) nearly 100-fold below inoculum density, indicating active killing. This effect is dose-dependent as we observed a significant reduction in the growth yield of *H. parainfluenzae* compared to monoculture when inoculums of *S. mitis* were either equivalent or 3-fold greater than *H. parainfluenzae*. However, when *S. mitis* inoculum was 10-fold lower than *H. parainfluenzae*, there was no significant change in the growth yield of *H. parainfluenzae* compared to monoculture.

The mechanism of dose-dependent killing of *H. parainfluenzae* involves H_2O_2 production by *S. mitis*. The reduction of *H. parainfluenzae* numbers in coculture was abolished if the cocultured strain of *S. mitis* lacked pyruvate oxidase (Δ*spxB*) and thus unable to produce H_2O_2. Figure 3 demonstrates that *H. parainfluenzae* growth yield when cocultured with *S. mitis* Δ*spxB* is not significantly different from *H. parainfluenzae* monoculture at any ratio tested, indicating that *S. mitis*-produced H_2O_2 is responsible for *H. parainfluenzae* inhibition. Additional coculture experiments indicate that *H. parainfluenzae* was unable to grow in pH neutralized supernatants of *S. mitis* unless they were pre-treated with exogenous catalase (data not shown), further supporting the finding that H_2O_2 production limits *H. parainfluenzae* growth in these conditions and that acid production is not sufficient to inhibit *H. parainfluenzae*. Thus, our observed density-dependent exclusion of *H. parainfluenzae* by *S. mitis* in *ex-vivo* samples (Fig. 2) can be explained by H_2O_2 toxicity.

Although the density-dependent killing of *H. parainfluenzae* by *S. mitis* implies an antagonistic interaction, the presence of *H. parainfluenzae* enhances *S. mitis* growth yield in biofilm coculture (Fig. S2). This enhancement was abolished when *S. mitis* was cocultured with *H. parainfluenzae* Δ*oxyR* but not with other catalase or cytochrome peroxidase mutants either individual or combined (Fig. S2A). The addition of exogenous catalase elevated *S. mitis* monoculture yields near to those observed in coculture without catalase which suggests that H_2O_2 detoxification is primarily responsible for this enhanced yield (Fig. S2B). However, a >10-fold yield enhancement was still observed in coculture with *H. parainfluenzae* supplemented with exogenous catalase indicating further interactions that benefit *S. mitis* fitness. The role of H_2O_2 decomposition in *S. mitis* yield increase was further confirmed when comparing mono vs coculture of *S. mitis* vs its *ΔspxB* mutant where the mutant demonstrated greater yield in monoculture and coculture vs the wild-type with a modest increase coculture yield (Fig. S2C) reminiscent of the wild-type coculture with exogenous catalase.

Individual H_2O_2 sensitive genes do not affect the fitness of H. parainfluenzae in coculture with S. mitis

The presence of *S. mitis* within a few micrometers of most *H. parainfluenzae* cells in natural plaque suggests that H_2O_2 and other inhibitory or promotive compounds excreted by *S. mitis* are reasonably expected to perfuse the substrate in which most *H. parainfluenzae* grow (32). We investigated the growth effects of known H_2O_2 relevant

gene products in *H. parainfluenzae* by constructing gene deletions and assessing the fitness of the deletion strains after H_2O_2 exposure. Genes in *H. parainfluenzae* relevant to peroxide metabolism include *oxyR* whose gene product is a global transcriptional regulator responsive to H_2O_2. Also present is a single catalase (*katA*) essential for H_2O_2 resistance in *H. influenzae* (33). Additionally, *H. parainfluenzae* possesses a cytochrome c peroxidase (*ccp*), orthologs of which are important for peroxide resistance in other *Pasteurellaceae* (34), *Campylobacter jejuni* (35), and *H. influenzae* (36). We also made deletions of the peroxiredoxin (*prx*), peroxiredoxin-glutaredoxin (*pdgX*) and glucose-6-phosphate dehydrogenase (*g6p*) genes known to contribute to oxidative stress protection in *H. influenzae* and other species (37–40).

We quantified changes in H_2O_2 resistance by a zone of inhibition assay (Fig. 4A), in which an agar plate inoculated with a lawn of wild-type or deletion-strain *H. parainfluenzae* is exposed to a small filter saturated with H_2O_2 and sensitivity is measured as the diameter of the zone of inhibition. As expected, the largest increase in sensitivity was observed in *H. parainfluenzae* with deletions of the global H_2O_2-responsive transcriptional regulator Δ*oxyR*, while all other individual gene deletion mutants were less sensitive to H_2O_2. A Δ*katA*+Δ*ccp* double mutant demonstrated a significant increase in sensitivity compared to individual mutants, indicating a combinatorial effect of these gene products. Surprisingly, MIC concentrations for many mutants were minor and nearly identical (Table S1) indicating that individual contributions of these genes to H_2O_2 tolerance are minimal. We next used the colony biofilm model to test the fitness of each mutant in coculture with H_2O_2-producing *S. mitis* (Fig. 4B). OxyR was shown

to be essential for *H. parainfluenzae* survival in coculture, while deletion of individual genes typically controlled by OxyR showed no significant difference compared to wildtype which contrasts greatly to similar mutants in *H. influenzae* (*katA*) (33) and other species (41–43). However, the Δ*katA*+Δ*ccp* mutants' growth yield was significantly inhibited in *S. mitis* coculture again indicating an additive effect of these gene products on H_2O_2 resistance. These data demonstrate that the mechanism of *H. parainfluenzae* resistance to H_2O_2 involves a complex multifactorial system unlike other *Haemophilus* spp. yet characterized.

S. mitis and other Streptococcus sp. support H. parainfluenzae growth

Like other *Haemophilus sp.*, *H. parainfluenzae* is a NAD auxotroph and must obtain NAD, nicotinamide mononucleotide (NMN) or nicotinamide riboside (NR) from the host or other microorganisms (44). We found that human saliva was unable to support *H. parainfluenzae* growth unless NAD was added (data not shown) suggesting that adjacent microbes are the source of NAD for *H. parainfluenzae* in the oral cavity. As *Corynebacterium* and *Streptococcus* are two of the most abundant genera in SUPP, we tested if species from these genera could complement NAD auxotrophy. Spot assays on *H. parainfluenzae* lawns on medium lacking NAD showed robust growth of *H. parainfluenzae* adjacent to *S. mitis* and *S. sanguinis* but no other taxa (Fig. 5). These data demonstrate that *H. parainfluenzae* obtains NAD from these taxa when they are in close

proximity. It is notable that the two species that significantly correlate with *H. parainfluenzae* in microbiome data (Fig. 1) also enhance its growth most strongly in the absence of NAD compared to other *Streptococcus* spp.

In vitro transcriptional responses of H. parainfluenzae to S. mitis

Transcriptome analysis of *H. parainfluenzae* in aerobic coculture with *S. mitis* indicated a multifaceted response to oxidative stress. We observed that *H. parainfluenzae* significantly differentially expressed 387 genes greater than 2-fold in coculture (Tables S2&S3), compared to monoculture. Surprisingly, the differentially expressed genes did not include catalase; however, based on transcript abundance catalase is well expressed under both conditions. Among genes typically involved in oxidative stress responses, *dps*, which encodes an iron sequestration protein, had a 2.2-fold increase in coculture suggesting that *H. parainfluenzae* is sequestering free intracellular Fe^{2+}, to prevent oxidative damage. Surprisingly however, several other genes involved in H_2O_2 were repressed in coculture, including *ccp, pdgX,* thioredoxin (*trxA*), glutaredoxin (*grx*) and thiol peroxidase (*tsa*), demonstrating the complex nature of the oxidative stress response in this species. *H. parainfluenzae* stress responses were induced in coculture, likely due to H_2O_2–related damage by *S. mitis*. We observed modest but significant upregulation of the *hfq* chaperone encoding gene, universal stress protein E (*uspE*) and repression of *lexA*. LexA is involved in the repression of genes involved in the SOS response of *E. coli* (44). Hfq is known to be involved in the stress responses of many species (45). Paralogs of the Universal stress proteins including *uspE*, are known to be involved in response to DNA damage (46). Genes likely involved in DNA repair are also induced

in coculture including those encoding DNA ligase, exodeoxyribonuclease V beta chain and endonuclease V.

Streptococcus spp. are known to rapidly consume carbohydrates, and transcriptional data suggest that *H. parainfluenzae* in coculture switches from carbohydrate consumption to alternative sources of carbon and energy. There was increased expression of genes suggesting the breakdown of glycerophospholipids resulting in the uptake and utilization of glycerol, including the predicted extracellular patatin-like phospholipase (2.5-fold), lysophospholipase L2 (3.8-fold), glycerol uptake facilitator protein (5.3-fold), glycerol kinase (3.4-fold), and a fatty acid degradation regulator (2.1-fold). Additionally, there was an increase in expression of fructose 1,6 bisphosphatase (2.8-fold), indicating active gluconeogenesis, consistent with *H. parainfluenzae* growth on 3-carbon intermediates such as glycerol. There was also evidence of the uptake and catabolism of the sialic acid, N-acetylneuraminic acid as suggested by an increase in expression of SHS family sialic acid transporter (2-fold), sialic acid utilization regulator (3.6-fold), N-acetylneuraminate lyase (2-fold), N-acetylmannosamine kinase (3.8-fold), and N-acetylmannosamine-6-phosphate 2-epimerase (3.1-fold). Lastly, there was an increase in the expression of genes involved in the oligopeptide transport system, *oppA* (3-fold), *oppB* (2.2-fold), *oppC* (2.3-fold), *oppD* (2.7-fold), and *oppF* (2.4-fold). These data together suggest uptake of alternate carbon and energy sources in coculture. *S. mitis* transcriptional responses to *H. parainfluenzae* are the focus of a separate study.

In vivo transcriptional responses of H. parainfluenzae vs in vitro

We hypothesized that *in vivo* gene expression of *H. parainfluenzae* is largely influenced by *S. mitis* due to their *in vivo* proximity (Fig. 2) and that our *in vitro* coculture data may be predictive of *H. parainfluenzae* behavior *in vivo*. To quantify this, we compared *in vitro H. parainfluenzae* transcriptomes to two separate *in vivo* metatranscriptome datasets from healthy SUPP (47,48). We aligned metatranscriptomes to the *H. parainfluenzae* genome generating a dataset of *H. parainfluenzae* transcription within the complex plaque biofilm. We then compared these samples to our *in vitro* monoculture and then determined which genes differentially expressed *in vivo* are also expressed in *in vitro* coculture.

Comparing significantly differentially expressed gene patterns shared between all 3 datasets (*in vitro* coculture and both *in vivo* metatranscriptomes) we observed that 18 genes were mutually upregulated including genes involved in glycerol catabolism, gluconeogenesis, and pili biogenesis (Table S4). We also observed 22 genes that were mutually downregulated including those involved in stringent response, methionine metabolism, and *fur* (Table S5, Fig. 6B). In individual metatranscriptome comparisons we saw even more genes that were significantly differentially expressed in the presence of *S. mitis in vitro*. This included repression of *ccp,* genes involved in methionine metabolism, stringent response, metal transport genes, *fur*, and induction of genes involved in glycerol catabolism, gluconeogenesis, cell stress, DNA damage/repair related pathways, and peptide/oligopeptide transport (Tables S6-S9).

These data suggest that aspects of *H. parainfluenzae* transcriptional responses in SUPP can be recapitulated in *in vitro* coculture with *S. mitis*. One notably absent overlap between *in vitro* cocultures vs *in vivo* datasets was the upregulation of genes involved in lactate oxidation observed *in vivo*. Since most *Streptococcus sp.* produce lactate as a metabolic end product (18), many oral taxa have evolved the ability to utilize lactate as a carbon source. Metatranscriptome data suggests that *H. parainfluenzae* catabolizes lactate *in vivo*, which it did not do in coculture indicating that further carbon source competition and crossfeeding is occurring *in vivo* that did not occur *in vitro* on complex medium. Overall, these data indicate numerous overlaps of *in vitro H. parainfluenzae* transcriptional responses to *S. mitis* that also occur *in vivo* where they exist in close proximity.

Discussion

Our findings reveal multiple factors that can dictate the spatial organization and behavior of two abundant oral commensal bacteria *in vivo*. The availability and distribution of oxygen has been hypothesized to dictate the spatial organization of bacteria within

oral biofilm structures and in mixed communities of soil bacteria, where bacterial respiration creates a reduced environment enabling the growth of strict anaerobes in the biofilm interior (2,17). An important facet of oxygen availability is the production of H_2O_2 by some microbes, which can be an important mechanism of protection against invading or competing species in a variety of environments from the oral cavity (21) to the surface of the oceans (49). Also, the exchange of nutrients including electron donors and cofactors or nutrients between taxa can determine growth and interaction between them (8,50). Here we demonstrate that streptococcal metabolism can dictate both spatial organization and constituency within a naturally occurring multispecies biofilm.

The production of H_2O_2 by early colonizing *Streptococcus sp.* is regarded as an important mechanism of protecting commensals from invading species and is believed to play a role in determining species composition (21). Our *in vitro* findings show that *S. mitis* can inhibit or kill *H. parainfluenzae* in a dose-dependent manner via the production of H_2O_2. This appears to be mirrored in our *in vivo* findings where streptococci seemingly exclude *H. parainfluenzae* above a certain density. We assert that this density dependent interaction between these taxa is important for driving heterogeneity and spatial organization within this complex community.

Given the close association between *H. parainfluenzae* and H_2O_2 producing streptococci we investigated mechanisms of H_2O_2 resistance in *H. parainfluenzae* and demonstrated that it possesses a highly redundant, multifactorial oxidative stress response that sub-

stantially differs from other closely related species, including *H. influenzae*. We demonstrated that while loss of OxyR caused a significant increase in H_2O_2 sensitivity, loss of catalase or other individual gene products that provide H_2O_2 resistance did not (Fig. 4A, Table S1) which directly contrasts with the importance of catalase in *H. influenzae*, whose deletion leads to its inability to survive high concentrations of H_2O_2 (refs. 33,37). Streptococcal H_2O_2 production is thought to provide a competitive advantage *in vivo* and presents a source of stress that coexisting bacterial species must tolerate. This ability to deal with streptococci-produced H_2O_2 has been demonstrated in multiple species (10,21,32,51). Given that *H. parainfluenzae* is found closely associated with *S. mitis* in SUPP and co-occur together in other sites of the oral cavity (52), an intriguing hypothesis is that this redundant system is born from *H. parainfluenzae's* constant proximity to a H_2O_2 producer in multispecies biofilms. Evaluating the regulation of this redundant system is under current investigation by our group. We also noted that the fitness of *S. mitis in vitro* was reduced when cocultured with *H. parainfluenzae* strains impaired in H_2O_2 resistance (Fig. S2) and that when exogenous H_2O_2 detoxification occurred this fitness was restored (Fig. S2B). However, we also observed that *H. parainfluenzae* still further increased *S. mitis* yield when H_2O_2 was not a factor indicating further mutual benefit beyond H_2O_2 responses.

Paradoxically, *H. parainfluenzae* can be inhibited by, but is found adjacent to, *S. mitis*. This could be due to the ability of *S. mitis* to complement the NAD auxotrophy of *H. parainfluenzae*. We observed that abundant SUPP *Corynebacterium spp*. were unable

to restore *H. parainfluenzae'*s growth, but some oral streptococci and *S. mitis* in particular could (Fig. 5) while host saliva could not. Perhaps this explains why 92% of *H. parainfluenzae* cells lie within 10 μm of *S. mitis in vivo* (Fig 2A). It is interesting to note that both *H. parainfluenzae* and *S. mitis* are found as commensals not just in the same sites of the human oral cavity (52), but also in other sites in the nasopharynx (53,54). Thus, *Streptococcus sp.*-produced NAD could, therefore, be an important determinant of *H. parainfluenzae'*s ability to survive and colonize various sites of the human body. While this may appear to be disadvantageous to *H. parainfluenzae*, it is also possible given the ubiquitous nature of Mitis group streptococci in the oral cavity, that *H. parainfluenzae* evolved this auxotrophy due to the constant availability of extracellular NAD. This is reminiscent of other cases in which auxotrophy development confers a fitness advantage (55).

When comparing the *H. parainfluenzae* coculture *in vitro* transcriptome to *in vivo* SUPP metatranscriptomes (Fig. 6) we observed similar patterns of carbon catabolism including the shift from utilization of sugars to small organic acids and alcohols while downregulating genes in the stringent response suggesting greater access to peptides. Given their *in vivo* proximity, it is extremely likely that Mitis group streptococci are what induce these same *H. parainfluenzae* behaviors *in vivo,* highlighting a facet of our reductionist approach that can uniquely explain behaviors in a complex multispecies *in vivo* biofilm. One notable pathway absent from our *in vitro* cocultures was lactate oxidation, which has previously been shown to be critical for co-infection between organisms with

Streptococcus spp. by cross-feeding on this fermentation product (7). *In vivo*, meta-transcriptome data indicated that *H. parainfluenzae* was also upregulating lactate oxidation gene products which would be expected in the more diverse, competitive SUPP environment compared to *in vitro* coculture alone.

H. parainfluenzae and *S. mitis* are found abundantly not just in supragingival plaque but also in other sites of the human oral cavity (26,52). The abundance of these two taxa has been associated with health and their reduction is associated with the development of oral squamous cell carcinomas (24,56). Both taxa have also been shown to prevent the adhesion and attachment of the oral pathogen *Porphyromonas gingivalis* (57) and their mutual proximity has been observed at the genus level (17). Therefore, further investigating the mechanistic interactions that take place between these two species could provide insights into maintaining their presence and thus prevention of disease. Overall, there is a wealth of information and techniques available to study the composition, structure, and gene expression of complex multispecies communities. However, specific mechanisms that exist between individual members of these communities can be hard to discern from broad observational methods. Using a reductionist approach on two highly abundant and prevalent species in the oral cavity we determined how these taxa can support growth of each other and dictate their micron-scale distribution within this environment while suggesting additional mechanisms in use in the greater *in vivo* community.

Materials and Methods

Strains and Media

Strains and plasmids used in this study are listed in Table S11. Unless indicated, *Streptococcus mitis* was cultured using Brain Heart Infusion (BHI) broth or solid agar supplemented with Yeast extract (YE), *Haemophilus parainfluenzae* had additional supplementation with 15µg/ml Nicotinamide Adenine Dinucleotide (Sigma-Aldrich) and 15µg/ml Hemin (Sigma-Aldrich) - (BHI-YE-HP). *Escherichia coli* was grown on Luria Broth (LB). *H. parainfluenzae* and *S. mitis* were grown at 37°C and 5% CO_2, *E. coli* at 37°C in standard atmospheric conditions with liquid cultures shaken at 200 RPM. Antibiotics were used at the following concentrations: kanamycin 40µg/ml, vancomycin 5µg/ml, and spectinomycin 50µg/ml for *E. coli* and *H. parainfluenzae.* 200µg/ml spectinomycin was used for selection of *H. parainfluenzae* transformants.

Genomic and plasmid DNA isolation

H. parainfluenzae Genomic DNA was isolated using the DNeasy Blood & Tissue kit (Qiagen) according to the manufacturer's instructions. Plasmid isolations were performed using QIAprep spin miniprep kits (Qiagen).

Genetic manipulation of H. parainfluenzae

Gene deletions were generated using derivatives of a suicide vector pMRKO (7) as listed in Table S8. *H. parainfluenzae* was transformed via conjugation and mutants screened via PCR and Sanger sequencing. Procedures involved in plasmid construction

and *H. parainfluenzae* transformation are outlined in the supplementary methods section.

Read abundance data

MetaPhlAn (58) species-assigned metagenomic sequence data from the Human Microbiome Project (Human Microbiome Project Consortium 2012) for the "Supragingival Plaque" oral site was 1st sorted based on predicted read abundance for *Haemophilus parainfluenzae*. Using the top quartile (highest 25% of samples enriched for *H. parainfluenzae*) we compared these samples to the bottom 75% and performed LEfSe analysis (29) to predict species significantly encountered at higher *H. parainfluenzae* abundance. LDA of a log10 score ≥ 3 were deemed significant.

Plaque Collection, Fixation, and Storage

Supragingival plaque was collected according to a protocol approved by New England IRB; all donors provided informed consent. Donors were instructed to refrain from practicing oral hygiene for 24 h before plaque collection. Plaque samples were collected from 7 donors by supervised self-sampling using a toothpick to scrape the supragingival surface of the teeth, avoiding the gingival margin. We fixed the plaque in a solution of 2% paraformaldehyde (PFA) in PBS buffer on ice for 2 to 6 h. The PFA was removed by three washes with 10 mM Tris HCl buffer (pH 7.5). The samples were stored in a 1:1 (vol/vol) solution of 10 mM Tris HCl (pH 7.5) and 100% ethanol at –20°C.

DNA FISH and Mounting

Aliquots of plaque were dried on UltraStick Slides (Thermo Scientific) for 10 min at 46°C. The plaque was hybridized with 2 μM of each probe in a 900 mM NaCl, 20 mM Tris HCl (pH 7.5), 0.01% SDS, and 20% formamide hybridization buffer for 3 h in a humid chamber at 46°C. Non-hybridized probe was removed by washing the slides in prewarmed 215 mM NaCl, 20 mM Tris HCl (pH 7.5), and 5 mM EDTA wash buffer for 15 min at 48°C. The slides were rocked once during the wash incubation. The slides were rinsed in chilled deionized water and allowed to mostly air-dry before the samples were mounted in ProLong Gold Antifade mounting medium (ThermoFisher) under a #1.5 coverslip. The slides were dried flat in the dark.

Imaging

We imaged the hybridized plaque with an LSM 780 Confocal Microscope (Zeiss) with a Plan-Apochromat 40x/1.4 NA objective. Each field of view was simultaneously excited by linear scanning with 405, 488, 561, and 633 nm laser lines. The emission spectra were decomposed by linear unmixing using ZEN software (Zeiss) using reference spectra recorded from pure cultures of reference cells (*Leptotrichia buccalis*) hybridized with the Eub338 probe labeled with the appropriate fluorophore as described above. To obtain a random sample of the masses of plaque large enough to permit spatial analysis, we scanned transects spaced every 5 μm along the coverslip at 40x magnification and imaged every mass of plaque that was at least 70 μm in diameter and 250 μm away from the previously imaged fields of view. For each donor, we imaged the first 20 fields of

view that satisfied these criteria or as many fields of view as were present on the slide. To maximize the number of bacteria captured in each image, we imaged the focal plane closest to the surface of the slide.

Image Analysis

To allow quantitative analysis of the spatial distribution of the taxa of interest, we used FIJI to create binarized *S. mitis*, *H. parainfluenzae,* and bacterial mass images (59) as described in the supplementary methods section.

We evaluated the pair correlations between *S. mitis* and *H. parainfluenzae* over different distances using a linear dipole analysis performed in Daime 2.2 (refs. 60,61). For this analysis, the reference space in each image was restricted to the area in the binary bacterial biomass image. We used all possible dipoles with lengths ranging from 0.15 to 99.90 μm in steps of 0.45 μm.

We evaluated trends between the local densities of both taxa, by dividing each field of view into 1024 6.64 μm by 6.64 μm blocks, discarding blocks that did not contain any of the binary bacterial mass image, and calculating the fraction of each block that was covered by the *S. mitis* and *H. parainfluenzae* binary images.

Mono and Coculture Assays

Colony biofilm assays were carried out as described previously (31). Briefly, equal volumes of *H. parainfluenzae* and/or *S. mitis* were spotted either in mono or coculture on sterile 25mm 0.2 µm polycarbonate membranes (MilliporeSigma™) and placed on BHIYE HP agar plates. *H. parainfluenzae* was spotted at an OD_{600} of 1 and *S. mitis* at OD_{600} of either 0.1, 1 or 3. The plates were then incubated for 24 hours at 37°C in 5% CO_2. The membranes were then transferred to sterile media, mixed to ensure complete resuspension of the colony into the media; serially diluted and plated for CFU enumeration. *S. mitis* was enumerated by counting CFUs on BHI-YE and *H. parainfluenzae* on BHI-YEHP with 5 µg/ml vancomycin.

Disk diffusion assays

Cultures of *H. parainfluenzae* were grown anaerobically in BHI-YEHP overnight. All strains were then adjusted to an OD_{600} of 1 and 100µl was spread plated on BHIYE HP plates and incubated aerobically for 2 hours at 37°C in 5% CO_2. 5 µl of 30% H_2O_2 was then added to a sterile 5mm paper disk and plates were incubated for 24 hours at 37°C in 5% CO_2. The diameters of the zones of inhibition were then measured using a caliper in at least 3 axes.

Coculture transcriptome sample preparation

RNASeq analyses were carried out on mono and coculture samples following the colony biofilm assays described above. Briefly, *H. parainfluenzae* was spotted on the polycarbonate membranes at an OD_{600} of 1 and *S. mitis* at OD_{600} 0.1. The plates were then

incubated for 22 hours at 37°C in 5% CO_2. The membranes were then transferred onto fresh media for 4 hours and immediately placed in RNAlater solution (Ambion™). Experiments were carried out in biological duplicates. RNA extraction, library preparation and sequencing were then carried out by the Microbial 'Omics Core facility at the Broad Institute. Sequences are submitted to the NIH SRA Gene Expression Omnibus (GEO) database and can be found under submission GSE158845.

Transcriptome analyses

The *H. parainfluenzae* ATCC 33392 genome (GCA_000191405.1) was obtained from NCBI and annotation were generated using RAST under default settings (62–64). RNASeq reads were aligned, mapped and differentially expressed genes were analyzed using bowtie2 (ref. 65), HTSeq (66) and DESeq2 (ref. 67) with a Unix based pipeline, generated in this paper (available at https://github.com/dasithperera-hub/RNASeq-analysis-toolkit). This pipeline was also used to carry out a pathway analysis by mapping DEGs to KEGG orthology (https://www.genome.jp/kegg-bin/get_htext?ko00001). This allowed for improved annotations and the identification of potential pathways that are involved in coculture. The same pipeline was used to analyze *H. parainfluenzae* gene expression in published metatranscriptome datasets (47,48).

Complementing Nicotinamide Adenine Dinucleotide (NAD) auxotrophy of H. parainfluenzae

Overnight cultures of *H. parainfluenzae* were washed 3 times in 1x Phosphate buffered saline (PBS) and diluted to an OD_{600} of 0.1 and spread plated on a plate containing BHI-YE supplemented with Hemin and 20units/ml catalase. 5µL of bacteria at an OD_{600} of 1 was added to a sterile paper disk and incubated for 48 hours. Strains used for spotting include *C. matruchotii, C. durum, S. mitis, S. sanguinis, S. cristatus,* and *S. gordonii*.

Figures

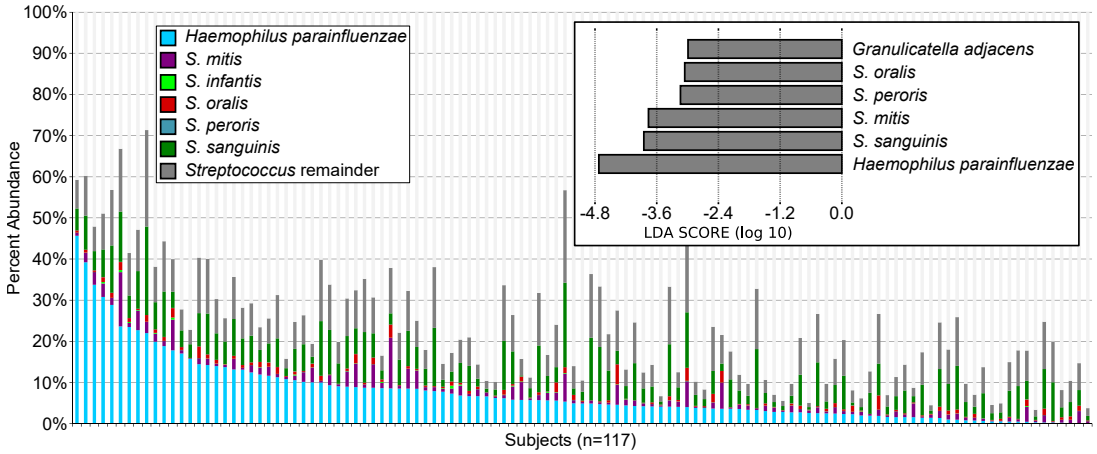

Figure 2.1: Read abundance data and predicted correlations between taxa in supragingival plaque. Human Microbiome Project (HMP) metagenome data of supragingival plaque was used to plot the relative abundance and prevalence of species of interest including *Haemophilus parainfluenzae* (blue), several Mitis group streptococci and all remaining *Streptococcus* spp. (dark grey). (Top Right) The top 25% of subjects based on *H. parainfluenzae* abundance were compared to the remainder via LEfSe analysis. Shown are species enriched in this comparison above an LDA score ≤ -3.0.

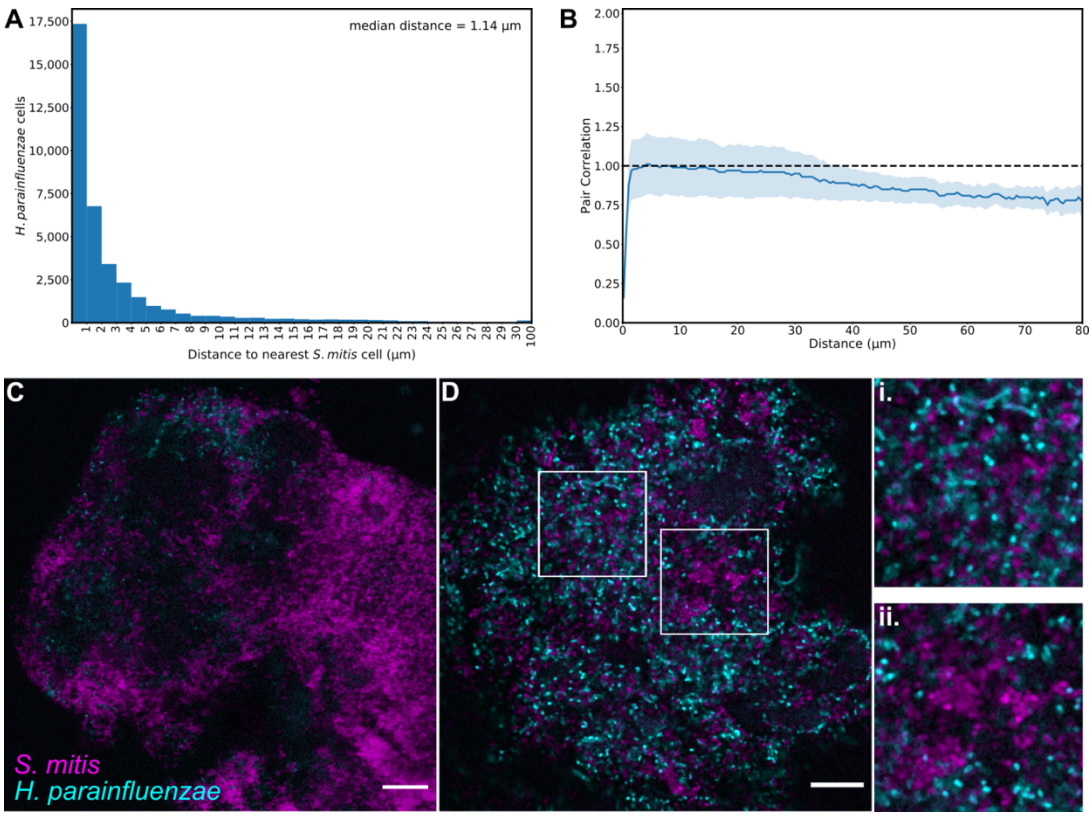

Figure 2.2. *H. parainfluenzae* distribution is related to the density of *S. mitis in vivo* (A) Histogram of the distance to the nearest *S. mitis* cell, measured edge-to-edge, from each of the 37,591 *H. parainfluenzae* cells in 41 fields of view. (B) Pair correlations between *H. parainfluenzae* and *S. mitis* cells. The lighter lines represent the bounds of the 95% confidence interval for the correlation values. The dashed line represents the null hypothesis: the pair correlation equals one. n = 41 fields of view. (C) Plaque with sparsely distributed *H. parainfluenzae* (cyan). (D) Plaque with high abundances of both *S. mitis* (magenta) and *H. parainfluenzae*. (i) Most *H. parainfluenzae* cells are within a few microns of the nearest *S. mitis* cell. Generally, *H. parainfluenzae* are randomly distributed with respect to *S. mitis*. (ii) *H. parainfluenzae* avoids the highest densities of *S. mitis*. Scale bars indicate 10 µm.

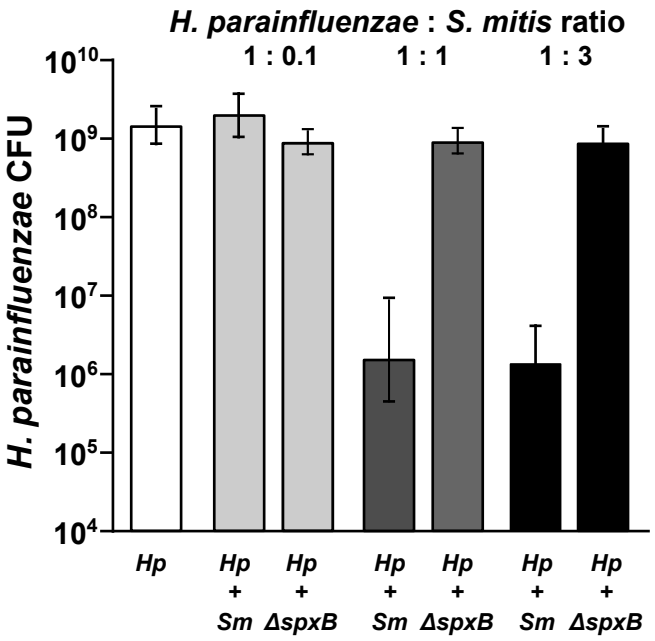

Figure 2.3: *H. parainfluenzae* growth is inhibited by *Streptococcus mitis* produced H_2O_2 in a dose dependent manner. *H. parainfluenzae* (*Hp*) CFU counts in mono and coculture with wildtype (*Sm*) or a pyruvate oxidase mutant (*ΔspxB*) of *S. mitis. Hp* had an initial inoculum using 10µL at an OD_{600} of 1, which corresponds to $4.65x10^6$ CFU/ml. Wildtype (*Sm*) and *S. mitis ΔspxB* with initial inoculums using 10µL at an OD_{600} of either 0.1, 1 or 3 which corresponds to an average of $2.45x10^5$, $1.55x10^6$ or $3.45x10^6$ CFU/ml. Data are mean CFU counts with error bars indicating standard deviation for n≥3. *denotes p< 0.001 using a Student's t-test compared to monoculture.

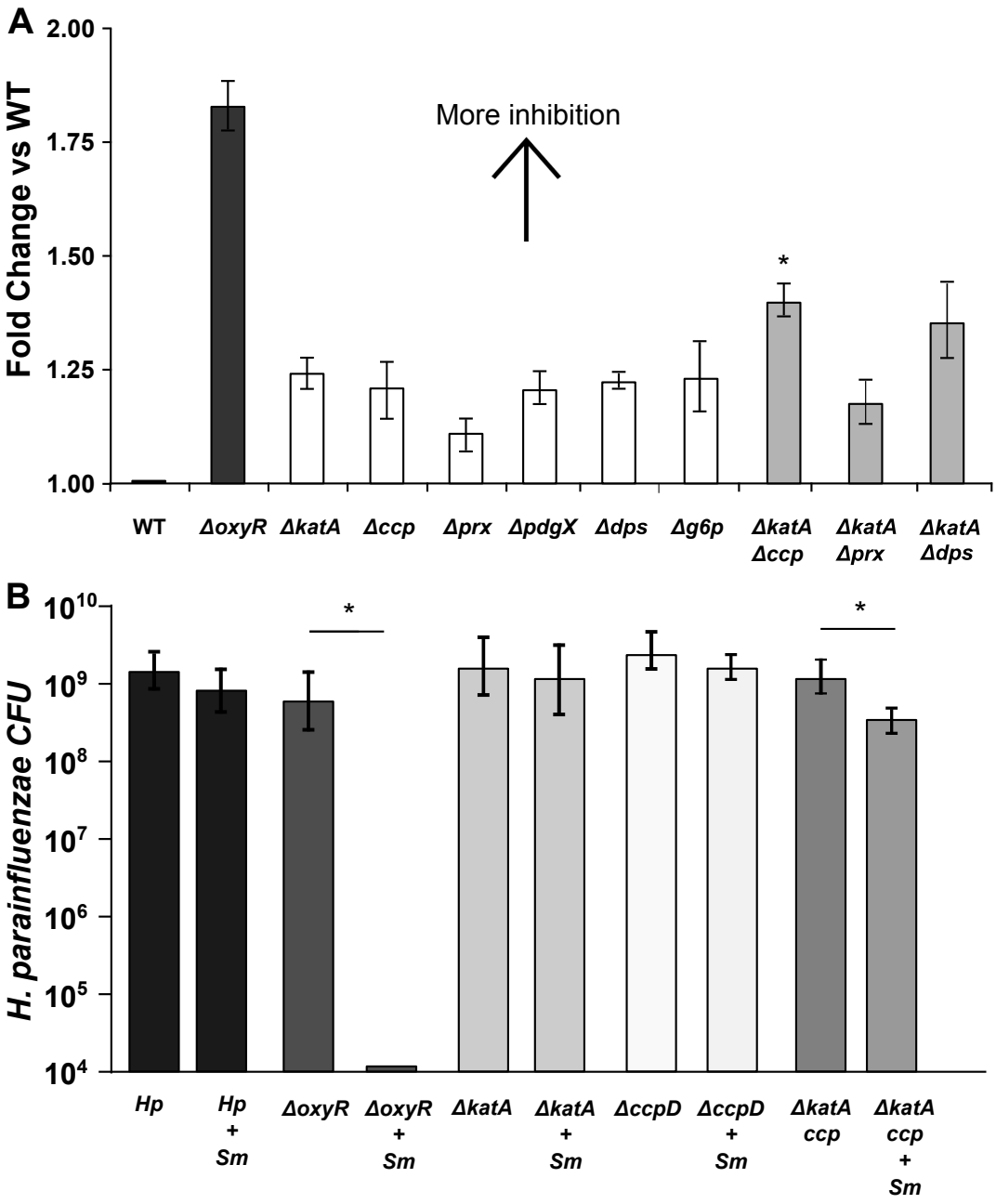

Figure 2.4: *H. parainfluenzae* resistance to H_2O_2 relies on the contribution of multiple genes. We assessed the sensitivity of wildtype *H. parainfluenzae* (WT) to H_2O_2 or coculture yield with *S. mitis* vs mutants lacking *oxyR*, catalase (*katA*), cytochrome c peroxidase (*ccp*), peroxiredoxin (*prx*), glutaredoxin-peroxiredoxin (*pdgX*), DNA-binding protein from starved cells (*dps*) and glucose-6-phosphate dehydrogenase (*g6p*).

(A) Zones of inhibition by 30% H_2O_2 exposure (areas of no visible *H. parainfluenzae* growth) were measured after 24 hours and fold change calculated compared to wildtype. Data are the mean fold change relative to WT; error bars indicate standard deviation for n≥3. All strains were significantly different from WT, while *ΔkatA-Δccp* was significantly different from *ΔkatA* (padj < 0.05), based on t-test with Bonferroni correction. (B) WT and mutant *H. parainfluenzae* CFU following 24h coculture with *S. mitis*. *H. parainfluenzae* inocula were 4.65 x10^6 CFU/ml. *S. mitis* inoculum was 2.45x10^5 CFU/ml. Data are represented as mean CFU, error bars indicate standard deviation for n≥3. *denotes p< 0.05 by Student's t-test compared to monoculture.

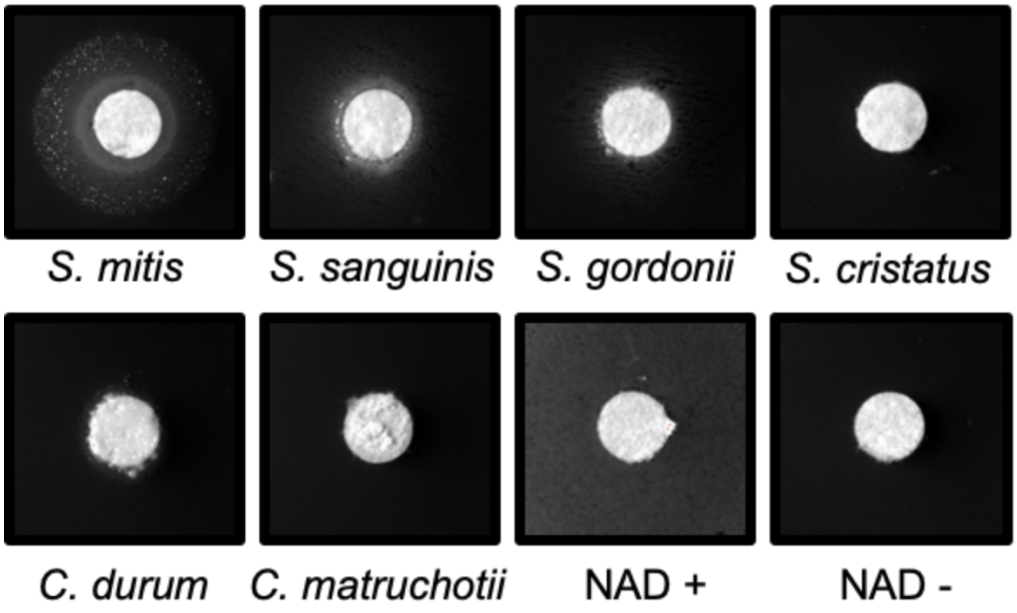

Figure 2.5: *Streptococcus*-produced Nicotinamide Adenine Dinucleotide (NAD) supports *H. parainfluenzae* growth. Cultures of *S. mitis, S. sanguinis, S. gordonii, S. cristatus, Corynebacterium matruchotii* and *C. durum* were grown overnight, normalized based on optical density, and spotted onto paper discs over lawns of *H. parainfluenzae* spread on solid agar medium lacking NAD. Plates were incubated for 48h before observation. Rings near the disc indicate *H. parainfluenzae* growth. NAD was added a positive control (NAD+).

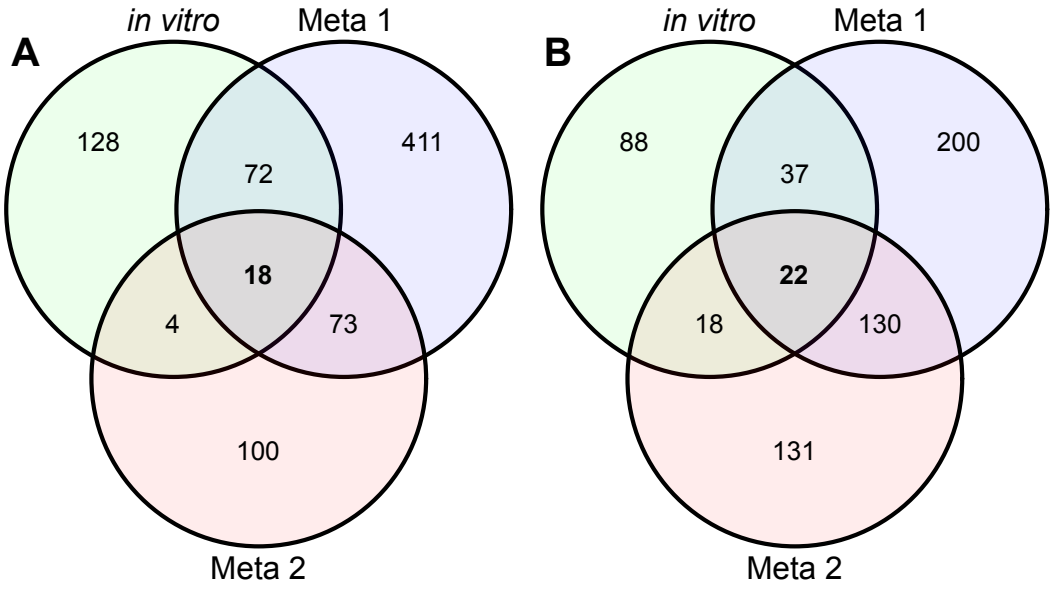

Figure 2.6: Comparison of coculture gene expression with meta-transcriptome datasets. Mono vs coculture RNASeq results (*in vitro*) for *H. parainfluenzae* indicated 387 significantly differentially expressed genes (DEG) above 2-fold. By comparing *in vitro* monoculture to *in vivo* metatranscriptome reads from Benítez-Páez 2014 (Meta 1) and Jorth 2014 (Meta 2) we were able to generate two sets of *in vivo*-specific DEGs to determine differences in (A) significantly upregulated or (B) significantly downregulated genes shared between *in vitro* coculture and *in vivo* conditions.

Acknowledgments:

We thank Janet Atoyan and the RI Genomics and sequencing center at URI for sequence generation, Jonathan Livny and the Microbial 'Omics Core and Genomics Platform for their help with RNASeq library sequencing and guidance on experimental design, the RI-INBRE/ SURF program for supporting summer undergraduate research for KCL, the URI Science and Engineering fellows program for supporting summer undergraduate research for KC and the Annual Mark Wilson conference attendees for many valuable suggestions and discussion.

Funding Sources: This work was funded by the NIDCR/NIH (R01DE027958 – MR, JMW), (R01DE022586 – JMW), NIGMS/RI-INBRE early career development award (P20GM103430 - MMR) and the Rhode Island Foundation Medical Research Fund (20164348 - MR). This work was supported by the USDA National Institute of Food and Agriculture, Hatch Formula project accession number 1017848.

Author Contributions: MR and JMW designed research; DP, AM, VML, KCL, EA, and KC performed research, JMW, AM, DP and MR wrote the paper.

Competing Interests: The authors declare that there are no competing financial interests with this work.

References

1. Stoodley P, Sauer K, Davies DG, Costerton JW. Biofilms as complex differentiated communities. Annu Rev Microbiol. 2002;56:187–209.

2. Borer B, Tecon R, Or D. Spatial organization of bacterial populations in response to oxygen and carbon counter-gradients in pore networks. Nat Commun. 2018 Feb 22;9(1):769.

3. Liu W, Jacquiod S, Brejnrod A, Russel J, Burmølle M, Sørensen SJ. Deciphering links between bacterial interactions and spatial organization in multispecies biofilms. ISME J. 2019 Dec;13(12):3054–66.

4. Liu W, Russel J, Burmølle M, Sørensen SJ, Madsen JS. Micro-scale intermixing: a requisite for stable and synergistic co-establishment in a four-species biofilm. ISME J. 2018 Aug;12(8):1940–51.

5. Shrivastava A, Patel VK, Tang Y, Yost SC, Dewhirst FE, Berg HC. Cargo transport shapes the spatial organization of a microbial community. Proc Natl Acad Sci U S A. 2018 Aug 21;115(34):8633–8.

6. Gralka M, Szabo R, Stocker R, Cordero OX. Trophic Interactions and the Drivers of Microbial Community Assembly. Curr Biol CB. 2020 Oct 5;30(19):R1176–88.

7. Ramsey MM, Rumbaugh KP, Whiteley M. Metabolite cross-feeding enhances virulence in a model polymicrobial infection. PLoS Pathog. 2011 Mar;7(3):e1002012.

8. Zengler K, Zaramela LS. The social network of microorganisms - how auxotrophies shape complex communities. Nat Rev Microbiol. 2018 Jun;16(6):383–90.

9. Mashimo PA, Yamamoto Y, Nakamura M, Reynolds HS, Genco RJ. Lactic acid production by oral Streptococcus mitis inhibits the growth of oral Capnocytophaga. J Periodontol. 1985 Sep;56(9):548–52.

10. Redanz S, Cheng X, Giacaman RA, Pfeifer CS, Merritt J, Kreth J. Live and let die: Hydrogen peroxide production by the commensal flora and its role in maintaining a symbiotic microbiome. Mol Oral Microbiol. 2018 Oct;33(5):337–52.

11. Kreth J, Zhang Y, Herzberg MC. Streptococcal antagonism in oral biofilms: Streptococcus sanguinis and Streptococcus gordonii interference with Streptococcus mutans. J Bacteriol. 2008 Jul;190(13):4632–40.

12. Liu W, Røder HL, Madsen JS, Bjarnsholt T, Sørensen SJ, Burmølle M. Interspecific Bacterial Interactions are Reflected in Multispecies Biofilm Spatial Organization. Front Microbiol. 2016;7:1366.

13. Ren D, Madsen JS, Sørensen SJ, Burmølle M. High prevalence of biofilm synergy among bacterial soil isolates in cocultures indicates bacterial interspecific cooperation. ISME J. 2015 Jan;9(1):81–9.

14. Lee KWK, Periasamy S, Mukherjee M, Xie C, Kjelleberg S, Rice SA. Biofilm development and enhanced stress resistance of a model, mixed-species community biofilm. ISME J. 2014 Apr;8(4):894–907.

15. Mikx FH. [The study of dental plaque by Antoni van Leeuwenhoek in 1683]. Ned Tijdschr Tandheelkd. 1983 Sep;90(9):421–4.

16. Kolenbrander PE, Andersen RN, Blehert DS, Egland PG, Foster JS, Palmer RJ. Communication among oral bacteria. Microbiol Mol Biol Rev MMBR. 2002 Sep;66(3):486–505, table of contents.

17. Mark Welch JL, Rossetti BJ, Rieken CW, Dewhirst FE, Borisy GG. Biogeography of a human oral microbiome at the micron scale. Proc Natl Acad Sci U S A. 2016 Feb 9;113(6):E791-800.

18. Kreth J, Merritt J, Qi F. Bacterial and host interactions of oral streptococci. DNA Cell Biol. 2009 Aug;28(8):397–403.

19. van der Hoeven JS, Toorop AI, Mikx RH. Symbiotic relationship of Veillonella alcalescens and Streptococcus mutans in dental plaque in gnotobiotic rats. Caries Res. 1978;12(3):142–7.

20. Mikx FH, Van der Hoeven JS. Symbiosis of Streptococcus mutans and Veillonella alcalescens in mixed continuous cultures. Arch Oral Biol. 1975 Jul;20(7):407–10.

21. Zhu L, Kreth J. The role of hydrogen peroxide in environmental adaptation of oral microbial communities. Oxid Med Cell Longev. 2012;2012:717843.

22. Zheng W, Tan TK, Paterson IC, Mutha NVR, Siow CC, Tan SY, et al. StreptoBase: An Oral Streptococcus mitis Group Genomic Resource and Analysis Platform. PloS One. 2016;11(5):e0151908.

23. Jensen A, Scholz CFP, Kilian M. Re-evaluation of the taxonomy of the Mitis group of the genus Streptococcus based on whole genome phylogenetic analyses, and proposed reclassification of Streptococcus dentisani as Streptococcus oralis subsp. dentisani comb. nov., Streptococcus tigurinus as Streptococcus oralis subsp. tigurinus

comb. nov., and Streptococcus oligofermentans as a later synonym of Streptococcus cristatus. Int J Syst Evol Microbiol. 2016 Nov;66(11):4803–20.

24. Liljemark WF, Bloomquist CG, Uhl LA, Schaffer EM, Wolff LF, Pihlstrom BL, et al. Distribution of oral Haemophilus species in dental plaque from a large adult population. Infect Immun. 1984 Dec;46(3):778–86.

25. Dewhirst FE, Chen T, Izard J, Paster BJ, Tanner ACR, Yu W-H, et al. The human oral microbiome. J Bacteriol. 2010 Oct;192(19):5002–17.

26. Eren AM, Borisy GG, Huse SM, Mark Welch JL. Oligotyping analysis of the human oral microbiome. Proc Natl Acad Sci U S A. 2014 Jul 15;111(28):E2875-2884.

27. Sen Yew H, Chambers ST, Roberts SA, Holland DJ, Julian KA, Raymond NJ, et al. Association between HACEK bacteraemia and endocarditis. J Med Microbiol. 2014 Jun;63(Pt 6):892–5.

28. Tseng Y-C, Yang H-Y, Lin W-T, Chang C-B, Chien H-C, Wang H-P, et al. Salivary dysbiosis in Sjögren's syndrome and a commensal-mediated immunomodulatory effect of salivary gland epithelial cells. NPJ Biofilms Microbiomes. 2021 Mar 11;7(1):21.

29. Segata N, Izard J, Waldron L, Gevers D, Miropolsky L, Garrett WS, et al. Metagenomic biomarker discovery and explanation. Genome Biol. 2011 Jun 24;12(6):R60.

30. Merritt JH, Kadouri DE, O'Toole GA. Growing and analyzing static biofilms. Curr Protoc Microbiol. 2005 Jul;Chapter 1:Unit 1B.1.

31. Ramsey MM, Freire MO, Gabrilska RA, Rumbaugh KP, Lemon KP. Staphylococcus aureus Shifts toward Commensalism in Response to Corynebacterium Species. Front Microbiol. 2016;7:1230.

32. Liu X, Ramsey MM, Chen X, Koley D, Whiteley M, Bard AJ. Real-time mapping of a hydrogen peroxide concentration profile across a polymicrobial bacterial biofilm using scanning electrochemical microscopy. Proc Natl Acad Sci U S A. 2011 Feb 15;108(7):2668–73.

33. Bishai WR, Howard NS, Winkelstein JA, Smith HO. Characterization and virulence analysis of catalase mutants of Haemophilus influenzae. Infect Immun. 1994 Nov;62(11):4855–60.

34. Takashima E, Konishi K. Characterization of a quinol peroxidase mutant in Aggregatibacter actinomycetemcomitans. FEMS Microbiol Lett. 2008 Sep;286(1):66–70.

35. Ishikawa T, Mizunoe Y, Kawabata S, Takade A, Harada M, Wai SN, et al. The iron-binding protein Dps confers hydrogen peroxide stress resistance to Campylobacter jejuni. J Bacteriol. 2003 Feb;185(3):1010–7.

36. Wong SMS, Alugupalli KR, Ram S, Akerley BJ. The ArcA regulon and oxidative stress resistance in Haemophilus influenzae. Mol Microbiol. 2007 Jun;64(5):1375–90.

37. Juneau RA, Pang B, Armbruster CE, Murrah KA, Perez AC, Swords WE. Peroxiredoxin-glutaredoxin and catalase promote resistance of nontypeable Haemophilus influenzae 86-028NP to oxidants and survival within neutrophil extracellular traps. Infect Immun. 2015 Jan;83(1):239–46.

38. Izawa S, Maeda K, Miki T, Mano J, Inoue Y, Kimura A. Importance of glucose-6-phosphate dehydrogenase in the adaptive response to hydrogen peroxide in Saccharomyces cerevisiae. Biochem J. 1998 Mar 1;330 (Pt 2):811–7.

39. Lundberg BE, Wolf RE, Dinauer MC, Xu Y, Fang FC. Glucose 6-phosphate dehydrogenase is required for Salmonella typhimurium virulence and resistance to reactive oxygen and nitrogen intermediates. Infect Immun. 1999 Jan;67(1):436–8.

40. Perkins A, Nelson KJ, Parsonage D, Poole LB, Karplus PA. Peroxiredoxins: guardians against oxidative stress and modulators of peroxide signaling. Trends Biochem Sci. 2015 Aug;40(8):435–45.

41. Panek HR, O'Brian MR. KatG is the primary detoxifier of hydrogen peroxide produced by aerobic metabolism in Bradyrhizobium japonicum. J Bacteriol. 2004 Dec;186(23):7874–80.

42. Kim J-S, Holmes RK. Characterization of OxyR as a negative transcriptional regulator that represses catalase production in Corynebacterium diphtheriae. PloS One. 2012;7(3):e31709.

43. Park B, Nizet V, Liu GY. Role of Staphylococcus aureus catalase in niche competition against Streptococcus pneumoniae. J Bacteriol. 2008 Apr;190(7):2275–8.

44. Kamenšek S, Podlesek Z, Gillor O, Zgur-Bertok D. Genes regulated by the Escherichia coli SOS repressor LexA exhibit heterogeneous expression. BMC Microbiol. 2010 Nov 11;10:283.

45. Deng Y, Chen C, Zhao Z, Zhao J, Jacq A, Huang X, et al. The RNA Chaperone Hfq Is Involved in Colony Morphology, Nutrient Utilization and Oxidative and Envelope Stress Response in Vibrio alginolyticus. PloS One. 2016;11(9):e0163689.

46. Gustavsson N, Diez A, Nyström T. The universal stress protein paralogues of Escherichia coli are co-ordinately regulated and co-operate in the defence against DNA damage. Mol Microbiol. 2002 Jan;43(1):107–17.

47. Jorth P, Turner KH, Gumus P, Nizam N, Buduneli N, Whiteley M. Meta-transcriptomics of the human oral microbiome during health and disease. mBio. 2014 Apr 1;5(2):e01012-01014.

48. Benítez-Páez A, Belda-Ferre P, Simón-Soro A, Mira A. Microbiota diversity and gene expression dynamics in human oral biofilms. BMC Genomics. 2014 Apr 27;15:311.

49. Ma L, Calfee BC, Morris JJ, Johnson ZI, Zinser ER. Degradation of hydrogen peroxide at the ocean's surface: the influence of the microbial community on the realized thermal niche of Prochlorococcus. ISME J. 2017 Oct 31;

50. Seth EC, Taga ME. Nutrient cross-feeding in the microbial world. Front Microbiol. 2014;5:350.

51. Zhu B, Macleod LC, Newsome E, Liu J, Xu P. Aggregatibacter actinomycetemcomitans mediates protection of Porphyromonas gingivalis from Streptococcus sanguinis hydrogen peroxide production in multi-species biofilms. Sci Rep. 2019 Mar 20;9(1):4944.

52. Mark Welch JL, Dewhirst FE, Borisy GG. Biogeography of the Oral Microbiome: The Site-Specialist Hypothesis. Annu Rev Microbiol. 2019 08;73:335–58.

53. Kosikowska U, Biernasiuk A, Rybojad P, Łoś R, Malm A. Haemophilus parainfluenzae as a marker of the upper respiratory tract microbiota changes under the

influence of preoperative prophylaxis with or without postoperative treatment in patients with lung cancer. BMC Microbiol. 2016 Apr 6;16:62.

54. Könönen E, Jousimies-Somer H, Bryk A, Kilpi T, Kilian M. Establishment of streptococci in the upper respiratory tract: longitudinal changes in the mouth and nasopharynx up to 2 years of age. J Med Microbiol. 2002 Sep;51(9):723–30.

55. Seif Y, Choudhary KS, Hefner Y, Anand A, Yang L, Palsson BO. Metabolic and genetic basis for auxotrophies in Gram-negative species. Proc Natl Acad Sci U S A. 2020 Mar 17;117(11):6264–73.

56. Yang C-Y, Yeh Y-M, Yu H-Y, Chin C-Y, Hsu C-W, Liu H, et al. Oral Microbiota Community Dynamics Associated With Oral Squamous Cell Carcinoma Staging. Front Microbiol. 2018;9:862.

57. Van Hoogmoed CG, Geertsema-Doornbusch GI, Teughels W, Quirynen M, Busscher HJ, Van der Mei HC. Reduction of periodontal pathogens adhesion by antagonistic strains. Oral Microbiol Immunol. 2008 Feb;23(1):43–8.

58. Segata N, Waldron L, Ballarini A, Narasimhan V, Jousson O, Huttenhower C. Metagenomic microbial community profiling using unique clade-specific marker genes. Nat Methods. 2012 Jun 10;9(8):811–4.

59. Schindelin J, Arganda-Carreras I, Frise E, Kaynig V, Longair M, Pietzsch T, et al. Fiji: an open-source platform for biological-image analysis. Nat Methods. 2012 Jun 28;9(7):676–82.

60. Daims H, Wagner M. In situ techniques and digital image analysis methods for quantifying spatial localization patterns of nitrifiers and other microorganisms in biofilm and flocs. Methods Enzymol. 2011;496:185–215.

61. Daims H, Lücker S, Wagner M. daime, a novel image analysis program for microbial ecology and biofilm research. Environ Microbiol. 2006 Feb;8(2):200–13.

62. Brettin T, Davis JJ, Disz T, Edwards RA, Gerdes S, Olsen GJ, et al. RASTtk: A modular and extensible implementation of the RAST algorithm for building custom annotation pipelines and annotating batches of genomes. Sci Rep. 2015 Jul;5(1):8365.

63. Overbeek R, Olson R, Pusch GD, Olsen GJ, Davis JJ, Disz T, et al. The SEED and the Rapid Annotation of microbial genomes using Subsystems Technology (RAST). Nucleic Acids Res. 2014 Jan;42(D1):D206–14.

64. Aziz RK, Bartels D, Best AA, DeJongh M, Disz T, Edwards RA, et al. The RAST Server: Rapid Annotations using Subsystems Technology. BMC Genomics. 2008;9(1):75.

65. Langmead B, Salzberg SL. Fast gapped-read alignment with Bowtie 2. Nat Methods. 2012 Mar 4;9(4):357–9.

66. Anders S, Pyl PT, Huber W. HTSeq--a Python framework to work with high-throughput sequencing data. Bioinformatics. 2015 Jan 15;31(2):166–9.

67. Love MI, Huber W, Anders S. Moderated estimation of fold change and dispersion for RNA-seq data with DESeq2. Genome Biol. 2014;15(12):550.

Appendix

Table S2.1: Minimum inhibitory concentrations in BHI-YE HP for H_2O_2

Strain	MIC (μM)
Wildtype	834
Δ*katA*	834
Δ*ccp*	834
Δ*oxyR*	104

Table S2.2: *H. parainfluenzae* genes induced in *in vitro* coculture

Fold change	ID	Description
37.19	fig|6666666.571729.peg.656	hypothetical protein
12.14	fig|6666666.571729.peg.1162	4-alpha-glucanotransferase (amylomaltase) (EC 2.4.1.25);Ontology_term
10.87	fig|6666666.571729.peg.747	Type IV pilin PilA
9.92	fig|6666666.571729.peg.1163	1%2C4-alpha-glucan (glycogen) branching enzyme%2C GH-13-type (EC 2.4.1.18);Ontology_term
9.42	fig|6666666.571729.peg.1164	Limit dextrin alpha-1%2C6-maltotetraose-hydrolase (EC 3.2.1.196);Ontology_term
6.52	fig|6666666.571729.peg.744	Leader peptidase (Prepilin peptidase) (EC 3.4.23.43) / N-methyltransferase (EC 2.1.1.-);Ontology_term
6.35	fig|6666666.571729.peg.265	Vitamin B12 ABC transporter%2C ATP-binding protein BtuD
5.65	fig|6666666.571729.peg.102	GALNS arylsulfatase regulator (Fe-S oxidoreductase)
5.56	fig|6666666.571729.peg.173	Putative ABC transporter of substrate X%2C permease subunit I
5.37	fig|6666666.571729.peg.1645	DNA ligase
5.36	fig|6666666.571729.peg.40	Hydroxymethylpyrimidine ABC transporter%2C transmembrane component
5.34	fig|6666666.571729.peg.593	hypothetical protein
5.3	fig|6666666.571729.peg.60	Glycerol uptake facilitator protein
5.13	fig|6666666.571729.peg.32	Type IV pilus biogenesis protein PilM
5.08	fig|6666666.571729.peg.105	Sodium-Choline Symporter
4.85	fig|6666666.571729.peg.1165	Glucose-1-phosphate adenylyltransferase (EC 2.7.7.27);Ontology_term

4.81	fig|6666666.571729.peg.592	hypothetical protein
4.72	fig|6666666.571729.peg.1288	Type III restriction-modification system methylation subunit (EC 2.1.1.72);Ontology_term
4.67	fig|6666666.571729.peg.595	FIG00847847: hypothetical protein
4.67	fig|6666666.571729.peg.174	Putative ABC transporter of substrate X%2C permease subunit II
4.65	fig|6666666.571729.peg.254	hypothetical protein
4.63	fig|6666666.571729.peg.1235	Oligopeptide/dipeptide ABC transporter%2C permease protein / Oligopeptide/dipeptide ABC transporter%2C ATP-binding protein
4.6	fig|6666666.571729.peg.131	Site-specific tyrosine recombinase XerC
4.58	fig|6666666.571729.peg.690	hypothetical protein
4.54	fig|6666666.571729.peg.95	Phosphoribosylformylglycinamidine synthase%2C synthetase subunit (EC 6.3.5.3) / Phosphoribosylformylglycinamidine synthase%2C glutamine amidotransferase subunit (EC 6.3.5.3);Ontology_term
4.5	fig|6666666.571729.peg.274	hypothetical protein
4.47	fig|6666666.571729.peg.101	small multidrug resistance family (SMR) protein
4.47	fig|6666666.571729.peg.25	AAA+ ATPase superfamily protein YifB/ComM%2C associated with DNA recombination
4.41	fig|6666666.571729.peg.1865	Dihydrofolate reductase (EC 1.5.1.3);Ontology_term
4.4	fig|6666666.571729.peg.649	hypothetical protein
4.16	fig|6666666.571729.peg.501	hypothetical protein
4.14	fig|6666666.571729.peg.930	hypothetical protein
4.09	fig|6666666.571729.peg.596	Efflux ABC transporter%2C ATP-binding protein
3.99	fig|6666666.571729.peg.502	hypothetical protein
3.99	fig|6666666.571729.peg.323	DNA transformation protein TfoX
3.97	fig|6666666.571729.peg.257	Tryptophanase (EC 4.1.99.1);Ontology_term
3.92	fig|6666666.571729.peg.849	Guanylate kinase (EC 2.7.4.8);Ontology_term
3.88	fig|6666666.571729.peg.252	hypothetical protein
3.84	fig|6666666.571729.peg.249	Lysophospholipase L2 (EC 3.1.1.5);Ontology_term
3.82	fig|6666666.571729.peg.435	Biofilm PGA synthesis deacetylase PgaB (EC 3.-)
3.8	fig|6666666.571729.peg.792	N-acetylmannosamine kinase (EC 2.7.1.60);Ontology_term
3.76	fig|6666666.571729.peg.969	Trehalose operon transcriptional repressor
3.75	fig|6666666.571729.peg.1138	Dihydrolipoamide succinyltransferase component (E2) of 2-oxoglutarate dehydrogenase complex (EC 2.3.1.61);Ontology_term

3.66	fig|6666666.571729.peg.648	Mobile element protein
3.6	fig|6666666.571729.peg.793	Sialic acid utilization regulator%2C RpiR family
3.54	fig|6666666.571729.peg.172	Putative ABC transporter of substrate X%2C ATP-binding subunit
3.54	fig|6666666.571729.peg.1075	Uncharacterized integral membrane protein GSU2901
3.52	fig|6666666.571729.peg.402	3'(2')%2C5'-bisphosphate nucleotidase (EC 3.1.3.7);Ontology_term
3.51	fig|6666666.571729.peg.470	hypothetical protein
3.48	fig|6666666.571729.peg.689	hypothetical protein
3.48	fig|6666666.571729.peg.1189	Zn-ribbon-containing%2C possibly nucleic-acid-binding protein
3.44	fig|6666666.571729.peg.171	Protein SlyX
3.43	fig|6666666.571729.peg.1122	Phage integrase
3.43	fig|6666666.571729.peg.1247	Iron(III) ABC transporter%2C ATP-binding protein
3.38	fig|6666666.571729.peg.61	Glycerol kinase (EC 2.7.1.30);Ontology_term
3.38	fig|6666666.571729.peg.17	Oligopeptide ABC transporter%2C substrate-binding protein OppA (TC 3.A.1.5.1)
3.37	fig|6666666.571729.peg.544	dTDP-glucose 4%2C6-dehydratase (EC 4.2.1.46);Ontology_term
3.35	fig|6666666.571729.peg.403	hypothetical protein
3.32	fig|6666666.571729.peg.1681	hypothetical protein
3.3	fig|6666666.571729.peg.134	Shikimate 5-dehydrogenase I alpha (EC 1.1.1.25);Ontology_term
3.29	fig|6666666.571729.peg.2	Methionine ABC transporter ATP-binding protein
3.27	fig|6666666.571729.peg.1011	CRISPR-associated endonuclease Cas9
3.24	fig|6666666.571729.peg.1141	Succinyl-CoA ligase [ADP-forming] alpha chain (EC 6.2.1.5);Ontology_term
3.23	fig|6666666.571729.peg.896	5'-deoxynucleotidase YfbR (EC 3.1.3.89);Ontology_term
3.22	fig|6666666.571729.peg.161	hypothetical protein
3.2	fig|6666666.571729.peg.475	Transcriptional regulator%2C AsnC family
3.19	fig|6666666.571729.peg.1639	Transcriptional factor MdcH
3.19	fig|6666666.571729.peg.1191	Cysteine desulfurase (EC 2.8.1.7) > sulfur transfer pathway protein CsdA;Ontology_term
3.16	fig|6666666.571729.peg.778	Cytochrome c552 precursor (EC 1.7.2.2);Ontology_term
3.14	fig|6666666.571729.peg.791	N-acetylmannosamine-6-phosphate 2-epimerase (EC 5.1.3.9);Ontology_term
3.13	fig|6666666.571729.peg.629	NADP-specific glutamate dehydrogenase (EC 1.4.1.4);Ontology_term
3.08	fig|6666666.571729.peg.525	D-glycerate transporter (predicted)
3.07	fig|6666666.571729.peg.597	hypothetical protein

3.06	fig|6666666.571729.peg.20	Oligopeptide ABC transporter%2C ATP-binding protein OppD (TC 3.A.1.5.1)
3.05	fig|6666666.571729.peg.748	1%2C6-anhydro-N-acetylmuramyl-L-alanine amidase
3.04	fig|6666666.571729.peg.1260	hypothetical protein
3.03	fig|6666666.571729.peg.1137	2-oxoglutarate dehydrogenase E1 component (EC 1.2.4.2);Ontology_term
3.03	fig|6666666.571729.peg.21	Oligopeptide ABC transporter%2C ATP-binding protein OppF (TC 3.A.1.5.1)
3.03	fig|6666666.571729.peg.1113	Uncharacterized DUF218 membrane proteinn PM0506
3	fig|6666666.571729.peg.560	hypothetical protein
3	fig|6666666.571729.peg.1814	Alanyl-tRNA synthetase (EC 6.1.1.7);Ontology_term
2.99	fig|6666666.571729.peg.1192	Micrococcal nuclease (thermonuclease) homologs
2.99	fig|6666666.571729.peg.1477	Uncharacterized protein MSMEG_6412
2.98	fig|6666666.571729.peg.176	Sodium-dependent anion transporter family
2.95	fig|6666666.571729.peg.1246	ABC transporter%2C substrate-binding protein (cluster 8%2C B12/iron complex)
2.95	fig|6666666.571729.peg.1927	Carbonic anhydrase%2C alpha class (EC 4.2.1.1);Ontology_term
2.95	fig|6666666.571729.peg.929	hypothetical protein
2.93	fig|6666666.571729.peg.106	Predicted permeases
2.91	fig|6666666.571729.peg.965	Permease of the drug/metabolite transporter (DMT) superfamily
2.91	fig|6666666.571729.peg.100	5'-nucleotidase (EC 3.1.3.5)%3B 2'%2C3'-cyclic-nucleotide 2'-phosphodiesterase (EC 3.1.4.16)%3B Putative UDP-sugar hydrolase (EC 3.6.1.45);Ontology_term
2.89	fig|6666666.571729.peg.1147	UPF0115 protein YfcN
2.89	fig|6666666.571729.peg.1234	Putative glutathione transporter%2C permease component
2.89	fig|6666666.571729.peg.511	DNA uptake protein and related DNA-binding proteins
2.88	fig|6666666.571729.peg.1502	Ferric iron ABC transporter%2C iron-binding protein
2.87	fig|6666666.571729.peg.1325	Ribulosamine/erythrulosamine 3-kinase potentially involved in protein deglycation
2.85	fig|6666666.571729.peg.1287	Type III restriction-modification system restriction subunit (EC 3.1.21.5);Ontology_term
2.85	fig|6666666.571729.peg.436	Biofilm PGA outer membrane secretin PgaA
2.84	fig|6666666.571729.peg.242	Fructose-1%2C6-bisphosphatase%2C GlpX type (EC 3.1.3.11);Ontology_term
2.75	fig|6666666.571729.peg.3	Methionine ABC transporter permease protein
2.74	fig|6666666.571729.peg.1446	Allophanate hydrolase 2 subunit 2 (EC 3.5.1.54);Ontology_term

2.74	fig|6666666.571729.peg.1273	Universal stress protein E
2.73	fig|6666666.571729.peg.158	Endonuclease V (EC 3.2.2.17);Ontology_term
2.7	fig|6666666.571729.peg.256	hypothetical protein
2.69	fig|6666666.571729.peg.1038	Tripeptide aminopeptidase (EC 3.4.11.4);Ontology_term
2.68	fig|6666666.571729.peg.720	hypothetical protein
2.67	fig|6666666.571729.peg.130	Histone acetyltransferase HPA2 and related acetyltransferases
2.67	fig|6666666.571729.peg.261	hypothetical protein
2.66	fig|6666666.571729.peg.775	NrfD protein
2.66	fig|6666666.571729.peg.258	Tyrosine-specific transport protein
2.65	fig|6666666.571729.peg.434	Biofilm PGA synthesis N-glycosyltransferase PgaC (EC 2.4.-.-);Ontology_term
2.65	fig|6666666.571729.peg.1258	hypothetical protein
2.65	fig|6666666.571729.peg.1017	Cell division inhibitor Slr1223 (YfcH in EC)%2C contains epimerase/dehydratase and DUF1731 domains
2.63	fig|6666666.571729.peg.1719	Aldose 1-epimerase (EC 5.1.3.3);Ontology_term
2.62	fig|6666666.571729.peg.1720	Galactokinase (EC 2.7.1.6);Ontology_term
2.62	fig|6666666.571729.peg.33	Multimodular transpeptidase-transglycosylase (EC 2.4.1.129) (EC 3.4.-.-);Ontology_term
2.61	fig|6666666.571729.peg.433	AagD
2.61	fig|6666666.571729.peg.19	Oligopeptide ABC transporter%2C permease protein OppC (TC 3.A.1.5.1)
2.6	fig|6666666.571729.peg.259	hypothetical protein
2.59	fig|6666666.571729.peg.1916	Glycosyl transferase
2.59	fig|6666666.571729.peg.1083	Peptide transport system ATP-binding protein sapF (TC 3.A.1.5.5)
2.59	fig|6666666.571729.peg.148	Nitrate/nitrite response regulator protein NarP
2.59	fig|6666666.571729.peg.583	FIGfam138462: Acyl-CoA synthetase%2C AMP-(fatty) acid ligase
2.59	fig|6666666.571729.peg.1315	hypothetical protein
2.58	fig|6666666.571729.peg.1775	Ribosome LSU-associated GTP-binding protein HflX
2.57	fig|6666666.571729.peg.1774	RNA-binding protein Hfq
2.56	fig|6666666.571729.peg.1657	VgrG protein
2.55	fig|6666666.571729.peg.159	hypothetical protein
2.55	fig|6666666.571729.peg.104	Choline-sulfatase (EC 3.1.6.6);Ontology_term
2.55	fig|6666666.571729.peg.1595	Ribonucleotide reductase of class III (anaerobic)%2C activating protein (EC 1.97.1.4);Ontology_term
2.55	fig|6666666.571729.peg.1078	Aspartokinase (EC 2.7.2.4);Ontology_term

2.54	fig|6666666.571729.peg.1085	ABC transporter%2C permease protein 2 (cluster 5%2C nickel/peptides/opines)
2.54	fig|6666666.571729.peg.1678	hypothetical protein
2.53	fig|6666666.571729.peg.322	Patatin-like phospholipase
2.51	fig|6666666.571729.peg.160	hypothetical protein
2.5	fig|6666666.571729.peg.18	Oligopeptide ABC transporter%2C permease protein OppB (TC 3.A.1.5.1)
2.49	fig|6666666.571729.peg.1406	Lysine exporter LysO
2.49	fig|6666666.571729.peg.855	Glutamine synthetase adenylyl-L-tyrosine phosphorylase (EC 2.7.7.89) / Glutamate-ammonia-ligase adenylyltransferase (EC 2.7.7.42);Ontology_term
2.49	fig|6666666.571729.peg.842	hypothetical protein
2.48	fig|6666666.571729.peg.23	GTP-binding protein EngB
2.48	fig|6666666.571729.peg.1726	Galactose/methyl galactoside ABC transporter%2C permease protein MglC (EC 3.6.3.17);Ontology_term
2.46	fig|6666666.571729.peg.1380	Phosphoenolpyruvate carboxylase (EC 4.1.1.31);Ontology_term
2.45	fig|6666666.571729.peg.1243	TonB-dependent receptor%3B Outer membrane receptor for ferrienterochelin and colicins
2.45	fig|6666666.571729.peg.1786	tRNA(Ile)-lysidine synthetase (EC 6.3.4.19);Ontology_term
2.45	fig|6666666.571729.peg.1877	hypothetical protein
2.43	fig|6666666.571729.peg.1	D-glycero-beta-D-manno-heptose-1%2C7-bisphosphate 7-phosphatase (EC 3.1.3.82);Ontology_term
2.42	fig|6666666.571729.peg.1447	Allophanate hydrolase 2 subunit 1 (EC 3.5.1.54);Ontology_term
2.42	fig|6666666.571729.peg.84	Aspartate--ammonia ligase (EC 6.3.1.1);Ontology_term
2.41	fig|6666666.571729.peg.933	hypothetical protein
2.41	fig|6666666.571729.peg.41	Hydroxymethylpyrimidine ABC transporter%2C ATPase component
2.41	fig|6666666.571729.peg.1359	Putative high-affinity iron permease
2.4	fig|6666666.571729.peg.1236	Oligopeptide ABC transporter%2C ATP-binding protein OppF (TC 3.A.1.5.1)
2.4	fig|6666666.571729.peg.400	6-phosphogluconolactonase (EC 3.1.1.31)%2C eukaryotic type;Ontology_term
2.4	fig|6666666.571729.peg.658	Ribosome-associated inhibitor A
2.39	fig|6666666.571729.peg.1391	ATPase component NikO of energizing module of nickel ECF transporter
2.39	fig|6666666.571729.peg.1223	Exodeoxyribonuclease V beta chain (EC 3.1.11.5);Ontology_term
2.37	fig|6666666.571729.peg.1233	ABC transporter%2C substrate-binding protein (cluster 5%2C nickel/peptides/opines)

2.37	fig|6666666.571729.peg.1455	NADP-dependent malic enzyme (EC 1.1.1.40);Ontology_term
2.36	fig|6666666.571729.peg.7	hypothetical protein
2.36	fig|6666666.571729.peg.1475	Aerobic respiration control sensor protein ArcB (EC 2.7.13.3);Ontology_term
2.36	fig|6666666.571729.peg.600	3-oxoacyl-[acyl-carrier-protein] synthase III (EC 2.3.1.41);Ontology_term
2.35	fig|6666666.571729.peg.1139	Predicted hydroxymethylpyrimidine transporter CytX
2.34	fig|6666666.571729.peg.1936	Uncharacterized protein YfgD%2C not an arsenate reductase
2.34	fig|6666666.571729.peg.687	Phosphoribosylamine--glycine ligase (EC 6.3.4.13);Ontology_term
2.34	fig|6666666.571729.peg.1724	Galactose/methyl galactoside ABC transporter%2C substrate-binding protein MglB (EC 3.6.3.17);Ontology_term
2.34	fig|6666666.571729.peg.1140	Succinyl-CoA ligase [ADP-forming] beta chain (EC 6.2.1.5);Ontology_term
2.34	fig|6666666.571729.peg.281	hypothetical protein
2.33	fig|6666666.571729.peg.730	Rod shape-determining protein RodA
2.33	fig|6666666.571729.peg.728	D-alanyl-D-alanine carboxypeptidase (EC 3.4.16.4);Ontology_term
2.32	fig|6666666.571729.peg.1723	Galactose operon repressor%2C GalR-LacI family of transcriptional regulators
2.31	fig|6666666.571729.peg.1636	Putative DNA-binding protein in cluster with Type I restriction-modification system
2.31	fig|6666666.571729.peg.1257	hypothetical protein
2.3	fig|6666666.571729.peg.1003	Ribonuclease G
2.3	fig|6666666.571729.peg.263	hypothetical protein
2.29	fig|6666666.571729.peg.920	Anaerobic respiratory reductase chaperone
2.29	fig|6666666.571729.peg.522	23S rRNA (uracil(1939)-C(5))-methyltransferase (EC 2.1.1.190);Ontology_term
2.26	fig|6666666.571729.peg.1402	Hydrogenase-4 component B
2.26	fig|6666666.571729.peg.1547	Cystathionine beta-lyase (EC 4.4.1.8);Ontology_term
2.25	fig|6666666.571729.peg.1248	Vitamin B12 ABC transporter%2C permease protein BtuC
2.25	fig|6666666.571729.peg.538	Glycosyltransferase
2.25	fig|6666666.571729.peg.1401	Hydrogenase-4 component C
2.24	fig|6666666.571729.peg.423	deoxyribose-phosphate aldolase(EC:4.1.2.4);Ontology_term
2.23	fig|6666666.571729.peg.284	Shikimate 5-dehydrogenase I gamma (EC 1.1.1.25);Ontology_term
2.23	fig|6666666.571729.peg.683	Aerobic respiration control response regulator ArcA
2.21	fig|6666666.571729.peg.794	N-acetylneuraminate lyase (EC 4.1.3.3);Ontology_term

2.21	fig|6666666.571729.peg.653	Phosphoserine phosphatase (EC 3.1.3.3);Ontology_term
2.21	fig|6666666.571729.peg.578	FIG021862: membrane protein%2C exporter
2.2	fig|6666666.571729.peg.119	Chloride channel protein EriC
2.19	fig|6666666.571729.peg.934	Pentapeptide repeat family protein
2.18	fig|6666666.571729.peg.1682	T6SS component Hcp
2.17	fig|6666666.571729.peg.1255	ABC-type antimicrobial peptide transport system%2C permease component
2.17	fig|6666666.571729.peg.175	Possible ABC transporter%2C periplasmic substrate X binding protein precursor
2.17	fig|6666666.571729.peg.913	ImpA
2.17	fig|6666666.571729.peg.776	NrfC protein
2.17	fig|6666666.571729.peg.1232	DNA protection during starvation protein
2.15	fig|6666666.571729.peg.1084	Peptide ABC transporter%2C ATP-binding protein SapD
2.15	fig|6666666.571729.peg.1588	Hypothetical protein VC0266 (sugar utilization related?)
2.13	fig|6666666.571729.peg.686	IMP cyclohydrolase (EC 3.5.4.10) / Phosphoribosylaminoimidazolecarboxamide formyltransferase (EC 2.1.2.3);Ontology_term
2.13	fig|6666666.571729.peg.153	Uncharacterized protein EC-HemY in Proteobacteria (unrelated to HemY-type PPO in GramPositives)
2.13	fig|6666666.571729.peg.1638	putative 5'(3')-deoxyribonucleotidase
2.13	fig|6666666.571729.peg.339	hypothetical protein
2.13	fig|6666666.571729.peg.866	beta-galactosidase (EC 3.2.1.23);Ontology_term
2.11	fig|6666666.571729.peg.112	tRNA 5-methylaminomethyl-2-thiouridine synthesis sulfur carrier protein TusA
2.11	fig|6666666.571729.peg.960	Inner membrane protein YedI
2.11	fig|6666666.571729.peg.1631	AAA ATPase%2C central region
2.09	fig|6666666.571729.peg.1901	Outer membrane protein P2 precursor
2.09	fig|6666666.571729.peg.693	hypothetical protein
2.09	fig|6666666.571729.peg.1112	Oxygen-insensitive NAD(P)H nitroreductase (EC 1.-.-.-) / Dihydropteridine reductase (EC 1.5.1.34);Ontology_term
2.07	fig|6666666.571729.peg.696	Na+/H+ antiporter NhaB
2.06	fig|6666666.571729.peg.177	Putative metabolite transport protein YjhB
2.06	fig|6666666.571729.peg.1369	pseudoazurin
2.06	fig|6666666.571729.peg.763	Phosphatidate cytidylyltransferase (EC 2.7.7.41);Ontology_term
2.06	fig|6666666.571729.peg.1976	UDP-2%2C3-diacylglucosamine diphosphatase (EC 3.6.1.54);Ontology_term
2.06	fig|6666666.571729.peg.697	Transcriptional regulator for fatty acid degradation FadR%2C GntR family

2.05	fig|6666666.571729.peg.1209	tRNA pseudouridine(65) synthase (EC 5.4.99.26);Ontology_term
2.05	fig|6666666.571729.peg.1372	ABC-type Fe3+-hydroxamate transport system%2C periplasmic component
2.05	fig|6666666.571729.peg.382	LSU rRNA pseudouridine(746) synthase (EC 5.4.99.29) @ tRNA pseudouridine(32) synthase (EC 5.4.99.28);Ontology_term
2.05	fig|6666666.571729.peg.729	Septum-associated rare lipoprotein A
2.02	fig|6666666.571729.peg.266	thiamine-phosphate pyrophosphorylase(EC:2.5.1.3);Ontology_term
2.02	fig|6666666.571729.peg.1919	FIG00696423: hypothetical protein
2.02	fig|6666666.571729.peg.1721	Galactokinase (EC 2.7.1.6);Ontology_term
2.01	fig|6666666.571729.peg.279	Ribonuclease BN
2	fig|6666666.571729.peg.1979	hypothetical protein

Table S2.3: *H. parainfluenzae* genes repressed in *in vitro* coculture

Fold change	ID	Description
-7.49	fig|6666666.571729.peg.756	FIG00697202: hypothetical protein
-5.51	fig|6666666.571729.peg.882	Monothiol glutaredoxin GrxD
-5.45	fig|6666666.571729.peg.904	hypothetical protein
-5.39	fig|6666666.571729.peg.666	UPF0394 inner membrane protein YeeE
-4.62	fig|6666666.571729.peg.680	LSU ribosomal protein L36p @ LSU ribosomal protein L36p%2C zinc-independent
-4.56	fig|6666666.571729.peg.1296	Exodeoxyribonuclease VII small subunit (EC 3.1.11.6);Ontology_term
-4.45	fig|6666666.571729.peg.1754	Dihydroneopterin triphosphate pyrophosphohydrolase type 2
-4.37	fig|6666666.571729.peg.1825	Lipid-A-disaccharide synthase (EC 2.4.1.182);Ontology_term
-4.36	fig|6666666.571729.peg.903	O-acetylhomoserine sulfhydrylase (EC 2.5.1.49) @ O-succinylhomoserine sulfhydrylase (EC 2.5.1.48);Ontology_term
-4.23	fig|6666666.571729.peg.1340	Transcription elongation factor GreA
-4.22	fig|6666666.571729.peg.665	UPF0033 protein YeeD
-4.09	fig|6666666.571729.peg.906	hypothetical protein

-4.03	fig|6666666.571729.peg.1728	Protein IscX%2C believed to be involved in assembly of Fe-S clusters
-3.98	fig|6666666.571729.peg.1700	Cytochrome c551 peroxidase (EC 1.11.1.5);Ontology_term
-3.97	fig|6666666.571729.peg.1108	hypothetical protein
-3.92	fig|6666666.571729.peg.1751	Crossover junction endodeoxyribonuclease RuvC (EC 3.1.22.4);Ontology_term
-3.76	fig|6666666.571729.peg.881	Beta-propeller domains of methanol dehydrogenase type
-3.66	fig|6666666.571729.peg.1884	Nucleoid-associated protein YaaK
-3.57	fig|6666666.571729.peg.1770	Phage integrase
-3.56	fig|6666666.571729.peg.1516	Thiol peroxidase%2C Tpx-type (EC 1.11.1.15);Ontology_term
-3.43	fig|6666666.571729.peg.241	Cell division protein ZapB
-3.41	fig|6666666.571729.peg.1305	Threonyl-tRNA synthetase (EC 6.1.1.3);Ontology_term
-3.4	fig|6666666.571729.peg.1644	D-sedoheptulose 7-phosphate isomerase (EC 5.3.1.28);Ontology_term
-3.36	fig|6666666.571729.peg.1897	Putative glutamine amidotransferase YafJ
-3.32	fig|6666666.571729.peg.838	Uracil permease @ Uracil:proton symporter UraA
-3.31	fig|6666666.571729.peg.338	Hybrid peroxiredoxin hyPrx5 (EC 1.11.1.15);Ontology_term
-3.26	fig|6666666.571729.peg.1769	hypothetical protein
-3.25	fig|6666666.571729.peg.45	DNA primase DnaG
-3.21	fig|6666666.571729.peg.1819	Heat shock protein 10 kDa family chaperone GroES
-3.16	fig|6666666.571729.peg.204	Xanthine-guanine phosphoribosyltransferase (EC 2.4.2.22);Ontology_term
-3.11	fig|6666666.571729.peg.1338	23S rRNA (uridine(2552)-2'-O)-methyltransferase (EC 2.1.1.166);Ontology_term
-3.07	fig|6666666.571729.peg.1743	Tol-Pal system-associated acyl-CoA thioesterase
-3.03	fig|6666666.571729.peg.360	LSU ribosomal protein L22p (L17e)
-2.94	fig|6666666.571729.peg.1051	Modulator of drug activity B
-2.94	fig|6666666.571729.peg.632	Twin-arginine translocation protein TatB
-2.92	fig|6666666.571729.peg.357	LSU ribosomal protein L23p (L23Ae)
-2.91	fig|6666666.571729.peg.1892	LSU ribosomal protein L31p @ LSU ribosomal protein L31p%2C zinc-dependent

-2.9	fig|6666666.571729.peg.1464	GTP cyclohydrolase II (EC 3.5.4.25);Ontology_term
-2.89	fig|6666666.571729.peg.1214	3-hydroxyacyl-[acyl-carrier-protein] dehydratase%2C FabA form (EC 4.2.1.59) @ Trans-2-decenoyl-[acyl-carrier-protein] isomerase (EC 5.3.3.14);Ontology_term
-2.88	fig|6666666.571729.peg.1849	tRNA (guanine(46)-N(7))-methyltransferase (EC 2.1.1.33);Ontology_term
-2.88	fig|6666666.571729.peg.364	SSU ribosomal protein S17p (S11e)
-2.88	fig|6666666.571729.peg.47	N(6)-L-threonylcarbamoyladenine synthase (EC 2.3.1.234);Ontology_term
-2.88	fig|6666666.571729.peg.1463	Phosphatidylglycerophosphatase B (EC 3.1.3.27);Ontology_term
-2.87	fig|6666666.571729.peg.1809	Copper(I) chaperone CopZ
-2.86	fig|6666666.571729.peg.1409	Outer membrane stress sensor protease DegQ%2C serine protease
-2.86	fig|6666666.571729.peg.1733	Iron-sulfur cluster assembly iron binding protein IscA
-2.82	fig|6666666.571729.peg.1242	Iron(III) ABC transporter%2C solute-binding protein
-2.81	fig|6666666.571729.peg.1643	Arginine ABC transporter%2C ATP-binding protein ArtP
-2.81	fig|6666666.571729.peg.1729	Ferredoxin%2C 2Fe-2S
-2.78	fig|6666666.571729.peg.949	Flavodoxin 1
-2.77	fig|6666666.571729.peg.717	Uncharacterized protease YegQ
-2.76	fig|6666666.571729.peg.187	Sigma factor RpoE negative regulatory protein RseB precursor
-2.76	fig|6666666.571729.peg.1740	TolA protein
-2.76	fig|6666666.571729.peg.355	LSU ribosomal protein L3p (L3e)
-2.74	fig|6666666.571729.peg.1710	Acid stress protein IbaG
-2.72	fig|6666666.571729.peg.69	hypothetical protein
-2.71	fig|6666666.571729.peg.1509	DNA polymerase III psi subunit (EC 2.7.7.7);Ontology_term
-2.7	fig|6666666.571729.peg.1123	Pyruvate kinase (EC 2.7.1.40);Ontology_term
-2.7	fig|6666666.571729.peg.774	Cytochrome c-type heme lyase subunit nrfE%2C nitrite reductase complex assembly
-2.69	fig|6666666.571729.peg.1602	FIG024746: hypothetical protein
-2.69	fig|6666666.571729.peg.358	LSU ribosomal protein L2p (L8e)

-2.68	fig|6666666.571729.peg.1730	Chaperone protein HscA
-2.67	fig|6666666.571729.peg.880	hypothetical protein
-2.67	fig|6666666.571729.peg.1482	hypothetical protein
-2.65	fig|6666666.571729.peg.359	SSU ribosomal protein S19p (S15e)
-2.65	fig|6666666.571729.peg.630	Porphobilinogen synthase (EC 4.2.1.24);Ontology_term
-2.64	fig|6666666.571729.peg.2003	Frataxin homolog CyaY%2C facilitates Fe-S cluster assembly%2C interacts with IscS
-2.63	fig|6666666.571729.peg.73	Purine nucleoside phosphorylase (EC 2.4.2.1);Ontology_term
-2.61	fig|6666666.571729.peg.353	hypothetical protein
-2.59	fig|6666666.571729.peg.354	SSU ribosomal protein S10p (S20e)
-2.59	fig|6666666.571729.peg.1858	Glutathionylspermidine synthase (EC 6.3.1.8) / Glutathionylspermidine amidohydrolase (EC 3.5.1.78);Ontology_term
-2.58	fig|6666666.571729.peg.1168	6%2C7-dimethyl-8-ribityllumazine synthase (EC 2.5.1.78);Ontology_term
-2.58	fig|6666666.571729.peg.1641	Arginine ABC transporter%2C permease protein ArtQ
-2.57	fig|6666666.571729.peg.948	Ferric uptake regulation protein FUR
-2.57	fig|6666666.571729.peg.1013	LSU ribosomal protein L25p
-2.57	fig|6666666.571729.peg.1169	Transcription termination protein NusB
-2.55	fig|6666666.571729.peg.1542	HesA/MoeB/ThiF family protein > sulfur transfer pathway protein CsdL
-2.55	fig|6666666.571729.peg.989	Iron compound ABC transporter%2C permease protein
-2.55	fig|6666666.571729.peg.1731	Uncharacterized protein YbfG
-2.52	fig|6666666.571729.peg.1750	Holliday junction ATP-dependent DNA helicase RuvA (EC 3.6.4.12);Ontology_term
-2.51	fig|6666666.571729.peg.565	FIG01269488: protein%2C clustered with ribosomal protein L32p
-2.51	fig|6666666.571729.peg.1485	Transcriptional activator MetR
-2.49	fig|6666666.571729.peg.1692	T6SS lysozyme-like component TssE
-2.48	fig|6666666.571729.peg.361	SSU ribosomal protein S3p (S3e)
-2.47	fig|6666666.571729.peg.1846	Transcriptional regulator%2C AcrR family

-2.46	fig|6666666.571729.peg.356	LSU ribosomal protein L4p (L1e)
-2.44	fig|6666666.571729.peg.1768	hypothetical protein
-2.42	fig|6666666.571729.peg.659	hypothetical protein
-2.42	fig|6666666.571729.peg.440	Iron(III) dicitrate transport system%2C periplasmic iron-binding protein FecB (TC 3.A.1.14.1)
-2.42	fig|6666666.571729.peg.416	tRNA pseudouridine(13) synthase (EC 5.4.99.27);Ontology_term
-2.42	fig|6666666.571729.peg.764	Alanine transaminase (EC 2.6.1.2);Ontology_term
-2.41	fig|6666666.571729.peg.676	LSU ribosomal protein L27p
-2.41	fig|6666666.571729.peg.1793	Membrane protein involved in the export of O-antigen and teichoic acid
-2.41	fig|6666666.571729.peg.186	Molybdopterin-guanine dinucleotide biosynthesis protein MobB
-2.36	fig|6666666.571729.peg.681	LSU ribosomal protein L31p @ LSU ribosomal protein L31p%2C zinc-independent
-2.36	fig|6666666.571729.peg.226	Threonine dehydratase biosynthetic (EC 4.3.1.19);Ontology_term
-2.36	fig|6666666.571729.peg.430	33 kDa chaperonin HslO
-2.35	fig|6666666.571729.peg.839	Uracil phosphoribosyltransferase (EC 2.4.2.9);Ontology_term
-2.33	fig|6666666.571729.peg.1800	Glutamyl-tRNA synthetase (EC 6.1.1.17);Ontology_term
-2.33	fig|6666666.571729.peg.1737	tRNA (cytidine(32)/uridine(32)-2'-O)-methyltransferase (EC 2.1.1.200);Ontology_term
-2.33	fig|6666666.571729.peg.57	L-cystine ABC transporter%2C substrate-binding protein TcyA
-2.32	fig|6666666.571729.peg.936	Nucleoside-diphosphate-sugar epimerases
-2.32	fig|6666666.571729.peg.1012	DedA protein
-2.32	fig|6666666.571729.peg.1245	Molybdate-binding domain of ModE
-2.32	fig|6666666.571729.peg.1297	(2E%2C6E)-farnesyl diphosphate synthase (EC 2.5.1.10);Ontology_term
-2.32	fig|6666666.571729.peg.1917	Lipooligosaccharide biosynthesis protein lex-1 (EC 2.-.-.-);Ontology_term
-2.32	fig|6666666.571729.peg.1316	Stringent starvation protein B
-2.31	fig|6666666.571729.peg.1566	UPF0307 protein YjgA
-2.3	fig|6666666.571729.peg.1573	N-succinyl-L%2CL-diaminopimelate desuccinylase (EC 3.5.1.18);Ontology_term
-2.3	fig|6666666.571729.peg.905	Chaperone protein DnaK

-2.3	fig|6666666.571729.peg.1603	FIG023677: hypothetical protein
-2.29	fig|6666666.571729.peg.1742	Tol-Pal system protein TolQ
-2.28	fig|6666666.571729.peg.1732	Chaperone protein HscB
-2.28	fig|6666666.571729.peg.755	Autonomous glycyl radical cofactor
-2.28	fig|6666666.571729.peg.67	hypothetical protein
-2.27	fig|6666666.571729.peg.467	Excinuclease ABC subunit A
-2.26	fig|6666666.571729.peg.735	Efflux ABC transporter%2C permease/ATP-binding protein
-2.26	fig|6666666.571729.peg.1487	Site-specific recombinase
-2.26	fig|6666666.571729.peg.1054	Peptide chain release factor 1
-2.26	fig|6666666.571729.peg.1039	Hypothetical metal-binding enzyme%2C YcbL homolog
-2.26	fig|6666666.571729.peg.841	Nitric-oxide reductase (EC 1.7.99.7)%2C quinol-dependent;Ontology_term
-2.25	fig|6666666.571729.peg.625	FAD:protein FMN transferase (EC 2.7.1.180) @ FAD:protein FMN transferase (EC 2.7.1.180)%2C NqrBC-associated;Ontology_term
-2.25	fig|6666666.571729.peg.871	DNA polymerase III chi subunit (EC 2.7.7.7);Ontology_term
-2.25	fig|6666666.571729.peg.318	Putative phosphatase YigL%2C haloacid dehalogenase-like phosphatase family
-2.23	fig|6666666.571729.peg.843	Signal recognition particle protein Ffh
-2.23	fig|6666666.571729.peg.1827	3-hydroxyacyl-[acyl-carrier-protein] dehydratase%2C FabZ form (EC 4.2.1.59);Ontology_term
-2.22	fig|6666666.571729.peg.1811	Methionine repressor MetJ
-2.21	fig|6666666.571729.peg.531	GTP-binding protein TypA/BipA
-2.2	fig|6666666.571729.peg.1716	Apolipoprotein N-acyltransferase / Copper homeostasis protein CutE
-2.2	fig|6666666.571729.peg.1850	FIG002060: uncharacterized protein YggL
-2.19	fig|6666666.571729.peg.782	LSU ribosomal protein L33p @ LSU ribosomal protein L33p%2C zinc-independent
-2.19	fig|6666666.571729.peg.142	Ketol-acid reductoisomerase (NADP(+)) (EC 1.1.1.86);Ontology_term
-2.18	fig|6666666.571729.peg.1493	Uridine kinase (EC 2.7.1.48);Ontology_term
-2.17	fig|6666666.571729.peg.1486	Site-specific recombinase

-2.16	fig|6666666.571729.peg.1318	SSU ribosomal protein S9p (S16e)
-2.16	fig|6666666.571729.peg.682	tmRNA-binding protein SmpB
-2.16	fig|6666666.571729.peg.1808	Copper-translocating P-type ATPase (EC 3.6.3.4);Ontology_term
-2.16	fig|6666666.571729.peg.1646	Thioredoxin
-2.16	fig|6666666.571729.peg.70	Transcription accessory protein (S1 RNA-binding domain)
-2.15	fig|6666666.571729.peg.367	LSU ribosomal protein L5p (L11e)
-2.15	fig|6666666.571729.peg.879	LemA family protein
-2.15	fig|6666666.571729.peg.362	LSU ribosomal protein L16p (L10e)
-2.14	fig|6666666.571729.peg.980	hypothetical protein
-2.13	fig|6666666.571729.peg.1741	Tol biopolymer transport system%2C TolR protein
-2.12	fig|6666666.571729.peg.1797	Soluble lytic murein transglycosylase (EC 4.2.2.n1)
-2.12	fig|6666666.571729.peg.1299	LSU ribosomal protein L20p
-2.11	fig|6666666.571729.peg.675	LSU ribosomal protein L21p
-2.1	fig|6666666.571729.peg.1437	Ribonucleotide reductase of class Ia (aerobic)%2C alpha subunit (EC 1.17.4.1);Ontology_term
-2.1	fig|6666666.571729.peg.1715	Phospholipid ABC transporter ATP-binding protein MlaF
-2.09	fig|6666666.571729.peg.1861	Phosphatidylserine decarboxylase (EC 4.1.1.65);Ontology_term
-2.09	fig|6666666.571729.peg.239	tRNA-5-carboxymethylaminomethyl-2-thiouridine(34) synthesis protein MnmG
-2.09	fig|6666666.571729.peg.1303	Translation initiation factor 3
-2.07	fig|6666666.571729.peg.1907	LSU ribosomal protein L9p
-2.07	fig|6666666.571729.peg.1818	Heat shock protein 60 kDa family chaperone GroEL
-2.06	fig|6666666.571729.peg.1183	Transcription termination protein NusA
-2.06	fig|6666666.571729.peg.144	histone H1
-2.05	fig|6666666.571729.peg.1341	D-alanyl-D-alanine carboxypeptidase (EC 3.4.16.4);Ontology_term
-2.04	fig|6666666.571729.peg.46	SSU ribosomal protein S21p

-2.03	fig|6666666.571729.peg.1587	Ribonucleotide reductase of class III (anaerobic)%2C large subunit (EC 1.17.4.2);Ontology_term
-2.03	fig|6666666.571729.peg.363	LSU ribosomal protein L29p (L35e)
-2.01	fig|6666666.571729.peg.496	2-haloalkanoic acid dehalogenase (EC 3.8.1.2);Ontology_term
-2.01	fig|6666666.571729.peg.1494	Deoxycytidine triphosphate deaminase (EC 3.5.4.13);Ontology_term
-2	fig|6666666.571729.peg.1468	DNA topoisomerase IV subunit B (EC 5.99.1.3);Ontology_term
-2	fig|6666666.571729.peg.1096	Thiol:disulfide interchange protein DsbC
-2	fig|6666666.571729.peg.1929	SOS-response repressor and protease LexA (EC 3.4.21.88);Ontology_term

Table S2.4: *H. parainfluenzae* genes induced in *in vitro* coculture and both *in vivo* metatranscriptomes

id	Description
fig|6666666.571729.peg.60	Glycerol uptake facilitator protein
fig|6666666.571729.peg.32	Type IV pilus biogenesis protein PilM
fig|6666666.571729.peg.40	Hydroxymethylpyrimidine ABC transporter transmembrane component
fig|6666666.571729.peg.629	NADP-specific glutamate dehydrogenase (EC 1.4.1.4);Ontology_term
fig|6666666.571729.peg.1372	ABC-type Fe3+-hydroxamate transport system periplasmic component
fig|6666666.571729.peg.1681	hypothetical protein
fig|6666666.571729.peg.25	AAA+ ATPase superfamily protein YifB/ComM associated with DNA recombination
fig|6666666.571729.peg.687	Phosphoribosylamine--glycine ligase (EC 6.3.4.13);Ontology_term
fig|6666666.571729.peg.119	Chloride channel protein EriC
fig|6666666.571729.peg.95	Phosphoribosylformylglycinamidine synthase synthetase subunit (EC 6.3.5.3) / Phosphoribosylformylglycinamidine synthase glutamine amidotransferase subunit (EC 6.3.5.3);Ontology_term
fig|6666666.571729.peg.1446	Allophanate hydrolase 2 subunit 2 (EC 3.5.1.54);Ontology_term
fig|6666666.571729.peg.522	23S rRNA (uracil(1939)-C(5))-methyltransferase (EC 2.1.1.190);Ontology_term
fig|6666666.571729.peg.173	Putative ABC transporter of substrate X permease subunit I

fig|6666666.571729.peg.242	Fructose-16-bisphosphatase GlpX type (EC 3.1.3.11);Ontology_term
fig|6666666.571729.peg.502	hypothetical protein
fig|6666666.571729.peg.866	beta-galactosidase (EC 3.2.1.23);Ontology_term
fig|6666666.571729.peg.1078	Aspartokinase (EC 2.7.2.4);Ontology_term
fig|6666666.571729.peg.61	Glycerol kinase (EC 2.7.1.30);Ontology_term

Table S2.5: *H. parainfluenzae* genes repressed in *in vitro* coculture and both *in vivo* metatranscriptomes

id	Description
fig|6666666.571729.peg.903	O-acetylhomoserine sulfhydrylase (EC 2.5.1.49) @ O-succinylhomoserine sulfhydrylase (EC 2.5.1.48);Ontology_term
fig|6666666.571729.peg.905	Chaperone protein DnaK
fig|6666666.571729.peg.1409	Outer membrane stress sensor protease DegQ serine protease
fig|6666666.571729.peg.1340	Transcription elongation factor GreA
fig|6666666.571729.peg.1811	Methionine repressor MetJ
fig|6666666.571729.peg.1850	FIG002060: uncharacterized protein YggL
fig|6666666.571729.peg.980	hypothetical protein
fig|6666666.571729.peg.430	33 kDa chaperonin HslO
fig|6666666.571729.peg.904	hypothetical protein
fig|6666666.571729.peg.906	hypothetical protein
fig|6666666.571729.peg.69	hypothetical protein
fig|6666666.571729.peg.496	2-haloalkanoic acid dehalogenase (EC 3.8.1.2);Ontology_term
fig|6666666.571729.peg.57	L-cystine ABC transporter substrate-binding protein TcyA
fig|6666666.571729.peg.73	Purine nucleoside phosphorylase (EC 2.4.2.1);Ontology_term
fig|6666666.571729.peg.1316	Stringent starvation protein B
fig|6666666.571729.peg.1858	Glutathionylspermidine synthase (EC 6.3.1.8) / Glutathionylspermidine amidohydrolase (EC 3.5.1.78);Ontology_term
fig|6666666.571729.peg.1884	Nucleoid-associated protein YaaK
fig|6666666.571729.peg.1861	Phosphatidylserine decarboxylase (EC 4.1.1.65);Ontology_term
fig|6666666.571729.peg.226	Threonine dehydratase biosynthetic (EC 4.3.1.19);Ontology_term
fig|6666666.571729.peg.1013	LSU ribosomal protein L25p
fig|6666666.571729.peg.948	Ferric uptake regulation protein FUR
fig|6666666.571729.peg.1305	Threonyl-tRNA synthetase (EC 6.1.1.3);Ontology_term

Table S2.6: *H. parainfluenzae* genes upregulated in *in vitro* coculture and *in vivo* meta-transcriptome Benítez-Páez et al., (2014)

id	Description
fig|6666666.571729.peg.60	Glycerol uptake facilitator protein
fig|6666666.571729.peg.32	Type IV pilus biogenesis protein PilM
fig|6666666.571729.peg.40	Hydroxymethylpyrimidine ABC transporter transmembrane component
fig|6666666.571729.peg.629	NADP-specific glutamate dehydrogenase (EC 1.4.1.4);Ontology_term
fig|6666666.571729.peg.1372	ABC-type Fe3+-hydroxamate transport system periplasmic component
fig|6666666.571729.peg.1681	hypothetical protein
fig|6666666.571729.peg.25	AAA+ ATPase superfamily protein YifB/ComM associated with DNA recombination
fig|6666666.571729.peg.687	Phosphoribosylamine--glycine ligase (EC 6.3.4.13);Ontology_term
fig|6666666.571729.peg.119	Chloride channel protein EriC
fig|6666666.571729.peg.95	Phosphoribosylformylglycinamidine synthase synthetase subunit (EC 6.3.5.3) / Phosphoribosylformylglycinamidine synthase glutamine amidotransferase subunit (EC 6.3.5.3);Ontology_term
fig|6666666.571729.peg.1446	Allophanate hydrolase 2 subunit 2 (EC 3.5.1.54);Ontology_term
fig|6666666.571729.peg.522	23S rRNA (uracil(1939)-C(5))-methyltransferase (EC 2.1.1.190);Ontology_term
fig|6666666.571729.peg.173	Putative ABC transporter of substrate X permease subunit I
fig|6666666.571729.peg.686	IMP cyclohydrolase (EC 3.5.4.10) / Phosphoribosylaminoimidazolecarboxamide formyltransferase (EC 2.1.2.3);Ontology_term
fig|6666666.571729.peg.896	5'-deoxynucleotidase YfbR (EC 3.1.3.89);Ontology_term
fig|6666666.571729.peg.242	Fructose-16-bisphosphatase GlpX type (EC 3.1.3.11);Ontology_term
fig|6666666.571729.peg.502	hypothetical protein
fig|6666666.571729.peg.866	beta-galactosidase (EC 3.2.1.23);Ontology_term
fig|6666666.571729.peg.3	Methionine ABC transporter permease protein
fig|6666666.571729.peg.792	N-acetylmannosamine kinase (EC 2.7.1.60);Ontology_term
fig|6666666.571729.peg.1078	Aspartokinase (EC 2.7.2.4);Ontology_term
fig|6666666.571729.peg.61	Glycerol kinase (EC 2.7.1.30);Ontology_term

Table S2.7: *H. parainfluenzae* genes downregulated in *in vitro* coculture and *in vivo* meta-transcriptome Benítez-Páez et al., (2014)

id	Description
fig|6666666.571729.peg.1245	Molybdate-binding domain of ModE

fig|6666666.571729.peg.903	O-acetylhomoserine sulfhydrylase (EC 2.5.1.49) @ O-succinylhomoserine sulfhydrylase (EC 2.5.1.48);Ontology_term
fig|6666666.571729.peg.1768	hypothetical protein
fig|6666666.571729.peg.905	Chaperone protein DnaK
fig|6666666.571729.peg.1409	Outer membrane stress sensor protease DegQ serine protease
fig|6666666.571729.peg.1340	Transcription elongation factor GreA
fig|6666666.571729.peg.1811	Methionine repressor MetJ
fig|6666666.571729.peg.1700	Cytochrome c551 peroxidase (EC 1.11.1.5);Ontology_term
fig|6666666.571729.peg.1850	FIG002060: uncharacterized protein YggL
fig|6666666.571729.peg.980	hypothetical protein
fig|6666666.571729.peg.430	33 kDa chaperonin HslO
fig|6666666.571729.peg.904	hypothetical protein
fig|6666666.571729.peg.906	hypothetical protein
fig|6666666.571729.peg.665	UPF0033 protein YeeD
fig|6666666.571729.peg.1242	Iron(III) ABC transporter solute-binding protein
fig|6666666.571729.peg.1809	Copper(I) chaperone CopZ
fig|6666666.571729.peg.1012	DedA protein
fig|6666666.571729.peg.1818	Heat shock protein 60 kDa family chaperone GroEL
fig|6666666.571729.peg.67	hypothetical protein
fig|6666666.571729.peg.69	hypothetical protein
fig|6666666.571729.peg.496	2-haloalkanoic acid dehalogenase (EC 3.8.1.2);Ontology_term
fig|6666666.571729.peg.57	L-cystine ABC transporter substrate-binding protein TcyA
fig|6666666.571729.peg.73	Purine nucleoside phosphorylase (EC 2.4.2.1);Ontology_term
fig|6666666.571729.peg.782	LSU ribosomal protein L33p @ LSU ribosomal protein L33p zinc-independent
fig|6666666.571729.peg.1316	Stringent starvation protein B
fig|6666666.571729.peg.1858	Glutathionylspermidine synthase (EC 6.3.1.8) / Glutathionylspermidine amidohydrolase (EC 3.5.1.78);Ontology_term
fig|6666666.571729.peg.46	SSU ribosomal protein S21p
fig|6666666.571729.peg.1797	Soluble lytic murein transglycosylase (EC 4.2.2.n1)
fig|6666666.571729.peg.1731	Uncharacterized protein YbfG
fig|6666666.571729.peg.1884	Nucleoid-associated protein YaaK
fig|6666666.571729.peg.717	Uncharacterized protease YegQ
fig|6666666.571729.peg.838	Uracil permease @ Uracil:proton symporter UraA
fig|6666666.571729.peg.1299	LSU ribosomal protein L20p
fig|6666666.571729.peg.1730	Chaperone protein HscA
fig|6666666.571729.peg.1861	Phosphatidylserine decarboxylase (EC 4.1.1.65);Ontology_term

fig|6666666.571729.peg.1800	Glutamyl-tRNA synthetase (EC 6.1.1.17);Ontology_term
fig|6666666.571729.peg.226	Threonine dehydratase biosynthetic (EC 4.3.1.19);Ontology_term
fig|6666666.571729.peg.1013	LSU ribosomal protein L25p
fig|6666666.571729.peg.948	Ferric uptake regulation protein FUR
fig|6666666.571729.peg.1305	Threonyl-tRNA synthetase (EC 6.1.1.3);Ontology_term

Table S2.8: *H. parainfluenzae* genes induced in *in vitro* coculture and *in vivo* meta-transcriptome Jorth et al., (2014)

id	Description
fig|6666666.571729.peg.1083	Peptide transport system ATP-binding protein sapF (TC 3.A.1.5.5)
fig|6666666.571729.peg.747	Type IV pilin PilA
fig|6666666.571729.peg.656	hypothetical protein
fig|6666666.571729.peg.1288	Type III restriction-modification system methylation subunit (EC 2.1.1.72);Ontology_term
fig|6666666.571729.peg.40	Hydroxymethylpyrimidine ABC transporter transmembrane component
fig|6666666.571729.peg.1084	Peptide ABC transporter ATP-binding protein SapD
fig|6666666.571729.peg.1446	Allophanate hydrolase 2 subunit 2 (EC 3.5.1.54);Ontology_term
fig|6666666.571729.peg.25	AAA+ ATPase superfamily protein YifB/ComM associated with DNA recombination
fig|6666666.571729.peg.254	hypothetical protein
fig|6666666.571729.peg.1645	DNA ligase
fig|6666666.571729.peg.583	FIGfam138462: Acyl-CoA synthetase AMP-(fatty) acid ligase
fig|6666666.571729.peg.160	hypothetical protein
fig|6666666.571729.peg.1223	Exodeoxyribonuclease V beta chain (EC 3.1.11.5);Ontology_term
fig|6666666.571729.peg.629	NADP-specific glutamate dehydrogenase (EC 1.4.1.4);Ontology_term
fig|6666666.571729.peg.32	Type IV pilus biogenesis protein PilM
fig|6666666.571729.peg.60	Glycerol uptake facilitator protein
fig|6666666.571729.peg.1192	Micrococcal nuclease (thermonuclease) homologs
fig|6666666.571729.peg.95	Phosphoribosylformylglycinamidine synthase synthetase subunit (EC 6.3.5.3) / Phosphoribosylformylglycinamidine synthase glutamine amidotransferase subunit (EC 6.3.5.3);Ontology_term
fig|6666666.571729.peg.279	Ribonuclease BN

fig|6666666.571729.peg.687	Phosphoribosylamine--glycine ligase (EC 6.3.4.13);Ontology_term
fig|6666666.571729.peg.1141	Succinyl-CoA ligase [ADP-forming] alpha chain (EC 6.2.1.5);Ontology_term
fig|6666666.571729.peg.242	Fructose-16-bisphosphatase GlpX type (EC 3.1.3.11);Ontology_term
fig|6666666.571729.peg.102	GALNS arylsulfatase regulator (Fe-S oxidoreductase)
fig|6666666.571729.peg.382	LSU rRNA pseudouridine(746) synthase (EC 5.4.99.29) @ tRNA pseudouridine(32) synthase (EC 5.4.99.28);Ontology_term
fig|6666666.571729.peg.649	hypothetical protein
fig|6666666.571729.peg.1287	Type III restriction-modification system restriction subunit (EC 3.1.21.5);Ontology_term
fig|6666666.571729.peg.1163	14-alpha-glucan (glycogen) branching enzyme GH-13-type (EC 2.4.1.18);Ontology_term
fig|6666666.571729.peg.1475	Aerobic respiration control sensor protein ArcB (EC 2.7.13.3);Ontology_term
fig|6666666.571729.peg.595	FIG00847847: hypothetical protein
fig|6666666.571729.peg.18	Oligopeptide ABC transporter permease protein OppB (TC 3.A.1.5.1)
fig|6666666.571729.peg.403	hypothetical protein
fig|6666666.571729.peg.61	Glycerol kinase (EC 2.7.1.30);Ontology_term
fig|6666666.571729.peg.592	hypothetical protein
fig|6666666.571729.peg.322	Patatin-like phospholipase
fig|6666666.571729.peg.593	hypothetical protein
fig|6666666.571729.peg.648	Mobile element protein
fig|6666666.571729.peg.597	hypothetical protein
fig|6666666.571729.peg.173	Putative ABC transporter of substrate X permease subunit I
fig|6666666.571729.peg.172	Putative ABC transporter of substrate X ATP-binding subunit
fig|6666666.571729.peg.1147	UPF0115 protein YfcN
fig|6666666.571729.peg.475	Transcriptional regulator AsnC family
fig|6666666.571729.peg.1258	hypothetical protein
fig|6666666.571729.peg.522	23S rRNA (uracil(1939)-C(5))-methyltransferase (EC 2.1.1.190);Ontology_term
fig|6666666.571729.peg.119	Chloride channel protein EriC
fig|6666666.571729.peg.1122	Phage integrase
fig|6666666.571729.peg.1372	ABC-type Fe3+-hydroxamate transport system periplasmic component
fig|6666666.571729.peg.134	Shikimate 5-dehydrogenase I alpha (EC 1.1.1.25);Ontology_term
fig|6666666.571729.peg.1681	hypothetical protein
fig|6666666.571729.peg.252	hypothetical protein
fig|6666666.571729.peg.693	hypothetical protein
fig|6666666.571729.peg.249	Lysophospholipase L2 (EC 3.1.1.5);Ontology_term

fig|6666666.571729.peg.1636	Putative DNA-binding protein in cluster with Type I restriction-modification system
fig|6666666.571729.peg.501	hypothetical protein
fig|6666666.571729.peg.323	DNA transformation protein TfoX
fig|6666666.571729.peg.1477	Uncharacterized protein MSMEG_6412
fig|6666666.571729.peg.969	Trehalose operon transcriptional repressor
fig|6666666.571729.peg.1916	Glycosyl transferase
fig|6666666.571729.peg.423	deoxyribose-phosphate aldolase(EC:4.1.2.4);Ontology_term
fig|6666666.571729.peg.161	hypothetical protein
fig|6666666.571729.peg.1209	tRNA pseudouridine(65) synthase (EC 5.4.99.26);Ontology_term
fig|6666666.571729.peg.720	hypothetical protein
fig|6666666.571729.peg.730	Rod shape-determining protein RodA
fig|6666666.571729.peg.502	hypothetical protein
fig|6666666.571729.peg.855	Glutamine synthetase adenylyl-L-tyrosine phosphorylase (EC 2.7.7.89) / Glutamate-ammonia-ligase adenylyltransferase (EC 2.7.7.42);Ontology_term
fig|6666666.571729.peg.1078	Aspartokinase (EC 2.7.2.4);Ontology_term
fig|6666666.571729.peg.470	hypothetical protein
fig|6666666.571729.peg.525	D-glycerate transporter (predicted)
fig|6666666.571729.peg.1189	Zn-ribbon-containing possibly nucleic-acid-binding protein
fig|6666666.571729.peg.1786	tRNA(Ile)-lysidine synthetase (EC 6.3.4.19);Ontology_term
fig|6666666.571729.peg.866	beta-galactosidase (EC 3.2.1.23);Ontology_term
fig|6666666.571729.peg.960	Inner membrane protein YedI
fig|6666666.571729.peg.1017	Cell division inhibitor Slr1223 (YfcH in EC) contains epimerase/dehydratase and DUF1731 domains
fig|6666666.571729.peg.578	FIG021862: membrane protein exporter
fig|6666666.571729.peg.1011	CRISPR-associated endonuclease Cas9
fig|6666666.571729.peg.176	Sodium-dependent anion transporter family
fig|6666666.571729.peg.1248	Vitamin B12 ABC transporter permease protein BtuC
fig|6666666.571729.peg.19	Oligopeptide ABC transporter permease protein OppC (TC 3.A.1.5.1)
fig|6666666.571729.peg.689	hypothetical protein
fig|6666666.571729.peg.1260	hypothetical protein
fig|6666666.571729.peg.258	Tyrosine-specific transport protein
fig|6666666.571729.peg.148	Nitrate/nitrite response regulator protein NarP
fig|6666666.571729.peg.21	Oligopeptide ABC transporter ATP-binding protein OppF (TC 3.A.1.5.1)
fig|6666666.571729.peg.1140	Succinyl-CoA ligase [ADP-forming] beta chain (EC 6.2.1.5);Ontology_term

fig|6666666.571729.peg.1235	Oligopeptide/dipeptide ABC transporter permease protein / Oligopeptide/dipeptide ABC transporter ATP-binding protein
fig|6666666.571729.peg.1631	AAA ATPase central region
fig|6666666.571729.peg.763	Phosphatidate cytidylyltransferase (EC 2.7.7.41);Ontology_term
fig|6666666.571729.peg.653	Phosphoserine phosphatase (EC 3.1.3.3);Ontology_term
fig|6666666.571729.peg.1236	Oligopeptide ABC transporter ATP-binding protein OppF (TC 3.A.1.5.1)
fig|6666666.571729.peg.104	Choline-sulfatase (EC 3.1.6.6);Ontology_term
fig|6666666.571729.peg.965	Permease of the drug/metabolite transporter (DMT) superfamily

Table S2.9: *H. parainfluenzae* genes repressedin *in vitro* coculture and *in vivo* metatranscriptome Jorth et al., (2014)

id	Description
fig|6666666.571729.peg.1646	Thioredoxin
fig|6666666.571729.peg.905	Chaperone protein DnaK
fig|6666666.571729.peg.1013	LSU ribosomal protein L25p
fig|6666666.571729.peg.1850	FIG002060: uncharacterized protein YggL
fig|6666666.571729.peg.1409	Outer membrane stress sensor protease DegQ serine protease
fig|6666666.571729.peg.1884	Nucleoid-associated protein YaaK
fig|6666666.571729.peg.73	Purine nucleoside phosphorylase (EC 2.4.2.1);Ontology_term
fig|6666666.571729.peg.948	Ferric uptake regulation protein FUR
fig|6666666.571729.peg.1793	Membrane protein involved in the export of O-antigen and teichoic acid
fig|6666666.571729.peg.903	O-acetylhomoserine sulfhydrylase (EC 2.5.1.49) @ O-succinylhomoserine sulfhydrylase (EC 2.5.1.48);Ontology_term
fig|6666666.571729.peg.338	Hybrid peroxiredoxin hyPrx5 (EC 1.11.1.15);Ontology_term
fig|6666666.571729.peg.1737	tRNA (cytidine(32)/uridine(32)-2'-O)-methyltransferase (EC 2.1.1.200);Ontology_term
fig|6666666.571729.peg.906	hypothetical protein
fig|6666666.571729.peg.1340	Transcription elongation factor GreA
fig|6666666.571729.peg.353	hypothetical protein
fig|6666666.571729.peg.1811	Methionine repressor MetJ
fig|6666666.571729.peg.1482	hypothetical protein
fig|6666666.571729.peg.1733	Iron-sulfur cluster assembly iron binding protein IscA

fig|6666666.571729.peg.1858	Glutathionylspermidine synthase (EC 6.3.1.8) / Glutathionylspermidine amidohydrolase (EC 3.5.1.78);Ontology_term
fig|6666666.571729.peg.142	Ketol-acid reductoisomerase (NADP(+)) (EC 1.1.1.86);Ontology_term
fig|6666666.571729.peg.1108	hypothetical protein
fig|6666666.571729.peg.1168	67-dimethyl-8-ribityllumazine synthase (EC 2.5.1.78);Ontology_term
fig|6666666.571729.peg.764	Alanine transaminase (EC 2.6.1.2);Ontology_term
fig|6666666.571729.peg.57	L-cystine ABC transporter substrate-binding protein TcyA
fig|6666666.571729.peg.430	33 kDa chaperonin HslO
fig|6666666.571729.peg.904	hypothetical protein
fig|6666666.571729.peg.1728	Protein IscX believed to be involved in assembly of Fe-S clusters
fig|6666666.571729.peg.1929	SOS-response repressor and protease LexA (EC 3.4.21.88);Ontology_term
fig|6666666.571729.peg.1316	Stringent starvation protein B
fig|6666666.571729.peg.666	UPF0394 inner membrane protein YeeE
fig|6666666.571729.peg.632	Twin-arginine translocation protein TatB
fig|6666666.571729.peg.1123	Pyruvate kinase (EC 2.7.1.40);Ontology_term
fig|6666666.571729.peg.1464	GTP cyclohydrolase II (EC 3.5.4.25);Ontology_term
fig|6666666.571729.peg.1214	3-hydroxyacyl-[acyl-carrier-protein] dehydratase FabA form (EC 4.2.1.59) @ Trans-2-decenoyl-[acyl-carrier-protein] isomerase (EC 5.3.3.14);Ontology_term
fig|6666666.571729.peg.226	Threonine dehydratase biosynthetic (EC 4.3.1.19);Ontology_term
fig|6666666.571729.peg.841	Nitric-oxide reductase (EC 1.7.99.7) quinol-dependent;Ontology_term
fig|6666666.571729.peg.1861	Phosphatidylserine decarboxylase (EC 4.1.1.65);Ontology_term
fig|6666666.571729.peg.980	hypothetical protein
fig|6666666.571729.peg.1303	Translation initiation factor 3
fig|6666666.571729.peg.871	DNA polymerase III chi subunit (EC 2.7.7.7);Ontology_term
fig|6666666.571729.peg.359	SSU ribosomal protein S19p (S15e)
fig|6666666.571729.peg.1643	Arginine ABC transporter ATP-binding protein ArtP
fig|6666666.571729.peg.1741	Tol biopolymer transport system TolR protein
fig|6666666.571729.peg.1338	23S rRNA (uridine(2552)-2'-O)-methyltransferase (EC 2.1.1.166);Ontology_term
fig|6666666.571729.peg.1516	Thiol peroxidase Tpx-type (EC 1.11.1.15);Ontology_term
fig|6666666.571729.peg.1644	D-sedoheptulose 7-phosphate isomerase (EC 5.3.1.28);Ontology_term
fig|6666666.571729.peg.1587	Ribonucleotide reductase of class III (anaerobic) large subunit (EC 1.17.4.2);Ontology_term
fig|6666666.571729.peg.69	hypothetical protein

fig|6666666.571729.peg.1305	Threonyl-tRNA synthetase (EC 6.1.1.3);Ontology_term
fig|6666666.571729.peg.989	Iron compound ABC transporter permease protein
fig|6666666.571729.peg.1341	D-alanyl-D-alanine carboxypeptidase (EC 3.4.16.4);Ontology_term
fig|6666666.571729.peg.1096	Thiol:disulfide interchange protein DsbC
fig|6666666.571729.peg.949	Flavodoxin 1
fig|6666666.571729.peg.1494	Deoxycytidine triphosphate deaminase (EC 3.5.4.13);Ontology_term
fig|6666666.571729.peg.358	LSU ribosomal protein L2p (L8e)
fig|6666666.571729.peg.1602	FIG024746: hypothetical protein
fig|6666666.571729.peg.1729	Ferredoxin 2Fe-2S
fig|6666666.571729.peg.496	2-haloalkanoic acid dehalogenase (EC 3.8.1.2);Ontology_term
fig|6666666.571729.peg.1566	UPF0307 protein YjgA

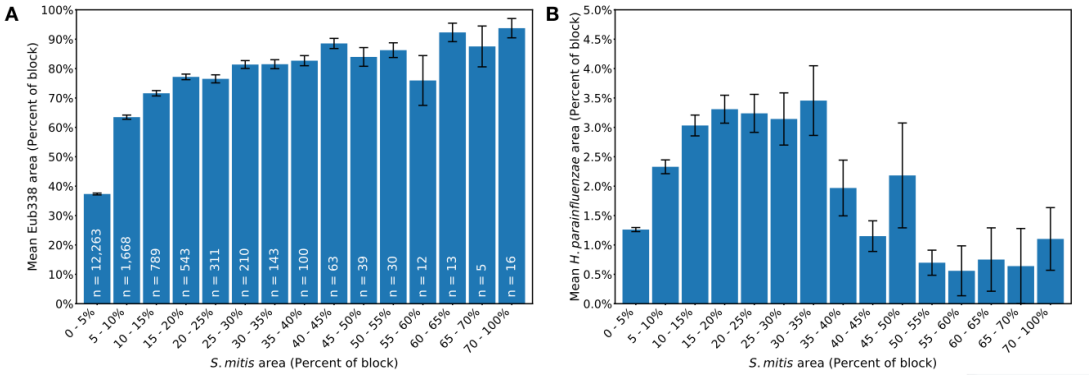

Figure S2.1: Total bacteria and *H. parainfluenzae* density relative to *S. mitis*. Bar heights represent the mean densities of (A) Eub338-labeled bacteria and (B) *H. parainfluenzae* with respect to the mean *S. mitis* densities for 16,205 blocks of 6.64 µm by 6.64 µm, from 41 fields of view. The number of blocks for each range of *S. mitis* densities is shown in S1A. The error bars represent ± 1 standard error.

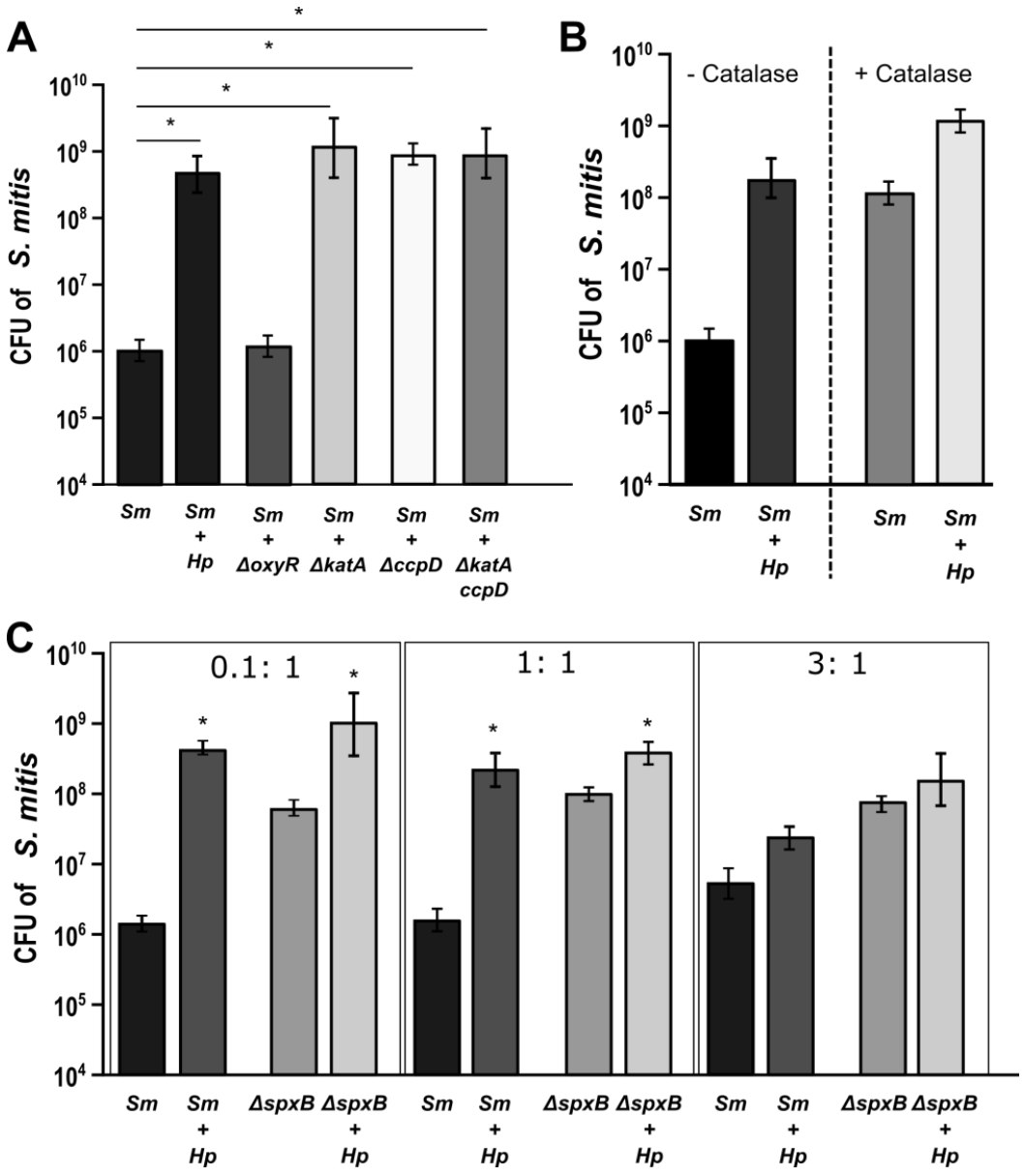

Figure S2.2: *H. parainfluenzae* H_2O_2 detoxification aids *S. mitis* growth. (A) *S. mitis* CFU when cocultured with *H. parainfluenzae* WT and indicated H_2O_2 resistance gene deletion mutants. Data are mean CFU, error bars indicate standard deviation for n=3. *denotes $p < 0.001$ by Student's t-test compared to monoculture CFU. (B) *S. mitis* CFU in mono and coculture with the addition of 20U/ml of exogenous catalase following incubation for 24 hours. (C)

CFU counts of *S. mitis* (*Sm*) and the pyruvate oxidase mutant of *S. mitis* (*ΔspxB*) in mono and coculture with wildtype *H. parainfluenzae* (*Hp*). *Hp* had an initial inoculum of 4.65 x 10^6 CFU/ml. Wildtype (*Sm*) and *S. mitis ΔspxB* with initial inoculums of 2.45x10^5, 1.55x10^6 or 3.45x10^6 CFU/ml. Data are mean CFU and error bars indicate standard deviation for n≥3. *denotes p< 0.05 by Student's t-test compared to monoculture.

A

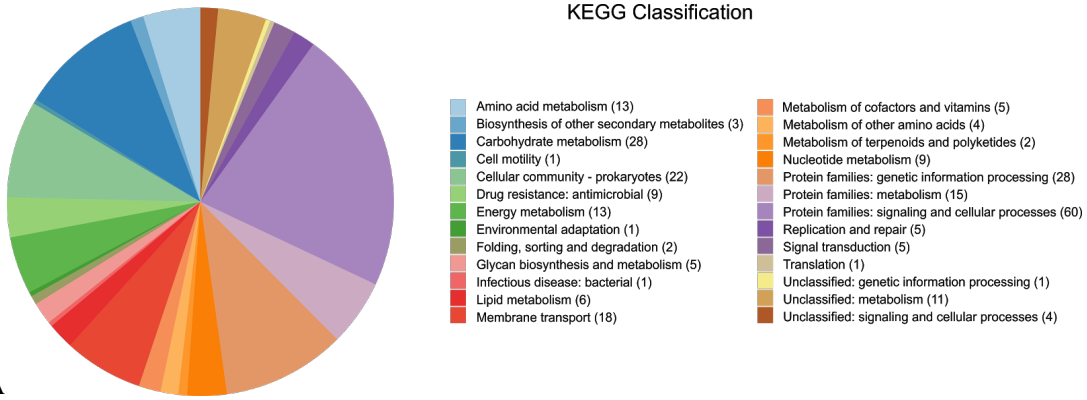

B

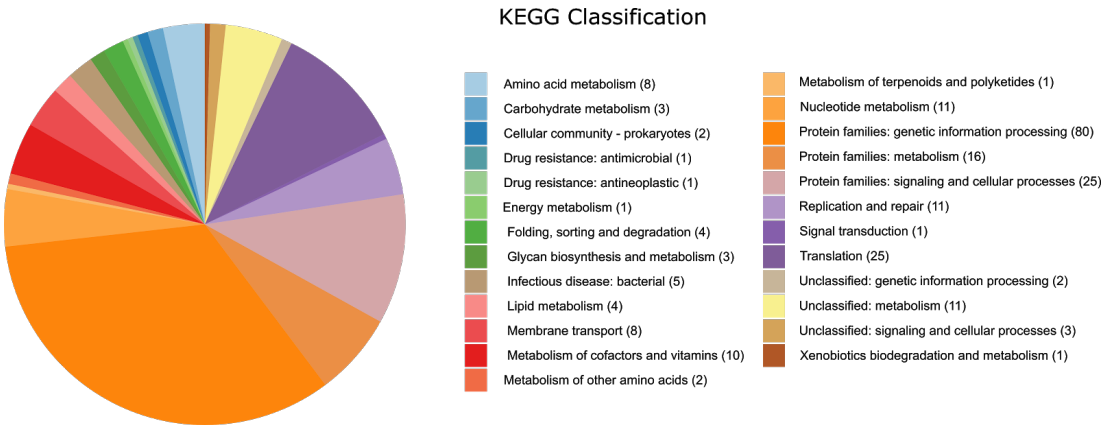

Figure S2.3: *H. parainfluenzae* transcriptional response to *S. mitis*. (A) Pathways induced in *H. parainfluenzae* when cocultured with *S. mitis* based on number of genes that have > 2-fold increase in expression. **(B)** Pathways repressed when *H. parainfluenzae* is cocultured with *S. mitis* based on a 2-fold decrease in coculture.

Table S2.10: DNA FISH probes

Probe	Fluorophore	Target Taxon	Probe Sequence 5'-3'	Reference
Eub338	Dual At655	Bacteria (domain)	GCTGCCTCCCGTAGGAGT	Amann et al. 1990
Pas111	Dual Dy615	Pasteurallaceae (family)	TCCCAAGCATTACTCACC	Valm et al. 2011
Str405	RRX	Streptococcus (genus)	TAGCCGTCCCTTTCTGGT	Paster et al. 1998
Smit651	Dual Dy415	*S. mitis*	CCCCTCTTGCACTCAA	Wilbert et al. 2020
Hpar441	Dual Dy490	*H. parainfluenzae*	ACTAAATGCCTTCCTCGCTAC	this paper

Table S2.11: Strains used in this study

Plasmids	Identifier	Host	Details
pDP863K	MR0203	NEB5-α	pMRKO (1) derivative used for the deletion of the *katA* gene in *H.parainfluenzae* via allelic exchange
pDP865K	MR0259	NEB5-α	pMRKO derivative used for the deletion of the *oxyR* gene in *H.parainfluenzae* via allelic exchange
pDP801K	MR0275	NEB5-α	A pMRKO derivative used for the deletion of the *ccp* gene in *H.parainfluenzae* via allelic exchange
pDP111K	MR0307	NEB5-α	A pMRKO derivative used for the deletion of the *g6p* gene in *H.parainfluenzae* via allelic exchange
pDP821K	MR0314	NEB5-α	A pMRKO derivative used for the deletion of the *pdgx* gene in *H.parainfluenzae* via allelic exchange
pEAKO	MR0254	NEB5-α	pMRKO containing a sacB cassette used in generating clean deletion vectors
pKC865K	MR0323	NEB5-α	A pEAKO derivative used for the deletion of the *prx* gene in *H.parainfluenzae* via clean deletion
pDP863C	MR0339	NEB5-α	A pEAKO derivative used for the deletion of the *katA* gene in *H.parainfluenzae* via markerless deletion.

Species	Identifier	Strain	Details
E. coli		NEB5-α	Cloning strain (New England Biolabs)
E. coli	MR0142	MFD-pir	Donor strain (2), Diaminopimelic acid auxotroph.
Haemophilus parainfluenzae	MR0160	ATCC 33392	*Haemophilus parainfluenzae* ATCC 33392TM
Haemophilus parainfluenzae	MR0205	*ΔkatA*	KatA deletion of *H. parainfluenzae* made via allelic exchange with a kanamycin resistance gene.
Haemophilus parainfluenzae	MR0266	*ΔoxyR*	OxyR deletion of *H. parainfluenzae* made via allelic exchange with a kanamycin resistance gene.
Haemophilus parainfluenzae	MR0277	*Δccp*	Cytochrome C Peroxidase deletion of *H. parainfluenzae* made via allelic exchange with a kanamycin resistance gene.
Haemophilus parainfluenzae	MR0312	*Δg6p*	Glucose-6 phosphate dehydrogenase deletion of *H. parainfluenzae* made via allelic exchange with a kanamycin resistance gene.
Haemophilus parainfluenzae	MR0316	*Δpdgx*	Peroxiredoxin/Glutaredoxin deletion of *H. parainfluenzae* made via allelic exchange with a kanamycin resistance gene.
Haemophilus parainfluenzae	MR0341	*Δprx*	Peroxiredoxin deletion of *H. parainfluenzae* made via markerless deletion using sucrose counterselection.
Haemophilus parainfluenzae	MR0406	*ΔccpkatA*	Catalase and Cytochrome C peroxidase double deletion, constructed using the markerless deletion of the catalase gene in the *Δccp* strain of *H. parainfluenzae*.
Haemophilus parainfluenzae	MR0359	*ΔprxkatA*	Peroxiredoxin and Catalase double deletion, constructed using the markerless deletion of the catalase gene in the *Δprx* strain of *H. parainfluenzae*.
S. mitis	MR0181	ATCC 49456	*Streptococcus mitis* ATCC 49456TM
S. mitis	MR0289	*ΔspxB*	Pyruvate oxidase deletion of *S. mitis* (3)

Gene deletion in *H. parainfluenzae*

1kb flanking regions of the target gene were amplified via PCR using Q5 High-fidelity 2X Mastermix and primers indicated in Table S9. For allelic exchange, these fragments were assembled to flank a kanamycin resistance cassette via isothermal assembly using the NEBuilder HiFi DNA Assembly MasterMix (New England Biolabs) and cloned into pMRKO. This resulting reaction was then transformed into NEB5α competent cells using the manufacturer's instructions (New England Biolabs). Plasmid constructs were verified via restriction digests and Sanger sequencing. After screening, plasmids were transformed into the donor strain MFD-pir, using the TSS transformation method (6).

These strains were then used to conjugate into *H. parainfluenzae*. Briefly, washed cells of *H. parainfluenzae* overnight cultures were subjected to heat-shock (46°C for 6 minutes) and combined with the donor strain by spread plating on a BHI-YE HP agar plate supplemented with 0.3 mM di-amino pimelate (DAP). Plates were then incubated overnight at 37°C in 5% CO_2. Cells were then harvested, and dilutions were plated on BHI-YE HP with 40 μg/ml of kanamycin and incubated for 24-48 hours at 37°C in 5% CO_2. Mutants were then screened by testing for sensitivity to spectinomycin (spectinomycin resistance cassette on pMRKO backbone), PCR and Sanger sequencing.

The markerless deletion of genes in *H. parainfluenzae* involved modifications to the above protocol. 1kb flanking regions were amplified and cloned into a pMRKO derivative containing a *sacB* gene (pEAKO - Table S8). Plasmids were then transformed into *H. parainfluenzae* via conjugation as described above. After transformation, cells were subjected to counterselection by plating on BHI-YE HP containing 10% sucrose for 4-5 days. Mutants were then screened via PCR and Sanger sequencing.

Image Analysis

To allow quantitative analysis of the spatial distribution of the taxa of interest, we used FIJI to create binarized *S. mitis*, *H. parainfluenzae,* and bacterial mass images. A slight misalignment of the Smit651 channel was brought into closer alignment with the other channels by shifting it up by 2 pixels, cropping 3 pixels off each edge, and re-scaling the channel image to regain the original 2,048 by 2,048 resolution. The noise in each channel was reduced by applying a median filter with a radius of 3 pixels. To create a bacterial biomass mask, the Eub338 channel was automatically segmented by thresholding with the global Otsu method (7) and dilating the segmented area by 3 pixels. The *S. miti*s channel was created by segmenting the Str405 and Smit651 channels with the local Bernsen and global RenyiEntropy automatic thresholding methods, respectively (8,9). Both segmented images were combined using the Boolean "AND" operator to retain the pixels appearing in both images. The *H. parainfluenzae* channel was created by segmenting the Pas111 and Hpar441 channels with the local Bernsen and global RenyiEntropy automatic thresholding methods, respectively. Both segmented images were combined using the Boolean "AND" operator. To ensure that there was a sufficiently large area of *H. parainfluenzae* in the images for reliable analysis, only the 41 fields of view in which at least 1% of the bacteria mass was covered by *H. parainfluenzae* in the associated binary image were used for the following analyses.

References

1. Ramsey MM, Rumbaugh KP, Whiteley M. Metabolite cross-feeding enhances virulence in a model polymicrobial infection. PLoS Pathog. 2011 Mar;7(3):e1002012.

2. Ferrières L, Hémery G, Nham T, Guérout A-M, Mazel D, Beloin C, et al. Silent mischief: bacteriophage Mu insertions contaminate products of Escherichia coli random mutagenesis performed using suicidal transposon delivery plasmids mobilized by broad-host-range RP4 conjugative machinery. J Bacteriol. 2010 Dec;192(24):6418–27.

3. Redanz S, Treerat P, Mu R, Redanz U, Zou Z, Koley D, et al. Pyruvate secretion by oral streptococci modulates hydrogen peroxide dependent antagonism. ISME J. 2020 May;14(5):1074–88.

4. Narayanan AM, Ramsey MM, Stacy A, Whiteley M. Defining Genetic Fitness Determinants and Creating Genomic Resources for an Oral Pathogen. Appl Environ Microbiol. 2017 Jul 15;83(14).

5. Schäfer A, Tauch A, Jäger W, Kalinowski J, Thierbach G, Pühler A. Small mobilizable multi-purpose cloning vectors derived from the Escherichia coli plasmids pK18 and pK19: selection of defined deletions in the chromosome of Corynebacterium glutamicum. Gene. 1994 Jul 22;145(1):69–73.

6. Chung CT, Niemela SL, Miller RH. One-step preparation of competent Escherichia coli: transformation and storage of bacterial cells in the same solution. Proc Natl Acad Sci U S A. 1989 Apr;86(7):2172–5.

7. Otsu N. A Threshold Selection Method from Gray-Level Histograms. IEEE Trans Syst Man Cybern. 1979 Jan;9(1):62–6.

8. Bernsen, John. Dynamic Thresholding of Grey-Level Images. 8th Int Conf Pattern Recognit Paris Fr. 1986 Aug;1251–5.

9. Kapur JN, Sahoo PK, Wong AKC. A new method for gray-level picture thresholding using the entropy of the histogram. Comput Vis Graph Image Process. 1985 Mar;29(3):273–85.

10. Amann RI, Krumholz L, Stahl DA. Fluorescent-oligonucleotide probing of whole cells for determinative, phylogenetic, and environmental studies in microbiology. J Bacteriol. 1990 Feb;172(2):762–70.

11. Valm AM, Mark Welch JL, Rieken CW, Hasegawa Y, Sogin ML, Oldenbourg R, et al. Systems-level analysis of microbial community organization through combinatorial labeling and spectral imaging. Proc Natl Acad Sci U S A. 2011 Mar 8;108(10):4152–7.

12. Paster BJ, Bartoszyk IM, Dewhirst FE. Identification of oral streptococci using PCR-based, reverse-capture, checkerboard hybridization. Methods Cell Sci. 1998 Mar 1;20(1):223–31.

13. Wilbert SA, Mark Welch JL, Borisy GG. Spatial Ecology of the Human Tongue Dorsum Microbiome. Cell Rep. 2020 Mar 24;30(12):4003-4015.e3.

Begin typing or pasting the rest of your chapter 3 text here. This template is best used for directly typing in your content. However, you can paste text into the document, but use caution as pasting can produce varying results.

CHAPTER 4: Understanding responses to hydrogen peroxide in *H. parainfluenzae*

Written in format required by the ISME Journal. *Unpublished.*

Dasith Perera, Matthew Ramsey

The University of Rhode Island, Department of Cell and Molecular Biology, Kingston, RI 02881, USA.

Abstract

The abundant commensal bacterium, *Haemophilus parainfluenzae* has been shown to be closely associated with hydrogen peroxide producing *Streptococcus sp. in vivo.* The response of *H. parainfluenzae* to streptococci-produced hydrogen peroxide revealed a redundant OxyR-controlled mechanism of dealing with this antimicrobial. Little is known about the mechanism of how *H. parainfluenzae* achieves this redundancy and why it evolved in this manner. Through transcriptome analyses we discovered that there appears to be a reduced preference for catalase, suggesting a mechanism for its redundancy which is currently under further investigation. The overall effects of being exposed to H_2O_2 on a consistent basis is not known. However, studies in other species have shown that H_2O_2 can induce the SOS response, which has been shown to be a mechanism of generating genetic diversity as a means of surviving stress. Interestingly, *H. parainfluenzae* has been shown to possess a high degree of strain variation within the human oral cavity. We observed that *H. parainfluenzae* appears to elicit an SOS-like response to H_2O_2 based on transcriptome analyses, suggesting a potential mechanism for genetic diversity seen within this species.

Introduction

Haemophilus parainfluenzae is a Gram-negative facultative anaerobe and commensal of the human nasopharynx and oral cavity (1,2). It has previously been shown to be found in close proximity to Mitis group Streptococci in supragingival plaque and are found to overlap in other sites of the oral cavity and nasopharynx (2,3). Mitis group Streptococci are known to rapidly consume high-energy carbohydrates and produce the inhibitory anti-microbial, hydrogen peroxide (H_2O_2) and use it as a competitive advantage against other species. Therefore, in order to constantly co-exist alongside Mitis group Streptococci, *H. parainfluenzae* would need to tolerate H_2O_2. We have previously shown that *H. parainfluenzae* can tolerate *S. mitis* produced H_2O_2 except at high *S. mitis* inoculums and that *H. parainfluenzae'*s response to H_2O_2 involves a redundant system involving multiple genes that aid in detoxification of H_2O_2, which is in contrast to other closely related species (2). The mechanism by which *H. parainfluenzae* achieves this redundancy and what benefit this type of system bestows is currently unknown and warrants investigation.

To examine the overall response to H_2O_2, we carried out transcriptome analyses to determine the genes that are affected following the deletion of *oxyR*, the transcriptional regulator that controls response to H_2O_2. These data indicated that catalase is not the gene most affected by loss of *oxyR*, which is in contrast to close relatives like *H. influenzae* where loss of *oxyR* results in a 334-fold loss in catalase expression (4), compared to a 35-fold decline in *H. parainfluenzae*. This is consistent with our previous findings where catalase is redundant in this species (2). We also demonstrated that overexpression of catalase (*katA*), in an *oxyR* deletion mutant (*ΔoxyR*) generated a

strain more resistant to H_2O_2 than wildtype, suggesting that the regulation of catalase could explain its redundancy. Therefore, we sought to examine the OxyR regulon by carrying out Chromatin Immunoprecipitation sequencing (ChIPSeq); however, we found that C-terminal tagging of OxyR resulted in either the tag being inaccessible or affected the function of the protein, preventing binding of the tagged protein to DNA, preventing us from further investigation. Further work is currently being done to evaluate this hypothesis and new tag types need to be tested.

A key feature about *H. parainfluenzae in vivo* is that there is a high degree of genome variability within this species that has resulted in strain specific niche associations (5,6). Given that *H. parainfluenzae* is found in close association with Mitis group Streptococci and is found in the same host body sites, it would be interesting to determine whether *Streptococcus sp.* produced H_2O_2 could play a role in the genetic diversity seen in strains of *H. parainfluenzae*. Apart from its anti-microbial activity, H_2O_2 can have other effects on a cell. It has been shown to result in DNA damage, including the formation of double and single-strand breaks (7,8). The addition of H_2O_2 has been shown to induce the SOS response in *Escherichia coli* which can result in mutagenesis (9). In fact, the induction of the SOS system in *E. coli* has been implicated in the generation of a transient genome-wide state of hypermutation that can be induced as a mechanism of generating genetic variability in times of stress (10). The overall effects of H_2O_2 on *H. parainfluenzae* are currently unknown despite H_2O_2 likely being a frequent feature of *H. parainfluenzae*'s microenvironment due to its proximity to *Streptococcus sp*.

To investigate this, we re-examined previous transcriptome analyses (2) that suggested that when *H. parainfluenzae* is cocultured with *S. mitis* aerobically there appears to be induction of an SOS-like response involving DNA polymerase IV (DNA pol IV) among other genes. DNA pol IV is a low fidelity polymerase that lacks proof reading activity and has thus been shown to be an important component of the SOS response(11). This response is similar to mechanisms of induced mutagenesis seen with *E. coli* in response to H_2O_2 (12,13); however, the lack of induction of key genes including *recA* suggested only partial induction of this system. This was corroborated by our assays involving experimentally evolved strains of *H. parainfluenzae* that suggested that there were only minor changes in the genome following a coculture period of 30 days (this paper). Further transcriptome analyses showed induction of a more complete SOS-like response following addition of H_2O_2, suggesting that the concentration of *S. mitis* used in the previous assays may have been insufficient to induce a complete response.

Results

H. parainfluenzae redundant H_2O_2 response is influenced by OxyR

To determine which genes are controlled either directly or indirectly by OxyR, we carried out transcriptome comparisons via RNASeq following addition of a sublethal dose of H_2O_2 in wildtype *H. parainfluenzae* vs a strain lacking the regulator OxyR (*ΔoxyR*). We observed the induction of 23 genes and repression of 46 genes when comparing *ΔoxyR* to wildtype (Table S1-S2). The gene most affected by loss of OxyR

is *oxyR* itself (63-fold), suggesting a mechanism of autoregulation, which is a consistent property of many LysM- type regulators (14). The expression of DNA protection during starvation (*dps*) is increased 37-fold in wildtype compared to *ΔoxyR* while catalase (*katA*) is increased 20-fold. Other enzymes capable of reacting with H_2O_2 are also significantly induced more that 3-fold, including peroxiredoxin (*prx*) and cytochrome C peroxidase (*ccp*). This response appears to contrast that of *H. influenzae* where catalase is the gene most affected (334-fold) following loss of OxyR (4), suggesting a reduced preference for catalase in *H. parainfluenzae*. Genes involved in the pentose phosphate pathway are also significantly induced greater than 2-fold including glucose-6-phosphate dehydrogenase (*g6pD*), 6-phosphogluconolactonase, transketolase, transaldolase. This is consistent with autoregulation of OxyR as NADPH produced by the pentose phosphate is important for the activity of glutathione reductase (4-fold increased in wildtype), which along with glutaredoxin (4-fold increase) and thioredoxin (2.5-fold increase) are involved in the reduction of OxyR, which is important for recycling OxyR (15). The gene with the greatest repression in wildtype compared to *ΔoxyR* is an iron transport system permease (*fecD*), repressed 3.8-fold, while a few other transporters involved in lipid and fatty acid metabolism are also repressed (Table S2).

Regulation of genes by OxyR enables redundant response to H_2O_2

To rule out the possibility of a malfunctioning catalase being responsible for catalase redundancy in *H. parainfluenzae*, we expressed *katA in trans*, under the control of a

strong constitutively active promoter in the*ΔoxyR* strain background. This generated a strain four-times more tolerant to H_2O_2 than the wildtype (Fig. 1), demonstrating that the catalase protein is functional, and that it is likely the mechanism of catalase regulation that is responsible for its reduced importance in this species.

As previous data indicated that deletion of *oxyR* was essential for survival of *H. parainfluenzae* following exposure to *S. mitis* produced H_2O_2, but deletion of *katA* and multiple other genes showed no effects(2), it is important to determine whether these genes are under the control of OxyR. To determine whether catalase and other genes involved in H_2O_2 detoxification are likely directly controlled by the same regulator, we carried out a motif prediction analysis using the tool MEME (16). This suggested that genes including *katA*, *prx* and *ccp* contained a putative protein binding site with similarities to that of an OxyR binding site in other species (Fig. 3), however there also appears to be some redundancy in this potential consensus site. As expected OxyR itself contains a domain that is predicted to bind to DNA in a helix-turn-helix conformation, based on computational prediction (data not shown).

In order to confirm the identity of the genes that are directly controlled by OxyR and to quantify the relative occupancies of OxyR at different location we attempted to carry out ChIPSeq (chromatin immunoprecipitation sequencing). This initially involved generating a strain of *H. parainfluenzae* with the chromosomal copy of *oxyR* modified to encode OxyR with a vesicular stomatitis virus-glycoprotein (VSV-G) epitope tag fused to the C-terminal end of the protein. The construction of this strain

was confirmed by sequencing. Chromatin Immunoprecipitation quantitative-polymerase chain reaction (ChIP-qPCR) was then carried out to look for enrichment of known OxyR controlled genes. However, after several attempts we failed to observe enrichment of *katA*, *dps* or *oxyR* following ChIP (Table 1), suggesting that either OxyR does not control these genes or that the OxyR VSV-G tag cannot be accessed. To rule out the latter, we constructed a strain where *oxyR* was modified to encode OxyR with a tandem affinity purification (TAP) epitope tag. However, this resulted in a phenotype similar to that of *ΔoxyR* (Fig. 2), indicating that the function of OxyR is severely affected by the presence of the TAP tag. Due to time constrains we decided to find alternative methods of testing our hypotheses.

The addition of H_2O_2 elicits an SOS response in H. parainfluenzae

Apart from resulting in the induction of the OxyR regulon, H_2O_2 can have other effects on the cell. To determine the effects of H_2O_2 on *H. parainfluenzae* we compared the transcriptomes of *H. parainfluenzae* grown aerobically with the addition of H_2O_2 to a strain grown aerobically without addition of H_2O_2 (Table S3-S4). This showed the significant induction of 313 genes greater than 2-fold (Table S3). Unsurprisingly, this included genes typically induced by H_2O_2 including *dps* and *g6pD*, *prx* and iron transporters, notably *katA* was not induced, suggesting maximal induction of catalase without addition of exogenous H_2O_2. Interestingly, we observed induction of genes that suggest initiation of an SOS-like response. This included induction of genes like DNA polymerase IV (4.3-fold), inner membrane protein *impA* (4.5-fold), regulatory protein

recX (4.2-fold), DNA repair proteins *recN* (3.2-fold) and *recA* (2-fold) as well as genes involved in competence, including type IV pilin *pilA* (9.1-fold), type IV biogenesis protein *pilM* (3.4-fold), regulator of competence *tfox* (2.6-fold), competence protein *comEC* (4.5-fold). Induction of competence is a mechanism of DNA uptake and a key component of horizontal gene transfer (17). Competence has also been shown to be a mechanism of inducing the SOS-response in *Vibrio cholerae* (18), while H_2O_2 itself can trigger the SOS response in *E.coli* (19). DNA pol IV and RecA play key roles in the SOS response (11,20) and its induction has been shown to be an important mechanism of adaptation and diversification (21).

Coculture with S. mitis results in partial expression of genes involved in SOS response due to H_2O_2 and only minor changes in protein coding sequences

We examined previously generated RNASeq data (2), that looked at gene expression in *H. parainfluenzae* in coculture with *S. mitis*, compared to monoculture. This analysis indicated the induction of some of the genes implicated in the SOS response. This includes *pilA* (10.9-fold), *pilM* (5.2-fold), *tfox* (4.0-fold), *impA* (2.2-fold), DNA pol IV (2.0-fold) and competence protein *comEA* (2.9-fold). The expression of other key genes including *comEC* and *recA* appear to be modestly higher in coculture; however, this difference is not significant, suggesting variability between the coculture replicates or scant induction of the SOS system at the time of collection.

H. parainfluenzae genome shows only minor changes following coculture with S. mitis

To determine whether *H. parainfluenzae* shows evidence of some level of diversification following coculture with *S. mitis* we analyzed reads generated from RNASeq experiments involving *H. parainfluenzae* in monoculture and coculture with *S. mitis*. This analysis was carried out using the GATK pipeline (22) and involved detection of single nucleotide polymorphisms (SNPs) and insertion-deletion (INDELs) in the reads compared to the reference genome. This analysis detected only minor, insignificant differences between the mono and coculture reads (Table 2).

Since the analysis of RNASeq reads involved only coding sequences and was carried out following a single 24 hour mono or coculture incubation, we hypothesized that there would be greater observable differences if the conditions involved multiple exposures to *S. mitis* and utilized whole genome sequencing and these differences were due to *S. mitis* produced H_2O_2. We therefore subcultured *H. parainfluenzae* over a course of 10 consecutive 24-hour periods of either mono or coculture with either wildtype or *S. mitis* Δ*spxB* and examined whole genome sequences for sequentially passaged strains vs the initial inoculum. This analysis showed no detectable SNPs in monoculture or coculture with Δ*spxB S. mitis*. However, we detected 1 SNP in both the replicates involving coculture with wildtype *S. mitis* (Table 3). We hypothesize that more significant differences may be observed following a longer duration and this is the subject of further investigation.

Discussion

H. parainfluenzae is a commensal of the human oral cavity and is associated with beneficial immunomodulatory effects (23). Since *H.* parainfluenzae was previously shown to coexist alongside the H_2O_2 producing Mitis group Streptococci (2), it is important to understand the overall effects of H_2O_2 on *H. parainfluenzae*. Our findings reveal a complex, redundant OxyR- controlled response to H_2O_2, that suggest a reduced affinity for catalase. We also observed what appears to be induction of an SOS response in the presence of H_2O_2, however this appears to be attenuated in our coculture experimental design.

The transcriptional regulator, OxyR is responsible for the overall response to H_2O_2 in many species including *E. coli, Salmonella typhimurium* and *H. influenzae* (24,25). We therefore looked at the effects of the deletion of OxyR on *H. parainfluenzae*. We previously showed that OxyR was essential for survival of *H. parainfluenzae* in coculture with *S. mitis* (2). In this study we looked at the genes affected by deletion of OxyR, through transcriptome analysis. This suggested the autoregulation of OxyR as the expression of *oxyR* was among the genes that were affected, which is consistent with other OxyR systems (15,25). Genes involved in the reduction of oxidized OxyR were also affected, suggesting that OxyR is involved in both activating and inactivat-

ing its own response. The observation of *oxyR* being the gene most affected in this dataset is also interesting, as similar datasets in close relatives including *H. influenzae* show catalase as being the gene most affected with over 300-fold effect in that species(4), while in *H. parainfluenzae* catalase is the 3rd most affected gene with a 20-fold effect. This suggests that gene regulation by OxyR may be responsible for the redundant H_2O_2 response seen in *H. parainfluenzae.* This is further corroborated by the observation that the overexpression of catalase in the Δ*oxyR* strain resulted in a strain that is more tolerant to H_2O_2 than wildtype, suggesting that catalase is sufficiently functional, and that regulation may play a role in redundancy; however, plasmid copy number and effects of being under a strong promoter may be factors that could limit our inferences. To further evaluate this, we are currently working on generating a strain of *H. parainfluenzae*, where the catalase gene has been replaced by catalase from *H. influenzae*, which could absolve the limitations of the previous construct. To evaluate whether regulation of catalase alone plays a role in redundancy we are currently working on replacing the catalase promoter region of *H. parainfluenzae* with the catalase promoter region of *H. influenzae* to determine whether this increases the affinity of OxyR for the catalase promoter, and therefore, increase the relative expression of catalase.

Since *H. parainfluenzae* has been shown to possess a high degree of strain variation (5,6) and is associated with the H_2O_2 producing Mitis group Streptococci we hypothesized that constant exposure to H_2O_2 might be a potential mechanism of genome diversification. We observed through transcriptome analyses that the addition of H_2O_2 to *H.*

parainfluenzae induced the expression of genes implicated in the SOS response. This response in other species has been shown to be a mechanism of generating genome diversity in response to stress (21). However, transcriptome analyses involving *H. parainfluenzae* in mono or coculture with *S. mitis* showed only a handful of these genes being expressed in coculture. Subsequently we didn't observe any significant differences in number of nucleotide changes between mono and coculture. We hypothesized that coculturing *H. parainfluenzae* with *S. mitis* over multiple passages would enable us to see a greater number of nucleotide differences between mono and coculture. However, after 10 rounds of coculture with *S. mitis* we only observed 1 SNP in each replicate. It is interesting to note that there were no SNPs in either monoculture or coculture with Δ*spxB*. A potential flaw in this experimental design is that this involved a single colony being passaged overtime in either mono or coculture. We hypothesize that greater changes maybe observed if this assay involved a pool of colonies rather than a single colony as this would enable the detection of greater variation.

In this study, we investigated the effects of H_2O_2 on *H. parainfluenzae* and observed differences in the OxyR regulon of *H. parainfluenzae* compared to closely related species suggesting that gene regulation by OxyR is responsible for the redundant response to H_2O_2 we observed previously(2). We observed evidence of induction of the SOS response in *H. parainfluenzae* following the addition of H_2O_2 however, this was attenuated in coculture with *S. mitis* suggesting insufficient H_2O_2 production or exposure in our experimental conditions, which was mirrored by our findings that failed to detect any significant genome variability following coculture with *S. mitis*. We attempted an

increased inoculum of *S. mitis*; however, we observed poor survival of *H. parainfluenzae*. Therefore, balancing survival and induction should be a key consideration in future experimental design.

Materials and Methods

Strains and Media

Strains and plasmids used in this study are listed in table 4. Unless indicated *S. mitis* was cultured using Brain Heart Infusion BHI broth or solid agar supplemented with Yeast extract (BHIYE). *H. parainfluenzae* was cultured using BHIYE, supplemented with 14µg/ml Nicotinamide Adenine Dinucleotide (Sigma-Aldrich) and 14µg/ml Hemin (Sigma-Aldrich) - (BHIYE-HP). *H. parainfluenzae* and S. mitis were grown at 37℃ and 5% CO2. E. coli was grown on Luria broth (LB) at 37℃ in standard atmospheric conditions with liquid cultures shaken at 200 RPM. Antibiotics were used at the following concentrations: Kanamycin 40µg/ml, and Spectinomycin 50µg/ml for E. coli, 200µg/ml for *H. parainfluenzae*.

OxyR transcriptome sample preparation

RNASeq analyses were carried out on strains using a colony biofilm model (2,26). Briefly, equal numbers of either wildtype or Δ*oxyR H. parainfluenzae* were spotted on sterile 25mm 0.2µm polycarbonate membranes that were placed on BHIYE HP agar plates. The plates were then incubated for 20 hours at 37℃ and 5% CO2, then transferred to fresh pre-warmed plates that were incubated for a further 4 hours. Thereafter,

membranes were transferred to pre-warmed plates containing 50μM H_2O_2 and incubated for an additional 20 minutes. Membranes were then immediately placed in RNAlater solution (Ambion™). Experiments were carried out in biological duplicates.

RNA extraction and sequencing

RNA was extracted using the Direct-zol™ RNA MiniPrep Plus kit (Zymo Research) according to manufacturer's instructions. Ribsomal RNA was then depleted using the Ribo-zero rRNA removal kit (Illumina) according to the manufacturer's instructions. The resulting products were then purified using the RNease MinElute cleanup kit (Qiagen). Library prep and sequencing were carried out as part of an Illumina RNA-Seq library preparation workshop.

Transcriptome analyses

Genome data for *H. parainfluenzae* ATCC 33392 was obtained from NCBI and genome annotations were generated using RAST as previously described (2). RNASeq reads were aligned, mapped and differentially expressed genes analyzed using our previously built pipeline, the RNASeq-analysis-toolkit (2).

Effects of catalase overexpression

The catalase gene of *H. parainfluenzae* was amplified and ligated into pJAK16 (ATCC) using gibson assembly, where it was placed under the control of a tac promoter which we had verified to be constitutively active in *H. parainfluenzae*. The re-

sulting plasmid was then transformed into Δ*oxyR H. parainfluenzae* via electroporation as described previously (27). The Minimum inhibitory concentration for H_2O_2 was then calculated via 2-fold serial dilutions.

OxyR VSV-G and TAP-tag strain construction

To determine the genes directly controlled by OxyR and quantify the relative occupancy of OxyR at different promoter regions, we sort to carry out ChIPSeq. To carry out these experiments we sort to generate a strain of *H. parainfluenzae* containing a VSV-G-tagged OxyR. A VSV-G-tagged OxyR was generated using a well-established method of tagging proteins (28). Briefly, the last 381bp of *oxyR* and a DNA sequence for the VSV-G protein were cloned into a non-replicating plasmid (pMRKO) using Gibson assembly. To ensure accurate translation of the VSV-G tag, the DNA sequence was generated after accounting for codon bias using the Kazusa tool (29). An alanine linker separating the *oxyR* fragment and VSV-G epitope tag was also generated to ensure that the tag would be generated in frame. Cells in which a single homologous recombination event occurred were selected on Spectinomycin and sequenced to confirm the generation of OxyR-VSV-G genotypically. To ensure that the generation of OxyR-VSV-G did not affect the function of OxyR we carried zone of inhibition assays for H_2O_2 to confirm that the strain had similar sensitivity to wildtype *H. parainfluenzae*. The same process was carried out to generate OxyR-TAP tag.

ChIP-qPCR of OxyR

To evaluate whether the OxyR tag is accessible and functioning as expected we sort to carry out ChIP-qPCR. ChIP was carried out as outlined previously (30). Briefly, mid-log cells of wildtype *H. parainfluenzae* and OxyR-VSV-G *H. parainfluenzae* treated with 50mM H_2O_2 and OxyR-VSV-G *H. parainfluenzae* grown anaerobically were harvested and then crosslinked using 1% formaldehyde. Crosslinking was abated using 250mM Glycine. Cells were then washed with PBS and stored at -80°C. The resulting pellets were then washed in sonication buffer (20mM KHEPES, 50mM Kcl, 0.5mM DTT, 10% Glycerol and protease inhibitor). Cells were then sonicated at an amplitude of 40% with a pulse setting of 6 seconds on, 2 seconds off using the Sonic Dismembrator Model 500 (Fisher). ChIP was then carried out in biological triplicate using anti-VSV-G agarose beads (Sigma). Prior to ChIP, aliquots were obtained as input controls. qPCR was then carried out to determine whether there was enrichment of known OxyR controlled promoter sites following ChIP. We tested for the enrichment of the promoter regions of *katA*, *dps*, *oxyR* vs enrichment for the control gene DNA gyrase *gyrA*.

OxyR Motif prediction

To predict which genes are most likely to be directly controlled by OxyR we sort to detect conserved motifs in the promoter region of genes that had the potential to be controlled by OxyR. To determine these motifs we used regions 150bp upstream of the starting site of all genes that had 3x greater expression in wildtype compared to

Δ*oxyR*. These were then submitted to MEME (31) for the detection of conserved binding motifs.

Detection of SNPs and INDELs from coculture RNASeq reads

To evaluate the possibility of genomic variation following coculture we examined nucleotide differences following mono and coculture using reads generated from previous RNASeq experiments (2). This analysis was carried out using the best practices principles and GATK analysis for the detection of RNASeq short variant discovery (32). Briefly, this involved reads generated from biological duplicates of *H. parainfluenzae* in monoculture and coculture with *S. mitis*. These reads were then mapped to the reference using Burrows-Wheeler Aligner (BWA) (33), duplicated reads condensed, quality recalibrated and variants called using the recommended tools within the GATK best practices pipeline and package (32).

Detection of SNPs and INDELs in genome following multiple rounds of coculture

As the analysis of RNASeq reads failed to show significant differences between mono and coculture we reasoned that this may have been due to the *post hoc* nature of our experimental design, as we were examining nucleotide differences only in protein coding sequences following a single round of coculture. We hypothesized that we would see greater differences if we were to examine whole genome sequences following multiple rounds of coculture. In order to do this biological duplicates originating from

two colonies of *H. parainfluenzae* were cultured and passaged either through mono-culture, coculture with *S. mitis* or coculture with *ΔspxB S.mitis* for 10 rounds of culture using a colony biofilm model (2,34). The latter was carried out to determine whether *S. mitis* produced H_2O_2 plays a role in any differences. Following the last round of culture, genomic DNA was isolated from the initial day 0 strains as well as the final day strains generated from mono and coculture using the MasterPure Complete DNA kit (Lucigen). The purified DNA was then submitted for Illumina sequencing at the Microbial Genome Sequencing Center, Pittsburgh, PA. The detection of SNPs and indels were carried out using samtools and bcftools (35). Briefly, reads were aligned using BWA (33), genomes indexed and likelihood scores calculated using samtools and variants called using bcftools.

Figures

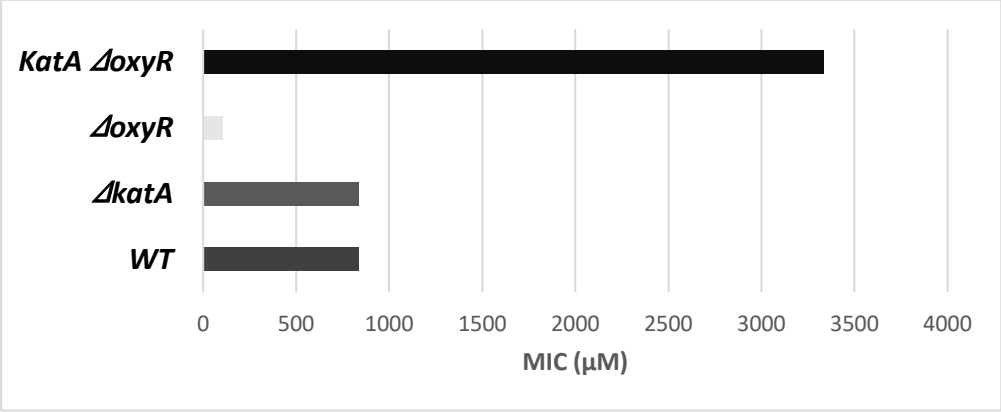

Figure 1: Effect of catalase overexpression on sensitivity to H_2O_2. Minimum inhibitory concentration assays for H_2O_2 were carried out on wildtype *H. parainfluenzae*

(WT), *H. parainfluenzae* lacking catalase (Δ*katA*), OxyR (Δ*oxyR*) and overexpression of catalase in Δ*oxyR* (*katA*$^{+}$ Δ*oxyR*).

Table 1: qPCR for enrichment of different putative OxyR controlled promoter regions

	Cp Values		
gyrA input	17.04	17.01	17
gyrA ChIP	26.26	26.18	26.14
katA input	16.5	16.48	16.41
katA ChIP	25.72	25.68	25.67
dps input	16.24	16.19	16.2
dps ChIP	25.6	25.47	25.5
oxyR input	16.77	16.76	16.77
oxyR ChIP	26.04	26	25.97

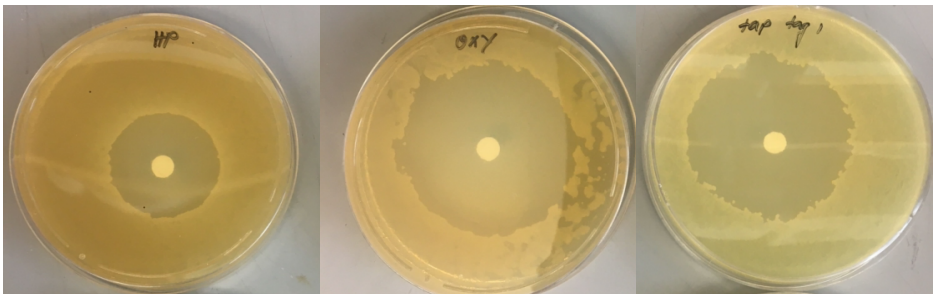

Figure 2: Zone of inhibition assays for H_2O_2. Zone of inhibition assays for H_2O_2 were carried out on (left to right) wildtype *H. parainfluenzae* (WT), *H. parainfluenzae* lacking OxyR (Δ*oxyR*) and *H. parainfluenzae* OxyR-TAP tag.

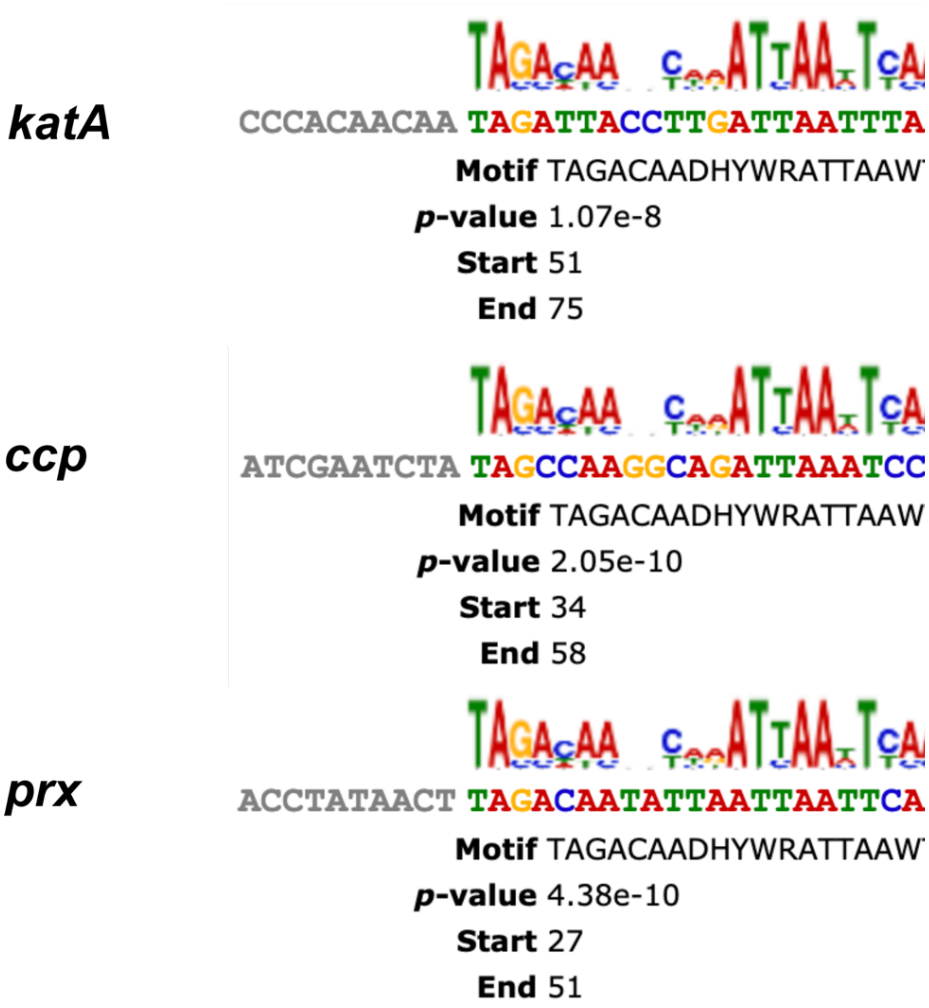

Figure 3: MEME motif prediction analysis of putative OxyR binding sites. Conserved putative OxyR binding sites were computationally predicted to be located within 150bp of the start sites of *katA*, *ccp*, *prx*. Ambiguous nucleotides in the predicted binding motif are denoted by noncanonical base denominations (R=AG, Y=CT, K=GT, M=AC, S=CG, W=AT, B=CGT, D=GAT, H=ACT, V=ACG) (16).

Table 2: Quantification of SNPs in RNASeq reads in *H.* parainfluenzae following mono and coculture with *S. mitis*.

Condition	Number of SNPs
H. parainfluenzae monoculture rep1	10
H. parainfluenzae monoculture rep2	12
H. parainfluenzae coculture with *S.mitis* rep1	50
H. parainfluenzae coculture with *S. mitis* rep2	14

Table 3: Quantification of SNPs in *H.* parainfluenzae following mono and coculture with wildtype and Δ*spxB S. mitis*.

Condition	Number of SNPs
H. parainfluenzae monoculture rep1	0
H. parainfluenzae monoculture rep2	0
H. parainfluenzae coculture with *S.mitis* rep1	1
H. parainfluenzae coculture with *S. mitis* rep2	1
H. parainfluenzae coculture with *ΔspxB S.mitis* rep1	0
H. parainfluenzae coculture with *ΔspxB S. mitis* rep2	0

References

1. Pang B, Swords WE. Haemophilus parainfluenzae Strain ATCC 33392 Forms Biofilms In Vitro and during Experimental Otitis Media Infections. Infect Immun. 2017 Sep;85(9):e01070-16.
2. Perera D, McLean A, Lopez VM, Cloutier-Leblanc K, Almeida E, Cabana K, et al. Mechanisms underlying proximity between oral commensal bacteria. bioRxiv. 2020 Jan 1;2020.09.29.318816.
3. Mark Welch JL, Rossetti BJ, Rieken CW, Dewhirst FE, Borisy GG. Biogeography of a human oral microbiome at the micron scale. Proc Natl Acad Sci U S A. 2016 Feb 9;113(6):E791-800.
4. Harrison A, Ray WC, Baker BD, Armbruster DW, Bakaletz LO, Munson RS. The OxyR regulon in nontypeable Haemophilus influenzae. J Bacteriol. 2007 Feb;189(3):1004–12.
5. Lloyd-Price J, Mahurkar A, Rahnavard G, Crabtree J, Orvis J, Hall AB, et al. Erratum: Strains, functions and dynamics in the expanded Human Microbiome Project. Nature. 2017 09;551(7679):256.
6. Utter DR, Borisy GG, Eren AM, Cavanaugh CM, Mark Welch JL. Metapangenomics of the oral microbiome provides insights into habitat adaptation and cultivar diversity. Genome Biol. 2020 Dec 16;21(1):293.
7. Imlay JA, Chin SM, Linn S. Toxic DNA damage by hydrogen peroxide through the Fenton reaction in vivo and in vitro. Science. 1988 Apr 29;240(4852):640–2.
8. Driessens N, Versteyhe S, Ghaddhab C, Burniat A, De Deken X, Van Sande J, et al. Hydrogen peroxide induces DNA single- and double-strand breaks in thyroid cells and is therefore a potential mutagen for this organ. Endocr Relat Cancer. 2009 Sep;16(3):845–56.
9. Imlay JA, Linn S. Mutagenesis and stress responses induced in Escherichia coli by hydrogen peroxide. J Bacteriol. 1987 Jul;169(7):2967–76.
10. McKenzie GJ, Harris RS, Lee PL, Rosenberg SM. The SOS response regulates adaptive mutation. Proc Natl Acad Sci U S A. 2000 Jun 6;97(12):6646–51.
11. Kuban W, Banach-Orlowska M, Schaaper RM, Jonczyk P, Fijalkowska IJ. Role of DNA polymerase IV in Escherichia coli SOS mutator activity. J Bacteriol. 2006 Nov;188(22):7977–80.
12. Rodríguez-Rojas A, Kim JJ, Johnston PR, Makarova O, Eravci M, Weise C, et al. Non-lethal exposure to H2O2 boosts bacterial survival and evolvability against oxidative stress. PLoS Genet. 2020 Mar;16(3):e1008649.
13. McKenzie GJ, Lee PL, Lombardo MJ, Hastings PJ, Rosenberg SM. SOS mutator DNA polymerase IV functions in adaptive mutation and not adaptive amplification. Mol Cell. 2001 Mar;7(3):571–9.
14. Song N, Nguyen Duc T, van Oeffelen L, Muyldermans S, Peeters E, Charlier D. Expanded target and cofactor repertoire for the transcriptional activator LysM from Sulfolobus. Nucleic Acids Res. 2013 Mar 1;41(5):2932–49.

15. Aslund F, Zheng M, Beckwith J, Storz G. Regulation of the OxyR transcription factor by hydrogen peroxide and the cellular thiol-disulfide status. Proc Natl Acad Sci U S A. 1999 May 25;96(11):6161–5.
16. Bailey TL, Boden M, Buske FA, Frith M, Grant CE, Clementi L, et al. MEME SUITE: tools for motif discovery and searching. Nucleic Acids Res. 2009 Jul;37(Web Server issue):W202-208.
17. Dubnau D. DNA uptake in bacteria. Annu Rev Microbiol. 1999;53:217–44.
18. Baharoglu Z, Krin E, Mazel D. Connecting environment and genome plasticity in the characterization of transformation-induced SOS regulation and carbon catabolite control of the Vibrio cholerae integron integrase. J Bacteriol. 2012 Apr;194(7):1659–67.
19. Goerlich O, Quillardet P, Hofnung M. Induction of the SOS response by hydrogen peroxide in various Escherichia coli mutants with altered protection against oxidative DNA damage. J Bacteriol. 1989 Nov;171(11):6141–7.
20. Maslowska KH, Makiela-Dzbenska K, Fijalkowska IJ. The SOS system: A complex and tightly regulated response to DNA damage. Environ Mol Mutagen. 2019 May;60(4):368–84.
21. Podlesek Z, Žgur Bertok D. The DNA Damage Inducible SOS Response Is a Key Player in the Generation of Bacterial Persister Cells and Population Wide Tolerance. Front Microbiol. 2020;11:1785.
22. Van der Auwera GA, Carneiro MO, Hartl C, Poplin R, Del Angel G, Levy-Moonshine A, et al. From FastQ data to high confidence variant calls: the Genome Analysis Toolkit best practices pipeline. Curr Protoc Bioinformatics. 2013;43:11.10.1-11.10.33.
23. Tseng Y-C, Yang H-Y, Lin W-T, Chang C-B, Chien H-C, Wang H-P, et al. Salivary dysbiosis in Sjögren's syndrome and a commensal-mediated immunomodulatory effect of salivary gland epithelial cells. NPJ Biofilms Microbiomes. 2021 Mar 11;7(1):21.
24. Storz G, Tartaglia LA, Ames BN. The OxyR regulon. Antonie Van Leeuwenhoek. 1990 Oct;58(3):157–61.
25. Whitby PW, Morton DJ, Vanwagoner TM, Seale TW, Cole BK, Mussa HJ, et al. Haemophilus influenzae OxyR: characterization of its regulation, regulon and role in fitness. PLoS One. 2012;7(11):e50588.
26. Ramsey MM, Rumbaugh KP, Whiteley M. Metabolite cross-feeding enhances virulence in a model polymicrobial infection. PLoS Pathog. 2011 Mar;7(3):e1002012.
27. Young REB, Twelkmeyer B, Vitiazeva V, Power PM, Schweda EKH, Hood DW. Haemophilus parainfluenzae expresses diverse lipopolysaccharide O-antigens using ABC transporter and Wzy polymerase-dependent mechanisms. Int J Med Microbiol. 2013 Dec;303(8):603–17.
28. Ramsey KM, Dove SL. A response regulator promotes Francisella tularensis intramacrophage growth by repressing an anti-virulence factor. Mol Microbiol. 2016 Aug;101(4):688–700.
29. Nakamura Y, Gojobori T, Ikemura T. Codon usage tabulated from international DNA sequence databases: status for the year 2000. Nucleic Acids Res. 2000 Jan 1;28(1):292.

30. Ramsey KM, Osborne ML, Vvedenskaya IO, Su C, Nickels BE, Dove SL. Ubiquitous promoter-localization of essential virulence regulators in Francisella tularensis. PLoS Pathog. 2015 Apr;11(4):e1004793.
31. Bailey TL, Elkan C. Fitting a mixture model by expectation maximization to discover motifs in biopolymers. Proc Int Conf Intell Syst Mol Biol. 1994;2:28–36.
32. DePristo MA, Banks E, Poplin R, Garimella KV, Maguire JR, Hartl C, et al. A framework for variation discovery and genotyping using next-generation DNA sequencing data. Nat Genet. 2011 May;43(5):491–8.
33. Li H, Durbin R. Fast and accurate long-read alignment with Burrows-Wheeler transform. Bioinformatics. 2010 Mar 1;26(5):589–95.
34. Ramsey MM, Freire MO, Gabrilska RA, Rumbaugh KP, Lemon KP. Staphylococcus aureus Shifts toward Commensalism in Response to Corynebacterium Species. Front Microbiol. 2016;7:1230.
35. Danecek P, Bonfield JK, Liddle J, Marshall J, Ohan V, Pollard MO, et al. Twelve years of SAMtools and BCFtools. Gigascience. 2021 Feb 16;10(2):giab008.

Appendix

Table S1: Genes induced in *ΔoxyR* compared to wildtype following addition of H_2O_2

Fold change	ID	Description
3.76	fig|6666666.571729.peg.1371	Iron(III) dicitrate transport system permease protein FecD (TC 3.A.1.14.1)
3.23	fig|6666666.571729.peg.847	Long-chain-fatty-acid--CoA ligase (EC 6.2.1.3);Ontology_term
3.18	fig|6666666.571729.peg.635	High-affinity choline uptake protein BetT
3.13	fig|6666666.571729.peg.1840	hypothetical protein
3.12	fig|6666666.571729.peg.30	Competence protein C%3B Chromosome segregation ATPases
3.04	fig|6666666.571729.peg.1590	Xanthine permease
3.01	fig|6666666.571729.peg.60	Glycerol uptake facilitator protein
2.82	fig|6666666.571729.peg.1443	Cytosine permease
2.74	fig|6666666.571729.peg.295	Lipid A export permease/ATP-binding protein MsbA
2.60	fig|6666666.571729.peg.1748	Chromosome segregation ATPases
2.51	fig|6666666.571729.peg.1229	hypothetical protein
2.43	fig|6666666.571729.peg.296	COG1132: ABC-type multidrug transport system%2C ATPase and permease components
2.31	fig|6666666.571729.peg.1095	hypothetical protein
2.30	fig|6666666.571729.peg.176	Sodium-dependent anion transporter family
2.29	fig|6666666.571729.peg.1995	Uncharacterized ferredoxin-like protein YfhL
2.28	fig|6666666.571729.peg.1214	3-hydroxyacyl-[acyl-carrier-protein] dehydratase%2C FabA form (EC 4.2.1.59) @ Trans-2-decenoyl-[acyl-carrier-protein] isomerase (EC 5.3.3.14);Ontology_term

2.18	fig|6666666.571729.peg.2004	Diaminopimelate decarboxylase and/or diaminopimelate epimerase leader peptide
2.18	fig|6666666.571729.peg.241	Cell division protein ZapB
2.10	fig|6666666.571729.peg.474	Uncharacterized inner membrane protein RarD
2.05	fig|6666666.571729.peg.1274	ABC-type Co2+ transport system%2C periplasmic component
2.03	fig|6666666.571729.peg.1810	Transcriptional regulator%2C MerR family
2.00	fig|6666666.571729.peg.313	TonB-dependent hemin%2C ferrichrome receptor
2.00	fig|6666666.571729.peg.319	Fluoride ion transporter CrcB

Table S2: Genes repressed in in *ΔoxyR* compared to wildtype following addition of H_2O_2

Fold change	ID	Description
-62.81	fig|6666666.571729.peg.337	Hydrogen peroxide-inducible genes activator > OxyR
-37.41	fig|6666666.571729.peg.1232	DNA protection during starvation protein (dps)
-20.38	fig|6666666.571729.peg.1459	Catalase KatA (EC 1.11.1.6);Ontology_term
-8.87	fig|6666666.571729.peg.401	Glucose-6-phosphate 1-dehydrogenase (EC 1.1.1.49);Ontology_term
-7.09	fig|6666666.571729.peg.929	hypothetical protein
-7.01	fig|6666666.571729.peg.930	hypothetical protein
-6.31	fig|6666666.571729.peg.1548	Alkyl hydroperoxide reductase subunit C-like protein
-5.03	fig|6666666.571729.peg.1700	Cytochrome c551 peroxidase (EC 1.11.1.5);Ontology_term

-4.52	fig|6666666.571729.peg.1089	Superoxide dismutase [Cu-Zn] precursor (EC 1.15.1.1);Ontology_term
-4.34	fig|6666666.571729.peg.1898	Glutathione reductase (EC 1.8.1.7);Ontology_term
-3.98	fig|6666666.571729.peg.867	Glutaredoxin 1
-3.69	fig|6666666.571729.peg.400	6-phosphogluconolactonase (EC 3.1.1.31)%2C eukaryotic type;Ontology_term
-3.59	fig|6666666.571729.peg.84	Aspartate--ammonia ligase (EC 6.3.1.1);Ontology_term
-3.59	fig|6666666.571729.peg.813	Manganese ABC transporter%2C ATP-binding protein SitB
-3.55	fig|6666666.571729.peg.1126	Glucose-6-phosphate isomerase (EC 5.3.1.9);Ontology_term
-3.40	fig|6666666.571729.peg.1464	GTP cyclohydrolase II (EC 3.5.4.25);Ontology_term
-3.18	fig|6666666.571729.peg.629	NADP-specific glutamate dehydrogenase (EC 1.4.1.4);Ontology_term
-3.16	fig|6666666.571729.peg.931	hypothetical protein
-3.16	fig|6666666.571729.peg.655	Transketolase (EC 2.2.1.1);Ontology_term
-2.95	fig|6666666.571729.peg.812	Manganese ABC transporter%2C inner membrane permease protein SitC
-2.86	fig|6666666.571729.peg.399	DUF1176 domain-containing protein
-2.86	fig|6666666.571729.peg.1430	NAD(P) transhydrogenase N-domain of subunit alpha (EC 1.6.1.2) / NAD(P) transhydrogenase C-domain of subunit alpha (EC 1.6.1.2);Ontology_term
-2.78	fig|6666666.571729.peg.934	Pentapeptide repeat family protein
-2.73	fig|6666666.571729.peg.2003	Frataxin homolog CyaY%2C facilitates Fe-S cluster assembly%2C interacts with IscS
-2.65	fig|6666666.571729.peg.932	hypothetical protein

-2.64	fig|6666666.571729.peg.814	Manganese ABC transporter%2C periplasmic-binding protein SitA
-2.62	fig|6666666.571729.peg.933	hypothetical protein
-2.61	fig|6666666.571729.peg.776	NrfC protein
-2.57	fig|6666666.571729.peg.1413	Exodeoxyribonuclease III (EC 3.1.11.2);Ontology_term
-2.50	fig|6666666.571729.peg.1337	Cell division-associated%2C ATP-dependent zinc metalloprotease FtsH
-2.50	fig|6666666.571729.peg.1646	Thioredoxin
-2.48	fig|6666666.571729.peg.826	ABC transporter involved in cytochrome c biogenesis%2C CcmB subunit
-2.42	fig|6666666.571729.peg.16	Transaldolase (EC 2.2.1.2);Ontology_term
-2.41	fig|6666666.571729.peg.777	Cytochrome c-type protein NrfB precursor
-2.39	fig|6666666.571729.peg.949	Flavodoxin 1
-2.36	fig|6666666.571729.peg.829	Cytochrome c-type biogenesis protein CcmE%2C heme chaperone
-2.32	fig|6666666.571729.peg.1429	NAD(P) transhydrogenase subunit beta (EC 1.6.1.2);Ontology_term
-2.30	fig|6666666.571729.peg.1412	DNA for glycosyltransferase%2C lytic transglycosylase%2C dTDP-4-rhamnose reductase
-2.29	fig|6666666.571729.peg.1903	Fumarate reductase flavoprotein subunit (EC 1.3.5.4);Ontology_term
-2.26	fig|6666666.571729.peg.398	DUF1176 domain-containing protein
-2.15	fig|6666666.571729.peg.1403	Hydrogenase-4 component A
-2.10	fig|6666666.571729.peg.1392	Formate dehydrogenase H (EC 1.2.1.2) @ selenocysteine-containing;Ontology_term
-2.10	fig|6666666.571729.peg.775	NrfD protein

-2.09	fig|6666666.571729.peg.661	DEAD-box ATP-dependent RNA helicase DeaD (CshA) (EC 3.6.4.13);Ontology_term
-2.05	fig|6666666.571729.peg.26	[4Fe-4S] cluster carrier protein NfuA
-2.04	fig|6666666.571729.peg.662	Lipoprotein NlpI

Table S3: Genes induced in *H. parainfluenzae* following addition of H_2O_2

Fold change	ID	Description
34.51	fig|6666666.571729.peg.602	hypothetical protein
31.85	fig|6666666.571729.peg.1707	hypothetical protein
24.78	fig|6666666.571729.peg.1635	DNA translocase FtsK
19.94	fig|6666666.571729.peg.816	hypothetical protein
19.80	fig|6666666.571729.peg.1271	hypothetical protein
13.75	fig|6666666.571729.peg.1301	hypothetical protein
12.75	fig|6666666.571729.peg.941	Sulfate and thiosulfate binding protein CysP
11.05	fig|6666666.571729.peg.1232	DNA protection during starvation protein
9.96	fig|6666666.571729.peg.888	Type II secretory pathway%2C pseudopilin PulG
9.89	fig|6666666.571729.peg.1893	Outer membrane receptor proteins%2C mostly Fe transport
9.80	fig|6666666.571729.peg.30	Competence protein C%3B Chromosome segregation ATPases
9.10	fig|6666666.571729.peg.747	Type IV pilin PilA

8.98	fig|6666666.571729.peg.93	hypothetical protein
8.19	fig|6666666.571729.peg.1633	Serine/threonine protein phosphatase (EC 3.1.3.16);Ontology_term
7.98	fig|6666666.571729.peg.159	hypothetical protein
7.75	fig|6666666.571729.peg.890	hypothetical protein
7.74	fig|6666666.571729.peg.842	hypothetical protein
7.56	fig|6666666.571729.peg.629	NADP-specific glutamate dehydrogenase (EC 1.4.1.4);Ontology_term
7.50	fig|6666666.571729.peg.677	Uncharacterized inner membrane transporter YhbE
6.93	fig|6666666.571729.peg.1182	Bacterial ribosome SSU maturation protein RimP
6.56	fig|6666666.571729.peg.1986	Cobalt/zinc/cadmium resistance protein CzcD
6.17	fig|6666666.571729.peg.1638	putative 5'(3')-deoxyribonucleotidase
6.12	fig|6666666.571729.peg.889	Type II secretory pathway%2C component PulJ
6.05	fig|6666666.571729.peg.586	Acyl carrier protein
6.02	fig|6666666.571729.peg.1631	AAA ATPase%2C central region
5.92	fig|6666666.571729.peg.1634	NAD-dependent protein deacetylase of SIR2 family
5.85	fig|6666666.571729.peg.268	hypothetical protein
5.78	fig|6666666.571729.peg.942	Precorrin-2 oxidase (EC 1.3.1.76) @ Sirohydrochlorin ferrochelatase activity of CysG (EC 4.99.1.4) / Uro-
5.60	fig|6666666.571729.peg.945	Sulfate adenylyltransferase subunit 1 (EC 2.7.7.4);Ontology_term
5.48	fig|6666666.571729.peg.939	Sulfate transport system permease protein CysW

5.45	fig|6666666.571729.peg.41	Hydroxymethylpyrimidine ABC transporter%2C ATPase component
5.41	fig|6666666.571729.peg.1780	Iron compound ABC uptake transporter permease protein
5.23	fig|6666666.571729.peg.1028	Inorganic triphosphatase (EC 3.6.1.25);Ontology_term
5.03	fig|6666666.571729.peg.1736	Iron-sulfur cluster regulator IscR
4.96	fig|6666666.571729.peg.678	Uncharacterized inner membrane transporter YhbE
4.95	fig|6666666.571729.peg.431	IroE protein
4.93	fig|6666666.571729.peg.1636	Putative DNA-binding protein in cluster with Type I restriction-modification system
4.80	fig|6666666.571729.peg.943	Adenylyl-sulfate reductase [thioredoxin] (EC 1.8.4.10);Ontology_term
4.79	fig|6666666.571729.peg.501	hypothetical protein
4.70	fig|6666666.571729.peg.366	LSU ribosomal protein L24p (L26e)
4.68	fig|6666666.571729.peg.1994	hypothetical protein
4.65	fig|6666666.571729.peg.2004	Diaminopimelate decarboxylase and/or diaminopimelate epimerase leader peptide
4.64	fig|6666666.571729.peg.1942	Ferric siderophore transport system%2C biopolymer transport protein ExbB
4.64	fig|6666666.571729.peg.502	hypothetical protein
4.60	fig|6666666.571729.peg.1288	Type III restriction-modification system methylation subunit (EC 2.1.1.72);Ontology_term
4.56	fig|6666666.571729.peg.401	Glucose-6-phosphate 1-dehydrogenase (EC 1.1.1.49);Ontology_term
4.56	fig|6666666.571729.peg.1894	TonB-dependent receptor%3B Outer membrane receptor for ferrienterochelin and colicins
4.51	fig|6666666.571729.peg.913	ImpA

4.50	fig|6666666.571729.peg.1530	DNA internalization-related competence protein ComEC/Rec2
4.49	fig|6666666.571729.peg.339	hypothetical protein
4.47	fig|6666666.571729.peg.1302	hypothetical protein
4.37	fig|6666666.571729.peg.84	Aspartate--ammonia ligase (EC 6.3.1.1);Ontology_term
4.34	fig|6666666.571729.peg.1230	Sel1 domain protein repeat-containing protein
4.32	fig|6666666.571729.peg.1049	DNA polymerase IV (EC 2.7.7.7);Ontology_term
4.30	fig|6666666.571729.peg.1632	hypothetical protein
4.29	fig|6666666.571729.peg.1481	Putative permease
4.26	fig|6666666.571729.peg.940	Sulfate transport system permease protein CysT
4.21	fig|6666666.571729.peg.320	Regulatory protein RecX
4.14	fig|6666666.571729.peg.1959	L-lactate dehydrogenase
4.12	fig|6666666.571729.peg.587	Acyl carrier protein
4.12	fig|6666666.571729.peg.407	hypothetical protein
4.12	fig|6666666.571729.peg.1408	hypothetical protein
4.11	fig|6666666.571729.peg.744	Leader peptidase (Prepilin peptidase) (EC 3.4.23.43) / N-methyltransferase (EC 2.1.1.-);Ontology_term
4.09	fig|6666666.571729.peg.691	hypothetical protein
4.07	fig|6666666.571729.peg.260	hypothetical protein
4.01	fig|6666666.571729.peg.601	Dialkylrecorsinol condensing enzyme

4.00	fig|6666666.571729.peg.92	hypothetical protein
3.96	fig|6666666.571729.peg.633	Twin-arginine translocation protein TatA
3.92	fig|6666666.571729.peg.261	hypothetical protein
3.84	fig|6666666.571729.peg.672	hypothetical protein
3.80	fig|6666666.571729.peg.596	Efflux ABC transporter%2C ATP-binding protein
3.80	fig|6666666.571729.peg.208	Protein YihD
3.79	fig|6666666.571729.peg.72	hypothetical protein
3.79	fig|6666666.571729.peg.465	Integrase
3.79	fig|6666666.571729.peg.835	hypothetical protein
3.77	fig|6666666.571729.peg.1417	Na+/H+ antiporter
3.76	fig|6666666.571729.peg.186	Molybdopterin-guanine dinucleotide biosynthesis protein MobB
3.72	fig|6666666.571729.peg.992	SSU ribosomal protein S15p (S13e)
3.71	fig|6666666.571729.peg.66	hypothetical protein
3.71	fig|6666666.571729.peg.907	hypothetical protein
3.71	fig|6666666.571729.peg.1149	Protein YecM
3.70	fig|6666666.571729.peg.464	Integrase
3.69	fig|6666666.571729.peg.376	LSU ribosomal protein L36p @ LSU ribosomal protein L36p%2C zinc-dependent
3.68	fig|6666666.571729.peg.1570	PTS IIA-like nitrogen-regulatory protein PtsN

3.68	fig|6666666.571729.peg.1852	Periplasmic nitrate reductase component NapD
3.68	fig|6666666.571729.peg.1985	Transcriptional regulator%2C MerR family
3.68	fig|6666666.571729.peg.2011	16S rRNA processing protein RimM
3.67	fig|6666666.571729.peg.160	hypothetical protein
3.66	fig|6666666.571729.peg.162	hypothetical protein
3.64	fig|6666666.571729.peg.313	TonB-dependent hemin%2C ferrichrome receptor
3.62	fig|6666666.571729.peg.1482	hypothetical protein
3.60	fig|6666666.571729.peg.814	Manganese ABC transporter%2C periplasmic-binding protein SitA
3.60	fig|6666666.571729.peg.597	hypothetical protein
3.60	fig|6666666.571729.peg.252	hypothetical protein
3.58	fig|6666666.571729.peg.1220	Anticodon nuclease
3.57	fig|6666666.571729.peg.1841	SAM-dependent methyltransferase
3.52	fig|6666666.571729.peg.254	hypothetical protein
3.52	fig|6666666.571729.peg.1743	Tol-Pal system-associated acyl-CoA thioesterase
3.51	fig|6666666.571729.peg.1412	DNA for glycosyltransferase%2C lytic transglycosylase%2C dTDP-4-rhamnose reductase
3.50	fig|6666666.571729.peg.1238	RNA:NAD 2'-phosphotransferase
3.50	fig|6666666.571729.peg.1952	Carbonic anhydrase (EC 4.2.1.1);Ontology_term
3.49	fig|6666666.571729.peg.298	hypothetical protein

3.49	fig|6666666.571729.peg.949	Flavodoxin 1
3.48	fig|6666666.571729.peg.256	hypothetical protein
3.47	fig|6666666.571729.peg.560	hypothetical protein
3.47	fig|6666666.571729.peg.1576	hypothetical protein
3.45	fig|6666666.571729.peg.269	hypothetical protein
3.44	fig|6666666.571729.peg.39	Hydroxymethylpyrimidine ABC transporter%2C substrate-binding component
3.42	fig|6666666.571729.peg.1601	FIG035246: DoxX family protein
3.40	fig|6666666.571729.peg.32	Type IV pilus biogenesis protein PilM
3.40	fig|6666666.571729.peg.435	Biofilm PGA synthesis deacetylase PgaB (EC 3.-)
3.39	fig|6666666.571729.peg.1779	Iron compound ABC uptake transporter permease protein
3.38	fig|6666666.571729.peg.879	LemA family protein
3.34	fig|6666666.571729.peg.1794	Intracellular septation protein IspA
3.32	fig|6666666.571729.peg.262	hypothetical protein
3.32	fig|6666666.571729.peg.1122	Phage integrase
3.29	fig|6666666.571729.peg.1656	hypothetical protein
3.29	fig|6666666.571729.peg.1943	Biopolymer transport protein ExbD/TolR
3.28	fig|6666666.571729.peg.67	hypothetical protein
3.28	fig|6666666.571729.peg.1010	CRISPR-associated protein Cas1

3.25	fig|6666666.571729.peg.1806	Copper-sensing two-component system response regulator CpxR
3.23	fig|6666666.571729.peg.1438	hypothetical protein
3.23	fig|6666666.571729.peg.1445	Lactam utilization protein LamB
3.22	fig|6666666.571729.peg.1846	Transcriptional regulator%2C AcrR family
3.21	fig|6666666.571729.peg.916	Putative molybdenum transport ATP-binding protein modF
3.20	fig|6666666.571729.peg.470	hypothetical protein
3.20	fig|6666666.571729.peg.1231	Sel1-like repeat
3.19	fig|6666666.571729.peg.22	Membrane protein LAPB
3.19	fig|6666666.571729.peg.1584	DNA repair protein RecN
3.16	fig|6666666.571729.peg.592	hypothetical protein
3.12	fig|6666666.571729.peg.379	SSU ribosomal protein S4p (S9e) @ SSU ribosomal protein S4p (S9e)%2C zinc-independent
3.11	fig|6666666.571729.peg.1579	Protein SprT
3.11	fig|6666666.571729.peg.253	hypothetical protein
3.09	fig|6666666.571729.peg.161	hypothetical protein
3.08	fig|6666666.571729.peg.1443	Cytosine permease
3.07	fig|6666666.571729.peg.1	D-glycero-beta-D-manno-heptose-1%2C7-bisphosphate 7-phosphatase (EC 3.1.3.82);Ontology_term
3.07	fig|6666666.571729.peg.812	Manganese ABC transporter%2C inner membrane permease protein SitC
3.05	fig|6666666.571729.peg.1185	Ribosome-binding factor A

3.03	fig|6666666.571729.peg.1460	Na+/alanine symporter
3.02	fig|6666666.571729.peg.40	Hydroxymethylpyrimidine ABC transporter%2C transmembrane component
3.02	fig|6666666.571729.peg.1654	hypothetical protein
3.00	fig|6666666.571729.peg.1291	Molybdopterin synthase sulfur carrier subunit
2.96	fig|6666666.571729.peg.1987	Dihydroneopterin aldolase (EC 4.1.2.25);Ontology_term
2.96	fig|6666666.571729.peg.503	hypothetical protein
2.96	fig|6666666.571729.peg.538	Glycosyltransferase
2.95	fig|6666666.571729.peg.877	Uncharacterized protein YdiJ
2.94	fig|6666666.571729.peg.535	hypothetical protein
2.93	fig|6666666.571729.peg.64	hypothetical protein
2.93	fig|6666666.571729.peg.369	SSU ribosomal protein S8p (S15Ae)
2.92	fig|6666666.571729.peg.248	hypothetical protein
2.89	fig|6666666.571729.peg.500	hypothetical protein
2.88	fig|6666666.571729.peg.1655	hypothetical protein
2.87	fig|6666666.571729.peg.476	Na+/H+ antiporter NhaA type
2.86	fig|6666666.571729.peg.1428	hypothetical protein
2.82	fig|6666666.571729.peg.1272	Fumarate and nitrate reduction regulatory protein
2.82	fig|6666666.571729.peg.649	hypothetical protein

2.81	fig|6666666.571729.peg.118	SSU ribosomal protein S12p (S23e)
2.81	fig|6666666.571729.peg.1765	hypothetical protein
2.81	fig|6666666.571729.peg.1645	DNA ligase
2.79	fig|6666666.571729.peg.10	hypothetical protein
2.78	fig|6666666.571729.peg.455	Transcriptional regulator%2C MarR family
2.78	fig|6666666.571729.peg.1969	Tyrosine-specific transport protein
2.77	fig|6666666.571729.peg.1277	Mobile element protein
2.74	fig|6666666.571729.peg.914	ImpA
2.74	fig|6666666.571729.peg.322	Patatin-like phospholipase
2.73	fig|6666666.571729.peg.380	DNA-directed RNA polymerase alpha subunit (EC 2.7.7.6);Ontology_term
2.72	fig|6666666.571729.peg.235	Permease of the drug/metabolite transporter (DMT) superfamily
2.71	fig|6666666.571729.peg.896	5'-deoxynucleotidase YfbR (EC 3.1.3.89);Ontology_term
2.71	fig|6666666.571729.peg.403	hypothetical protein
2.71	fig|6666666.571729.peg.1237	FIG00847315: hypothetical protein
2.70	fig|6666666.571729.peg.606	hypothetical protein
2.69	fig|6666666.571729.peg.1544	Putative Ton-B dependent hemine receptor
2.69	fig|6666666.571729.peg.662	Lipoprotein NlpI
2.68	fig|6666666.571729.peg.593	hypothetical protein

2.67	fig|6666666.571729.peg.929	hypothetical protein
2.65	fig|6666666.571729.peg.265	Vitamin B12 ABC transporter%2C ATP-binding protein BtuD
2.63	fig|6666666.571729.peg.5	hypothetical protein
2.63	fig|6666666.571729.peg.533	hypothetical protein
2.62	fig|6666666.571729.peg.42	23S rRNA (adenine(2030)-N(6))-methyltransferase (EC 2.1.1.266);Ontology_term
2.60	fig|6666666.571729.peg.745	Type II secretory pathway%2C component PulF%3B Type IV fimbrial assembly protein PilC
2.60	fig|6666666.571729.peg.1737	tRNA (cytidine(32)/uridine(32)-2'-O)-methyltransferase (EC 2.1.1.200);Ontology_term
2.59	fig|6666666.571729.peg.1011	CRISPR-associated endonuclease Cas9
2.59	fig|6666666.571729.peg.263	hypothetical protein
2.58	fig|6666666.571729.peg.1681	hypothetical protein
2.58	fig|6666666.571729.peg.590	hypothetical protein
2.58	fig|6666666.571729.peg.402	3'(2')%2C5'-bisphosphate nucleotidase (EC 3.1.3.7);Ontology_term
2.57	fig|6666666.571729.peg.370	LSU ribosomal protein L6p (L9e)
2.56	fig|6666666.571729.peg.184	Dipeptide ABC transporter%2C substrate-binding protein DppA (TC 3.A.1.5.2)
2.56	fig|6666666.571729.peg.946	Sulfite reductase [NADPH] flavoprotein alpha-component (EC 1.8.1.2);Ontology_term
2.56	fig|6666666.571729.peg.323	DNA transformation protein TfoX
2.55	fig|6666666.571729.peg.1974	Transcriptional regulator of glmS gene%2C DeoR family
2.54	fig|6666666.571729.peg.645	hypothetical protein

2.54	fig|6666666.571729.peg.368	SSU ribosomal protein S14p (S29e) @ SSU ribosomal protein S14p (S29e)%2C zinc-independent
2.54	fig|6666666.571729.peg.837	DnaA inactivator Hda (shorter homolog of DnaA)
2.53	fig|6666666.571729.peg.1868	hypothetical protein
2.53	fig|6666666.571729.peg.1386	Transcriptional regulator%2C MerR family
2.52	fig|6666666.571729.peg.1183	Transcription termination protein NusA
2.52	fig|6666666.571729.peg.964	Permease of the drug/metabolite transporter (DMT) superfamily
2.50	fig|6666666.571729.peg.986	ABC transporter%2C ATP-binding protein
2.50	fig|6666666.571729.peg.746	Type IV fimbrial assembly%2C ATPase PilB
2.48	fig|6666666.571729.peg.423	deoxyribose-phosphate aldolase(EC:4.1.2.4);Ontology_term
2.48	fig|6666666.571729.peg.1463	Phosphatidylglycerophosphatase B (EC 3.1.3.27);Ontology_term
2.47	fig|6666666.571729.peg.1750	Holliday junction ATP-dependent DNA helicase RuvA (EC 3.6.4.12);Ontology_term
2.47	fig|6666666.571729.peg.679	GTP-binding protein Obg
2.46	fig|6666666.571729.peg.1100	TonB-dependent receptor
2.46	fig|6666666.571729.peg.1287	Type III restriction-modification system restriction subunit (EC 3.1.21.5);Ontology_term
2.46	fig|6666666.571729.peg.285	hypothetical protein
2.44	fig|6666666.571729.peg.1164	Limit dextrin alpha-1%2C6-maltotetraose-hydrolase (EC 3.2.1.196);Ontology_term
2.44	fig|6666666.571729.peg.60	Glycerol uptake facilitator protein
2.43	fig|6666666.571729.peg.635	High-affinity choline uptake protein BetT

2.42	fig|6666666.571729.peg.1172	L-lysine permease
2.42	fig|6666666.571729.peg.1523	Ferric iron ABC transporter%2C ATP-binding protein
2.41	fig|6666666.571729.peg.65	hypothetical protein
2.41	fig|6666666.571729.peg.999	Glycine cleavage system transcriptional activator GcvA
2.40	fig|6666666.571729.peg.1865	Dihydrofolate reductase (EC 1.5.1.3);Ontology_term
2.40	fig|6666666.571729.peg.325	hypothetical protein
2.39	fig|6666666.571729.peg.1603	FIG023677: hypothetical protein
2.38	fig|6666666.571729.peg.1581	Para-aminobenzoate synthase%2C amidotransferase component (EC 2.6.1.85);Ontology_term
2.38	fig|6666666.571729.peg.1187	Chorismate mutase I (EC 5.4.99.5) / Cyclohexadienyl dehydrogenase (EC 1.3.1.12)(EC 1.3.1.43);Ontol-
2.38	fig|6666666.571729.peg.1328	Possible protease sohB (EC 3.4.21.-);Ontology_term
2.37	fig|6666666.571729.peg.7	hypothetical protein
2.37	fig|6666666.571729.peg.1658	hypothetical protein
2.36	fig|6666666.571729.peg.540	UDP-glucose 4-epimerase (EC 5.1.3.2);Ontology_term
2.35	fig|6666666.571729.peg.1905	Fumarate reductase subunit C
2.34	fig|6666666.571729.peg.1916	Glycosyl transferase
2.33	fig|6666666.571729.peg.441	Permease of the drug/metabolite transporter (DMT) superfamily
2.33	fig|6666666.571729.peg.236	16S rRNA (guanine(527)-N(7))-methyltransferase (EC 2.1.1.170);Ontology_term
2.33	fig|6666666.571729.peg.1478	Biotin operon repressor / Biotin--protein ligase (EC 6.3.4.9)(EC 6.3.4.10)(EC 6.3.4.11)(EC

2.33	fig|6666666.571729.peg.1413	Exodeoxyribonuclease III (EC 3.1.11.2);Ontology_term
2.33	fig|6666666.571729.peg.1756	hypothetical protein
2.33	fig|6666666.571729.peg.1694	T6SS component TssB (ImpB/VipA)
2.32	fig|6666666.571729.peg.155	ABC transporter%2C permease protein (cluster 3%2C basic aa/glutamine/opines)
2.32	fig|6666666.571729.peg.100	5'-nucleotidase (EC 3.1.3.5)%3B 2'%2C3'-cyclic-nucleotide 2'-phosphodiesterase (EC 3.1.4.16)%3B Pu-
2.32	fig|6666666.571729.peg.1759	hypothetical protein
2.31	fig|6666666.571729.peg.1547	Cystathionine beta-lyase (EC 4.4.1.8);Ontology_term
2.31	fig|6666666.571729.peg.373	LSU ribosomal protein L30p (L7e)
2.31	fig|6666666.571729.peg.154	ABC transporter%2C permease protein (cluster 3%2C basic aa/glutamine/opines)
2.30	fig|6666666.571729.peg.1128	Protein tyrosine/serine phosphatase
2.30	fig|6666666.571729.peg.55	Sulfate transporter%2C CysZ-type
2.29	fig|6666666.571729.peg.1691	T6SS component TssF (ImpG/VasA)
2.27	fig|6666666.571729.peg.971	Glycogen phosphorylase (EC 2.4.1.1);Ontology_term
2.27	fig|6666666.571729.peg.1637	NAD-dependent protein deacetylase of SIR2 family
2.26	fig|6666666.571729.peg.57	L-cystine ABC transporter%2C substrate-binding protein TcyA
2.25	fig|6666666.571729.peg.49	Thymidine kinase (EC 2.7.1.21);Ontology_term
2.25	fig|6666666.571729.peg.404	Predicted membrane protein
2.24	fig|6666666.571729.peg.1879	hypothetical protein

2.24	fig|6666666.571729.peg.1909	Primosomal replication protein N
2.23	fig|6666666.571729.peg.875	COG2315: Uncharacterized protein conserved in bacteria
2.23	fig|6666666.571729.peg.377	SSU ribosomal protein S13p (S18e)
2.23	fig|6666666.571729.peg.1711	Phospholipid ABC transporter-binding protein MlaB
2.22	fig|6666666.571729.peg.813	Manganese ABC transporter%2C ATP-binding protein SitB
2.22	fig|6666666.571729.peg.994	Hypothetical protein DUF454
2.21	fig|6666666.571729.peg.1647	Cystathionine gamma-synthase (EC 2.5.1.48);Ontology_term
2.20	fig|6666666.571729.peg.2013	hypothetical protein
2.20	fig|6666666.571729.peg.539	Lipid carrier : UDP-N-acetylgalactosaminyltransferase (EC 2.4.1.-) / Alpha-1%2C3-N-acetylgalactosa-
2.20	fig|6666666.571729.peg.1876	Putative inner membrane protein
2.20	fig|6666666.571729.peg.1712	Phospholipid ABC transporter shuttle protein MlaC
2.18	fig|6666666.571729.peg.781	Formamidopyrimidine-DNA glycosylase (EC 3.2.2.23);Ontology_term
2.18	fig|6666666.571729.peg.1933	1%2C4-dihydroxy-2-naphthoate polyprenyltransferase (EC 2.5.1.74);Ontology_term
2.18	fig|6666666.571729.peg.463	hypothetical protein
2.18	fig|6666666.571729.peg.1317	Stringent starvation protein A
2.17	fig|6666666.571729.peg.1684	T6SS component TssA (ImpA)
2.17	fig|6666666.571729.peg.1477	Uncharacterized protein MSMEG_6412
2.16	fig|6666666.571729.peg.1668	hypothetical protein

2.16	fig|6666666.571729.peg.1085	ABC transporter%2C permease protein 2 (cluster 5%2C nickel/peptides/opines)
2.16	fig|6666666.571729.peg.965	Permease of the drug/metabolite transporter (DMT) superfamily
2.15	fig|6666666.571729.peg.1221	Type I restriction-modification system%2C specificity subunit S
2.15	fig|6666666.571729.peg.584	FIG017861: hypothetical protein
2.15	fig|6666666.571729.peg.1610	Protein PhnA
2.15	fig|6666666.571729.peg.1827	3-hydroxyacyl-[acyl-carrier-protein] dehydratase%2C FabZ form (EC 4.2.1.59);Ontology_term
2.15	fig|6666666.571729.peg.944	Sulfate adenylyltransferase subunit 2 (EC 2.7.7.4);Ontology_term
2.14	fig|6666666.571729.peg.187	Sigma factor RpoE negative regulatory protein RseB precursor
2.14	fig|6666666.571729.peg.416	tRNA pseudouridine(13) synthase (EC 5.4.99.27);Ontology_term
2.13	fig|6666666.571729.peg.660	Membrane-bound lytic murein transglycosylase F (EC 4.2.2.n1)
2.13	fig|6666666.571729.peg.87	Anaerobic glycerol-3-phosphate dehydrogenase subunit B (EC 1.1.5.3);Ontology_term
2.13	fig|6666666.571729.peg.1690	T6SS component TssG (ImpH/VasB)
2.13	fig|6666666.571729.peg.1652	hypothetical protein
2.13	fig|6666666.571729.peg.62	hypothetical protein
2.13	fig|6666666.571729.peg.1006	Riboflavin synthase eubacterial/eukaryotic (EC 2.5.1.9);Ontology_term
2.12	fig|6666666.571729.peg.224	hypothetical protein
2.11	fig|6666666.571729.peg.389	hypothetical protein
2.11	fig|6666666.571729.peg.869	hypothetical protein

2.11	fig|6666666.571729.peg.107	Nucleoside triphosphate pyrophosphohydrolase MazG (EC 3.6.1.8);Ontology_term
2.11	fig|6666666.571729.peg.1452	hypothetical protein
2.10	fig|6666666.571729.peg.595	FIG00847847: hypothetical protein
2.10	fig|6666666.571729.peg.316	Pantothenate kinase (EC 2.7.1.33);Ontology_term
2.10	fig|6666666.571729.peg.506	Lipoprotein signal peptidase (EC 3.4.23.36);Ontology_term
2.09	fig|6666666.571729.peg.1456	Exopolysaccharide biosynthesis protein
2.09	fig|6666666.571729.peg.1222	Type I restriction-modification system%2C DNA-methyltransferase subunit M (EC 2.1.1.72);Ontol-
2.09	fig|6666666.571729.peg.735	Efflux ABC transporter%2C permease/ATP-binding protein
2.09	fig|6666666.571729.peg.536	Alpha-1%2C4-N-acetylgalactosamine transferase PglH (EC 2.4.1.-);Ontology_term
2.09	fig|6666666.571729.peg.1825	Lipid-A-disaccharide synthase (EC 2.4.1.182);Ontology_term
2.08	fig|6666666.571729.peg.375	Protein translocase subunit SecY
2.08	fig|6666666.571729.peg.1176	Protein ygiW precursor
2.08	fig|6666666.571729.peg.1393	Formate hydrogenlyase maturation protease (EC 3.4.23.51);Ontology_term
2.08	fig|6666666.571729.peg.1262	tRNA-(cytosine32)-2-thiocytidine synthetase TtcA
2.08	fig|6666666.571729.peg.292	converved hypothetical protein
2.07	fig|6666666.571729.peg.1807	Copper sensory histidine kinase CpxA
2.07	fig|6666666.571729.peg.321	RecA protein
2.06	fig|6666666.571729.peg.95	Phosphoribosylformylglycinamidine synthase%2C synthetase subunit (EC 6.3.5.3) / Phosphoribosylformyl-

2.05	fig|6666666.571729.peg.237	Redox-sensing transcriptional regulator QorR
2.05	fig|6666666.571729.peg.1280	Transcriptional regulator%2C LysR family
2.04	fig|6666666.571729.peg.1686	T6SS outer membrane component TssL (ImpK/VasF)
2.04	fig|6666666.571729.peg.648	Mobile element protein
2.03	fig|6666666.571729.peg.1378	LPS-core synthesis glycosyltransferase PM0509
2.03	fig|6666666.571729.peg.1336	Dihydropteroate synthase (EC 2.5.1.15);Ontology_term
2.03	fig|6666666.571729.peg.1913	LOS biosynthesis enzyme LBGB
2.02	fig|6666666.571729.peg.750	Uncharacterized UPF0721 integral membrane protein
2.02	fig|6666666.571729.peg.271	S-ribosylhomocysteine lyase (EC 4.4.1.21) @ Autoinducer-2 production protein LuxS;Ontology_term
2.02	fig|6666666.571729.peg.1088	Conserved protein YcjX with nucleoside triphosphate hydrolase domain
2.02	fig|6666666.571729.peg.1082	Signal peptide peptidase SppA (protease 4)
2.01	fig|6666666.571729.peg.763	Phosphatidate cytidylyltransferase (EC 2.7.7.41);Ontology_term
2.00	fig|6666666.571729.peg.1548	Alkyl hydroperoxide reductase subunit C-like protein

Table S4: Genes repressed in *H. parainfluenzae* following addition of H_2O_2 compared to no added H_2O_2

Fold change	ID	Description

-4683.91	fig|6666666.571729.peg.756	FIG00697202: hypothetical protein
-90.59	fig|6666666.571729.peg.537	hypothetical protein
-68.30	fig|6666666.571729.peg.458	Putative Dihydrolipoamide dehydro-genase (EC 1.8.1.4)%3B Mercuric ion reductase (EC 1.16.1.1)%3B PF00070 family%2C FAD-dependent NAD(P)
-37.22	fig|6666666.571729.peg.646	hypothetical protein
-32.75	fig|6666666.571729.peg.1745	Cytochrome d ubiquinol oxidase sub-unit X (EC 1.10.3.-);Ontology_term
-29.18	fig|6666666.571729.peg.388	Osmotically-inducible lipoprotein OsmB
-28.32	fig|6666666.571729.peg.1020	hypothetical protein
-25.31	fig|6666666.571729.peg.742	DNA gyrase inhibitor YacG
-17.45	fig|6666666.571729.peg.607	hypothetical protein
-16.26	fig|6666666.571729.peg.347	hypothetical protein
-13.98	fig|6666666.571729.peg.704	5-formyltetrahydrofolate cyclo-ligase (EC 6.3.3.2);Ontology_term
-11.51	fig|6666666.571729.peg.1289	hypothetical protein
-11.44	fig|6666666.571729.peg.1275	hypothetical protein
-11.25	fig|6666666.571729.peg.1389	Substrate-specific component NikM of nickel ECF transporter
-11.19	fig|6666666.571729.peg.1796	YciL protein
-10.86	fig|6666666.571729.peg.461	Inner membrane protein%2C KefB/KefC family
-10.46	fig|6666666.571729.peg.218	hypothetical protein

-9.73	fig|6666666.571729.peg.1884	Nucleoid-associated protein YaaK
-9.51	fig|6666666.571729.peg.1299	LSU ribosomal protein L20p
-9.25	fig|6666666.571729.peg.566	LSU ribosomal protein L32p @ LSU ribosomal protein L32p%2C zinc-independent
-8.62	fig|6666666.571729.peg.251	hypothetical protein
-8.29	fig|6666666.571729.peg.1473	hypothetical protein
-8.01	fig|6666666.571729.peg.1409	Outer membrane stress sensor protease DegQ%2C serine protease
-7.81	fig|6666666.571729.peg.562	Carboxymuconolactone decarboxylase family protein
-7.48	fig|6666666.571729.peg.676	LSU ribosomal protein L27p
-7.11	fig|6666666.571729.peg.13	2-iminobutanoate/2-iminopropanoate deaminase RidA/TdcF (EC 3.5.99.10);Ontology_term
-6.68	fig|6666666.571729.peg.1818	Heat shock protein 60 kDa family chaperone GroEL
-6.62	fig|6666666.571729.peg.1982	ABC transporter%2C permease protein (cluster 10%2C nitrate/sulfonate/bicarbonate)
-6.59	fig|6666666.571729.peg.1360	Periplasmic protein p19 involved in high-affinity Fe2+ transport
-6.14	fig|6666666.571729.peg.1862	FKBP-type peptidyl-prolyl cis-trans isomerase FklB (EC 5.2.1.8);Ontology_term
-6.13	fig|6666666.571729.peg.1738	Tol-Pal system peptidoglycan-associated lipoprotein PAL
-6.01	fig|6666666.571729.peg.1908	SSU ribosomal protein S18p @ SSU ribosomal protein S18p%2C zinc-independent
-6.00	fig|6666666.571729.peg.1586	Heat shock protein GrpE

-5.96	fig|6666666.571729.peg.433	AagD
-5.96	fig|6666666.571729.peg.1950	Uncharacterized protein YhdT
-5.90	fig|6666666.571729.peg.453	putative phage shock protein E precursor
-5.80	fig|6666666.571729.peg.685	Rhomboid family protein
-5.55	fig|6666666.571729.peg.905	Chaperone protein DnaK
-5.54	fig|6666666.571729.peg.1720	Galactokinase (EC 2.7.1.6);Ontology_term
-5.52	fig|6666666.571729.peg.1013	LSU ribosomal protein L25p
-5.44	fig|6666666.571729.peg.1552	ADP-ribose pyrophosphatase (EC 3.6.1.13);Ontology_term
-5.39	fig|6666666.571729.peg.1768	hypothetical protein
-5.28	fig|6666666.571729.peg.903	O-acetylhomoserine sulfhydrylase (EC 2.5.1.49) @ O-succinylhomoserine sulfhydrylase (EC 2.5.1.48);Ontology_term
-5.19	fig|6666666.571729.peg.1821	Uncharacterized transporter YfbS
-5.10	fig|6666666.571729.peg.250	2-oxoglutarate/malate translocator
-5.08	fig|6666666.571729.peg.69	hypothetical protein
-5.07	fig|6666666.571729.peg.902	Chaperone protein DnaJ
-5.04	fig|6666666.571729.peg.1395	Hydrogenase-4 component I
-4.98	fig|6666666.571729.peg.1809	Copper(I) chaperone CopZ
-4.96	fig|6666666.571729.peg.524	Diacylglycerol kinase (EC 2.7.1.107);Ontology_term

-4.82	fig|6666666.571729.peg.508	hypothetical protein
-4.70	fig|6666666.571729.peg.1284	N5-carboxyaminoimidazole ribonucleotide mutase (EC 5.4.99.18);Ontology_term
-4.60	fig|6666666.571729.peg.1040	FIG001587: exported protein
-4.59	fig|6666666.571729.peg.1077	Adenylosuccinate synthetase (EC 6.3.4.4);Ontology_term
-4.55	fig|6666666.571729.peg.1403	Hydrogenase-4 component A
-4.54	fig|6666666.571729.peg.836	hypothetical protein
-4.48	fig|6666666.571729.peg.546	Nucleoside diphosphate kinase (EC 2.7.4.6);Ontology_term
-4.41	fig|6666666.571729.peg.446	PTS system%2C mannose-specific IID component
-4.41	fig|6666666.571729.peg.306	Hydrogenase maturation protease
-4.39	fig|6666666.571729.peg.1072	3-oxoacyl-[acyl-carrier-protein] synthase%2C KASI (EC 2.3.1.41);Ontology_term
-4.37	fig|6666666.571729.peg.183	Pyridoxamine 5'-phosphate oxidase (EC 1.4.3.5);Ontology_term
-4.36	fig|6666666.571729.peg.1934	tRNA (adenine(37)-N6)-methyltransferase
-4.33	fig|6666666.571729.peg.680	LSU ribosomal protein L36p @ LSU ribosomal protein L36p%2C zinc-independent
-4.33	fig|6666666.571729.peg.977	Lipid A biosynthesis lauroyl acyltransferase (EC 2.3.1.241);Ontology_term
-4.29	fig|6666666.571729.peg.1819	Heat shock protein 10 kDa family chaperone GroES
-4.28	fig|6666666.571729.peg.447	PTS system%2C mannose-specific IIC component
-4.27	fig|6666666.571729.peg.310	Ni/Fe-hydrogenase 2 small subunit HybO (EC 1.12.99.6);Ontology_term

-4.25	fig|6666666.571729.peg.862	Phosphotransferase system%2C phosphocarrier protein HPr
-4.23	fig|6666666.571729.peg.906	hypothetical protein
-4.20	fig|6666666.571729.peg.96	Orf2
-4.19	fig|6666666.571729.peg.1858	Glutathionylspermidine synthase (EC 6.3.1.8) / Glutathionylspermidine amidohydrolase (EC 3.5.1.78);Ontology_term
-4.15	fig|6666666.571729.peg.789	Cyclic AMP receptor protein
-4.13	fig|6666666.571729.peg.1588	Hypothetical protein VC0266 (sugar utilization related?)
-4.05	fig|6666666.571729.peg.1322	Integration host factor alpha subunit
-4.03	fig|6666666.571729.peg.48	hypothetical protein
-4.00	fig|6666666.571729.peg.1388	Additional component NikL of nickel ECF transporter
-3.94	fig|6666666.571729.peg.451	Uncharacterized protein YnbE
-3.92	fig|6666666.571729.peg.665	UPF0033 protein YeeD
-3.88	fig|6666666.571729.peg.1021	Ribose-phosphate pyrophosphokinase (EC 2.7.6.1);Ontology_term
-3.86	fig|6666666.571729.peg.1925	DnaJ-like protein DjlA
-3.86	fig|6666666.571729.peg.785	Phosphopantothenoylcysteine decarboxylase (EC 4.1.1.36) / Phosphopantothenoylcysteine synthetase (EC
-3.81	fig|6666666.571729.peg.1998	Fructose-bisphosphate aldolase class II (EC 4.1.2.13);Ontology_term
-3.81	fig|6666666.571729.peg.550	TonB-dependent receptor
-3.80	fig|6666666.571729.peg.686	IMP cyclohydrolase (EC 3.5.4.10) / Phosphoribosylaminoimidazolecarboxamide formyltransferase (EC

-3.71	fig|6666666.571729.peg.1436	Uncharacterized protein YraP
-3.70	fig|6666666.571729.peg.1089	Superoxide dismutase [Cu-Zn] precursor (EC 1.15.1.1);Ontology_term
-3.65	fig|6666666.571729.peg.1563	hypothetical protein
-3.63	fig|6666666.571729.peg.496	2-haloalkanoic acid dehalogenase (EC 3.8.1.2);Ontology_term
-3.61	fig|6666666.571729.peg.801	Ribonuclease P protein component (EC 3.1.26.5);Ontology_term
-3.61	fig|6666666.571729.peg.2016	VgrG protein
-3.60	fig|6666666.571729.peg.716	Lactoylglutathione lyase (EC 4.4.1.5);Ontology_term
-3.58	fig|6666666.571729.peg.278	D-aminoacyl-tRNA deacylase (EC 3.1.1.96);Ontology_term
-3.58	fig|6666666.571729.peg.787	Transcriptional regulator SlmA%2C TetR family
-3.55	fig|6666666.571729.peg.659	hypothetical protein
-3.54	fig|6666666.571729.peg.270	Formate-dependent phosphoribosyl-glycinamide formyltransferase
-3.51	fig|6666666.571729.peg.1808	Copper-translocating P-type ATPase (EC 3.6.3.4);Ontology_term
-3.50	fig|6666666.571729.peg.210	UPF0438 protein YifE
-3.49	fig|6666666.571729.peg.1907	LSU ribosomal protein L9p
-3.49	fig|6666666.571729.peg.1883	Recombination protein RecR
-3.48	fig|6666666.571729.peg.1835	Ribosome recycling factor
-3.46	fig|6666666.571729.peg.2001	Uncharacterized glycine randical protein HI_0521

-3.44	fig|6666666.571729.peg.1961	N-acetylmuramic acid 6-phosphate etherase (EC 4.2.1.126);Ontology_term
-3.44	fig|6666666.571729.peg.457	hypothetical protein
-3.40	fig|6666666.571729.peg.226	Threonine dehydratase biosynthetic (EC 4.3.1.19);Ontology_term
-3.38	fig|6666666.571729.peg.1937	Alternative ribosome-rescue factor A
-3.37	fig|6666666.571729.peg.1081	Putative NAD(P)H nitroreductase YdjA
-3.35	fig|6666666.571729.peg.1512	Phospholipid-binding protein
-3.34	fig|6666666.571729.peg.1722	Galactose-1-phosphate uridylyltransferase (EC 2.7.7.10);Ontology_term
-3.34	fig|6666666.571729.peg.1485	Transcriptional activator MetR
-3.33	fig|6666666.571729.peg.1516	Thiol peroxidase%2C Tpx-type (EC 1.11.1.15);Ontology_term
-3.31	fig|6666666.571729.peg.1542	HesA/MoeB/ThiF family protein > sulfur transfer pathway protein CsdL
-3.29	fig|6666666.571729.peg.11	LSU ribosomal protein L7p/L12p (P1/P2)
-3.27	fig|6666666.571729.peg.411	ATP-dependent protease subunit HslV (EC 3.4.25.2);Ontology_term
-3.27	fig|6666666.571729.peg.1264	Bacterial non-heme ferritin (EC 1.16.3.2);Ontology_term
-3.25	fig|6666666.571729.peg.1261	tRNA 2-thiouridine synthesis protein TusE
-3.23	fig|6666666.571729.peg.1168	6%2C7-dimethyl-8-ribityllumazine synthase (EC 2.5.1.78);Ontology_term
-3.23	fig|6666666.571729.peg.1169	Transcription termination protein NusB
-3.20	fig|6666666.571729.peg.334	Cell division protein DivIC (FtsB)%2C stabilizes FtsL against RasP cleavage

-3.19	fig|6666666.571729.peg.2000	ADP-heptose--lipooligosaccharide heptosyltransferase II
-3.17	fig|6666666.571729.peg.1660	VgrG protein
-3.16	fig|6666666.571729.peg.1143	LSU rRNA pseudouridine(2605) synthase (EC 5.4.99.22);Ontology_term
-3.14	fig|6666666.571729.peg.1074	Acetolactate synthase small subunit (EC 2.2.1.6);Ontology_term
-3.14	fig|6666666.571729.peg.700	Putative pre-16S rRNA nuclease YqgF
-3.13	fig|6666666.571729.peg.336	Unsaturated fatty acid biosythesis repressor FabR%2C TetR family
-3.09	fig|6666666.571729.peg.180	Uncharacterized oxidoreductase YjhC
-3.07	fig|6666666.571729.peg.495	Large exoproteins involved in heme utilization or adhesion
-3.05	fig|6666666.571729.peg.68	hypothetical protein
-3.05	fig|6666666.571729.peg.1954	Biotin carboxyl carrier protein of acetyl-CoA carboxylase
-3.03	fig|6666666.571729.peg.1427	UPF0033 protein YedF
-2.97	fig|6666666.571729.peg.73	Purine nucleoside phosphorylase (EC 2.4.2.1);Ontology_term
-2.96	fig|6666666.571729.peg.1875	5-methyltetrahydrofolate--homocysteine methyltransferase (EC 2.1.1.13);Ontology_term
-2.96	fig|6666666.571729.peg.1873	3-isopropylmalate dehydratase large subunit (EC 4.2.1.33);Ontology_term
-2.96	fig|6666666.571729.peg.1509	DNA polymerase III psi subunit (EC 2.7.7.7);Ontology_term
-2.95	fig|6666666.571729.peg.820	(E)-4-hydroxy-3-methylbut-2-enyl-diphosphate synthase (flavodoxin) (EC 1.17.7.3);Ontology_term
-2.94	fig|6666666.571729.peg.1453	Repair of Iron Centers di-iron protein

-2.90	fig|6666666.571729.peg.179	probable oxidoreductase protein
-2.89	fig|6666666.571729.peg.705	Chaperone protein ClpB (ATP-dependent unfoldase)
-2.87	fig|6666666.571729.peg.841	Nitric-oxide reductase (EC 1.7.99.7)%2C quinol-dependent;Ontology_term
-2.86	fig|6666666.571729.peg.608	Protein translocase subunit SecA
-2.83	fig|6666666.571729.peg.1067	probable membrane protein YPO3565
-2.83	fig|6666666.571729.peg.1404	[NiFe] hydrogenase metallocenter assembly protein HypC
-2.82	fig|6666666.571729.peg.699	UPF0301 protein YqgE
-2.82	fig|6666666.571729.peg.1211	Cold shock protein of CSP family > CspD (naming convention as in E.coli)
-2.80	fig|6666666.571729.peg.430	33 kDa chaperonin HslO
-2.78	fig|6666666.571729.peg.422	Deoxyribose-phosphate aldolase (EC 4.1.2.4);Ontology_term
-2.78	fig|6666666.571729.peg.1240	5-methyltetrahydropteroyltriglutamate--homocysteine methyltransferase (EC 2.1.1.14);Ontology_term
-2.77	fig|6666666.571729.peg.497	hypothetical protein
-2.77	fig|6666666.571729.peg.1382	[NiFe] hydrogenase metallocenter assembly protein HypE
-2.77	fig|6666666.571729.peg.1993	Uncharacterized MFS-type transporter
-2.77	fig|6666666.571729.peg.1135	Putative TEGT family carrier/transport protein
-2.76	fig|6666666.571729.peg.1310	Anthranilate phosphoribosyltransferase (EC 2.4.2.18);Ontology_term
-2.76	fig|6666666.571729.peg.1867	6-phosphofructokinase (EC 2.7.1.11);Ontology_term

-2.76	fig|6666666.571729.peg.290	L-asparaginase (EC 3.5.1.1);Ontology_term
-2.76	fig|6666666.571729.peg.687	Phosphoribosylamine--glycine ligase (EC 6.3.4.13);Ontology_term
-2.74	fig|6666666.571729.peg.413	FKBP-type peptidyl-prolyl cis-trans isomerase SlyD (EC 5.2.1.8);Ontology_term
-2.74	fig|6666666.571729.peg.439	Iron(III) dicitrate transport system permease protein FecC (TC 3.A.1.14.1)
-2.74	fig|6666666.571729.peg.717	Uncharacterized protease YegQ
-2.72	fig|6666666.571729.peg.1506	Formate dehydrogenase O gamma subunit (EC 1.2.1.2);Ontology_term
-2.71	fig|6666666.571729.peg.526	Glycerate kinase (EC 2.7.1.31);Ontology_term
-2.70	fig|6666666.571729.peg.1387	Additional periplasmic component NikK of nickel ECF transporter
-2.70	fig|6666666.571729.peg.701	FIG00003370: Multicopper polyphenol oxidase
-2.69	fig|6666666.571729.peg.894	Diaminohydroxyphosphoribosylaminopyrimidine deaminase (EC 3.5.4.26) / 5-amino-6-(5-phosphoribosylamino)uracil reductase (EC 1.1.1.193);Ontology_term
-2.68	fig|6666666.571729.peg.529	Pyrroline-5-carboxylate reductase (EC 1.5.1.2);Ontology_term
-2.68	fig|6666666.571729.peg.521	DNA recombination and repair protein RecO
-2.68	fig|6666666.571729.peg.61	Glycerol kinase (EC 2.7.1.30);Ontology_term
-2.68	fig|6666666.571729.peg.2005	Diaminopimelate decarboxylase (EC 4.1.1.20);Ontology_term
-2.68	fig|6666666.571729.peg.1306	FMN-dependent NADH-azoreductase (EC 1.7.1.6);Ontology_term
-2.67	fig|6666666.571729.peg.1857	Cytochrome c-type protein NapC

-2.67	fig|6666666.571729.peg.1076	Protein of unknown function DUF484
-2.66	fig|6666666.571729.peg.129	Triosephosphate isomerase (EC 5.3.1.1);Ontology_term
-2.65	fig|6666666.571729.peg.1316	Stringent starvation protein B
-2.63	fig|6666666.571729.peg.301	ATP-dependent protease La (EC 3.4.21.53) Type I;Ontology_term
-2.63	fig|6666666.571729.peg.1903	Fumarate reductase flavoprotein subunit (EC 1.3.5.4);Ontology_term
-2.62	fig|6666666.571729.peg.821	Histidyl-tRNA synthetase (EC 6.1.1.21);Ontology_term
-2.61	fig|6666666.571729.peg.1365	Putative thioredoxin precursor
-2.61	fig|6666666.571729.peg.1206	UPF0319 protein YccT precursor
-2.60	fig|6666666.571729.peg.206	Protease HtpX
-2.60	fig|6666666.571729.peg.1139	Predicted hydroxymethylpyrimidine transporter CytX
-2.58	fig|6666666.571729.peg.609	Mutator MutT protein (7%2C8-dihydro-8-oxoguanine-triphosphatase) (EC 3.6.1.-);Ontology_term
-2.57	fig|6666666.571729.peg.766	2-succinyl-5-enolpyruvyl-6-hydroxy-3-cyclohexene-1-carboxylic-acid synthase (EC 2.2.1.9);Ontology_term
-2.54	fig|6666666.571729.peg.412	ATP-dependent hsl protease ATP-binding subunit HslU
-2.54	fig|6666666.571729.peg.417	5'-nucleotidase SurE (EC 3.1.3.5);Ontology_term
-2.52	fig|6666666.571729.peg.135	Threonylcarbamoyl-AMP synthase (EC 2.7.7.87);Ontology_term
-2.52	fig|6666666.571729.peg.682	tmRNA-binding protein SmpB
-2.50	fig|6666666.571729.peg.353	hypothetical protein

-2.49	fig|6666666.571729.peg.139	Thiosulfate sulfurtransferase GlpE (EC 2.8.1.1);Ontology_term
-2.48	fig|6666666.571729.peg.1850	FIG002060: uncharacterized protein YggL
-2.48	fig|6666666.571729.peg.1402	Hydrogenase-4 component B
-2.47	fig|6666666.571729.peg.1782	Zinc ABC transporter%2C ATP-binding protein ZnuC
-2.46	fig|6666666.571729.peg.1751	Crossover junction endodeoxyribonuclease RuvC (EC 3.1.22.4);Ontology_term
-2.46	fig|6666666.571729.peg.1144	Cys regulon transcriptional activator CysB
-2.46	fig|6666666.571729.peg.1541	Zinc ABC transporter%2C substrate-binding protein ZnuA
-2.46	fig|6666666.571729.peg.667	UPF0597 protein YhaM
-2.45	fig|6666666.571729.peg.472	Multidrug efflux system EmrAB-OMF%2C inner-membrane proton/drug antiporter EmrB (MFS type)
-2.44	fig|6666666.571729.peg.1968	UPF0701 protein YicC
-2.44	fig|6666666.571729.peg.1405	[NiFe] hydrogenase metallocenter assembly protein HypF
-2.44	fig|6666666.571729.peg.838	Uracil permease @ Uracil:proton symporter UraA
-2.43	fig|6666666.571729.peg.893	Ribonucleotide reductase transcriptional regulator NrdR
-2.43	fig|6666666.571729.peg.886	Biotin synthase (EC 2.8.1.6);Ontology_term
-2.42	fig|6666666.571729.peg.217	2'%2C3'-cyclic-nucleotide 2'-phosphodiesterase (EC 3.1.4.16) / 3'-nucleotidase (EC 3.1.3.6);Ontology_term
-2.42	fig|6666666.571729.peg.1227	FIG023911: putative membrane protein

-2.42	fig|6666666.571729.peg.734	Putative transport protein YidE
-2.42	fig|6666666.571729.peg.532	Glutamine synthetase type I (EC 6.3.1.2);Ontology_term
-2.42	fig|6666666.571729.peg.527	Site-specific tyrosine recombinase XerD
-2.40	fig|6666666.571729.peg.966	hypothetical protein
-2.39	fig|6666666.571729.peg.1708	Pyridoxal phosphate-containing protein YggS
-2.39	fig|6666666.571729.peg.1836	Uridylate kinase (EC 2.7.4.22);Ontology_term
-2.38	fig|6666666.571729.peg.1073	Acetolactate synthase large subunit (EC 2.2.1.6);Ontology_term
-2.38	fig|6666666.571729.peg.1919	FIG00696423: hypothetical protein
-2.38	fig|6666666.571729.peg.1346	BioD-like N-terminal domain / Phosphate acetyltransferase (EC 2.3.1.8);Ontology_term
-2.36	fig|6666666.571729.peg.692	Serine hydroxymethyltransferase (EC 2.1.2.1);Ontology_term
-2.35	fig|6666666.571729.peg.493	NADH-dependent butanol dehydrogenase A (EC 1.1.1.-);Ontology_term
-2.35	fig|6666666.571729.peg.466	Single-stranded DNA-binding protein
-2.33	fig|6666666.571729.peg.1286	Aspartate aminotransferase (EC 2.6.1.1);Ontology_term
-2.33	fig|6666666.571729.peg.1046	3-deoxy-D-manno-octulosonate 8-phosphate phosphatase (EC 3.1.3.45);Ontology_term
-2.32	fig|6666666.571729.peg.1101	Cytidylate kinase (EC 2.7.4.25);Ontology_term
-2.31	fig|6666666.571729.peg.1719	Aldose 1-epimerase (EC 5.1.3.3);Ontology_term

-2.31	fig|6666666.571729.peg.280	UPF0225 protein YchJ
-2.30	fig|6666666.571729.peg.1304	Aldose 1-epimerase
-2.30	fig|6666666.571729.peg.752	Thymidylate synthase (EC 2.1.1.45);Ontology_term
-2.29	fig|6666666.571729.peg.1775	Ribosome LSU-associated GTP-binding protein HflX
-2.29	fig|6666666.571729.peg.142	Ketol-acid reductoisomerase (NADP(+)) (EC 1.1.1.86);Ontology_term
-2.29	fig|6666666.571729.peg.721	UDP-glucose 4-epimerase (EC 5.1.3.2);Ontology_term
-2.28	fig|6666666.571729.peg.492	LSU ribosomal protein L1p (L10Ae)
-2.28	fig|6666666.571729.peg.1695	T6SS PAAR-repeat protein
-2.27	fig|6666666.571729.peg.193	PTS system%2C fructose-specific IIA component (EC 2.7.1.202) / Fructose-specific phosphocarrier protein HPr;Ontology_term
-2.27	fig|6666666.571729.peg.548	FIG00782388: hypothetical protein
-2.27	fig|6666666.571729.peg.1353	Glutamate-1-semialdehyde 2%2C1-aminomutase (EC 5.4.3.8);Ontology_term
-2.27	fig|6666666.571729.peg.848	NAD-dependent glyceraldehyde-3-phosphate dehydrogenase (EC 1.2.1.12);Ontology_term
-2.26	fig|6666666.571729.peg.1787	DNA mismatch repair endonuclease MutH
-2.24	fig|6666666.571729.peg.1151	Outer membrane lipoprotein
-2.24	fig|6666666.571729.peg.1810	Transcriptional regulator%2C MerR family
-2.23	fig|6666666.571729.peg.1783	Zinc ABC transporter%2C permease protein ZnuB

-2.22	fig|6666666.571729.peg.825	ABC transporter involved in cyto-chrome c biogenesis%2C ATPase component CcmA
-2.22	fig|6666666.571729.peg.478	23S rRNA (guanosine(2251)-2'-O)-methyltransferase (EC 2.1.1.185);On-tology_term
-2.22	fig|6666666.571729.peg.1005	Multidrug efflux transporter MdtK/NorM (MATE family)
-2.22	fig|6666666.571729.peg.1104	probable membrane protein YPO2224
-2.21	fig|6666666.571729.peg.138	Flavin-utilizing monoxygenase
-2.21	fig|6666666.571729.peg.1777	ABC transporter%2C substrate-bind-ing protein (cluster 8%2C B12/iron complex)
-2.21	fig|6666666.571729.peg.1642	Arginine ABC transporter%2C sub-strate-binding protein ArtI
-2.21	fig|6666666.571729.peg.1800	Glutamyl-tRNA synthetase (EC 6.1.1.17);Ontology_term
-2.20	fig|6666666.571729.peg.975	Enoyl-[acyl-carrier-protein] reductase [NADH] (EC 1.3.1.9);Ontology_term
-2.20	fig|6666666.571729.peg.783	LSU ribosomal protein L28p @ LSU ribosomal protein L28p%2C zinc-in-dependent
-2.20	fig|6666666.571729.peg.1320	5%2C10-methylenetetrahydrofolate reductase (EC 1.5.1.20);Ontol-ogy_term
-2.19	fig|6666666.571729.peg.706	Molybdopterin adenylyltransferase (EC 2.7.7.75);Ontology_term
-2.19	fig|6666666.571729.peg.1880	PTS system%2C sucrose-specific IIB component (EC 2.7.1.211) / PTS sys-tem%2C sucrose-specific IIC compo-nent;Ontology_term
-2.19	fig|6666666.571729.peg.674	Octaprenyl diphosphate synthase (EC 2.5.1.90);Ontology_term
-2.19	fig|6666666.571729.peg.574	3-oxoacyl-[ACP] reductase (EC 1.1.1.100) FadG2%2C NOT involved in fatty acid synthesis;Ontology_term

-2.18	fig|6666666.571729.peg.71	Transcription elongation factor GreB
-2.18	fig|6666666.571729.peg.1314	Tryptophan synthase alpha chain (EC 4.2.1.20);Ontology_term
-2.18	fig|6666666.571729.peg.2003	Frataxin homolog CyaY%2C facilitates Fe-S cluster assembly%2C interacts with IscS
-2.18	fig|6666666.571729.peg.822	UPF0070 protein YfgM
-2.17	fig|6666666.571729.peg.1766	hypothetical protein
-2.17	fig|6666666.571729.peg.1623	UDP-N-acetylmuramoyl-tripeptide--D-alanyl-D-alanine ligase (EC 6.3.2.10);Ontology_term
-2.17	fig|6666666.571729.peg.1236	Oligopeptide ABC transporter%2C ATP-binding protein OppF (TC 3.A.1.5.1)
-2.16	fig|6666666.571729.peg.89	Glycerol-3-phosphate transporter
-2.16	fig|6666666.571729.peg.199	Thymidylate kinase (EC 2.7.4.9);Ontology_term
-2.16	fig|6666666.571729.peg.1233	ABC transporter%2C substrate-binding protein (cluster 5%2C nickel/peptides/opines)
-2.15	fig|6666666.571729.peg.1726	Galactose/methyl galactoside ABC transporter%2C permease protein MglC (EC 3.6.3.17);Ontology_term
-2.15	fig|6666666.571729.peg.266	thiamine-phosphate pyrophosphorylase(EC:2.5.1.3);Ontology_term
-2.14	fig|6666666.571729.peg.1199	Electron transport complex protein RnfE
-2.13	fig|6666666.571729.peg.153	Uncharacterized protein EC-HemY in Proteobacteria (unrelated to HemY-type PPO in GramPositives)
-2.13	fig|6666666.571729.peg.309	Hydrogenase-2 operon protein HybA

-2.13	fig|6666666.571729.peg.774	Cytochrome c-type heme lyase subunit nrfE%2C nitrite reductase complex assembly
-2.13	fig|6666666.571729.peg.81	Spermidine/putrescine import ABC transporter substrate-binding protein PotD (TC 3.A.1.11.1)
-2.12	fig|6666666.571729.peg.1997	Phosphoglycerate kinase (EC 2.7.2.3);Ontology_term
-2.12	fig|6666666.571729.peg.319	Fluoride ion transporter CrcB
-2.12	fig|6666666.571729.peg.27	Competence protein F homolog%2C phosphoribosyltransferase domain%3B protein YhgH required for utilization of DNA as sole source of carbon and energy
-2.12	fig|6666666.571729.peg.924	FIG005121: SAM-dependent methyltransferase (EC 2.1.1.-);Ontology_term
-2.11	fig|6666666.571729.peg.1617	D-alanine--D-alanine ligase (EC 6.3.2.4);Ontology_term
-2.10	fig|6666666.571729.peg.1771	Ribonuclease E (EC 3.1.26.12);Ontology_term
-2.10	fig|6666666.571729.peg.70	Transcription accessory protein (S1 RNA-binding domain)
-2.10	fig|6666666.571729.peg.1239	Cytidine deaminase (EC 3.5.4.5);Ontology_term
-2.09	fig|6666666.571729.peg.1763	Histidine permease YuiF
-2.09	fig|6666666.571729.peg.114	Selenocysteine-specific translation elongation factor
-2.09	fig|6666666.571729.peg.4	Methionine ABC transporter substrate-binding protein
-2.09	fig|6666666.571729.peg.658	Ribosome-associated inhibitor A
-2.08	fig|6666666.571729.peg.1075	Uncharacterized integral membrane protein GSU2901

-2.08	fig|6666666.571729.peg.1305	Threonyl-tRNA synthetase (EC 6.1.1.3);Ontology_term
-2.08	fig|6666666.571729.peg.221	Acetolactate synthase large subunit (EC 2.2.1.6);Ontology_term
-2.07	fig|6666666.571729.peg.420	Murein hydrolase activator NlpD
-2.07	fig|6666666.571729.peg.1225	Glutaredoxin 2
-2.06	fig|6666666.571729.peg.227	ATP synthase epsilon chain (EC 3.6.3.14);Ontology_term
-2.06	fig|6666666.571729.peg.937	Argininosuccinate synthase (EC 6.3.4.5);Ontology_term
-2.06	fig|6666666.571729.peg.1333	hypothetical protein
-2.05	fig|6666666.571729.peg.1923	Ribonuclease PH (EC 2.7.7.56);Ontology_term
-2.05	fig|6666666.571729.peg.1494	Deoxycytidine triphosphate deaminase (EC 3.5.4.13);Ontology_term
-2.05	fig|6666666.571729.peg.145	Phosphoglycerate mutase (EC 5.4.2.11);Ontology_term
-2.04	fig|6666666.571729.peg.467	Excinuclease ABC subunit A
-2.03	fig|6666666.571729.peg.1640	Arginine ABC transporter%2C permease protein ArtM
-2.03	fig|6666666.571729.peg.1454	Phosphatidylglycerol--membrane-oligosaccharide glycerophosphotransferase (EC 2.7.8.20);Ontology_term
-2.02	fig|6666666.571729.peg.76	UPF0381 protein HI_0636
-2.02	fig|6666666.571729.peg.1397	Hydrogenase-4 component G
-2.02	fig|6666666.571729.peg.1614	Cell division protein FtsZ
-2.01	fig|6666666.571729.peg.1379	Purine nucleotide synthesis repressor

-2.01	fig|6666666.571729.peg.390	6-phosphogluconate dehydrogen-ase%2C decarboxylating (EC 1.1.1.44);Ontology_term
-2.00	fig|6666666.571729.peg.1953	Biotin carboxylase of acetyl-CoA car-boxylase (EC 6.3.4.14);Ontol-ogy_term